



Two-Photon Sensitive Biomaterials for Dynamic Control of Cellular Microenvironments

Dissertation

zur Erlangung des Grades
des Doktors der Naturwissenschaften
der Naturwissenschaftlich-Technischen Fakultät
der Universität des Saarlandes

von

Qiyang Jiang

Saarbrücken, 2022

Tag des Kolloquiums: 26 July, 2022

Dekan: Prof. Dr. rer. nat. Jörn Walter

Berichterstatter: Prof. Dr. Aránzazu del Campo Bécares

Prof. Dr. Karen Lienkamp

Akad. Mitglied: Dr. Lola Gonzalez-Garcia

Vorsitz: Prof. Dr.-Ing. Markus Galle

Two-Photon Sensitive Biomaterials for Dynamic Control of Cellular Microenvironments

Qiyang Jiang

geb. in JiLin, China

DISSERTATION

INM- Leibniz Institut für Neue Materialien, Saarbrücken

I hereby declare that I wrote the dissertation submitted without any unauthorized external assistance and used only sources acknowledged in the work. All textual passages which are appropriated verbatim or paraphrased from published and unpublished texts as well as all information obtained from oral sources are duly indicated and listed in accordance with bibliographical rules. In carrying out this research, I complied with the rules of standard scientific practice as formulated in the statutes of Saarland University in Saarbrücken to insure standard scientific practice.

Qiyang Jiang

Dedicated to my family

Acknowledgements

This thesis was performed at INM- Leibniz Institute for New Materials, Saarbrücken. The completion of this thesis work would not have been possible without the support of many individuals. Especially, I would like to give special thanks to China Scholarship Council (CSC) for financially supporting my stay in Germany.

First and foremost, I would like to express my sincere gratitude and appreciation to my supervisor, Prof. Dr. Aránzazu del Campo Bécares, for her continuous support, guidance, motivation, and profound knowledge. I am grateful for the opportunity to join and work in her interdisciplinary group and for providing a creative working atmosphere. I further appreciate the opportunities to participate in scientific conferences, courses, and discussions.

Deepest gratitude to my mentor, Assist. Prof. Dr. Julieta Paez, for her continuous support, encouragement, and constant motivation. I am very thankful for her useful advice, discussions and for always being so understanding to support me both in my professional and personal life.

I would like to express my sincere gratitude to my second supervisor, Prof. Dr. Uli Kazmaier, University of Saarland, for his suggestions and support.

Furthermore, I would like to thank Dr. Aleeza Farrukh and Dr. Roshna Vakkeel, for introducing me to the field of photochemistry and for guiding me in my research.

I also thank Rocío Valbuena Mendoza, for her collaboration in performing cell migration experiments and for all the discussions and advice.

Special thanks to my colleagues and friends, Dr. Maria Villiou, Dr. Desna Joseph, Dr. Essak Khan and Rebecca Ludwig, for their invaluable support, scientific and non-scientific discussions and constant encouragement.

I am also very thankful to Dr. Lulu Xue and Dr. Xinhong Xiong, for their true friendship, to cheer me up and for sharing incredible moments together. Also to Dr. Jingnan Zhang, for his kind help and support.

I would like to thank Dr. Emmanuel Terriac and Dr. Mitchell Han, for their help in microscopy; and to Prof. Dr. Yijun Zheng, for introducing me to the peptide synthesizer. Thanks to Dr. Malgorzata Wlodarczyk-Biegun and Dr. Jun Feng, for introducing me to rheology techniques. To Dr. Lena Barnefske, for her help in NaonoScribe technique; to Dr. Bernd Reinhard for his help with the microwave reactor. I am grateful to Dieter Anschütz, Dr. Claudia Fink-Straube and Ha Rimbach-Nguyen, for mass spectrometry measurements. I would also thank Dr. Samuel Pearson, Dr. Maria Puertas Bartolome, Minye Jin, Adrián de Miguel Jimenez, for their help, discussions and support. I thank Stefan Brück for all his technical support and for the fun in the labs.

I am especially thankful to Martina Bonnard, for her assistance and support during the extremely difficult time of my sickness. Thanks to Mr. Bernd Rus, Ms. Sabine Müller and Ms. Miriam Badziong for their help in solving various social issues in Germany.

Special thanks to Dr. Bin Li, Dr. Shifang Zhao, Dr. Vaishali Chopra, Lisa Sold, Priyanka Dhakane, Ana Diaz Alvarez, Shardul Bhusari and all my friends for their kind support in Germany.

My deepest gratitude to my parents and my sister, for their unconditional love and support, who brighten me with virtue and selflessly encourage me to explore my life. I am also sincerely grateful to my parents-in-law for their support.

Finally, I would like to thank my wonderful husband Bo Chen, for all his love, companionship, patience, and support. Without you, I would have not been able to reach this milestone. Thanks for always being there and help me going through all the hard times throughout this journey.

Abstract

Two-photon (2P) activable photocleavable protecting groups (PPGs) can be introduced in polymer networks as photodegradation sites or as blocking groups for active sites, which enable the alternation of mechanical properties and biochemical signals and allow to study consequent cell response in a spatiotemporal controlled manner. So far, the design of high efficient 2P activable hydrogels is challenging. This Thesis presents novel designs of photodegradable hydrogels that contain the 4'-methoxy-4-nitrobiphenyl-3-yleth-2-yl)methyl (PMNB) PPG. PMNB-gels formed under physiological conditions and showed tuneable hydrolytic stability and adequate rate for cell encapsulation. Moreover, PMNB-gels can be photodegraded efficiently upon 2P excitation ($\lambda = 740$ nm). Preliminary experiments of PMNB-gels as 4D matrices for the investigation of cell response are presented. In a second part, a 2P-activatable PPGs endowed with an extended π conjugation was demonstrated and introduced to yield the RGD cell adhesive peptide. The targeted peptide is obtained but only in low yield due to its low stability. The results of this Thesis provide new tools for instructing cells in 3D cultures using 2P-activated processes and demonstrate the potential of photochemistry for the realization of 4D biomaterials.

Zusammenfassung

Zwei-Photonen-(2P)-aktivierbare photolytisch spaltbare Schutzgruppen (PPGs) können in Polymernetzwerke als photokysetellen oder als Schutzgruppen für aktive Stellen eingeführt werden, das Alternieren von mechanischen Eigenschaften und biochemischen Signalen ermöglichen und es erlauben, die daraus resultierende Zellreaktion in einer räumlich-zeitlich kontrollierten Weise zu untersuchen. Bisher ist das Design von hocheffizienten 2P-aktivierbaren Hydrogelen eine Herausforderung. In dieser Arbeit werden neuartige Designs von photodegradierbaren Hydrogelen vorgestellt, die 4'-Methoxy-4-nitrobiphenyl-3-yleth-2-yl)methyl (PMNB) PPG enthalten. PMNB-Gele bildeten sich unter physiologischen Bedingungen und zeigten eine einstellbare hydrolytische Stabilität und eine angemessene Geschwindigkeit für die Immobilisierung von Zellen. Darüber hinaus können PMNB-Gele bei 2P-Anregung ($\lambda = 740 \text{ nm}$) effizient photolytisch abgebaut werden. Es werden erste Experimente mit PMNB-Gelen als 4D-Matrizen für die Untersuchung der Zellreaktion vorgestellt. In einem zweiten Teil wurde ein 2P-aktivierbares PPGs mit einer verlängerten π -Konjugation demonstriert und eingeführt, um das zelladhäsive RGD-Peptid zu erhalten. Das angestrebte Peptid wurde gewonnen, allerdings aufgrund seiner geringen Stabilität nur in geringer Ausbeute. Die Ergebnisse dieser Arbeit liefern neue Werkzeuge für die Steuerung von Zellen in 3D-Kulturen mit Hilfe von 2P-aktivierbaren Prozessen und zeigen das Potenzial der Photochemie für die Realisierung von 4D-Biomaterialien.

Abbreviations

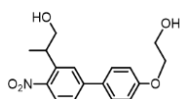
ϵ	Molar extinction coefficient
λ_{\max}	Wavelength of the absorbance maximum
Φ	Quantum yield
δ	Two-photon cross-section
δ	Chemical shift
GM	Goeppert-Mayer
$t_{1/2}$	Half-time
ACN	Acetonitrile
AcOH	Acetic acid
Arg	Arginine
Asp	Aspartic acid
Boc	Tert-butoxycarbonyl
Bu ₄ NBr	Tetrabutylammonium bromide
CDCl ₃	Deuterated chloroform
c[RGDfC]	Cyclo[arginine-glycine-aspartic acid-D-phenylalanine-cysteine]
c[RGDfK]	Cyclo[arginine-glycine-aspartic acid-D-phenylalanine-lysine]
c[RGDfK(Mal)]	Cyclo[arginine-glycine-aspartic acid-D-phenylalanine-lysine(maleimide)]
CuAAC	Copper-catalysed azide–alkyne cycloadditions
Cys	Cysteine
d	Doublet (NMR)
DBCO	Azodibenzocyclooctyne
DCC	<i>N,N'</i> -Dicyclohexylcarbodiimide
DCM	Dichloromethane
DIBAL-H	Diisobutylaluminiumhydride
DIPEA	<i>N,N'</i> -Diisopropylethylamine
DMAP	4-Dimethylaminopyridine

DMF	<i>N,N'</i> -dimethylformamide
DPPA	Diphenylphosphoryl azide
DTT	Dithiothreitol
ECM	Extracellular matrix
ESI-MS	Electrospray ionization mass spectroscopy
EtN ₃	Triethylamine
EtOAc	Ethyl acetate
Fmoc	9-fluorenylmethoxycarbonyl protecting group
G´	Storage modulus
G´´	Loss modulus
Gly	Glycine
h	Hour
HBTU	(2-(1H-benzotriazol-1-yl)-1,1,3,3-tetramethyluronium hexafluorophosphate
HCl	Hydrochloric acid
HEPES	4-(2-hydroxyethyl)-1-piperazineethanesulfonic acid)
HOBt	Hydroxybenzotriazole
HPLC	High performance liquid chromatography
HUVEC	Human umbilical vein endothelial cells
Hz	Hertz
IC ₅₀	Half-maximal inhibitory concentration
J	Coupling constant in Hz (NMR)
K ₂ CO ₃	Potassium carbonate
LiAlH ₄	Lithium aluminium hydride
Lys	Lysine
mCPBA	meta-chloroperoxybenzoic acid
M	Molarity (mol/L)
m	Multiplet (NMR)
X	

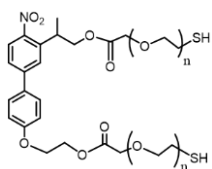
Mal	Maleimide
Mel	Iodomethane
MgSO ₄	Magnesium sulfate
min	Minute
N ₃	Azide
NaHCO ₃	Sodium bicarbonate
Na ₂ SO ₄	Sodium sulfate
NHS	<i>N</i> -Hydroxysuccinimide
NH ₂	Amino group
NIR	Near-infrared
NMM	<i>N</i> -Methylmorpholine
OH	Hydroxy
OMe	Methoxy
<i>o</i> NB	ortho-nitrobenzyl group
Ox-MS	Oxadiazole methanesulfone
Pbf	2,2,4,6,7-pentamethyl-dihydro-benzofuran-5-sulfonyl
PBS	Phosphate-buffered saline
Pd(OAc) ₂	Palladium(II) acetate
PDMS	Polydimethylsiloxane
PEG	Polyethylene glycol
PENP-OH	2-(5-((4-methoxyphenyl)ethynyl)-2-nitrophenyl)propan-1-ol
Phe	Phenylalanine
<i>p</i> -TsOH	<i>p</i> -Toluenesulfonic acid
q	Quartet (NMR)
s	Singlet (NMR)
SH	Thiol
SPAAC	Strain-promoted azide-alkyne cycloaddition
SPPS	Solid phase peptide synthesis

RT	Room temperature
t-BuOK	Potassium tert-butoxide
TFA	Trifluoroacetic acid
TFE	2,2,2-trifluoroethanol
THF	Tetrahydrofuran
TIS	Triisopropylsilane
TLC	Thin-layer chromatography
Trt	Triphenylmethyl
Tz-MS	Tetrazole methysulfone
UV/Vis	Linear optical absorption spectroscopy in the ultraviolet and visible spectral region
wt%	Weight percentage
w/v	Weight by volume
¹ H-NMR	Proton NMR spectroscopy
¹³ C-NMR	Carbon NMR spectroscopy
1P	One-photon
2P	Two-photon
2D	Two-dimensional
3D	Three-dimensional

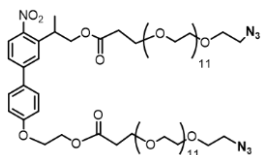
PMNB(OH)₂



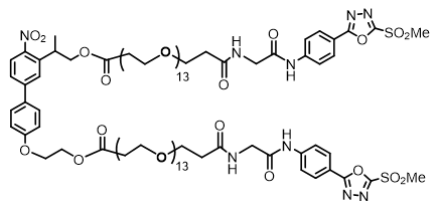
PMNB(E-PEG_n-SH)₂



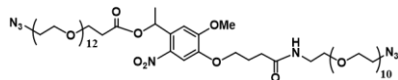
PMNB(E-EG₁₂-N₃)₂



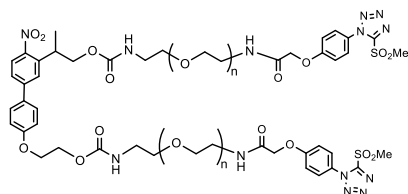
PMNB(E-EG₁₃-Ox-MS)₂



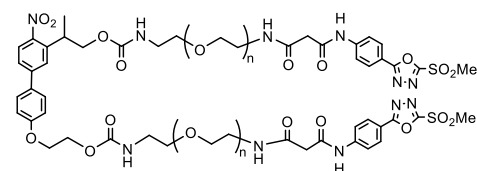
NB-E-(EG_n-N₃)₂



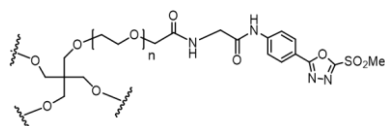
PMNB(C-EG_n-Tz-MS)₂



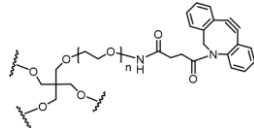
PMNB(C-EG_n-Ox-MS)₂



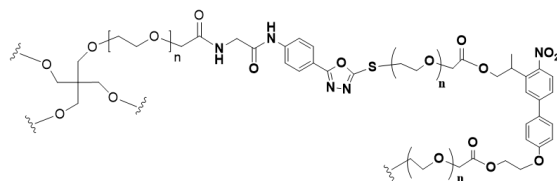
Star PEG-Ox-MS



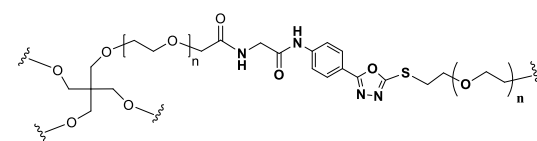
Star PEG-DBCO



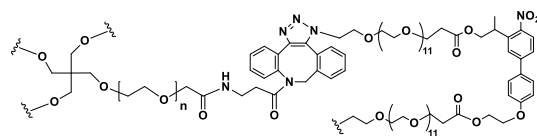
PEG-OxS-E-PMNB gel



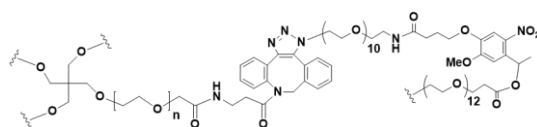
PEG-OxS gel



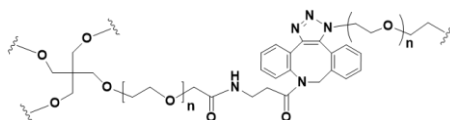
PEG-T-E-PMNB gel



PEG-T-E-NB gel



PEG-T gel



All other abbreviations, such as physical and chemical units, have their usual meaning if not stated otherwise.

INDEX

Motivation	1
Chapter 1: Introduction	3
1.1 Hydrogels as mimics of the native extracellular matrix	3
1.1.1 Hydrogel properties for cell encapsulation	3
1.1.2 PEG hydrogels for cell encapsulation	7
1.1.3 Crosslinking reactions used for cell encapsulation.....	8
1.2 Light-regulated hydrogels for cell culture.....	14
1.2.1 Light-responsive hydrogels with photoregulated degradation	16
1.2.2 Hydrogels with photoactivatable biochemical signals	19
1.3 Two-photon responsive hydrogels for cell encapsulation.....	21
1.4 Photocleavable protecting groups for efficient two-photon activation.....	23
1.4.1 General design rules for efficient two-photon activatable chromophores	23
1.4.2 The (<i>o</i> -nitrobiphenyl)propyl family	24
1.4.3 The (<i>o</i> -nitrobiphenylacetylene)propyl family	25
1.4.4 Alternative PPGs	26
1.5 References.....	27
Chapter 2: Synthesis of two-photon degradable crosslinkers and PEG-precursors.....	37
2.1 Introduction.....	37
2.2 Molecular design of photodegradable hydrogels for cell encapsulation	40
2.3 Synthesis of photodegradable crosslinkers	43
2.3.1 Synthesis of PMNB ester crosslinkers.....	43
2.3.2 Synthesis of control crosslinker	47
2.3.3 Synthesis of PMNB carbamate crosslinkers.....	48
2.4 Synthesis of star PEG-hydrogel precursors.....	52
2.5 Photochemical properties of PMNB(E-PEG _n -SH) ₂ and NB-E-(EG _n -N ₃) ₂	55
2.6 Hydrolytic stability of PMNB ester and carbamate crosslinkers	61
2.7 Conclusion	62
2.8 References.....	63
Chapter 3: Synthesis and physicochemical properties of photodegradable PEG-hydrogels	67
3.1 Introduction.....	67
3.2 Synthesis of hydrogels	68
3.3 Characterization of crosslinking kinetics and mechanical properties of the hydrogels by rheology	72
3.4 Study of hydrolytic stability of the hydrogels.....	74

3.5 Study of hydrogel photodegradation with UV/Vis light by rheology	75
3.5.1 1P degradation of hydrogel at UV/Vis	75
3.5.2 2P degradation of PEG-OxS-E-PMNB hydrogels	82
3.6 Cytocompatibility of photodegradable hydrogels and application for dynamic cell culture	89
3.7 Conclusions	92
3.8 References.....	94
Chapter 4: Synthesis of two-photon activatable cell adhesive peptide.....	99
4.1 Introduction.....	99
4.2 Molecular design of two-photon activatable RGD cell adhesive peptides	102
4.3 Synthesis of cyclo[RGD(PNEP)fX]	103
4.3.1 Synthesis PNEP-Asp	103
4.3.2 Stability study of Fmoc-Asp(PENP)-OH.....	105
4.3.3 Synthesis of c[RGD(PENP)fC] via solid phase peptide synthesis	106
4.4 Photochemical properties of Fmoc-Asp(PENP)-OH in solution.....	108
4.5 Photochemical properties of c[RGD(PENP)fK-N ₃] in solution	110
4.6 Discussion.....	112
4.7 Reference	112
Appendix	119
List of Scientific Contributions	162

Motivation

Photoresponsive biomaterials attract interest as models of the dynamic properties of the extracellular matrix (ECM) in natural tissues, and as useful platforms for in vitro cell culture to study the response of cellular responses (e.g., adhesion, migration, proliferation, or differentiation) to spatiotemporally regulated changes in vitro. Light as external trigger is especially convenient to manipulate the properties of materials in the presence of cells, as it is non-invasive, easily available, tunable (in terms of wavelength and dose), and it allows for high spatial resolution and temporal control. Additionally, light can be incorporated into medical devices and, therefore, it is considered convenient for future application of photoresponsive biomaterials in cell-based therapies for tissue regeneration.

For this purpose, hydrogels with increasing sophistication have been developed in the field of biomaterials for engineering tissues. These incorporate functionalities necessary as ECM mimics, including the possibility to be formed in the presence of living cells, high hydration and mechanical stability at low polymer contents, and also phototunable biophysical (e.g., mechanics, porosity) and biochemical (e.g., adhesive cues) properties. Despite the significant progress, there are still challenges around the development of photoactivatable hydrogels that need to be addressed, such as the efficient response to wavelengths in the NIR range to avoid cell damage during exposure and to increase penetration depth.

Photocleavable protecting groups (PPGs), which can be cleaved upon light illumination, have been extensively used for the realization of photoactivatable hydrogels. In most cases, these groups have their absorption maxima within the UV range and are cleaved using one-photon (1P) excitation. However, 1P irradiation does not allow deep penetration in the hydrogel or 3D resolution of the photoactivation process. In this regard, two-photon (2P) excitation using light in the NIR would be advantageous, as it allows improving the penetration depth and spatial resolution. However, reported 2P-activatable hydrogels contain photoresponsive groups with low 2P efficiency. This leads to the need of applying high exposure doses for activation, which can lead to cell photodamage and loss of cell function.

In this context, this Thesis aims to develop more efficient 2P-light responsive hydrogels with tuneable mechanical properties, and to demonstrate their suitability for in situ cell encapsulation and the activation and study of cell migration.

This Thesis has the following specific objectives:

- To design and synthesize efficient 2P photoactivatable macromers as crosslinkers, and to study the effect of diverse structural components (e.g., photolabile bonds, flanking spacers) on the reactivity, stability and functionality (e.g., photocleavage, water solubility and stability).
- To develop 2P degradable PEG-based hydrogels using biocompatible crosslinking reactions to allow the direct encapsulation of living cells during the gelation process.
- To 3D pattern hydrogels by using 2P lasers at a light dosage at wavelengths which do not damage cells and to direct cell migration by activating degradation of the polymer network.

- To synthesize efficient 2P photoactivable cell adhesive peptides for the biofunctionalization of 4D hydrogels to be used for dynamic cell culture.

With these objectives in mind, the Thesis is organized as follows:

Chapter 1 presents a literature review. It describes hydrogels as ECM mimics and summarizes materials properties and crosslinking methods used for cell encapsulation. Additionally, the progress and the current limitations of light-triggerable hydrogels used for 4D cell culture upon 1P and 2P excitation are presented. The state of the art of 2P-activable PPGs in cell biology is also described and current molecular approaches to improve their shortcomings are described.

Chapter 2 describes the chemical design and synthesis of a library of photodegradable crosslinkers with various structural variations. Studied and optimized molecular parameters are water solubility, hydrolytic stability, 2P-activation efficiency, and the type of crosslinking chemistry for hydrogel formation. The properties of the novel crosslinkers in solution are benchmarked against reported photodegradable molecules used in biomaterials research.

Using the novel crosslinkers synthesized and characterized in the previous chapter, in **Chapter 3** these are used for the synthesis of PEG hydrogels by polymerization with complementary macromers. The derived PEG gels are prepared via diverse crosslinking chemistries, all of them effective under cytocompatible conditions, and their materials properties characterized, including their gelation kinetics and mechanical strength. 1P and 2P-induced photodegradation of the obtained hydrogels is evaluated by rheology and 3D laser scanning microscope. The impact of photolabile bonds on the hydrolytic stability of hydrogels under cell culture conditions is investigated. Finally, preliminary experiments of cytocompatibility and 2P-degradation of such hydrogels are shown, to test the potential of the developed platform for directing cell migration in vitro.

Chapter 4 describes a novel 2P PPG designed to increase the 2P efficiency by extending the π -conjugation length of the compound. This group is incorporated to at the COOH group of the Asp residue within the cell-adhesive peptide RGDfC via solid phase peptide synthesis (SPPS), with the purpose of regulating its bioactivity. The characterization of the photochemical properties of the photoactivatable peptide is presented. The hydrolytic stability of obtained photoactivatable aspartic acid is studied under the conditions used in SPPS and the opportunities for further developments in this area are identified.

A **Conclusions** section summarizes the main results of the presented work and provides a brief outlook on future directions.

Finally, the **Appendix** section includes all the supplementary information about the materials and methods, instrumentation and experimental protocols; compound characterization (NMR, HPLC, mass spectrometry data), photolysis studies (UV/Vis, mass spectrometry and HPLC data), as well as complementary photorheological, microscopy and biological studies of hydrogels.

Chapter 1: Introduction

1.1 Hydrogels as mimics of the native extracellular matrix

Hydrogels are three-dimensional (3D) networks of crosslinked hydrophilic polymer chains, which can uptake high amount of water, up to more than thousand times their own dry weight.^{1,2} Their hydrated state and their softness and 3D porous structure resemble the characteristics of native extracellular matrix (ECM), and motivate their use as biomaterials to encapsulate cells to be used for cell culture, tissue engineering or cell therapies.³⁻⁶ Hydrophilic polymers of natural, synthetic or hybrid composition are used to form hydrogel networks and embed living cells for this purpose.^{7,8}

In conventional 2D cell culture, hydrogels are used as flat substrates onto which cells can grow. In this geometry cells exhibit abnormal polarization, and show different responses to their in vivo environment.^{9,10} In 3D cell cultures, cells are fully surrounded by a hydrogel matrix. When properly designed, in terms of biofunctionalization, diffusion and mechanical properties, such microenvironments provide a more realistic representation of the natural ECM. **Figure 1.1** describes and compares the most relevant cell features in 2D vs. 3D culture types. Hyaluronic acid (HA), collagen, alginate and poly(ethylene glycol) (PEG) hydrogels, among others, are widely used as polymeric backbones in 3D cell culture scaffolds, and have shown high compatibility to the cells.

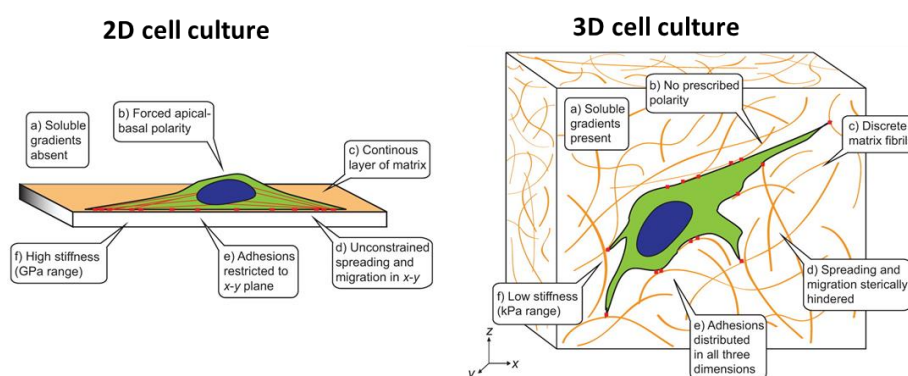


Figure 1.1 Cells microenvironments in 2D and 3D hydrogels. Adapted with permission from Journal of Cell Science.¹¹

1.1.1 Hydrogel properties for cell encapsulation

For cell encapsulation, hydrogels must fulfil a number of biochemical and physical design criteria in order to support cell growth and function as in the natural microenvironment (**Figure 1.2**). The gelation process for cell encapsulation should occur under physiological conditions in order to have high cytocompatibility. Hydrogels of Young's moduli in the physiological range of 1-100 kPa should form at solid content of <10 wt%. Ideally, the mechanical properties can be adjusted to meet the individual needs of the encapsulated cells. Moreover, the hydrogel should be degradable to allow cells enough space for migration and proliferation, and to be replaced by the matrix secreted by the cells. Diffusion properties is also a crucial factor to ensure continuous supply of the essential nutrients and

Chapter 1

removal of waste products, thus maintain the cell viability and functions. Biofunctionalization can also be adapted for desired application with the incorporation of different bioactive molecules. Ideally, hydrogel biochemical and mechanical properties can be tuned over time to mimic the dynamic evolution of tissues in developmental and pathological states.

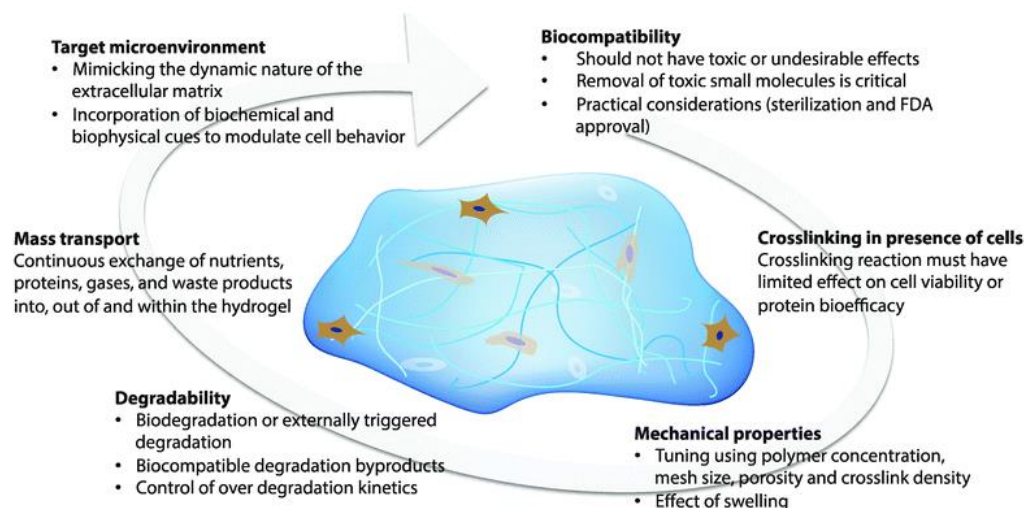


Figure 1.2 Hydrogel design criteria for cell encapsulation. Reprinted with permission from the Royal Society of Chemistry.¹²

Cytocompatibility

Cytocompatibility is a key criterion for a host material designed to encapsulate a living cell. Biocompatibility depends on different factors, e.g. the chemical and mechanical properties of the material, the presence of biofunctional groups and the degradation ability and kinetics. For cell encapsulation, hydrogels should not be toxic. If the hydrogels are to be used *in vivo*, they should also not cause an immunological response. Synthetic polymers like PEG, PHEMA or PLGA, and natural polymers like alginate or collagen present adequate biocompatibility and were well tolerated *in vitro* and *in vivo*. Modification with cell adhesive molecules increases the cytocompatibility of the hydrogel (see section “biofunctionalization”). The reactive functionalities or the chemical reactions during hydrogel synthesis (e.g. release of toxic side product or the catalysts or initiators of the gelation reaction) can also lead to cell damage. For example, unreacted maleimides, widely used in thiol-maleimide crosslinking reactions, are cytotoxic to neuronal cells.¹³ The reaction conditions for crosslinking (e.g. pH, ionic strength, polymer concentration) also play an important role in keeping high cell viability and should remain close to physiological values (pH~6-8, temperature~20-40°C).^{14, 15} Overall, biocompatibility of hydrogels need to be evaluated for the particular cell type and application.

Gelation kinetics

Gelation kinetics is an important parameter that determines the time window for encapsulating cells in the hydrogels. It can influence the cell distribution, viability and function of the cells inside the

hydrogel. The gelation kinetics is strongly dependent on the type of crosslinking approach applied.¹⁶
¹⁷ Gelation kinetics depends on several intrinsic factors pertaining to the gel precursors such as polymer concentration and molar mass, concentration and distribution of crosslinkable groups, but also on external factors such as temperature, pH, initiator concentration or presence of catalysts. Gelation times between 30 s and a few minutes are typically considered ideal for crosslinking hydrogels in the presence of cells while keeping high cell viability.¹⁸

Bio-functionality

In the native cell microenvironment, the ECM presents cell adhesive sites and growth factors that are recognized by cell surface receptors and regulate cell function. Therefore, such biological cues need to be incorporated in hydrogels for cell culture. Natural hydrogels present inherent bioactive sites, for example HA polymer presents repeating disaccharides of D-glucuronic acid and N-acetyl-d-glucosamine cues that bind to cell surface receptors CD44, but show some batch-to-batch variability in the functionalization depending on the source and isolation process.¹⁹ In the case of synthetic hydrogels, such as PEG, no biological signals are offered intrinsically, but they can be added at desired concentration by chemical derivatization of the polymer precursors before cell encapsulation. Hybrid hydrogels combine the inherent bioactive features with well-defined molecular architectures and properties.²⁰ Different kinds of bioactive ligands, proteins and growth factors have been incorporated into hydrogels. For example, the arginine-glycine-aspartic acid (RGD) tripeptide sequence was identified as the smallest cell adhesion motif within ECM proteins (including fibronectin, vitronectin and laminin) and can be recognized by the ECM adhesion receptors known as integrins (including $\alpha_v\beta_3$, $\alpha_5\beta_1$ and $\alpha_{IIb}\beta_3$).²¹ RGD can be easily incorporated into hydrogel backbone without disturbing the overall structure due to its small size. The cyclic RGD peptide is preferred instead of linear RGD peptide since the linear RGD peptide showed lower stability under enzymatic conditions and lower biological activity. Additionally, Pfaff et al. demonstrated that the cyclic RGDfV pentapeptide had higher activity to soluble and immobilized $\alpha_v\beta_3$ (3.2-fold ($IC_{50} = 11.3 \pm 1.2 \mu M$) and 5.8-fold ($IC_{50} = 0.4 \pm 0.2 \mu M$) respectively) compared to the linear RGDfV peptide.²² Dahlin et. al. studied the biocompatibility of PEG hydrogels modified with RGD cell adhesion peptide motif in vitro. Human periosteum-derived cells (hPDCs) were encapsulated in the enzymatically degradable PEG-based hydrogels with RGD peptide functionalization (Ac-GCGYGRGDSPG-NH₂). After 4 weeks in vitro culture, higher cell viability (~85%) were maintained in RGD-functionalized PEG hydrogel (150 μM) compared to the non-functionalized hydrogels (~40 %). Moreover, RGD peptide also showed a significant impact on the cell proliferation when culturing with growth medium (GM).²³

Mechanical properties

Mechanical properties of in vivo ECM microenvironments vary across types of tissue (**Figure 1.3**). A wide range of tissue elasticity, signed by a Young's modulus $E < 1$ kPa (brain, lung, breast), 1–10 kPa (endothelial tissue, muscle) and 10-100 kPa (skeletal muscle tissue) has been reported. Such range

Chapter 1

defines the possible stiffness for mimicking the native ECM by using the hydrogel-based biomaterials (0.01-100 kDa), which can be achieved by varying hydrogel composition and crosslinking degree.^{24, 25} The mechanical properties of matrix play an important role in regulating cell fate, including migration, proliferation and differentiation. For instance, Ehrbar et al. studied the effect of matrix stiffness on regulating cell fate (preosteoblastic cells MC3T3-E) within enzymatically degradable transglutaminase-poly (ethylene) glycol(TG-PEG) hydrogels. Cells showed round morphology, decreased cell mobility and improved the onset of migration (from 4 h to 6 h) when the increased stiffness (94±25 Pa to 482±77 Pa).²⁶ The hydrogels stiffness can also govern cell differentiation. Mesenchymal stem cells (MSCs) differentiate into neuronal lineage or glial cells at 1 kPa and 10 kPa in collagen-hyaluronic acid 3D matrices respectively.²⁷ Other studies also support this finding: MSCs differentiate into osteogenic lineages and adipogenic lineage in RGD-modified alginate hydrogels with a stiffness of 11-30 kPa and 2.5-5 kPa, respectively.²⁸

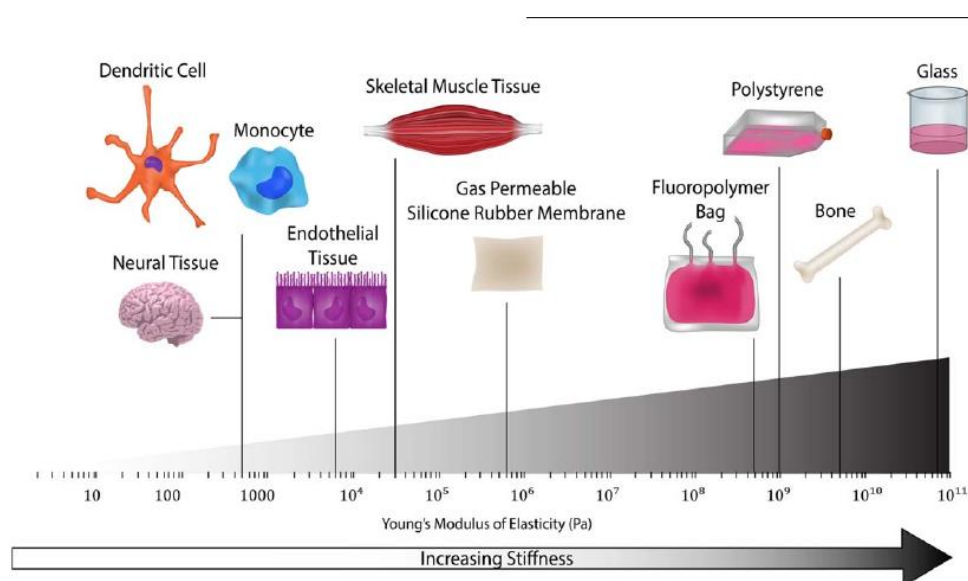


Figure 1.3 Mechanical properties of in vivo ECM microenvironments across native tissues. Republished with permission from Journal of Wiley online library.²⁵

Degradability

In native tissues, cells can remodel their surrounding ECM by a degradation process (typically by enzymatic degradation), therefore increasing matrix porosity and enabling cell migration and cell-cell interactions.²⁹ Natural hydrogels (e.g. collagen or fibrin) are normally enzymatically degradable, while the synthetic hydrogels typically degrade through hydrolytically unstable chemical bonds. A lack of control over degradation rate of above approaches has motivated novel strategies. Degradability can be achieved by introducing biodegradable sequences, like peptides that can be enzymatically cleaved by metalloproteases.

For example, the matrix metalloproteinases (MMP)-cleavable peptide sequences (e.g., CGPQGIWGQC and GCRDVPMSMRGGDRCG (VPM)) are widely used as crosslinkers to fabricate enzymatically degradable hydrogels, and have been proved to play a key role in cell migration and ECM remodeling.³⁰

³¹ Side functional groups of those peptide sequences (e.g. thiol groups) also capable for crosslinking via multi-type of chemistry approach. In addition, hydrogels can be designed with degradable sites by hydrolysis or by using reversible reactions (e.g. retro Michael-type cleavage and retro Diels–Alder cycloreversion) or including photolytic sites (**Figure 1.4**). The modulation of hydrogel degradation can lead to changes in stiffness, porosity, swelling ratio and structural integrity. Leach et al. reported hydrolytically degradable PEG hydrogel using PEG vinyl sulfone (PEG-VS) and PEG-diester-dithiol. The hydrolysis rate varied from hours to days by changing the crosslinker's molecular weight (3.4-8 kDa), varying the number of methylene moieties between the ester and the thiol group of the crosslinker and polymer concentration (5-15% w/v).²⁹ Lueckgen et al. reported enzymatically degradable alginate hydrogels using UV-initiated thiol-ene chemistry between alginate and enzymatically-degradable peptide crosslinkers (VPM or VpMSmRGG). The degradation kinetics was varied by using different enzymatically-degradable peptide sequence and the effect on cell spreading was studied.³² Baldwin et al. reported degradable hydrogels by using reversible Michael-type addition reactions based on the reduction of arylthioether-succinimide adducts by glutathione (GSH). The degradation rate varied depending on the structure of mercaptoacid under a reducing environment.³³ Recently, photodegradation pathway has attracted a great attention since the degradation can be spatiotemporally controlled. Anseth et al. reported photodegradable PEG hydrogels by using acrylated *o*-nitrobenzyl (*o*NB) based crosslinker. These hydrogels can be degraded upon exposure at $\lambda = 365$ nm, 405 nm and 740 nm.³⁴

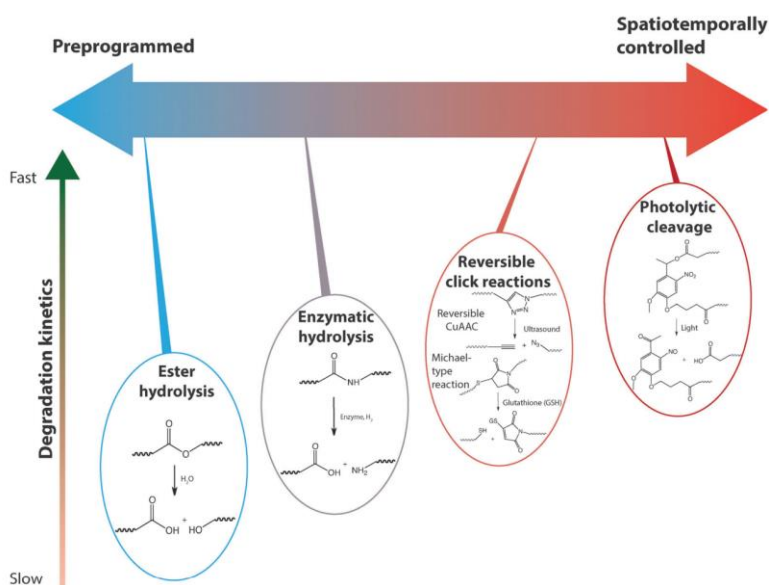


Figure 1.4 Modes of hydrogel degradation by hydrolysis, enzymolysis, reversible click reactions or photolytic cleavage. Republished with permission from Royal Society of Chemistry.¹²

1.1.2 PEG hydrogels for cell encapsulation

PEG synthesis and derivatization

Poly(ethylene glycol)(PEG) (also known as poly(oxyethylene) or poly(ethylene oxide) (PEO)) is a synthetic polymer that contains oxyethylene repeat unit ($-\text{O}-\text{CH}_2-\text{CH}_2-$) and have proven useful as 3D

Chapter 1

scaffold to mimic ECM microenvironments for a variety of biomedical applications, such as drug delivery and tissue engineering. PEG hydrogels present high biocompatibility, non-toxicity, high swelling capacity, tunable mechanical and chemical properties and are approved to be used in several clinical applications.³⁵

PEG can be synthesized by a ring-opening polymerization of ethylene oxide with a broad range of molecular weights from 0.3 kDa to 10,000 kDa. It can be functionalized by reacting the terminal hydroxyl groups to create telechelic PEG polymers with end-functionalities like thiol (-SH), maleimide (-Mal), hydroxysuccinimide ester (-NHS ester), amine (-NH₂), azide (-N₃), carboxylic acid (-COOH), norbornenes, alkynes, acrylates/methacrylate, vinyl sulfone or cyclooctyne. This offers chemical versatility for crosslinking and gel formation (**Figure 1.5**). For example, PEG hydrogels can be obtained by crosslinking reactions between -SH and -Mal or vinyl sulfone via Michael-type chemistry;^{36, 37} acrylate/methacrylate can photocrosslink via free-radical polymerization;³⁸ thiol and norbornene can crosslink via photoclick reaction.³⁹ Moreover, heterofunctional PEGs can also be synthesized under controlled conditions. PEG precursor molecules are also commercially available in different geometries such as linear, branched, Y-shaped, star shape or comb shape geometries. Among these, Star PEGs are branched polymers with several linear chains (>3) linked to a central core. Star PEGs with controlled molecular architecture, molar mass and high mono-dispersity are advantageous to develop hydrogels with controlled architecture. Star PEG macromolecules have a small hydrodynamic radius, a low degree of dynamic entanglement and a high density of functional groups. This results in low intrinsic viscosity of hydrogel precursor solutions and high rate constant of gel formation compared to linear analogues of the same molecular weight, which is an advantageous property for cell encapsulation since they allow mixing at low shear forces.⁴⁰ Star PEGs with a range of molar mass from 5 kDa-40 kDa are commonly used as hydrogel backbone for cell encapsulation and lead to hydrogel networks with typical mesh sizes between 40 and 200 Å⁴¹ and Young's Modulus up to elasticities of 30 kPa.^{16, 42}

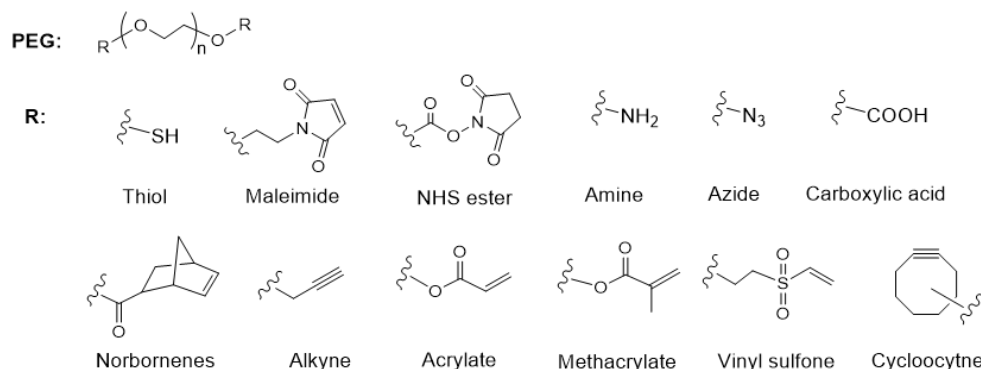


Figure 1.5 Commercial PEG polymers with different end-functional groups.

1.1.3 Crosslinking reactions used for cell encapsulation

Different physical and chemical crosslinking approaches have been used for preparing biomimetic ECM scaffolds. Physically crosslinked hydrogels are formed by non-covalent interactions, such as hydrogen bonding, ionic interactions, host-guest interactions, hydrophobic interactions, or peptide

assembly. The advantage of physically crosslinked hydrogels is the high biocompatibility due to the absence of reactive chemical crosslinking agents. However, physical gels have weak mechanical properties. In chemically crosslinked hydrogels the crosslinking density and the final mechanical properties of the hydrogel are defined by tuning the composition of the reactive precursors. Since polymer chains in the network are connected by covalent bonds, chemically crosslinked hydrogels are more stable than physical hydrogels.

In order to be suitable for hydrogel formation in the presence of cells, the ideal crosslinking reaction needs to work at physiological conditions, i.e. at pH (~6-8), temperature (20-40°C) and in buffer of adequate ionic strength (Typically 10-50 mM)⁴³. The kinetics of the crosslinking reaction determines the gelation rate. In general coupling reactions with a second-order reaction rate constant between 10^{-2} to $10^2 \text{ M}^{-1} \text{ s}^{-1}$ have been demonstrated to lead to homogeneous hydrogels with uniform cell distribution. **Table 1.1** summarizes the most common chemical approaches for gelation. The following sections shortly introduce the general features of each reaction.

Table 1.1 Comparison of the different commonly used chemical crosslinking coupling reactions for hydrogel formation in the presence of living cells

Crosslinking chemistry	Chemical reactions	Conditions	Gelation time	Features
Free-radical acrylic polymerization ⁴⁴		Initiator	Seconds-mins	High conversion (+) Highly sensitive to oxygen (-) Inhomogeneous structure (-)
Radical thiol-ene: photocrosslinking ⁴⁵		$h\nu$ Photoinitiator or pH 6-8	seconds-hours	Spatiotemporal control (+) UV irradiation (-) Radical generation (-)
SPAAC ^{46, 47}		pH 7.4	seconds-hours	Bioorthogonal (+) Biocompatibility (+) Homogeneous structure (+)
Thiol-mediated Michael additions ⁴⁸⁻⁵²		pH 6-8	seconds-mins	Kinetics: too slow or too fast (-)
Amine-NHS ester coupling ⁵³⁻⁵⁶		pH 6.6-9	Seconds-mins	Highly pH dependent (-) Water sensitive precursor (-)
Schiff-base crosslinking ^{57, 58}		pH 3-10	seconds-hours	Benign byproduct (+) Biocompatibility (+) Potential toxicity (-) pH sensitivity of Schiff base linkage (-) Reversibility (\pm)
Thiol-methylsulfone (MS) chemistry ^{59, 60}		pH 6-9	seconds-hours	pH dependent (+) Efficient and selective (+) Biocompatibility (+) Homogeneous structure (+)

Chapter 1

Free-radical polymerization of acrylic groups

Free-radical polymerization of acrylate functionalized polymer chains involves a chain-growth polymerization mechanism which can be initiated by free radicals formed by light, heat, pH or redox initiators. These radicals then react with vinyl monomers to generate a crosslinked network. Ammonium persulfate (APS)^{61, 62} is the most common initiator used for cell applications. Hydrogels prepared via radical polymerization present properties that depend on the concentrations of initiator and precursor polymers. Free-radical acrylic polymerizations are sensitive to oxygen, since the scavenging of the radical by oxygen is significantly faster than the rate constants of initiating and propagating radical species ($\sim 5 \times 10^8$ and $10^9 \text{ L mol}^{-1} \text{ s}^{-1}$, respectively)^{63, 64} Therefore, a degassing step of polymer precursor solutions is typically needed.

Acrylate polymerization is widely used to prepare hydrogels, and occurs at high conversion, mild crosslinking conditions and is tolerant to diverse functionalities (e.g. allyl, amino, epoxy, hydroxy and vinyl group).⁴⁴ However, the free radicals can oxidize proteins and damage cells through oxidative stress, therefore the amount of radicals should be controlled. Temenoff et al. studied the cytotoxicity of two different radical initiator (APS and sodium persulfate (NaPS)) with three reducing agents derived from ascorbic acid (AA, sodium ascorbate (Asc), and magnesium ascorbate 2-phosphate (Asc-2)) for oligo(poly(ethylene glycol) fumarate) (OPF)-based hydrogel system for MSCs. High MSC viability (> 90%) was demonstrated at low concentrations of the initiator combinations (10 mM), while a significant reduced viability was observed at high concentrations (100 mM).⁶⁵ Moreover, hydrogels may display inhomogeneous structure due to the heterogeneous nature of polymerization mechanism. Acrylated polymers such as poly(methyl methacrylate) (PMMA), poly(acrylamide) (PAAM), methacrylated hyaluronic acid (MeHA) and poly(ethylene glycol) diacrylate (PEGDA) have been used to prepare hydrogels via radical polymerization. The possibility to use radical photopolymerization has great advantages to control the polymerization in time and space. For example, Schesny et al. demonstrated a biocompatible implant using photo-crosslinked PEGDA scaffold which can promote bone marrow-derived stem cell migration and angiogenesis into cardiovascular cells via post myocardial infarction treatment.⁶⁶

Free-radical thiol-ene photopolymerization

Photocrosslinking of radical mediated thiol-ene chemistry is also a key approach for constructing platforms for cellular applications as this chemistry can be performed under physiological conditions under light illumination. Photocrosslinking can be controlled in a user-defined manner (spatial and temporal) by adjusting the initiator concentration, light wavelength and light intensity, especially for 3D matrix. Irgacure-2959,⁶⁷ eosin-Y⁶⁸ and lithium acylphosphinate (LAP)⁶⁹ are the most common used biocompatible photoinitiators. A cell compatible dose of light (e.g., $\sim 5\text{-}10 \text{ mW cm}^{-2}$ at 365 nm within 2-5 minutes) is needed for reducing phototoxicity.⁷⁰ Despite current development, approaches for polymerization using light of longer wavelengths (i.e. red and near infrared) to achieve deeper penetration and lower light intensity to minimize photodamage need to be developed. Free-radical thiol-ene photopolymerization follows a two-steps mechanism: i) an initial addition of thiyl radical to

an alkene (“ene”) functional group to form a carbon-centered radical followed by a subsequent hydrogen abstraction with a thiol group to give a thiyl radical, and ii) the reaction terminated by the radical and radical coupling.⁷¹ A photoinitiator is needed to generate radicals and initiate the crosslinking between -SH groups and alkene groups. Compared to the traditional free-radical crosslinking, radical thiol-ene crosslinking is not oxygen sensitive which can contribute to a higher degree of functional group conversion and a utilization of lower initiator concentration, as well as eliminating the degassing of precursor solutions. For example, McGann et al. reported a successful preparation of resilin-like polypeptide-PEG hydrogels via photoinitiated thiol-ene crosslinking between thiol functionalized star PEG and norbornene functionalized resilin-like polypeptides (RLPs). Hydrogel was formed in seconds using low cytocompatible doses (5 mW cm⁻² at 365 nm) with LAP photoinitiator (2.3 mM). Human mesenchymal stem cells (hMSC) were encapsulated within the hydrogels and presented high viability up to 28 days of culture, indicating the cytocompatibility of illumination dosage and crosslinking chemistry.⁴⁵

Strain-promoted azide-alkyne cycloaddition (SPAAC)

The strain-promoted azide-alkyne cycloaddition (SPAAC) reaction is a type of click reaction with moderate second order reaction rate constants ($\sim 1\text{--}60\text{ M}^{-1}\text{ s}^{-1}$) under aqueous conditions. As no catalyst is needed, this coupling was used to overcome toxicity issues of copper-catalyzed azide-alkyne cycloaddition (CuAAC). SPAAC click chemistry allows bioorthogonal conjugation under physiological conditions with high conversion and efficiency, and has been used in a broad of applications, such as cell encapsulation and drug delivery.⁷² Dibenzocyclooctyne (DBCO) (DBCO and azides, $k_2=1\text{--}60\text{ M}^{-1}\text{ s}^{-1}$) and bicyclononyne (BCN) (BCN and azides, $k_2=0.05\text{--}1\text{ M}^{-1}\text{ s}^{-1}$) are the most representative alkynes used for SPAAC.⁴⁶ Zhan et al. compared the bioorthogonality of different hydrogels prepared from star PEG-BCN or PEG-DBCO with star PEG-N₃ by encapsulating human mesenchymal stem cells (HMSCs) in the hydrogels in presence of azide-functionalized matrix metalloproteinases cleavable peptide (MMPcp-) and RGDS-peptide motif. DBCO/N₃ hydrogels showed faster gelation kinetics (gelation time \sim in the orders of minutes), thus higher homogeneity was achieved which was indicated by the homogeneous distribution of cells through the hydrogels, while cells sedimented to the bottom in BCN/N₃ hydrogels (gelation time ~ 1 hour). Moreover, HMSCs in these peptide-rich BCN/N₃ and DBCO/N₃ hydrogels (containing both MMPcp and RGDS motifs) were still viable after 5 days post-encapsulation.⁴⁷

Thiol-mediated Michael additions

Michael addition is defined as a nucleophilic addition of Michael donor (e.g., thiols) to an α,β -unsaturated carbonyl (Michael acceptor) resulting in the generation of C-C, C-N, C-S, C-O, and other C-X bonds with high conversion and high efficiency, including carbon-Michael reactions,⁴⁹ oxa-Michael addition,^{48, 49} aza-Michael addition,⁵⁰ and the thiol-Michael addition.^{51, 52} Among these, thiol-Michael addition attracts the most interest and has been extensively studied for developing biomaterials for cell studies. The thiol group presents high nucleophilicity under physiological conditions (partially

Chapter 1

deprotonated as thiolate at pH 7.4) thus offering the advantage of reacting under mild conditions with a broad range of compounds, however it might also offer the disadvantage of low hydrogel uniformity due to the high reactivity of thiol groups. For example, Phelps et al. studied the gelation kinetics and network structure of thiol-maleimide (Mal) and thiol-vinylsulfone (VS) PEG hydrogels. Mal groups present higher electrophilicity than VS groups due to the high ring strain imposed by the alkene bond, which can lead to a higher reaction rate. Hydrogels were prepared by crosslinking between star PEG (PEG-4MAL or PEG-4VS) and thiol-containing adhesive peptide GRGDSPC. Murine C2C12 myoblast cells were encapsulated in the PEG hydrogels and RGD peptide (2.0 mM) was also incorporated to support 3D cell adhesion and spreading. A fast-crosslinking kinetics (gelation time: 1–5 min) was obtained for PEG-4MAL hydrogels in PBS with triethanolamine (TEA) (4 mM, pH 7.4) which allowed a uniform distribution of cells throughout the hydrogels. Moreover, C2C12 cells presented high metabolic activities and maintained cell viability at 3 days in PEG-4MAL hydrogels after encapsulation. In comparison, a slower crosslinking kinetics (gelation time: ~30–60 min) was obtained for PEG-4VS hydrogels in PBS with higher TEA concentration (400 mM, pH 7.4), resulting in negative effects (e.g. lower metabolic activity and viability) on cells assayed by MTS assay.⁷³ Besides the differences observed in the crosslinking kinetics of MAL vs. VS electrophiles, thiol-VS gels were reported to present higher hydrolytic stability compared to thiol-Mal hydrogels under same conditions, which is advantageous for long term cell experiments that require longer lasting materials.⁵⁹

Amine-NHS ester coupling

The amine-NHS ester coupling reaction is a useful strategy that has also been applied for hydrogel formation and bioconjugation in aqueous media. Amine-NHS ester reactions involve the conjugation of NHS ester with primary amines to form amide bonds with release of hydroxysuccinimide under close-to-physiological conditions (pH 6.6 to 9). This coupling chemistry is strongly pH-dependent: i) at low pH (lower than the amine pKa), amine group is protonated and becomes less nucleophilic, therefore cannot react efficiently with activated NHS ester group.⁵³ ii) at high pH (typically higher than physiological pH), NHS ester hydrolyzes faster (e.g. the hydrolysis half-life for NHS-ester at pH 7.0 and 0°C is 4 to 5 h, while at pH 8.6 and 4°C is 10 min).⁵⁴ The optimal pH for amine-NHS ester coupling is near physiological region (pH~7.5). Furthermore, the ionic strength of the precursor solutions was also reported to have a big impact on the coupling reaction. For example, Yanagawa et al. used star PEG-amino and star PEG-NHS crosslinker to prepare hydrogels in high concentrated buffer conditions (10×10^{-3} M phthalic acid buffer (pH 4.0) with 140×10^{-3} M NaCl and 1:1 (v/v) mixture of PBS and 0.3 M 4-(2-hydroxyethyl)-1-piperazineethanesulfonic acid (HEPES) buffer (pH 7.0)). Gelation kinetics was controlled by adjusting pH from 6.6 to 7 and the gelation time varied from 3 min to 30 s. However, human umbilical vein endothelial cells (HUVECs) were only seeded onto the hydrogel surface instead of encapsulated into hydrogels due to the high concentrated buffer conditions which can be toxic to cells due to their high ionic strength.⁵⁵ Amine-NHS ester coupling reaction was also reported to take place in PBS buffer.⁵⁶ However, the low reproducibility and the difficulties to incorporate biologands limit further applications, such as cell encapsulation.

Schiff-base crosslinking

Schiff base crosslinking is an important family of click chemistry and involves the formation of imine bonds via reaction of aldehydes or ketones with amines or other amine derivatives (like hydrazide or hydroxylamine groups) to form hydrogel networks.⁵⁷ The ideal pH for Schiff base crosslinking is between pH 3-7 (typically 4.5) owing to the fast attack of amine group on the carbonyl. However, this pH is too acidic for maintaining high cell viability. These crosslinking reactions can also be performed under physiological conditions which allows the applications in cell encapsulation and drug delivery.⁵⁸ For example, Cao et al. prepared an injectable hydrogel from amino-functionalized chitosan and aldehyde-functionalized PEG via Schiff-base crosslinking chemistry under physiological conditions (in PBS buffer, 37°C). A short gelation time \sim 1-3 min was obtained by adjusting the concentration of PEG. Moreover, the hydrogels presented low degradation profile for long term both in vitro and in vivo microenvironments (up to 3 months). The 3D encapsulation of chondrocytes within hydrogels was reported and encapsulated chondrocytes were found to maintain a high viability and a round cell morphology, indicating the compatibility of Schiff-base crosslinking for constructing platforms for 3D cell studies.⁷⁴ Notably, Schiff base crosslinking is a reversible reaction under physiological conditions which can decrease the hydrogel stability due to the accelerated hydrolysis.

Thiol-methylsulfone (MS) chemistry

Thiol-MS coupling chemistry was reported by del Campo's group as an alternative chemistry to the thiol-Mal or thiol-VS coupling chemistries, Thiol-MS-based coupling reactions present an intermediate rate between thiol-Mal and thiol-VS chemistry, with gelation times between seconds to minutes.⁵⁹ Thiol groups can effectively react with heteroaromatic rings carrying methylsulfone electrophiles (**Figure 1.6**) under physiological conditions via a nucleophilic aromatic substitution (S_NAr) mechanism with the formation of stable, irreversible thiol-ether adducts and release of methanesulfinate as leaving group.⁶⁰ This coupling chemistry was demonstrated for a variety of applications, including selective cysteine conjugation,⁶⁰ thiol-blocking⁷⁵ and hydrogel formation for 2D and 3D cell culture.⁵⁹ ⁷⁶ A high reaction conversion, high chemoselectivity, moderate kinetics and high stability of formed adducts were observed, and the reaction kinetics could be regulated by adjusting pH and the electron-deficient character of heteroaromatic sulfone compounds. Paez et al. first used thiol-MS coupling chemistry to prepare hydrogels for 3D cell encapsulation by using star PEG-oxadiazole methylsulfone (star PEG-Ox-MS) and star PEG-SH. Compared with thiol-Mal and thiol-VS chemistry, this thiol-MS coupling allows an intermediate gelation kinetics and the reaction rate can be controlled by pH adjustment in the range 6.6 to 8, to obtain cell laden hydrogels with homogeneous distribution of cells. Fibroblasts and HUVECs were encapsulated in the hydrogels and cells showed high viability (>90%) after 6 days encapsulation which indicated the good cytocompatibility of resulting hydrogels.⁵⁹ More recently, the gelation kinetics of PEG hydrogels derived from star PEG-SH and star PEG-MS with different heteroaromatic sulfones (phenyl-tetrazole (Tz), benzothiazole (Bt), and oxadiazole (Ox) sulfones) were compared. Hydrogels were formed from few seconds to hours by varying the pH (8.0 to 6.6) and by using different MS heteroaryl units (i.e. relative gelation speed was thiol-Mal > Ox > Tz >

Chapter 1

Bt > thiol-VS). Compared with Ox- or Bt-based system, the most recent MS substrate, Tz-based, was demonstrated as a most promising candidate since the derived hydrogels showed higher hydrolytic stability during cell culture. Moreover, hydrogels derived from Tz-based MS substrate also showed high cytocompatibility and enabled homogeneous distribution of cells.¹⁸

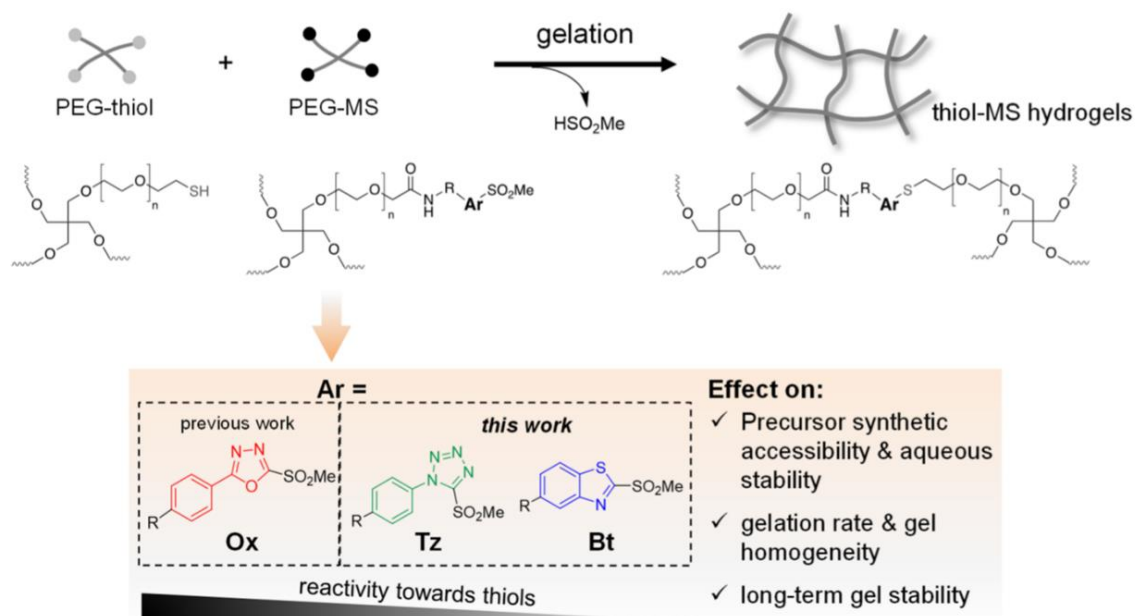


Figure 1.6 Thiol-methylsulfone coupling chemistry. Republished with permission from American Chemical Society.¹⁸

1.2 Light-regulated hydrogels for cell culture

Dynamic hydrogels are responsive materials designed to mimic the dynamic nature of the natural ECM. Different external stimuli (e.g. pH,⁷⁷ temperature,⁷⁸ mechanical force,⁷⁹ electrical signals,⁸⁰ light,⁸¹ et al.) have been used to dynamically manipulate the properties of hydrogels for cell encapsulation. Among these stimuli, light shows advantages, as it is readily available and can be easily dosed. More importantly, high spatial resolution and real-time manipulation of light enables to perturb the specific cellular or molecular interactions in 3D, therefore allowing the study of individual process of cells in a temporal and spatially controlled manner.

Light-responsive hydrogels have been used to generate 3D cell culture scaffolds with properties that can be modulated in space and time and guide cellular responses (e.g. cell migration,^{34, 82, 83} cell differentiation³⁴) on demand.⁸⁴ Light enables remote manipulation of hydrogels at any time point in both 2D and 3D. In most light-responsive systems for dynamic cell culture, photocleavable protecting groups (PPGs) are used as photoresponsive unit. When intercalated into the polymer backbone, PPGs can be used to dynamically control the mechanical properties of the hydrogel. Upon illumination, photodegradable hydrogels undergo a photodegradation process, which has a direct consequence on the mechanical properties and mesh size of the hydrogel, which might affect the behavior of cells. Apart from photodegradation, PPGs have been used to temporally block the bioactivity of biomolecules incorporated into the hydrogel. Photoactivation of the biochemical ligands within

hydrogels has been used to regulate adhesive cues or and to release cargos, and to control specific cell-material interactions. Importantly, light dosage needs to be considered in order to avoid photodamage to the cells. Typical light dosage at 365 nm light, Irradiance = 5–20 mW cm⁻², t = 2–20 min is total dose 5–10 J cm⁻²;^{85, 86} at 420 nm, irradiance 1.55 mW cm⁻², t = 6–12 h gives total dose 29–63 J cm⁻²⁸⁷ and at NIR light (e.g. 740-900 nm, 20-100 mW)^{88, 89} have been used for cell studies.

Conventionally, photoactivation of PPGs-based hydrogels is induced by one-photon excitation in the VIS range. Phototoxicity and low penetration are drawbacks of these illumination conditions. Two photon (2P) excitation involving NIR light (~700-1000 nm) has attracted considerable interest as an alternative to 1P processes. In 2P excitation process, the molecule is excited upon the simultaneous incidence of two photons of approximately half energy than that required for each photon compared to 1P process, thus 2P ultimately happens at longer wavelengths. Moreover, longer wavelength photons allow deeper penetration (~5 mm) in a 3D construct. 2P excitation offers high 3D spatial resolution (~0.1 μm³)^{90, 91} because the 2P excitation is proportional to the square of the excitation intensity, thus the 2P excitation is strictly confined within the focus region due to its nonlinear feature.⁹² As showed in **Figure 1.7**.

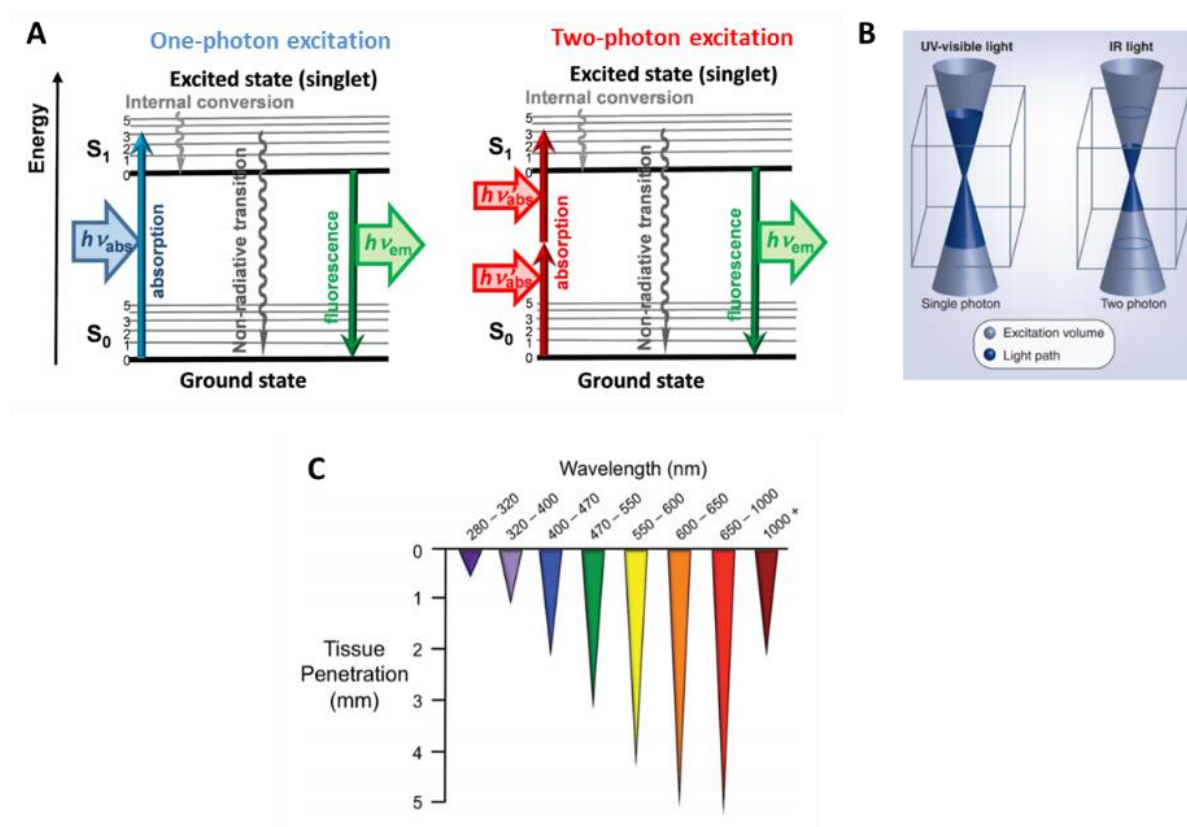


Figure 1.7. Comparison of 1P and 2P excitation processes. **(A)** Jablonski-type diagram of 1P and 2P excitation. Adapted with permission from Beilstein Journal of Organic Chemistry.⁹² **(B)** Spatial resolution achieved in 1P and 2P excitation. Adapted with permission from Future Medical Chemistry.⁹³ **(C)** Light penetration depth in tissue as function of wavelength. Adapted from ref.⁹⁴

Chapter 1

1.2.1 Light-responsive hydrogels with photoregulated degradation

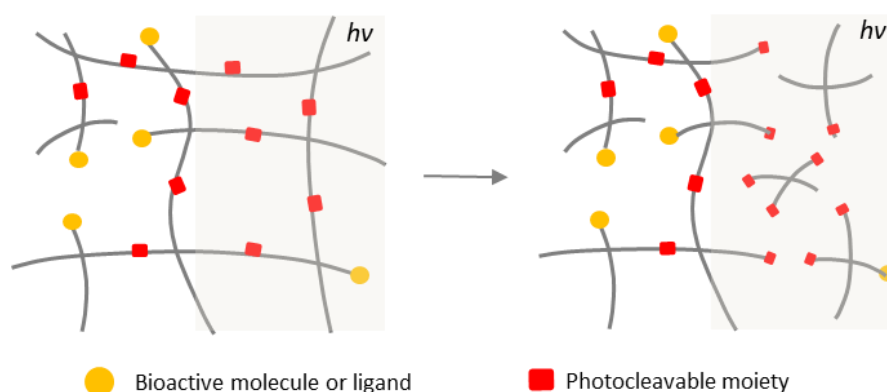


Figure 1.8. Schematics of photo-cleavage chemistry for controlled regulation of hydrogel degradation.

Hydrogel degradation in most examples of photodegradable hydrogels arises from photocleavage of PPGs incorporated in the hydrogel backbone, as shown in **Figure 1.8**. *o*-nitrobenzyl (*o*NB) derivatives are the most widely used PPGs due to their clean photolysis mechanism and commercial availability of suitable precursor reagents. Kloxin et al reported PEG-based photodegradable hydrogels via radical polymerization of a diacrylated *o*NB-based photocleavable crosslinker with PEG monoacrylate (PEGA) in PBS buffer. Precise control of degradation degree was achieved by illumination at 365 nm and 405 nm, and also using 2P excitation (740 nm). The bulk photodegradation of hydrogels was performed by flood irradiation at 365 nm and 405 nm and followed by the decrease of storage modulus (G') from photo rheology experiments, the time scale of photolabile group degradation time in hydrogels were observed in ~ 140 s, ~ 280 s and ~ 930 s with irradiation intensity and wavelength of 365 nm at 20 mW cm^{-2} , 365 nm at 10 mW cm^{-2} and 405 nm at 25 mW cm^{-2} respectively. hMSCs were encapsulated in the hydrogels and exhibited a rounded morphology and high viability. Upon UV exposure, the material was softened which consequently affected cell behavior, for example, cell migration and chondrogenic differentiation were also demonstrated within these photodegradable hydrogels (**Figure 1.9**).³⁴

In a follow-up work (**Figure 1.10**), the photodegradation approach was combined with an orthogonal photoconjugation step. A PEG hydrogel was prepared via the SPAAC reaction between star PEG tetracyclooctyne and photocleavable bis N_3 polypeptide bearing an intercalated *o*NB group. In a second step, thiol functionalized cell adhesive peptide RGD was incorporated to the network by thiol-ene photoreaction using eosin Y as photoinitiator and visible light irradiation (490–650 nm, 10 mW cm^{-2} , 0.5–2 min). At this wavelength range, the *o*NB group is stable. Photodegradation of the hydrogel was possible by subsequent illumination at 365 nm or 740 nm. A cell-laden (3T3 fibroblasts) fibrin clot was encapsulated within the hydrogels to demonstrate the wavelength-dependent, orthogonal control of cellular response. Adhesive RGD peptide sequence was conjugated into certain area of hydrogels in presence of cells and these were found to migrate into the degraded channels.⁹⁵

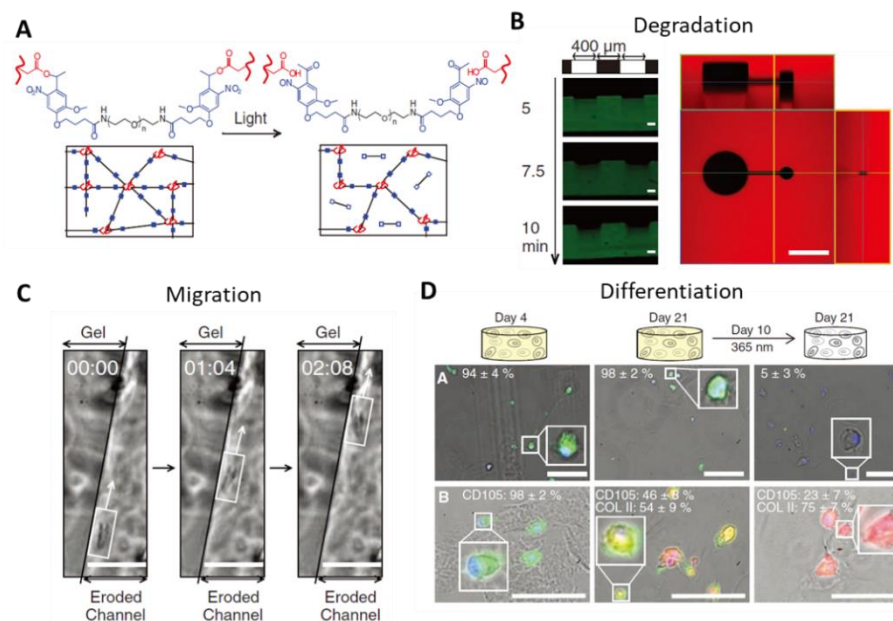


Figure 1.9. Photodegradable hydrogels from diacrylated oNB-based photocleavable crosslinker. **(A)** Hydrogel formation was done via free radical polymerization followed by photodegradation. **(B)** Surface erosion and 3D patterning upon exposure to 320-500 nm or 740 nm light. Scale bars= 100 μm . **(C)** Cell migration along the eroded channels. Scale bars= 50 μm . **(D)** Chondrogenic differentiation of hMSCs. Scale bars= 100 μm . Adapted with permission from Journal of Science.³⁴

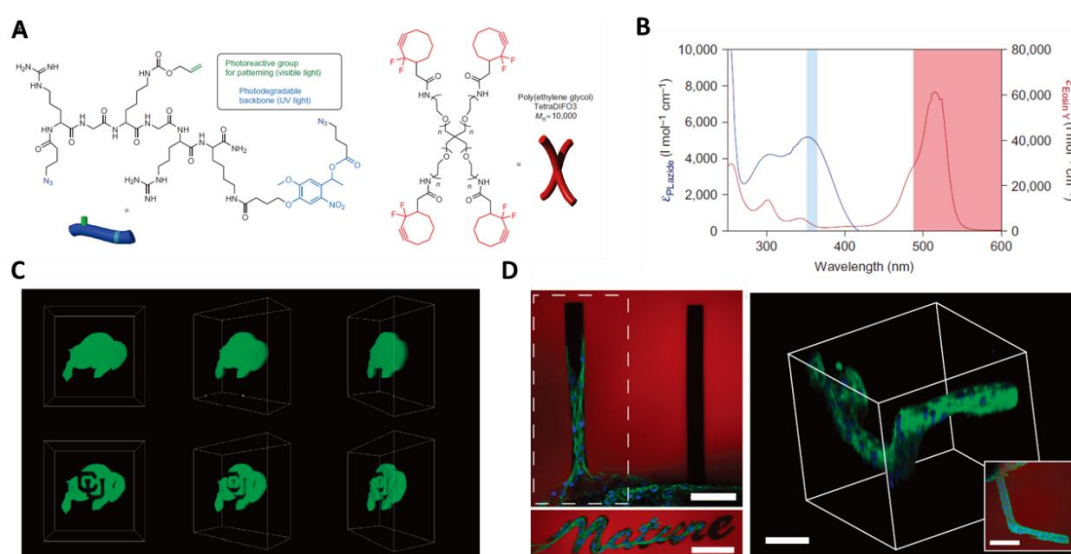


Figure 1.10. Orthogonal photoconjugation and photodegradation of oNB-based photodegradable hydrogels **(A)** Hydrogel formation via SPAAC. **(B)** UV spectra of the photoinitiator and the photolabile oNB group. **(C)** Orthogonality of photocoupling and photodegradation within hydrogels with subsequent illumination at different time point. Scale bars= 50 μm . **(D)** Directed cell migration within 3D patterned hydrogel. Scale bars = 100 μm . Adapted with permission from Journal of Nature chemistry.⁹⁵

Other oNB photodegradable hydrogels loaded with upconverting nanoparticles (UCNPs) were degraded using near infrared light (NIR). The UCNPs mediate conversion of NIR light into UV light and

Chapter 1

enable UV-light-induced photolysis of oNB functionalities using light of longer wavelength.⁹⁶ So far, no cell encapsulation was reported in photodegradable hydrogels in presence of UNCPS.

Coumarins are alternative chromophores to oNB group that present higher photoefficiency, moderate photostability, red-shifted absorption and exhibit weak fluorescence after photolysis. Only a few coumarin-based hydrogels have been reported. Azagarsamy et al. reported the synthesis of a hetero-functional coumarin with amine and azide groups and subsequently attached into star PEG backbone to yield star PEG tetra-azide. The hydrogel was prepared from star PEG tetra-alkyne (5 kDa) and star PEG tetra-azide (5 kDa) via CuAAC mechanism. Photodegradation kinetics was monitored by in situ photorheology. Upon light exposure (365 or 405 nm: 40, 10.4, 4.0, and 1.4 mW cm⁻²), nearly 2 orders of magnitude of degradation rate constant could be achieved from 1.0×10^{-4} s⁻¹ under exposure to 1.4 mW cm⁻² 405 nm light to 79×10^{-4} s⁻¹ under 10.4 mW cm⁻² 365 nm light. Hydrogel degradation was also demonstrated under 2P excitation (740 nm, 800 nm, 860 nm and 900 nm),⁹⁷ however, no cell studies were performed, probably due to toxicity of copper catalyst used for the CuAAC crosslinking. In another work (**Figure 1.11**), Lux et al. reported coumarin-based photodegradable polyacrylamide (PAA) hydrogels. Instead of serving as photodegradable crosslinker, bromohydroxycoumarin (Bhc) was used to block the -NH₂ group of ornithine in order to break ornithine lactamization under biologically relevant conditions. After UV or NIR light exposure, PAA hydrogel degraded due to the cleavage of Bhc through intramolecular cyclization. A high photoefficiency under UV exposure was demonstrated since only a very low irradiation dose (365 nm, 1 mW cm⁻²) was needed. These hydrogels were used to encapsulate small hydrophilic payloads such as Fluo-Bovine Serum Albumin (BSA). Murine mesenchymal stem cells expressing green fluorescent protein (GFP-mMSCs) were also successfully encapsulated in the hydrogels. Photorelease of mMSCs was also demonstrated upon illumination (365 nm, 1 mW cm⁻²). However, no cell viability studies were presented.⁹⁸

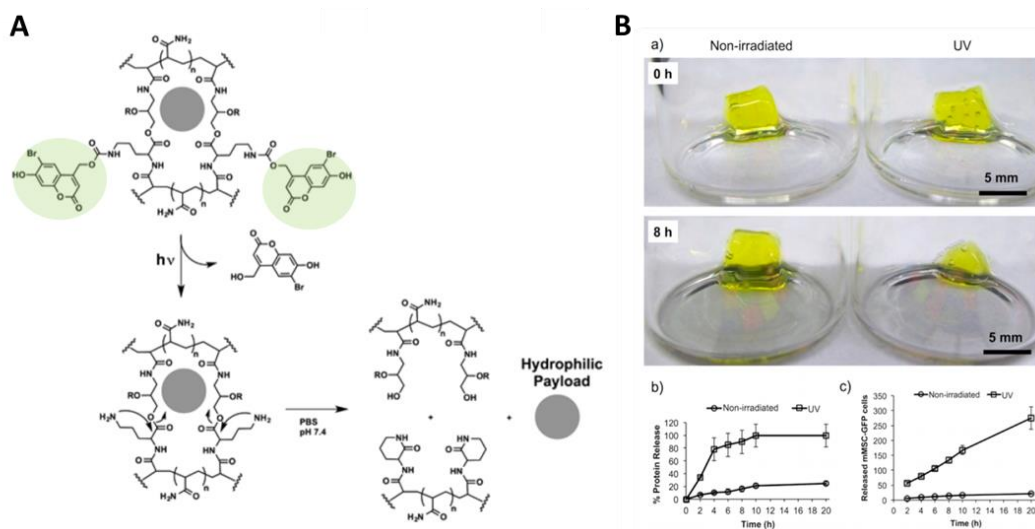


Figure 1.11. Coumarin-based photodegradable hydrogels (**A**) Light induced photodegradation PAA hydrogels due to the cleavage of Bhc through intramolecular cyclization. (**B**) Payload release from hydrogels under UV light exposure. Irradiation dose: 365 nm, 15 min, 1 mW·cm⁻². Adapted with permission from American Chemical Society.⁹⁸

Photocleavable bonds based on the allyl sulfide/thiol exchange have also been used for the design of photodegradable hydrogels via reversible addition fragmentation chain transfer (AFCT) mechanism. Brown et.al synthesized photodegradable hydrogels between star PEG-DBCO and bifunctional azide crosslinker containing allyl sulfide bonds via SPAAC mechanism (**Figure 1.12**). Photoinitiator (LAP) and a monofunctional thiol molecule were used to induce the generation of thiyl radicals, which attack the allyl group and results in fragmented macromolecules upon UV light exposure, thus leading to decrosslinking. Hydrogel can be degraded in 1 min under cytocompatible conditions (4 mM LAP, 25 mM mPEG-SH, 10 mW cm⁻² at 365 nm light) and demonstrated good cytocompatibility for cell encapsulation and subsequent release.⁹⁹

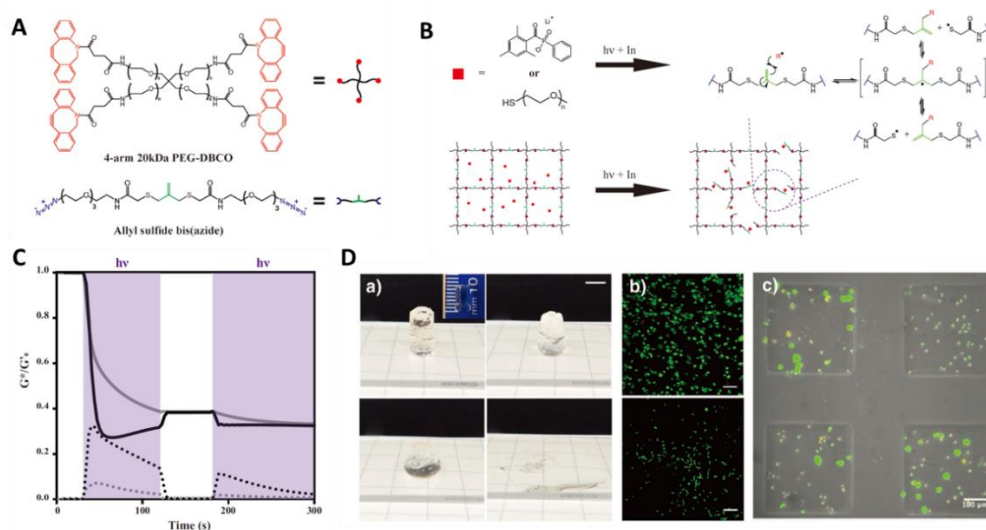


Figure 1.12. Photodegradation of allyl sulfide bond-based hydrogels via AFCT mechanism. **(A)** Chemical structures of star PEG-DBCO and bifunctional azide terminated crosslinker containing the allyl sulfide functionality. **(B)** Light induced photodegradation in presence of an initiator and free -SH molecules. **(C)** photo degradation followed by in situ rheology. Irradiation dose: 365 nm, 10 mW·cm⁻². **(D)** Bulk scale erosion and cytocompatible cell encapsulation and release. Scale bars: 100 μm. Adapted with permission from Wiley.⁹⁹

1.2.2 Hydrogels with photoactivatable biochemical signals

PPGs have been used to block the active site of biomolecules to temporarily inhibit their bioactivity, and later activation upon light exposure, as depicted in **Figure 1.13**.

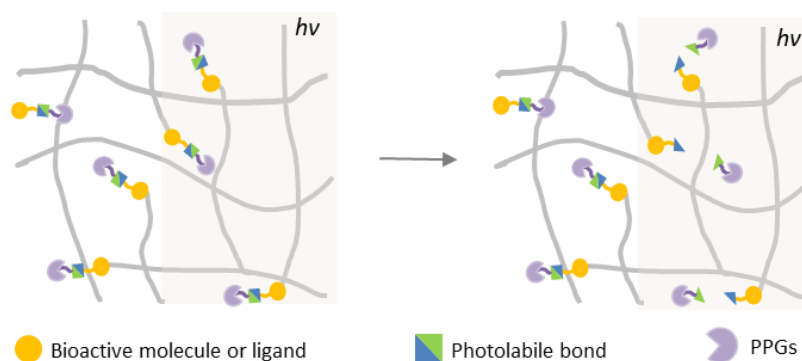


Figure 1.13. Schematics of photo-cleavage chemistry for controlled regulation of biochemical signals in hydrogels.

Chapter 1

Peptidomimetics of cell adhesive sites of matrix proteins are widely used to biofunctionalize hydrogels for cell culture. These can be synthesized with reduced synthetic effort and ease of purification compared to their complex protein counterparts.¹⁰⁰ Lee et.al reported implanted biomaterials based on PEG hydrogels with a photoprotected cyclic RGDfK peptide. Upon UV light illumination, the chromophore was cleaved and RGD peptide was exposed. This photoactivatable material was demonstrated in vivo useful for regulating cell adhesion and vascularization of biomaterials. Moreover, the chronic inflammation and fibrosis in vivo were significantly reduced with a delayed presentation of RGD peptide on implanted biomaterials, courtesy of the temporal controlled conferred by this approach. However, the spatial resolution and depth of penetration (1 mm) is still limited in terms of using UV light (**Figure 1.14**).¹⁰¹ Recently, biomaterials that present RGD motif with different chromophores were reported, to support spatiotemporal control over cell-materials interactions.¹⁰² Lin et.al demonstrated a cell-material interfacing system which can undergo a structural transition to expose a cell-penetrating peptide upon 1P or 2P excitation, thus trigger the uptake of different cargos loaded on the cell-penetrating peptide.¹⁰³

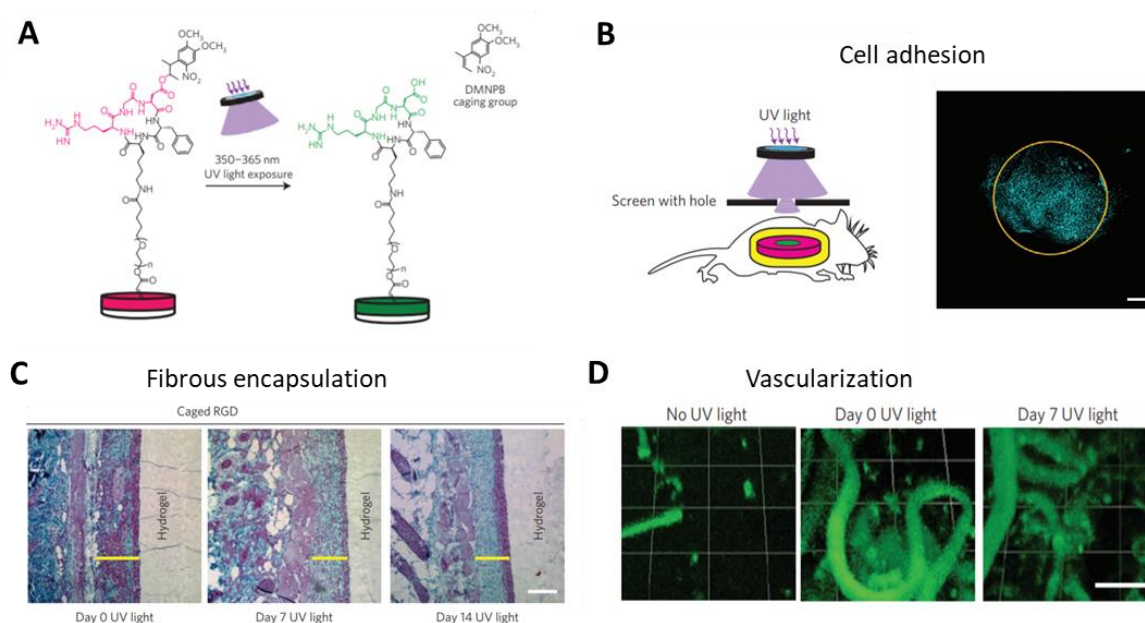


Figure 1.14. PEG hydrogels with photoactivatable cyclic RGDfK peptide. **(A)** Photolysis of photoprotected RGD peptide-functionalized PEGDA hydrogels at 350-365 nm. **(B)** Light-triggered in vivo cell adhesion. Scale bar: 200 μm . **(C)** Time-regulated presentation of RGD peptide on implanted biomaterials to modulate fibrous encapsulation in vivo. Scale bar: 100 μm . **(D)** Light-triggered in vivo vascularization. Scale bar: 100 μm . Irradiation dose(B-D): 351 nm, 10 $\text{mW}\cdot\text{cm}^{-2}$, 10 min. Adapted with permission from Nature Materials.¹⁰¹

The laminin mimetic peptide Ile-Lys-Val-Ala-Val (IKVAV) is another peptide used for control of cellular response, particularly for neuronal growth. Farrukh et. al reported hydrogels conjugated with IKVAV sequence protected with different PPGs at the amino side group of the K residue. Upon light exposure, IKVAV epitope was exposed and 2P-induced neuronal attachment and differentiation was demonstrated to pre-determined directions. Neuronal growth was obtained by using PPGs in a light-regulated manner (**Figure 1.15**).¹⁰⁴

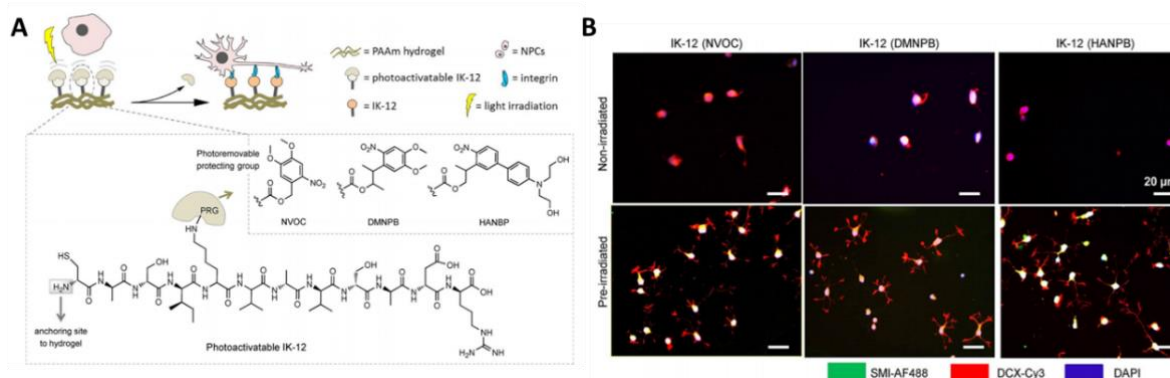


Figure 1.15. Light-guided neuronal growth with biomaterials presenting photoprotected IKVAV peptide. **(A)** Schematic representation of phototriggerable IKVAV peptides with different photocleavable groups. **(B)** Light-triggered neuronal growth. Adapted with permission from Wiley.¹⁰⁴

Other photoactivatable biomolecules, such as sortase A glycine (SAG) donor peptides was incorporated into hyaluronan hydrogels to orient axonal growth under 2P excitation at 770 nm (SP/Mai Tai MP system: 20-30% at a frame rate of 0.6 Hz) with high spatiotemporal resolution.¹⁰⁵

1.3 Two-photon responsive hydrogels for cell encapsulation

This section describes the few examples of photoresponsive hydrogels that have been tested for 2P activation in the presence of cells. To spatially manipulate hydrogel degradation, Arakawa et al. reported 2P degradable hydrogels and used them to fabricate endothelialized 3D microvascular networks with user-defined geometry in 3D in the presence of encapsulated cells (**Figure 1.16**).¹⁰⁶ Photodegradable hydrogels were prepared via SPAAC crosslinking between star PEG-BCN and a bisazide-functionalized peptide as crosslinker, which contained an intercalated *o*NB moiety. The hydrogel was also functionalized with the RDGS cell adhesive peptide and the enzymatically cleavable GPQGIWGQ peptide. A hydrogel with high cytocompatibility and user-defined manipulation possibilities was formulated. Illumination at 740 nm (1.9 W laser power, pixel dwell time of 2 μs and 5–7 frame repeat scans) was used to create 3D interconnected channels in presence of green fluorescent protein (GFP)-labeled human bone marrow-derived hS5 stromal cells. The channels were endothelialized with HUVECs for 4 days while the hS5 cells inside the hydrogel during illumination maintained high viability, as displayed in **Figure 1.16**.

In another work, Lunzer et al. reported a methodology to improve 2P efficiency of photodegradable, *o*NB-based photodegradable HA-PEG hydrogel by adding a water soluble two-photon sensitizer (P2CK). Upon illumination with light at 800 nm, the photosensitizer transferred energy to activate *o*NB functionalities via Förster resonance energy transfer (FRET) process. By adding 0.1 mM P2CK, irradiation power required for photoactivating *o*NB could be reduced from 70 to 50 mW, which did not cause phototoxicity. Spheroids of hTERT immortalized human adipose-derived mesenchymal stem cells (ASC/TERT1) were encapsulated in the hydrogels and migrated into horseshoe-shaped channels scanned at different laser powers. High cell viability was proven after 14 days (**Figure 1.17**).⁸⁹

Chapter 1

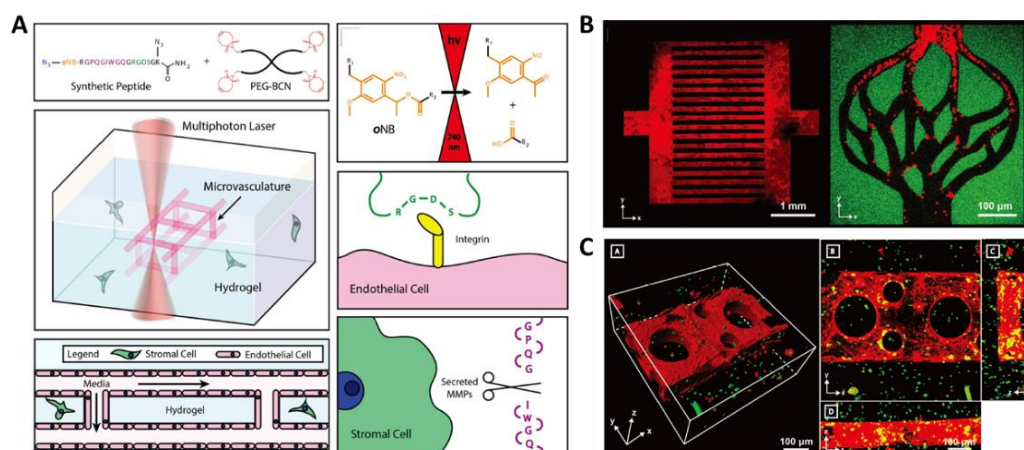


Figure 1.16. 2P degradable hydrogels to fabricate endothelialized 3D microvascular networks. **(A)** Hydrogel preparation via SPAAC chemistry between star PEG-BCN and a bisazide-functionalized peptide contains oNB moiety, RDGS peptide sequence and an enzymatically cleavable GPOGIWQG polypeptide sequence. **(B)** Photodegradation of biomimetic microvessel patterns. **(C)** Fabrication of endothelialized channels with HUVECs in the presence of encapsulated stromal cells. Adapted with permission from Wiley.¹⁰⁶

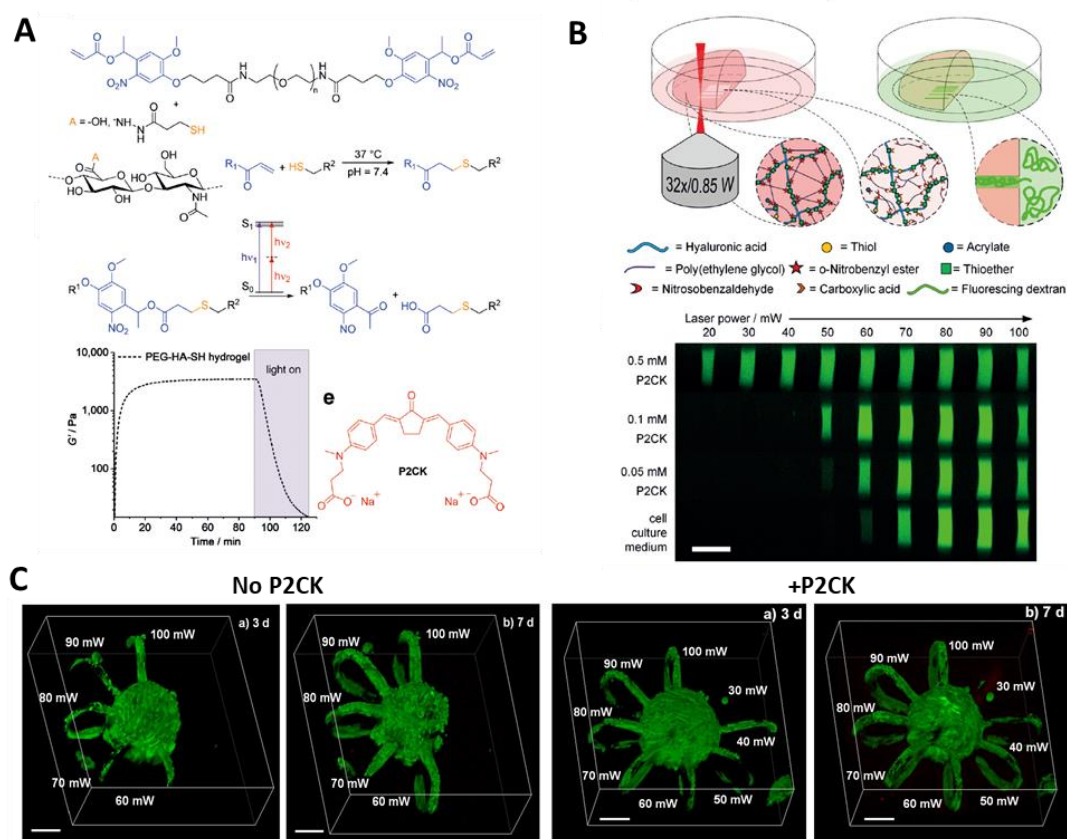


Figure 1.17. 2P degradable hydrogels for cell migration. **(A)** Hydrogel preparation and 1P degradation **(B)** 2P degradation in presence of 2P sensitizer P2CK. **(C)** 2P degradation of hydrogels to fabricate micro-channel to allow cell migration. Adapted with permission from Wiley.⁸⁹

Hydrogels with 2P-activatable bio-motifs have also been designed and used for spatiotemporal manipulation of cell behavior by light-driven modulation of photoactivatable adhesive ligands attached to the hydrogel. A two-photon activatable PMNB-protected RGD peptide, cyclo

[RGD(PMNB)fC], was developed for triggering angiogenesis with precise spatiotemporal control in PEG-based hydrogels. The active binding site of RGD peptide was blocked by PMNB groups, and was cleaved under 740 nm light to expose the RGD domain with appreciable biocompatibility. Well-defined microvasculature was formed in the activated area (**Figure 1.18**).¹⁰⁷

2P activable or degradable hydrogels for cell encapsulation allow for the study of the role of biomolecules and helping to understand the cellular responses in a high spatiotemporal manner. However, the high illumination dose were used may cause the damage for the living cells and no direct illumination on the cells are allowed due to the low efficiency of reported 2P PPGs. Moreover, the poor solubility and the poor hydrolytic stability of linking bonds (e.g. ester labile bond) are still need to be improved for long term cell studies.

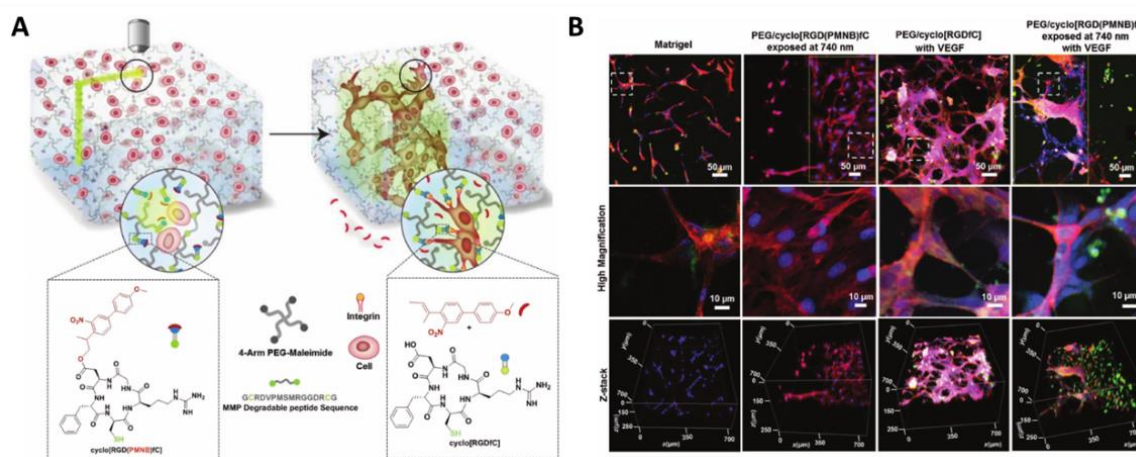


Figure 1.18. 2P light-Induced angiogenesis in hydrogels presenting PMNB-protected RGD peptide. **(A)** 2P activation of cyclo[RGD(PMNB)fC] functionalized PEG hydrogels. **(B)** 2P activated angiogenesis. (Irradiation conditions: 740 nm laser at $170 \mu\text{s} \mu\text{m}^{-1}$ scanning rate, 95% intensity). Adapted with permission from Wiley.¹⁰⁷

1.4 Photocleavable protecting groups for efficient two-photon activation

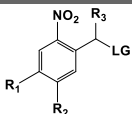
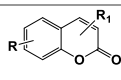
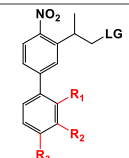
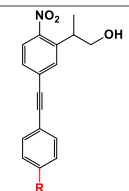
1.4.1 General design rules for efficient two-photon activatable chromophores

Currently, only a few PPGs with useful 2P sensitivity have been reported.¹⁰⁸ However, none of them satisfy all the criteria needed for biology applications (e.g. high photoefficiency, water solubility, hydrolytic stability). As summarized in **Table 1.2**. Increasing the photoefficiency of 2P PPGs is still needed to improve the performance of photoactivatable hydrogels. The 2P absorption cross-section (δ) is a key parameter to be considered for designing of 2P sensitive PPGs, which has units of GM ($1 \text{ GM} = 10^{-50} \text{ cm}^4 \text{ s photons}^{-1}$). In the last decade, the relationship between the structural factor and photoefficiency of PPGs has been extensively studied. Main features to improve photoefficiency are: i) extension of the π -conjugation, ii) introduction of substituents with strong electron-donor or acceptor character to promote strong internal charge transfer, and iii) alternation of molecular symmetry with multibranching or oligomer structures to improve cooperative effects.¹⁰⁹ Water solubility is a relevant parameter in a PPG to be used in biological applications. The solubility has been improved by incorporating charged¹¹⁰ or polar substituents¹¹¹, or hydrophilic segments (e.g. PEG

Chapter 1

chains)^{112, 113}. Good hydrolytic stability is also important to prevent undesired hydrolysis and to avoid materials degradation by other pathways than light exposure. The hydrolytic stability is related to the nature of chromophore's structure and the type of the linking group. Several types of linking group (e.g. ester, amide, carbonate and carbamate) have been studied, in which the ester and amide linking group are the most widely used. The *o*NB incorporated into PEG hydrogels by ester, amide, carbonate or carbamate linking group have been demonstrated to exhibit significant different hydrolysis speed at different time scale (ester: <1 h; carbonate:<2 h; amide:<12 h and carbamate:>72 h) under accelerated hydrolysis studies (in PBS, pH 10) over 72 h.

Table 1.2 Structure and summary of properties of reported 2P activable PPGs groups.

Chromophores	Structures	2P cross-section (δ)	Hydrolysis	Solubility	Applications
<i>o</i> NB		0.015–0.065 at 750 nm ¹⁰⁸	$t_{1/2}^a = 16.88$ h for <i>o</i> NB ester ¹¹⁴	-	Cell applications ^{34, 89, 95}
Coumarin		0.35 to 2 GM at 740 nm ¹⁰⁸	$\geq 95\%^b$ ¹¹⁵	>0.1 mM in H ₂ O ¹¹⁶	Drugs ¹¹⁷ Cell applications ¹¹⁸
(<i>o</i> -nitrobiphenyl)propyl family		3.2-11 GM at 740 nm or 800 nm ^{107, 119, 120}	<u>See next section</u>	<u>See next section</u>	Cell applications ¹⁰⁷
The (<i>o</i> -nitrobiphenyl acetylene)propyl family		19.8 GM at 800 nm ¹²¹ or 25.8 ± 3.2 GM at 690 nm ¹²²	-	20 μ M in cell medium with 0.1% DMSO ¹²¹	Cell applications ¹²¹

^a the time at which half of a bonds break in PBS pH 7.4.

^b in water for 24 h.

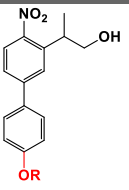
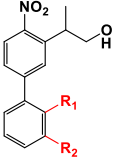
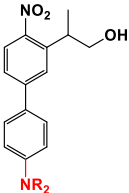
1.4.2 The (*o*-nitrobiphenyl)propyl family

The *o*-nitrobiphenylpropyl family was developed by Gug for more efficient 2P photolysis.¹²³ The two-photon cross section in the range of $\delta = 3.2$ -11 GM at 740 nm or 800 nm is significantly higher than that of *o*NB (0.015–0.065 at 750 nm).¹⁰⁸ The higher δ is a consequence of the extended conjugation and donor-acceptor structure. Among the different family members (**Table 1.3**), the 3-(2-propyl)-4'-methoxy-4-nitro-biphenyl (PMNB), with an electron donating methoxy group at the para position, has been used as PPG for cell biology experimentation.¹⁰⁷

A decrease on the 2P absorption cross section was observed by shifting the methoxy group from the para to the ortho or meta positions ($\delta = 2.2$ and 1.8 GM at 740 nm respectively).¹²⁴ Substitution effect at para position with different substitute dialkylamino groups was also studied by Specht et al.^{124, 125} Compared to methoxy, dialkylamino groups are better electron donors and can additionally enhance

the water solubility. In this case, a red shift ~ 90 nm, an increase of 2P cross-section (up to 11 GM at 800 nm) and higher water solubility were demonstrated. However, the presence of dialkylamino groups might lead to a poor hydrolytic stability.^{107, 119, 120} Therefore, the substitution group needs to be considered carefully.

Table 1.3 Structure and summary of properties of reported (*o*-nitrobiphenyl)propyl family groups.

Chromophores	Structures	λ_{\max} and 2P cross-section	Hydrolysis in PBS (pH 7.4) at r.t.	Solubility in PBS (pH 7.4) at r.t.
PMNB: R=Me PENB: R= (2-(2-(2-methoxyethoxy)ethyl)ethoxy)ethyl		λ_{\max} = 317 nm 3.1 GM at 740 nm ¹²⁴	PMNB-Glu 3% in 24 h. PMNB-RGD Stable >1 month ¹⁰⁷	PENB-Glu > 5 mM ¹²⁴
mMNB: R ₁ =H, R ₂ =OMe oMNB: R ₁ = OMe, R ₂ = H		mMNB-Glutamate (Glu) λ_{\max} = 296 nm 1.8 GM at 740 nm ¹²⁴ oMNB-Glutamate λ_{\max} = 302 nm 2.2 GM at 740 nm ¹²⁴	-	-
ANBP: R= Me HANBP: R=CH ₂ CH ₂ OH CANBP: R=CH ₂ COOH EANBP: R=(CH ₂ CH ₂ O) ₂ Me		up to 11 GM at 800 nm ¹²⁶	ANBP-RGD 63% in 1 week ¹⁰⁷ HANBP-RGD 58% in 1 week ¹⁰⁷ CANBP and EANBP-GABA $\leq 1\%$ in 24 h ¹²⁶	EANBP-GABA 10 mM ¹²⁴

1.4.3 The (*o*-nitrobiphenylacetylene)propyl family

A further extension of conjugation of *o*-nitrobiphenyl family by intercalating an alkyne spacer in the donor-acceptor biphenyl system has also been reported.¹²¹ The (*o*-nitrobiphenyl)acetylene unit with a bis(2-(2-methoxyethoxy)ethyl)amino group at para position was used as PPG to block the C-6 carboxy position of phytohormone gibberellic acid (GA₃), as showed in **Figure 1.19**. The resulting photoactivatable GA₃ (paGA₃-3) showed an absorption maximum around 400 nm, and the photolytic reaction had a 2P cross-section $\sim 1.8 \pm 0.4$ times higher than the chromophore without the alkynyl spacer. The high 2P efficiency enabled the photorelease of GA₃ in cultured COS-7 cells (incubated with paGA₃-3 (20 μ M in cell medium with 0.1% DMSO) for 5 min) to induce the translocation of mPlum-GID1 (far-red-fluorescent protein mPlum labeled GA₃-receptor) within seconds at 800 nm with 80 mW.¹²¹ However, hydrolytic stability was not demonstrated for paGA₃-3.

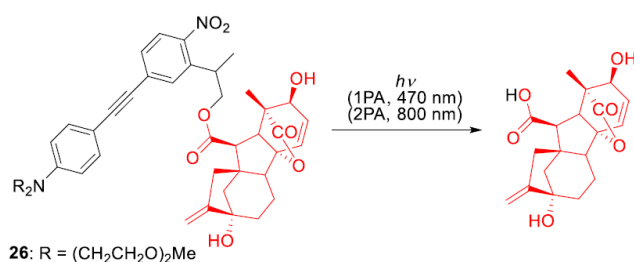


Figure 1.19. Photocleavage of plant hormone GA₃ from π -extended (*o*-nitrophenyl)acetylene chromophore. Reproduced after permission from American Chemical Society.¹²⁷

1.4.4 Alternative PPGs

Besides nitrophenyl^{107, 119, 120, 124} and *o*-nitrobenzyl derivatives,^{34, 128, 129} other PPG families have been tested for 2P activation in cell experiments, including coumarin derivatives^{98, 130, 131} and nitroindoline derivatives^{132, 133, 134}, summarized in **Figure 1.20**. These groups show low 2P efficiency due to their short conjugation length and internal charge transfer effects. 2P chromophores with branched structures or extended conjugation can lead to improved 2P properties, but the synthetic effort and expected low water solubility limit their development.^{135, 136}

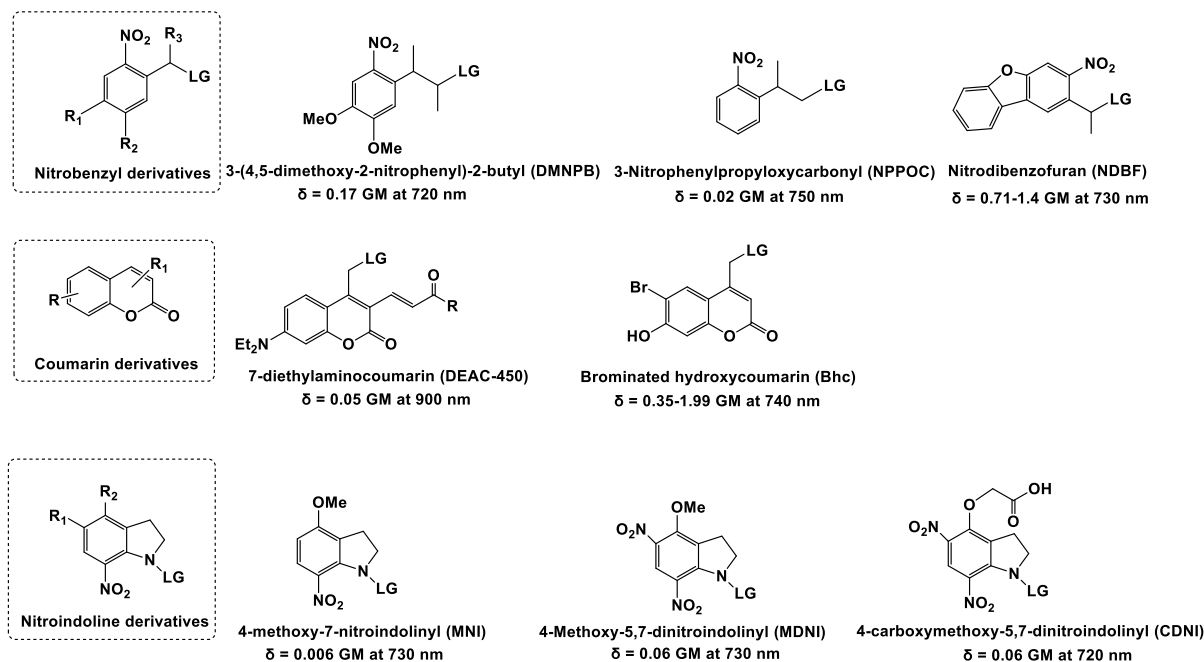


Figure 1.20. Chemical structures of common 2P chromophores used in cell studies.

1.5 References

1. Ahmed, E. M., Hydrogel: Preparation, characterization, and applications: A review. *J Adv Res* **2015**, *6* (2), 105-121.
2. Verhulsel, M.; Vignes, M.; Descroix, S.; Malaquin, L.; Vignjevic, D. M.; Viovy, J. L., A review of microfabrication and hydrogel engineering for micro-organs on chips. *Biomaterials* **2014**, *35* (6), 1816-32.
3. Caló, E.; Khutoryanskiy, V. V., Biomedical applications of hydrogels: A review of patents and commercial products. *European Polymer Journal* **2015**, *65*, 252-267.
4. Daniele, M. A.; Adams, A. A.; Naciri, J.; North, S. H.; Ligler, F. S., Interpenetrating networks based on gelatin methacrylamide and PEG formed using concurrent thiol click chemistries for hydrogel tissue engineering scaffolds. *Biomaterials* **2014**, *35* (6), 1845-56.
5. Hoffman, A. S., Hydrogels for biomedical applications. *Advanced Drug Delivery Reviews* **2012**, *64*, 18-23.
6. Ooi, H. W.; Hafeez, S.; van Blitterswijk, C. A.; Moroni, L.; Baker, M. B., Hydrogels that listen to cells: a review of cell-responsive strategies in biomaterial design for tissue regeneration. *Materials Horizons* **2017**, *4* (6), 1020-1040.
7. Zhu, T. X.; Mao, J. J.; Cheng, Y.; Liu, H. R.; Lv, L.; Ge, M. Z.; Li, S. H.; Huang, J. Y.; Chen, Z.; Li, H. Q.; Yang, L.; Lai, Y. K., Recent Progress of Polysaccharide-Based Hydrogel Interfaces for Wound Healing and Tissue Engineering. *Adv Mater Interfaces* **2019**, *6* (17), 1900761.
8. Weber, L. M.; He, J.; Bradley, B.; Haskins, K.; Anseth, K. S., PEG-based hydrogels as an in vitro encapsulation platform for testing controlled β -cell microenvironments. *Acta Biomaterialia* **2006**, *2* (1), 1-8.
9. Duval, K.; Grover, H.; Han, L. H.; Mou, Y.; Pegoraro, A. F.; Fredberg, J.; Chen, Z., Modeling Physiological Events in 2D vs. 3D Cell Culture. *Physiology (Bethesda)* **2017**, *32* (4), 266-277.
10. Caliari, S. R.; Burdick, J. A., A practical guide to hydrogels for cell culture. *Nature Methods* **2016**, *13* (5), 405-414.
11. Baker, B. M.; Chen, C. S., Deconstructing the third dimension – how 3D culture microenvironments alter cellular cues. *Journal of Cell Science* **2012**, *125* (13), 3015-3024.
12. Kharkar, P. M.; Kiick, K. L.; Kloxin, A. M., Designing degradable hydrogels for orthogonal control of cell microenvironments. *Chemical Society Reviews* **2013**, *42* (17), 7335-7372.
13. Khan, Y.; Laurencin, C. T., Regenerative engineering : advanced materials science principles. **2018**.
14. Kruse, C. R.; Singh, M.; Targosinski, S.; Sinha, I.; Sørensen, J. A.; Eriksson, E.; Nuutila, K., The effect of pH on cell viability, cell migration, cell proliferation, wound closure, and wound reepithelialization: In vitro and in vivo study. *Wound repair and regeneration : official publication of the Wound Healing Society [and] the European Tissue Repair Society* **2017**, *25* (2), 260-269.
15. Liu, B.; Poolman, B.; Boersma, A. J., Ionic Strength Sensing in Living Cells. *ACS Chem Biol* **2017**, *12* (10), 2510-2514.
16. Kim, J.; Kong, Y. P.; Niedzielski, S. M.; Singh, R. K.; Putnam, A. J.; Shikanov, A., Characterization of the crosslinking kinetics of multi-arm poly(ethylene glycol) hydrogels formed via Michael-type addition. *Soft Matter* **2016**, *12* (7), 2076-2085.

Chapter 1

17. Madl, C. M.; Heilshorn, S. C., Rapid Diels–Alder Cross-linking of Cell Encapsulating Hydrogels. *Chemistry of Materials* **2019**, *31* (19), 8035-8043.
18. Paez, J. I.; de Miguel-Jiménez, A.; Valbuena-Mendoza, R.; Rathore, A.; Jin, M.; Gläser, A.; Pearson, S.; del Campo, A., Thiol-Methylsulfone-Based Hydrogels for Cell Encapsulation: Reactivity Optimization of Aryl-Methylsulfone Substrate for Fine-Tunable Gelation Rate and Improved Stability. *Biomacromolecules* **2021**.
19. Wilson, J. L.; McDevitt, T. C., Biofunctional Hydrogels for Three-Dimensional Stem Cell Culture. **2017**, 345-362.
20. Jia, X.; Kiick, K. L., Hybrid multicomponent hydrogels for tissue engineering. *Macromol Biosci* **2009**, *9* (2), 140-156.
21. Pierschbacher, M. D.; Ruoslahti, E., Cell attachment activity of fibronectin can be duplicated by small synthetic fragments of the molecule. *Nature* **1984**, *309* (5963), 30-33.
22. Pfaff, M.; Tangemann, K.; Müller, B.; Gurrath, M.; Müller, G.; Kessler, H.; Timpl, R.; Engel, J., Selective recognition of cyclic RGD peptides of NMR defined conformation by alpha IIb beta 3, alpha V beta 3, and alpha 5 beta 1 integrins. *The Journal of biological chemistry* **1994**, *269* (32), 20233-8.
23. Kudva, A. K.; Luyten, F. P.; Patterson, J., RGD-functionalized polyethylene glycol hydrogels support proliferation and in vitro chondrogenesis of human periosteum-derived cells. *J Biomed Mater Res A* **2018**, *106* (1), 33-42.
24. Discher, D. E.; Mooney, D. J.; Zandstra, P. W., Growth factors, matrices, and forces combine and control stem cells. *Science* **2009**, *324* (5935), 1673-7.
25. Fekete, N.; Beland, A. V.; Campbell, K.; Clark, S. L.; Hoesli, C. A., Bags versus flasks: a comparison of cell culture systems for the production of dendritic cell-based immunotherapies. *Transfusion* **2018**, *58* (7), 1800-1813.
26. Ehrbar, M.; Sala, A.; Lienemann, P.; Ranga, A.; Mosiewicz, K.; Bittermann, A.; Rizzi, S. C.; Weber, F. E.; Lutolf, M. P., Elucidating the Role of Matrix Stiffness in 3D Cell Migration and Remodeling. *Biophysical Journal* **2011**, *100* (2), 284-293.
27. Her, G. J.; Wu, H.-C.; Chen, M.-H.; Chen, M.-Y.; Chang, S.-C.; Wang, T.-W., Control of three-dimensional substrate stiffness to manipulate mesenchymal stem cell fate toward neuronal or glial lineages. *Acta Biomaterialia* **2013**, *9* (2), 5170-5180.
28. Huebsch, N.; Arany, P. R.; Mao, A. S.; Shvartsman, D.; Ali, O. A.; Bencherif, S. A.; Rivera-Feliciano, J.; Mooney, D. J., Harnessing traction-mediated manipulation of the cell/matrix interface to control stem-cell fate. *Nature Materials* **2010**, *9* (6), 518-526.
29. Tibbitt, M. W.; Anseth, K. S., Hydrogels as extracellular matrix mimics for 3D cell culture. *Biotechnol Bioeng* **2009**, *103* (4), 655-663.
30. Chandrawati, R., Enzyme-responsive polymer hydrogels for therapeutic delivery. *Exp Biol Med (Maywood)* **2016**, *241* (9), 972-979.
31. Foster, G. A.; Headen, D. M.; González-García, C.; Salmerón-Sánchez, M.; Shirwan, H.; García, A. J., Protease-degradable microgels for protein delivery for vascularization. *Biomaterials* **2017**, *113*, 170-175.
32. Lueckgen, A.; Garske, D. S.; Ellinghaus, A.; Mooney, D. J.; Duda, G. N.; Cipitria, A., Enzymatically-degradable alginate hydrogels promote cell spreading and in vivo tissue infiltration.

Biomaterials **2019**, *217*, 119294.

33. Baldwin, A. D.; Kiick, K. L., Reversible maleimide–thiol adducts yield glutathione-sensitive poly(ethylene glycol)–heparin hydrogels. *Polymer Chemistry* **2013**, *4* (1), 133-143.
34. Kloxin, A. M.; Kasko, A. M.; Salinas, C. N.; Anseth, K. S., Photodegradable hydrogels for dynamic tuning of physical and chemical properties. *Science* **2009**, *324* (5923), 59-63.
35. Lin, C. C.; Anseth, K. S., PEG hydrogels for the controlled release of biomolecules in regenerative medicine. *Pharmaceutical research* **2009**, *26* (3), 631-43.
36. Chatani, S.; Nair, D. P.; Bowman, C. N., Relative reactivity and selectivity of vinyl sulfones and acrylates towards the thiol–Michael addition reaction and polymerization. *Polymer Chemistry* **2013**, *4* (4), 1048-1055.
37. Northrop, B. H.; Frayne, S. H.; Choudhary, U., Thiol–maleimide “click” chemistry: evaluating the influence of solvent, initiator, and thiol on the reaction mechanism, kinetics, and selectivity. *Polymer Chemistry* **2015**, *6* (18), 3415-3430.
38. Schamboeck, V.; Kryven, I.; Iedema, P. D., Acrylate Network Formation by Free-Radical Polymerization Modeled Using Random Graphs. *Macromol Theor Simul* **2017**, *26* (6), 1700047.
39. Choi, J. R.; Yong, K. W.; Choi, J. Y.; Cowie, A. C., Recent advances in photo-crosslinkable hydrogels for biomedical applications. *Biotechniques* **2019**, *66* (1), 40-53.
40. Aloorkar, N. H.; Kulkarni, A.; Patil, R. A.; Ingale, D. In *Star Polymers : An Overview*, 2012.
41. Bryant, S. J.; Anseth, K. S., Hydrogel properties influence ECM production by chondrocytes photoencapsulated in poly(ethylene glycol) hydrogels. *Journal of biomedical materials research* **2002**, *59* (1), 63-72.
42. Li, X.; Sun, Q.; Li, Q.; Kawazoe, N.; Chen, G., Functional Hydrogels With Tunable Structures and Properties for Tissue Engineering Applications. *Front Chem* **2018**, *6* (499), 499.
43. Feng, Y.; Taraban, M.; Yu, Y. B., The Effect of Ionic Strength on the Mechanical, Structural and Transport Properties of Peptide Hydrogels. *Soft matter* **2012**, *8* (46), 11723-11731.
44. Su, W.-F., Radical Chain Polymerization. In *Principles of Polymer Design and Synthesis*, Springer Berlin Heidelberg: Berlin, Heidelberg, 2013; pp 137-183.
45. McGann, C. L.; Dumm, R. E.; Jurusik, A. K.; Sidhu, I.; Kiick, K. L., Thiol-ene Photocrosslinking of Cytocompatible Resilin-Like Polypeptide-PEG Hydrogels. *Macromol Biosci* **2016**, *16* (1), 129-38.
46. Kim, E.; Koo, H., Biomedical applications of copper-free click chemistry: in vitro, in vivo, and ex vivo. *Chemical Science* **2019**, *10* (34), 7835-7851.
47. Zhan, H.; de Jong, H.; Löwik, D. W. P. M., Comparison of Bioorthogonally Cross-Linked Hydrogels for in Situ Cell Encapsulation. *ACS Applied Bio Materials* **2019**, *2* (7), 2862-2871.
48. Jiang, Q.; Zhang, Y.; Du, Y.; Tang, M.; Jiang, L.; Huang, W.; Yang, H.; Xue, X.; Jiang, B., Preparation of hyperbranched polymers by oxa-Michael addition polymerization. *Polymer Chemistry* **2020**, *11* (7), 1298-1306.
49. Hennen, D.; Hartmann, D.; Rieger, P. H.; Oesterreicher, A.; Wiener, J.; Arbeiter, F.; Feuchter, M.; Frohlich, E.; Pichelmayer, M.; Schlogl, S.; Griesser, T., Exploiting the Carbon and Oxa Michael Addition Reaction for the Synthesis of Yne Monomers: Towards the Conversion of Acrylates to Biocompatible Building Blocks. *Chemphotochem* **2020**, *4* (7), 476-480.
50. Bosica, G.; Abdilla, R., Aza-Michael Mono-addition Using Acidic Alumina under Solventless

Chapter 1

Conditions. *Molecules* **2016**, *21* (6), 815.

51. Nair, D. P.; Podgórski, M.; Chatani, S.; Gong, T.; Xi, W.; Fenoli, C. R.; Bowman, C. N., The Thiol-Michael Addition Click Reaction: A Powerful and Widely Used Tool in Materials Chemistry. *Chemistry of Materials* **2014**, *26* (1), 724-744.
52. Liu, Z. Q.; Wei, Z.; Zhu, X. L.; Huang, G. Y.; Xu, F.; Yang, J. H.; Osada, Y.; Zrínyi, M.; Li, J. H.; Chen, Y. M., Dextran-based hydrogel formed by thiol-Michael addition reaction for 3D cell encapsulation. *Colloids and Surfaces B: Biointerfaces* **2015**, *128*, 140-148.
53. Kurakazu, M.; Katashima, T.; Chijiishi, M.; Nishi, K.; Akagi, Y.; Matsunaga, T.; Shibayama, M.; Chung, U.-i.; Sakai, T., Evaluation of Gelation Kinetics of Tetra-PEG Gel. *Macromolecules* **2010**, *43* (8), 3935-3940.
54. Hermanson, G. T. In *Chapter 3 The Reactions of Bioconjugation*, 2013.
55. Yanagawa, F.; Sugiura, S.; Takagi, T.; Sumaru, K.; Camci-Unal, G.; Patel, A.; Khademhosseini, A.; Kanamori, T., Activated-ester-type photocleavable crosslinker for preparation of photodegradable hydrogels using a two-component mixing reaction. *Adv Healthc Mater* **2015**, *4* (2), 246-54.
56. Strehin, I.; Nahas, Z.; Arora, K.; Nguyen, T.; Elisseeff, J., A versatile pH sensitive chondroitin sulfate-PEG tissue adhesive and hydrogel. *Biomaterials* **2010**, *31* (10), 2788-97.
57. Dong, Y.; Wang, W., 14 - In situ-formed bioactive hydrogels for delivery of stem cells and biomolecules for wound healing. In *Wound Healing Biomaterials*, Ågren, M. S., Ed. Woodhead Publishing: 2016; pp 289-307.
58. Jalalvandi, E.; Hanton, L. R.; Moratti, S. C., Schiff-base based hydrogels as degradable platforms for hydrophobic drug delivery. *European Polymer Journal* **2017**, *90*, 13-24.
59. Paez, J. I.; Farrukh, A.; Valbuena-Mendoza, R.; Włodarczyk-Biegun, M. K.; del Campo, A., Thiol-Methylsulfone-Based Hydrogels for 3D Cell Encapsulation. *ACS Applied Materials & Interfaces* **2020**, *12* (7), 8062-8072.
60. Motiwala, H. F.; Kuo, Y.-H.; Stinger, B. L.; Palfey, B. A.; Martin, B. R., Tunable Heteroaromatic Sulfones Enhance in-Cell Cysteine Profiling. *Journal of the American Chemical Society* **2020**, *142* (4), 1801-1810.
61. Wilems, T. S.; Lu, X.; Kurosu, Y. E.; Khan, Z.; Lim, H. J.; Smith Callahan, L. A., Effects of free radical initiators on polyethylene glycol dimethacrylate hydrogel properties and biocompatibility. *J Biomed Mater Res A* **2017**, *105* (11), 3059-3068.
62. Berger, K. C.; Deb, P. C.; Meyerhoff, G., Radical Vinyl Polymerization. Reactions of Benzoyl Peroxide during Bulk Polymerization of Styrene with Labeled Initiator. *Macromolecules* **1977**, *10* (5), 1075-1080.
63. Turro, N. J., *Modern molecular photochemistry*. Benjamin/Cummings Pub. Co.: Menlo Park, Calif., 1991.
64. Lee, T. Y.; Guymon, C. A.; Jönsson, E. S.; Hoyle, C. E., The effect of monomer structure on oxygen inhibition of (meth)acrylates photopolymerization. *Polymer* **2004**, *45* (18), 6155-6162.
65. Temenoff, J. S.; Shin, H.; Conway, D. E.; Engel, P. S.; Mikos, A. G., In Vitro Cytotoxicity of Redox Radical Initiators for Cross-Linking of Oligo(poly(ethylene glycol) fumarate) Macromers. *Biomacromolecules* **2003**, *4* (6), 1605-1613.
66. Schesny, M. K.; Monaghan, M.; Bindermann, A. H.; Freund, D.; Seifert, M.; Eble, J. A.; Vogel,

- S.; Gawaz, M. P.; Hinderer, S.; Schenke-Layland, K., Preserved bioactivity and tunable release of a SDF1-GPVI bi-specific protein using photo-crosslinked PEGda hydrogels. *Biomaterials* **2014**, *35* (25), 7180-7187.
67. Toepke, M. W.; Impellitteri, N. A.; Theisen, J. M.; Murphy, W. L., Characterization of Thiol-Ene Crosslinked PEG Hydrogels. *Macromol Mater Eng* **2013**, *298* (6), 699-703.
68. Shih, H.; Lin, C. C., Visible-light-mediated thiol-ene hydrogelation using eosin-Y as the only photoinitiator. *Macromolecular rapid communications* **2013**, *34* (3), 269-73.
69. Fairbanks, B. D.; Schwartz, M. P.; Bowman, C. N.; Anseth, K. S., Photoinitiated polymerization of PEG-diacrylate with lithium phenyl-2,4,6-trimethylbenzoylphosphinate: polymerization rate and cytocompatibility. *Biomaterials* **2009**, *30* (35), 6702-6707.
70. Kharkar, P. M.; Rehmann, M. S.; Skeens, K. M.; Maverakis, E.; Kloxin, A. M., Thiol-ene click hydrogels for therapeutic delivery. *ACS Biomater Sci Eng* **2016**, *2* (2), 165-179.
71. Hoyle, C. E.; Lee, T. Y.; Roper, T., Thiol-enes: Chemistry of the past with promise for the future. *Journal of Polymer Science Part A: Polymer Chemistry* **2004**, *42* (21), 5301-5338.
72. Takayama, Y.; Kusamori, K.; Nishikawa, M., Click Chemistry as a Tool for Cell Engineering and Drug Delivery. *Molecules* **2019**, *24* (1), 172.
73. Phelps, E. A.; Enemchukwu, N. O.; Fiore, V. F.; Sy, J. C.; Murthy, N.; Sulchek, T. A.; Barker, T. H.; Garcia, A. J., Maleimide cross-linked bioactive PEG hydrogel exhibits improved reaction kinetics and cross-linking for cell encapsulation and in situ delivery. *Adv Mater* **2012**, *24* (1), 64-70, 2.
74. Cao, L.; Cao, B.; Lu, C.; Wang, G.; Yu, L.; Ding, J., An injectable hydrogel formed by in situ cross-linking of glycol chitosan and multi-benzaldehyde functionalized PEG analogues for cartilage tissue engineering. *Journal of Materials Chemistry B* **2015**, *3* (7), 1268-1280.
75. Toda, N.; Asano, S.; Barbas, C. F., 3rd, Rapid, stable, chemoselective labeling of thiols with Julia-Kociencki-like reagents: a serum-stable alternative to maleimide-based protein conjugation. *Angewandte Chemie (International ed. in English)* **2013**, *52* (48), 12592-6.
76. Farrukh, A.; Paez, J. I.; Salierno, M.; del Campo, A., Bioconjugating Thiols to Poly(acrylamide) Gels for Cell Culture Using Methylsulfonyl Co-monomers. *Angewandte Chemie (International ed. in English)* **2016**, *55* (6), 2092-6.
77. Flinck, M.; Kramer, S. H.; Pedersen, S. F., Roles of pH in control of cell proliferation. *Acta Physiol (Oxf)* **2018**, *223* (3), e13068.
78. Fragal, V. H.; Catori, D. M.; Fragal, E. H.; Garcia, F. P.; Nakamura, C. V.; Rubira, A. F.; Silva, R., Two-dimensional thermoresponsive sub-microporous substrate for accelerated cell tissue growth and facile detachment. *Journal of Colloid and Interface Science* **2019**, *547*, 78-86.
79. Vining, K. H.; Mooney, D. J., Mechanical forces direct stem cell behaviour in development and regeneration. *Nature Reviews Molecular Cell Biology* **2017**, *18* (12), 728-742.
80. Lee, E. J.; Chan, E. W.; Yousaf, M. N., Spatio-temporal control of cell coculture interactions on surfaces. *ChemBiochem* **2009**, *10* (10), 1648-53.
81. Aonbangkhen, C.; Zhang, H.; Wu, D. Z.; Lampson, M. A.; Chenoweth, D. M., Reversible Control of Protein Localization in Living Cells Using a Photocaged-Photocleavable Chemical Dimerizer. *Journal of the American Chemical Society* **2018**, *140* (38), 11926-11930.
82. DeForest, C. A.; Anseth, K. S., Cytocompatible click-based hydrogels with dynamically tunable

Chapter 1

properties through orthogonal photoconjugation and photocleavage reactions. *Nat Chem* **2011**, *3* (12), 925-31.

83. Luo, Y.; Shoichet, M. S., A photolabile hydrogel for guided three-dimensional cell growth and migration. *Nature Materials* **2004**, *3* (4), 249-253.

84. Shin, D. S.; You, J.; Rahimian, A.; Vu, T.; Siltanen, C.; Ehsanipour, A.; Stybayeva, G.; Sutcliffe, J.; Revzin, A., Photodegradable hydrogels for capture, detection, and release of live cells. *Angewandte Chemie (International ed. in English)* **2014**, *53* (31), 8221-4.

85. Maeda, K., Analysis of Ultraviolet Radiation Wavelengths Causing Hardening and Reduced Elasticity of Collagen Gels In Vitro. **2018**, *5* (1), 14.

86. Wong, D. Y.; Ranganath, T.; Kasko, A. M., Low-Dose, Long-Wave UV Light Does Not Affect Gene Expression of Human Mesenchymal Stem Cells. *PLoS One* **2015**, *10* (9), e0139307-e0139307.

87. Youn, H. Y.; Chou, B. R.; Cullen, A. P.; Sivak, J. G., Effects of 400 nm, 420 nm, and 435.8 nm radiations on cultured human retinal pigment epithelial cells. *Journal of photochemistry and photobiology. B, Biology* **2009**, *95* (1), 64-70.

88. Tibbitt, M. W.; Kloxin, A. M.; Dyamenahalli, K. U.; Anseth, K. S., Controlled two-photon photodegradation of PEG hydrogels to study and manipulate subcellular interactions on soft materials. *Soft Matter* **2010**, *6* (20), 5100-5108.

89. Lunzer, M.; Shi, L.; Andriotis, O. G.; Gruber, P.; Markovic, M.; Thurner, P. J.; Ossipov, D.; Liska, R.; Ovsianikov, A., A Modular Approach to Sensitized Two-Photon Patterning of Photodegradable Hydrogels. *Angew Chem Int Ed Engl* **2018**, *57* (46), 15122-15127.

90. Croissant, J. G.; Zink, J. I.; Raehm, L.; Durand, J. O., Two-Photon-Excited Silica and Organosilica Nanoparticles for Spatiotemporal Cancer Treatment. *Adv Healthc Mater* **2018**, *7* (7), e1701248.

91. Svoboda, K.; Yasuda, R., Principles of Two-Photon Excitation Microscopy and Its Applications to Neuroscience. *Neuron* **2006**, *50* (6), 823-839.

92. Caminade, A.-M.; Zibarov, A.; Cueto Diaz, E.; Hameau, A.; Klausen, M.; Moineau-Chane Ching, K.; Majoral, J.-P.; Verlhac, J.-B.; Mongin, O.; Blanchard-Desce, M., Fluorescent phosphorus dendrimers excited by two photons: synthesis, two-photon absorption properties and biological uses. *Beilstein J Org Chem* **2019**, *15*, 2287-2303.

93. Kasko, A. M.; Wong, D. Y., Two-photon lithography in the future of cell-based therapeutics and regenerative medicine: a review of techniques for hydrogel patterning and controlled release. *Future medicinal chemistry* **2010**, *2* (11), 1669-80.

94. Barolet, D., Light-emitting diodes (LEDs) in dermatology. *Seminars in cutaneous medicine and surgery* **2008**, *27* (4), 227-38.

95. DeForest, C. A.; Anseth, K. S., Cytocompatible click-based hydrogels with dynamically tunable properties through orthogonal photoconjugation and photocleavage reactions. *Nature Chemistry* **2011**, *3* (12), 925-931.

96. Yan, B.; Boyer, J.-C.; Habault, D.; Branda, N. R.; Zhao, Y., Near Infrared Light Triggered Release of Biomacromolecules from Hydrogels Loaded with Upconversion Nanoparticles. *Journal of the American Chemical Society* **2012**, *134* (40), 16558-16561.

97. Azagarsamy, M. A.; McKinnon, D. D.; Alge, D. L.; Anseth, K. S., Coumarin-Based Photodegradable Hydrogel: Design, Synthesis, Gelation, and Degradation Kinetics. *ACS Macro Letters*

2014, 3 (6), 515-519.

98. de Gracia Lux, C.; Lux, J.; Collet, G.; He, S.; Chan, M.; Olejniczak, J.; Foucault-Collet, A.; Almutairi, A., Short Soluble Coumarin Crosslinkers for Light-Controlled Release of Cells and Proteins from Hydrogels. *Biomacromolecules* **2015**, 16 (10), 3286-3296.

99. Brown, T. E.; Marozas, I. A.; Anseth, K. S., Amplified Photodegradation of Cell-Laden Hydrogels via an Addition-Fragmentation Chain Transfer Reaction. *Adv Mater* **2017**, 29 (11), 1605001.

100. Patch, J. A.; Barron, A. E., Mimicry of bioactive peptides via non-natural, sequence-specific peptidomimetic oligomers. *Current opinion in chemical biology* **2002**, 6 (6), 872-7.

101. Lee, T. T.; García, J. R.; Paez, J. I.; Singh, A.; Phelps, E. A.; Weis, S.; Shafiq, Z.; Shekaran, A.; del Campo, A.; García, A. J., Light-triggered in vivo activation of adhesive peptides regulates cell adhesion, inflammation and vascularization of biomaterials. *Nature Materials* **2015**, 14 (3), 352-360.

102. Petersen, S.; Alonso, J. M.; Specht, A.; Duodu, P.; Goeldner, M.; del Campo, A., Phototriggering of cell adhesion by caged cyclic RGD peptides. *Angewandte Chemie (International ed. in English)* **2008**, 47 (17), 3192-5.

103. Lin, Y.; Mazo, M. M.; Skaalure, S. C.; Thomas, M. R.; Schultz, S. R.; Stevens, M. M., Activatable cell-biomaterial interfacing with photo-caged peptides. *Chemical Science* **2019**, 10 (4), 1158-1167.

104. Farrukh, A.; Fan, W.; Zhao, S.; Salierno, M.; Paez, J. I.; Del Campo, A., Photoactivatable Adhesive Ligands for Light-Guided Neuronal Growth. *ChemBiochem : a European journal of chemical biology* **2018**, 19 (12), 1271-1279.

105. Broguiere, N.; Luchtefeld, I.; Trachsel, L.; Mazunin, D.; Rizzo, R.; Bode, J. W.; Lutolf, M. P.; Zenobi-Wong, M., Morphogenesis Guided by 3D Patterning of Growth Factors in Biological Matrices. *Adv Mater* **2020**, 32 (25), e1908299.

106. Arakawa, C. K.; Badeau, B. A.; Zheng, Y.; DeForest, C. A., Multicellular Vascularized Engineered Tissues through User-Programmable Biomaterial Photodegradation. *Adv Mater* **2017**, 29 (37).

107. Farrukh, A.; Paez, J. I.; del Campo, A., 4D Biomaterials for Light-Guided Angiogenesis. *Advanced Functional Materials* **2019**, 29 (6), 1807734.

108. Klán, P.; Šolomek, T.; Bochet, C. G.; Blanc, A.; Givens, R.; Rubina, M.; Popik, V.; Kostikov, A.; Wirz, J., Photoremovable Protecting Groups in Chemistry and Biology: Reaction Mechanisms and Efficacy. *Chemical Reviews* **2013**, 113 (1), 119-191.

109. Bort, G.; Gallavardin, T.; Ogden, D.; Dalko, P. I., From one-photon to two-photon probes: "caged" compounds, actuators, and photoswitches. *Angewandte Chemie (International ed. in English)* **2013**, 52 (17), 4526-37.

110. Wang, L.; Corrie, J. E. T.; Wootton, J. F., Photolabile Precursors of Cyclic Nucleotides with High Aqueous Solubility and Stability. *The Journal of Organic Chemistry* **2002**, 67 (10), 3474-3478.

111. Olson, J. P.; Banghart, M. R.; Sabatini, B. L.; Ellis-Davies, G. C. R., Spectral Evolution of a Photochemical Protecting Group for Orthogonal Two-Color Uncaging with Visible Light. *Journal of the American Chemical Society* **2013**, 135 (42), 15948-15954.

112. Josa-Culleré, L.; Llebaria, A., In the Search for Photocages Cleavable with Visible Light: An Overview of Recent Advances and Chemical Strategies. *Chemphotochem* **2020**, 5 (4), 296-314.

113. Peterson, J. A.; Wijesooriya, C.; Gehrman, E. J.; Mahoney, K. M.; Goswami, P. P.; Albright, T. R.; Syed, A.; Dutton, A. S.; Smith, E. A.; Winter, A. H., Family of BODIPY Photocages Cleaved by

Chapter 1

Single Photons of Visible/Near-Infrared Light. *Journal of the American Chemical Society* **2018**, *140* (23), 7343-7346.

114. Kharkar, P. M.; Kiick, K. L.; Kloxin, A. M., Design of thiol- and light-sensitive degradable hydrogels using Michael-type addition reactions. *Polymer Chemistry* **2015**, *6* (31), 5565-5574.

115. Adatia, K. K.; Halbritter, T.; Reinfelds, M.; Michele, A.; Tran, M.; Laschat, D. S.; Heckel, A.; Tovar, G. E. M.; Southan, A., Coumarin-4-ylmethyl- and p-Hydroxyphenacyl-Based Photoacid Generators with High Solubility in Aqueous Media: Synthesis, Stability and Photolysis. *Chemphotochem* **2020**, *4* (3), 207-217.

116. Bojtár, M.; Kormos, A.; Kis-Petik, K.; Kellermayer, M.; Kele, P., Green-Light Activatable, Water-Soluble Red-Shifted Coumarin Photocages. *Organic Letters* **2019**, *21* (23), 9410-9414.

117. Shen, W.; Zheng, J.; Zhou, Z.; Zhang, D., Approaches for the synthesis of o-nitrobenzyl and coumarin linkers for use in photocleavable biomaterials and bioconjugates and their biomedical applications. *Acta Biomaterialia* **2020**, *115*, 75-91.

118. Jung, H. S.; Kwon, P. S.; Lee, J. W.; Kim, J. I.; Hong, C. S.; Kim, J. W.; Yan, S.; Lee, J. Y.; Lee, J. H.; Joo, T.; Kim, J. S., Coumarin-Derived Cu²⁺-Selective Fluorescence Sensor: Synthesis, Mechanisms, and Applications in Living Cells. *Journal of the American Chemical Society* **2009**, *131* (5), 2008-2012.

119. Donato, L.; Mourot, A.; Davenport, C. M.; Herbivo, C.; Warther, D.; Léonard, J.; Bolze, F.; Nicoud, J.-F.; Kramer, R. H.; Goeldner, M.; Specht, A., Water-soluble, donor-acceptor biphenyl derivatives in the 2-(o-nitrophenyl)propyl series: highly efficient two-photon uncaging of the neurotransmitter γ -aminobutyric acid at $\lambda = 800$ nm. *Angewandte Chemie (International ed. in English)* **2012**, *51* (8), 1840-1843.

120. Garcia-Fernandez, L.; Herbivo, C.; Arranz, V. S.; Warther, D.; Donato, L.; Specht, A.; del Campo, A., Dual photosensitive polymers with wavelength-selective photoresponse. *Adv Mater* **2014**, *26* (29), 5012-7.

121. Schelkle, K. M.; Griesbaum, T.; Ollech, D.; Becht, S.; Buckup, T.; Hamburger, M.; Wombacher, R., Light-induced protein dimerization by one- and two-photon activation of gibberellic acid derivatives in living cells. *Angewandte Chemie (International ed. in English)* **2015**, *54* (9), 2825-9.

122. Schelkle, K. M.; Becht, S.; Faraji, S.; Petzoldt, M.; Mullen, K.; Buckup, T.; Dreuw, A.; Motzkus, M.; Hamburger, M., Emission turn-on and solubility turn-off in conjugated polymers: one- and two-photon-induced removal of fluorescence-quenching solubilizing groups. *Macromol Rapid Commun* **2015**, *36* (1), 31-7.

123. Gug, S.; Charon, S.; Specht, A.; Alarcon, K.; Ogden, D.; Zietz, B.; Léonard, J.; Haacke, S.; Bolze, F.; Nicoud, J. F.; Goeldner, M., Photolabile glutamate protecting group with high one- and two-photon uncaging efficiencies. *Chembiochem : a European journal of chemical biology* **2008**, *9* (8), 1303-7.

124. Specht, A.; Bolze, F.; Donato, L.; Herbivo, C.; Charon, S.; Warther, D.; Gug, S.; Nicoud, J.-F.; Goeldner, M., The donor-acceptor biphenyl platform: A versatile chromophore for the engineering of highly efficient two-photon sensitive photoremovable protecting groups. *Photochemical & Photobiological Sciences* **2012**, *11* (3), 578-586.

125. Donato, L.; Mourot, A.; Davenport, C. M.; Herbivo, C.; Warther, D.; Leonard, J.; Bolze, F.; Nicoud, J. F.; Kramer, R. H.; Goeldner, M.; Specht, A., Water-soluble, donor-acceptor biphenyl

derivatives in the 2-(o-nitrophenyl)propyl series: highly efficient two-photon uncaging of the neurotransmitter gamma-aminobutyric acid at $\lambda = 800$ nm. *Angew Chem Int Ed Engl* **2012**, *51* (8), 1840-3.

126. Donato, L.; Mourot, A.; Davenport, C. M.; Herbivo, C.; Warther, D.; Léonard, J.; Bolze, F.; Nicoud, J.-F.; Kramer, R. H.; Goeldner, M.; Specht, A., Water-Soluble, Donor–Acceptor Biphenyl Derivatives in the 2-(o-Nitrophenyl)propyl Series: Highly Efficient Two-Photon Uncaging of the Neurotransmitter γ -Aminobutyric Acid at $\lambda=800$ nm. **2012**, *51* (8), 1840-1843.

127. Weinstain, R.; Slanina, T.; Kand, D.; Klán, P., Visible-to-NIR-Light Activated Release: From Small Molecules to Nanomaterials. *Chemical Reviews* **2020**, *120* (24), 13135-13272.

128. Kretschy, N.; Holik, A. K.; Somoza, V.; Stengele, K. P.; Somoza, M. M., Next-Generation o-Nitrobenzyl Photolabile Groups for Light-Directed Chemistry and Microarray Synthesis. *Angewandte Chemie (International ed. in English)* **2015**, *54* (29), 8555-9.

129. Hammers, M. D.; Hodny, M. H.; Bader, T. K.; Mahmoodi, M. M.; Fang, S.; Fenton, A. D.; Nurie, K.; Trial, H. O.; Xu, F.; Healy, A. T.; Ball, Z. T.; Blank, D. A.; Distefano, M. D., Two-photon uncaging of bioactive thiols in live cells at wavelengths above 800 nm. *Organic & Biomolecular Chemistry* **2021**, *19* (10), 2213-2223.

130. DeForest, C. A.; Tirrell, D. A., A photoreversible protein-patterning approach for guiding stem cell fate in three-dimensional gels. *Nature Materials* **2015**, *14* (5), 523-531.

131. Amatrudo, J. M.; Olson, J. P.; Lur, G.; Chiu, C. Q.; Higley, M. J.; Ellis-Davies, G. C. R., Wavelength-Selective One- and Two-Photon Uncaging of GABA. *ACS Chemical Neuroscience* **2014**, *5* (1), 64-70.

132. Canepari, M.; Nelson, L.; Papageorgiou, G.; Corrie, J. E. T.; Ogden, D., Photochemical and pharmacological evaluation of 7-nitroindolyl- and 4-methoxy-7-nitroindolyl-amino acids as novel, fast caged neurotransmitters. *Journal of Neuroscience Methods* **2001**, *112* (1), 29-42.

133. Fedoryak, O. D.; Sul, J.-Y.; Haydon, P. G.; Ellis-Davies, G. C. R., Synthesis of a caged glutamate for efficient one- and two-photon photorelease on living cells. *Chemical Communications* **2005**, (29), 3664-3666.

134. Matsuzaki, M.; Ellis-Davies, G. C. R.; Nemoto, T.; Miyashita, Y.; Iino, M.; Kasai, H., Dendritic spine geometry is critical for AMPA receptor expression in hippocampal CA1 pyramidal neurons. *Nature Neuroscience* **2001**, *4* (11), 1086-1092.

135. Piant, S.; Bolze, F.; Specht, A., Two-photon uncaging, from neuroscience to materials. *Opt. Mater. Express* **2016**, *6* (5), 1679-1691.

136. Xu, L.; Lin, W.; Huang, B.; Zhang, J.; Long, X.; Zhang, W.; Zhang, Q., The design strategies and applications for organic multi-branched two-photon absorption chromophores with novel cores and branches: a recent review. *Journal of Materials Chemistry C* **2021**, *9* (5), 1520-1536.

Chapter 1

Chapter 2: Synthesis of two-photon degradable crosslinkers and PEG-precursors

2.1 Introduction

Hydrogels engineered with photolabile groups are of interest for biological studies and applications. For example, photodegradable hydrogels have been used to control the migration¹⁻³ and differentiation² states of cells in 3D cultures. In other examples, proteins and drugs⁴⁻⁶ have been loaded into photodegradable hydrogels and released on demand upon light exposure. To this purpose, photocleavable moieties are incorporated into the hydrogel network.⁷ Examples so far have mainly made use of *o*-nitrobenzyl (*o*NB) derivatives,^{2, 8, 9 10} and occasionally coumarin.¹¹ Allyl sulfide groups were also demonstrated to as an efficient 1P cleavable moiety through reversible radical addition-fragmentation chain transfer (AFCT) reactions.¹² As summarized in **Table 2.1**. These groups absorb light in the UV range in most cases. To minimize the risk of photodamage to embedded cells, alternative systems that allow activation at longer wavelengths, VIS or NIR have been suggested¹³ and are currently an active field of research.

Table 2.1 Main chemical approaches for fabrication of photodegradable hydrogels

Functional group	Mechanism/approach	Relative use	
		One-photon (1P)	Two-photon (2P)
Photocleavable system			
<i>o</i> -nitrobenzyl chromophore ^{2, 8, 9}		√ ^a	√
<i>o</i> -nitrobenzyl chromophore + photosensitizer ¹⁰		√	√
Coumarin chromophore ¹¹		√	√
Reversible photocleavable system			
Allyl sulfide group ¹²		√	X ^b

^a The related chromophore or groups have been used for 1P or 2P activation.

^b The related chromophore or groups have not been used for 1P or 2P activation.

The *o*NB group can also be activated with femtosecond lasers in the NIR range if the dose used is enough to activate two-photon excitation processes.^{2, 8, 9} The sensitivity of a photoremovable group to two-photon activation depends on its two-photon absorption cross-section (δ), which is the

Chapter 2

capacity of a chromophore to absorb two photons of a particular wavelength and polarization, and is expressed in Göppert-Mayer ($1 \text{ GM} = 10^{-50} \text{cm}^4 \text{ s photon}^{-1}$). Two-photon absorption cross-section can be measured by z scan of two-photon photoluminescence excitation spectroscopy.¹⁴ The Anseth's group reported two-photon degradable PEG-based hydrogels based on the *o*NB photolabile moiety and demonstrated that spatially controlled photodegradation allowed controlled cell migration into the exposed areas. However, the low two-photon absorption cross section (0.02 at 750 nm)¹⁵ required high exposure doses for activation ($> 10 \text{ J cm}^{-2}$), and this can cause cell photodamage. In the photolysis of *o*-nitrobenzyl esters the primary aci-nitro intermediates is formed by the photoinduced H-atom transfer (HAT*), followed by the ground state cyclization between hydroxyl moiety of nitro group and the benzylic carbon (**Figure 2.1**). The molecule is deprotonated and cleaves to form ketone or aldehyde, with concomitant release of X-carboxylic acid.^{15, 16}

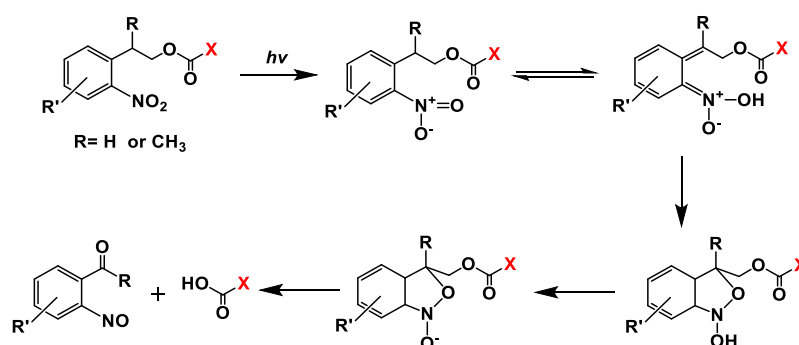
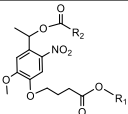
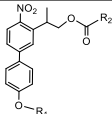


Figure 2.1 Reported photodegradation mechanism for *o*-nitrobenzyl ester groups.^{15, 16}

Synthetic efforts towards photodegradable hydrogels containing photoremovable groups with higher 2P photolysis efficiency have been made. For example, two-photon degradable hydrogels based on coumarin cleavable groups ($\delta = 0.35$ to 2 GM at 740 nm)¹⁵ were also developed. 2P degradation of the hydrogel network was achieved at 740 nm , 800 nm and 860 nm , but low efficiency was observed at 900 nm . Note, however, that these experiments were not done in the presence of cells.¹¹

An interesting alternative of photoremovable groups with higher 2P efficiency is the *o*-nitrobiphenylpropyl family.¹⁷⁻²⁰ They present a two-photon absorption cross-section $\delta = 3.1$ - 11 GM depending on the length of the extended π conjugated system, donor-acceptor structure and the attached substrate. The 4'-methoxy-4-nitrobiphenyl-3-yleth-2-yl)methyl (PMNB) candidate has a two-photon cross-section of 3.1 GM at 740 nm and 0.45 GM at 800 nm (**Table 2.2**), which is > 47 times higher than that of the *o*-nitrobenzyl group. This is due to the π -extended conjugated structure.^{17, 21} PMNB has been used as efficient photoremovable protecting group to block the active site of glutamate and neurotransmitter GABA.^{17, 18} In del Campo's group, PMNB was incorporated into crosslinked polymers to develop a positive photoresist.¹⁹ In this Chapter, photodegradable hydrogels based on the PMNB group are presented.

Table 2.2 Comparison of *o*NB and PMNB derivatives^{15, 22, 23}

Properties	<i>o</i> -Nitrobenzyl (<i>o</i> NB) based crosslinker	Methoxynitrophenyl (PMNB) based crosslinker
Structure		
λ_{max}^{abs} (nm)	352 nm ²⁴	317 nm ¹⁷
One-photon quantum yield (ϕ)	0.005 at 355 nm ²⁴	0.1 at 315 nm ¹⁷
Two-photon cross section (GM)	0.02 at 750 nm ²²	3.1 at 740 nm, 0.45 at 800 nm ¹⁷

The photolysis mechanism of PMNB-based ester and carbamate derivatives involves a β -elimination pathway (**Figure 2.2**). The photolysis of 2-nitro-2-phenethyl ester derivatives (that release -COOH groups upon cleavage) and 2-nitro-2-phenethyl carbamates (that release -NH₂ functionalities) have been studied.^{25, 26} As photolysis byproduct, an *o*-nitrobenzyl propene group is formed. Specifically, the photolysis of 2-nitro-2-phenethyl derivatives and 2-nitro-2-phenethyl carbamate derivatives occur through an aci-nitro intermediate (analogous to that for *o*-nitrobenzyloxycarbonyl and *o*-nitrobenzyloxycarbamate derivatives) as shown in **Figure 2.3**, followed by rearrangement to photolabile *o*-nitrostyrene with β -elimination of the protected group. Moreover, CO₂ is released by the decomposition of the carbamic acid intermediate of 2-nitro-2-phenethyl carbamate derivatives.^{15, 17, 25-28}

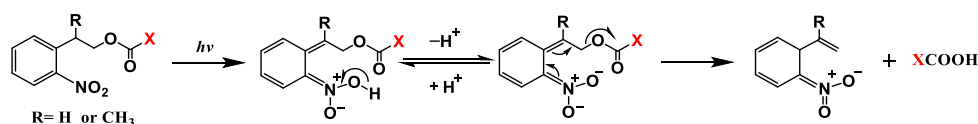


Figure 2.2 Reported photodegradation mechanism for *o*-nitrophenylethyl ester groups.^{13, 15}

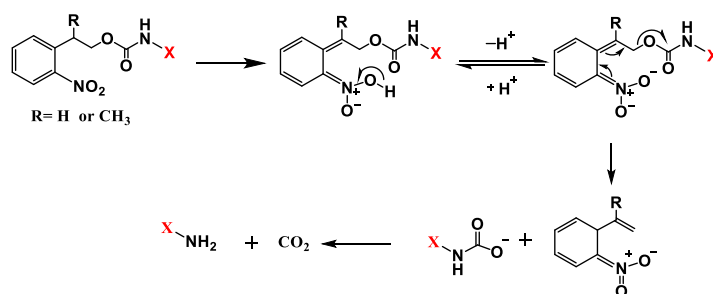


Figure 2.3 Reported photodegradation mechanism for *o*-nitrophenylethyl carbamate groups.^{25, 26}

In this chapter, the PMNB group will be used as an efficient 2P cleavable groups to construct the crosslinker for degradable hydrogels.

Chapter 2

2.2 Molecular design of photodegradable hydrogels for cell encapsulation

Polymer backbone

Star PEGs are commercially available in 5-40 kDa molar mass range, and this range has been proved adequate for cell encapsulation. In this Thesis, star PEGs (**Figure 2.4**) with molar mass 20 kDa were selected as it is the most widely used variant used successfully for cell encapsulation and 3D culture.^{29,}

30

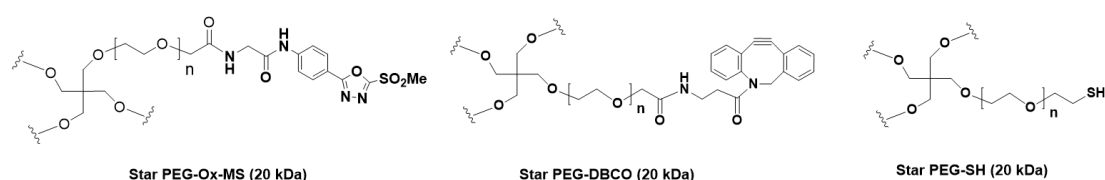


Figure 2.4 Chemical structures of star PEGs

Crosslinking chemistry

Star PEGs are available as homo- or hetero-functional stars with different terminal reactive functionalities. This allows high versatility for crosslinking and incorporation of bioactive cues for improving biocompatibility into cell laden hydrogels. Maleimide (Mal), *N*-hydroxysuccinimide (-NHS), cyclooctyne, thiol (-SH), amine (-NH₂) and azide (-N₃) are the most commonly used terminal groups used for gelation of star PEGs. The combinations Mal-SH, NHS-NH₂, and cyclooctyne-N₃ allow for gel formation under physiological conditions and have been extensively used for cell encapsulation and 3D cell culture. In addition, the methyl sulfone (-MS) group is another good candidate since it can react with -SH groups in seconds-minutes time scale under physiological conditions, and this reaction is orthogonal to alcohols, amines, carboxylic acids, and acrylate functional groups.³¹⁻³³

The selection of the crosslinking reaction for cell encapsulation is guided by the following considerations: i) high efficiency (i.e. with high conversions) under mild reaction conditions, ii) biocompatibility of precursors and crosslinked products and iii) adequate reaction rate for cell encapsulation applications. The crosslinking kinetics is a crucial parameter for preparing a homogenous cell culture platform. Gelation times should be typically between 30 s to 3-4 min to ensure proper mixing of precursors and cells under low shear forces (typical second-order reaction rate constants range $k_2 \sim 10^2$ to $10^{-1} \text{ M}^{-1}\text{s}^{-1}$), while avoiding cell sedimentation during crosslinking. Given the previous considerations, thiol-MS chemistry and strain-promoted azide-alkyne cycloaddition (SPAAC) were selected for the studies in this Thesis, since they exhibit crosslinking speed of seconds-minutes in buffer at pH 7.4.^{32, 34} An additional advantage of the thiol-MS chemistry is the pH tunability of the reaction rate, thus the gelation speed can be easily adjusted by altering pH within physiological range.

Photodegradable crosslinker

PEGs are non-degradable polymers and need to be crosslinked with degradable crosslinkers to support cell culture. In this Thesis, photodegradable crosslinkers are presented to allow spatiotemporal control of gel degradation.³⁵ The specific aim is the development of crosslinkers that can be degraded using

2P excitation processes at cell-compatible doses. A general scheme of photodegradable crosslinkers used is shown in **Figure 2.5**.

Relevant criteria for the selection of the photocleavable group in the crosslinker are: i) high efficiency of the photolytic process (i.e. high 2P absorption cross-section); ii) photolysis byproducts should be cell-compatible; iii) moderate synthetic effort and high yield; iv) high hydrolytic stability. Considering these criteria, and the information specified in the introductory part of this chapter, the photocleavable group (4'-methoxy-4-nitrobiphenyl-3-yleth-2-yl)methyl (PMNB) was selected. PMNB can be prepared in 5 steps with an overall yield of ~15% and has a high 2P cross section (3.1 GM at 740 nm and 0.45 GM at 800 nm), high hydrolytic stability, cell-compatible photo byproduct but considerably low water solubility.^{17, 20} PMNB has been used previously in the context of cell studies.³³ In previous work in the group¹⁹ the PMNB derivative 2-(4'-(2-hydroxy ethoxy)-4-nitro-[1,1'-biphenyl]-3-yl)propan-1-ol (PMNB(OH)₂) was synthesized (**Figure 2.5**). This intermediate has two hydroxyl groups that can be derivatized with OEG chains. To ensure solubility, OEG arms with number of repeat units $n > 10$ were attached to it.

Another point to consider for the photoefficiency is the leaving group in the photocleavage reaction, which are determined by the choice of the linking group (**Figure 2.5**). Ester and carbamate linking groups have been reported for *o*NB derivatives. The *o*NB carbamate exhibited ~1.5 times higher photolysis efficiency (quantum yield $\Phi = 0.054$ at 365 nm) than the *o*NB ester bond (quantum yield $\Phi = 0.034$ at 365 nm) within a hydrogel network.⁶ This could be explained that the carbamate linking group can better stabilize the corresponding *o*-nitrobenzyl type radicals, thus weaken the C–H bond that is cleaved in the photoinduced hydrogen atom transfer step and hence lower the barrier and released more efficiently.¹⁶

Ester groups have been used in photodegradable hydrogels reported by other groups^{2, 10}, but are prone to hydrolysis at physiological conditions. Star PEG-based hydrogels with linear photodegradable PEG (PEG-bis-NB-azide) crosslinker bearing ester labile bond showed appreciable hydrolysis within 2 hours at physiological conditions (neutral pH, aqueous medium).³⁶ A recent report quantifies the photolysis and hydrolysis kinetics of photodegradable PEG hydrogels with *o*NB group linked with different bonds (ester, amide, carbonate and carbamate) to the PEG backbone. *o*NB ester showed high hydrolysis rates (complete hydrogel degradation in 1 h in PBS at pH 10), whereas *o*NB carbamate showed similar hydrolysis behavior as nondegradable control hydrogels and ~1.5 times higher photolysis efficiency.⁶ Taking in to account these results, a PMNB-based crosslinker with esters and carbamate linkage to the OEG chains were synthesized to find out the best compromise between chemical and photolytic stability (**Figure 2.5**). Ester linkages are easy to introduce by esterification of the two pendant hydroxyl groups of PMNB(OH)₂ with a bifunctional COOH-PEG_n-X. Carbamate linkages are introduced by first activating the two pendant hydroxyl groups into carbonate intermediate to render the further reaction with NH₂-PEG_n-NHBoc under milder conditions. Boc protecting group was cleaved to obtain free -NH₂ group and was subsequently reacted with -COOH terminated small molecules to obtain PMNB carbamate crosslinkers.

Chapter 2

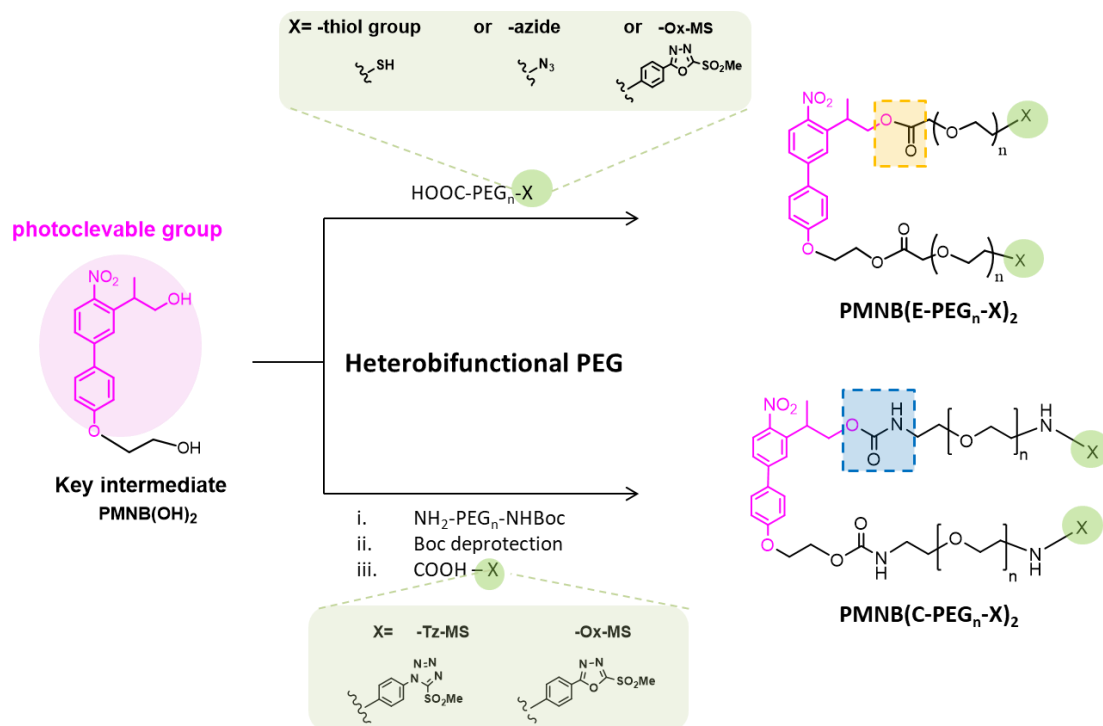


Figure 2.5 Chemical structures of functional two-photon degradable crosslinkers based on PMNB structure with ester labile bonds and carbamate labile bonds.

To compare the photolytic performance of PMNB hydrogels with previously reported chromophores from the literature, similar crosslinkers containing the *o*NB photocleavable group were also synthesized as control system (**Figure 2.6**). In this case, to minimize synthetic effort, the azide group ($X = \text{-N}_3$) was selected as terminal group for coupling to polymer backbones.

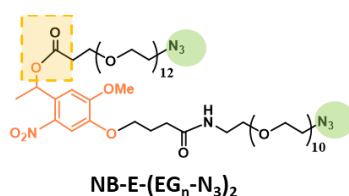


Figure 2.6 Chemical structure of NB-E-(EG_n-N₃)₂ with ester labile bond.

The crosslinker combinations used to prepare photodegradable hydrogels for cell encapsulation and dynamic cell culture in this **Thesis** are listed in **Table 2.3**.

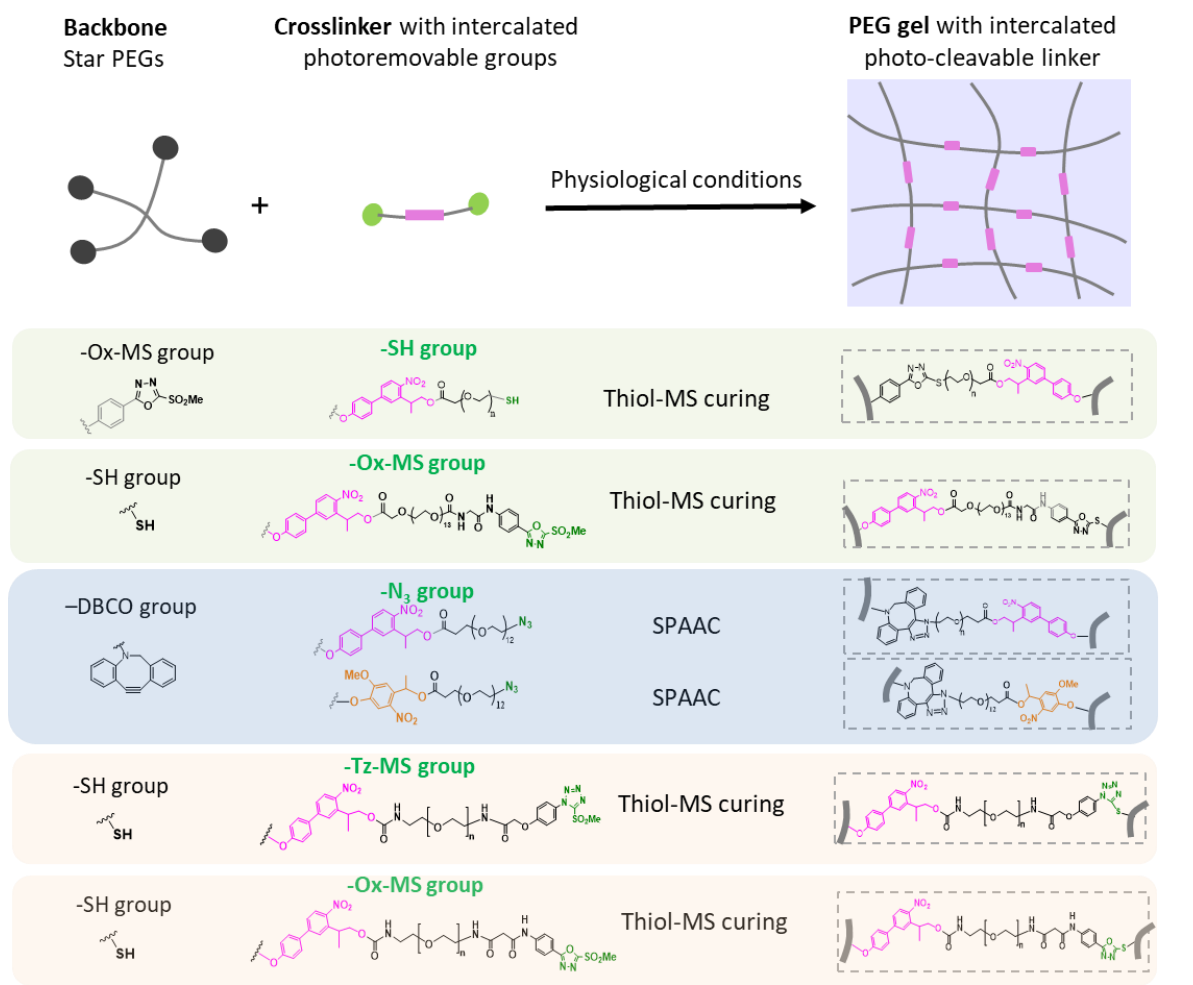


Table 2.3 Scheme of PEG hydrogels with intercalated photocleavable linker under physiological conditions.

2.3 Synthesis of photodegradable crosslinkers

2.3.1 Synthesis of PMNB ester crosslinkers

PMNB(OH)₂, (5)

The intermediate *PMNB(OH)₂* was synthesized in good yields following a previously described 5-step procedure with some modifications (**Figure 2.7**).¹⁹ The synthesis started with the acylation of *p*-bromo nitrobenzene at ortho position. The acylated compound **1** was obtained in good yield (70%). Its chemical structure was confirmed by ¹H-NMR after column purification. The singlet corresponding to the tert butyl ester (1.44 ppm, 9H) and a singlet corresponding to the methylene group (3.91 ppm, 2H) were visible in the spectrum. In the second step, the benzylic position was methylated by iodomethane through electrophilic methylation to afford **2** in 82% yield.¹⁵ The methyl substituent has been reported to enhance the quantum yield of derived chromophore.^{15, 37, 38} The success of the reaction was confirmed by the appearance of a doublet at 1.59 ppm (3H) corresponding to the methyl group and a multiplet at 4.20 ppm (1H) that corresponds to the -CH at the benzylic position. The bromide in **2** was reacted with 4-hydroxyphenylboronic acid by Suzuki coupling under microwave conditions to give **3**

Chapter 2

in 50% yield after column purification. The reaction product was confirmed by mass analysis ($m/z=366.2$ for $[M+Na]^+$) and the appearance of the signals corresponding to the aromatic ring (6.91-8.03 ppm) in 1H NMR. Compounds **1-3** were prepared in gram scale. Etherification of **3** with tert-butyl bromoacetate rendered **4** in 58% yield. The mass spectrum showed signal at 480.2 m/z corresponding to $[M+Na]^+$ of the expected product. The 1H -NMR spectrum showed a new singlet at 4.57 ppm (2H) corresponding to the methylene carbon, and a new singlet at 1.50 ppm (9H) from the tert butyl ester. The reduction of tert butyl ester groups to primary hydroxyls was achieved using DIBAL-H to afford **5** in 75% yield and high purity (>99%) after HPLC separation. Compound **5** was identified by mass spectrometry ($[M+H]^+$ 318.2 m/z) and by the disappearance of the tert butyl group signal and the appearance of multiplets at 3.84 ppm (2H), 4.01 ppm (2H) and 4.14 ppm (2H) that corresponds to the methylene carbons.

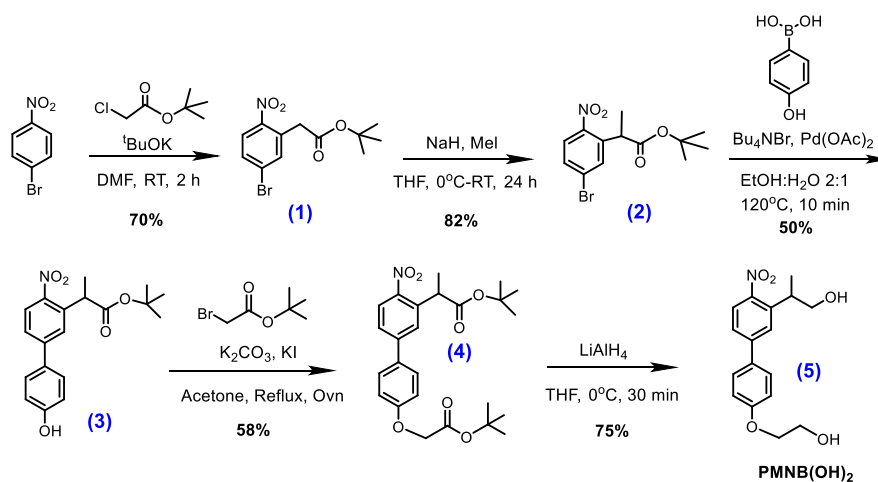


Figure 2.7 Synthetic route for the key intermediate PMNB(OH)₂ (**5**)

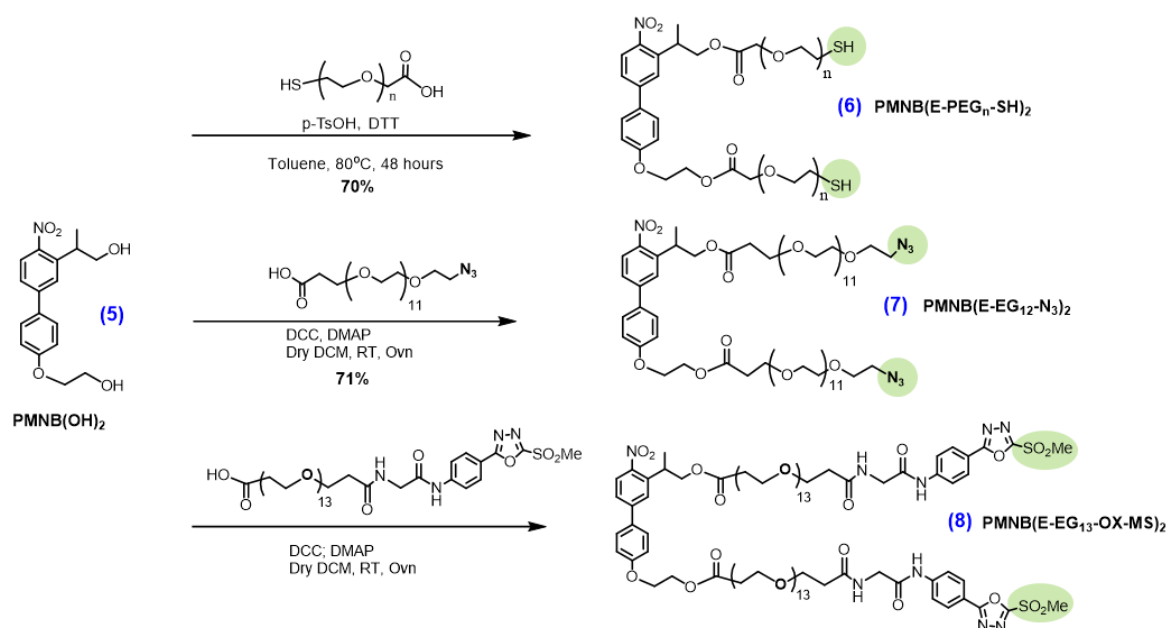


Figure 2.8 Synthesis route for PMNB(E-PEG_n-SH)₂, PMNB(E-EG₁₂-N₃)₂ and PMNB(E-EG₁₃-Ox-MS)₂

PMNB(E-PEG_n-SH)₂, (6)

The PMNB(E-PEG_n-SH)₂ crosslinker **6** was synthesized by reaction of PMNB(OH)₂ with COOH-PEG_n-SH (1 kDa) by modification of a previously described procedure (**Figure 2.8**).^{39, 40} DTT was used as reducing agent in order to avoid disulfide bond formation during the reaction and p-TsOH was used as catalyst. A large excess (10 eq.) of COOH-PEG_n-SH and a reaction time of 48 h was necessary to increase reaction yield of the disubstituted product to 70%. High yield of the disubstituted product was only achieved from commercial COOH-PEG_n-SH from Sigma Aldrich, which showed a narrower molecular weight distribution. The reason for this effect remains unknown at this point. The purity of **6** after purification was checked by HPLC (~90%) and the chemical structure was confirmed by ¹H-NMR and mass spectrometry. A complete consumption of PMNB(OH)₂ was observed (peak consumed at retention time 25 min) and a new peak at retention time 28 min was evident from analytical HPLC chromatogram (**Figure 2.9**). Mass analysis (**Appendix**) showed [M+2NH₄]²⁺ signal at m/z = 1307.2. The ¹H-NMR (**Appendix**) spectrum showed a new proton signal corresponding to -SH at 1.61 ppm and a multiplet at 3.5-3.7 ppm corresponding to the methylene units of the PEG chain. These results demonstrated the successful synthesis of the target compound with high purity. PMNB(E-PEG_n-SH)₂ was soluble in PBS, HEPES buffer and cell culture medium at up to 10 wt% concentration.

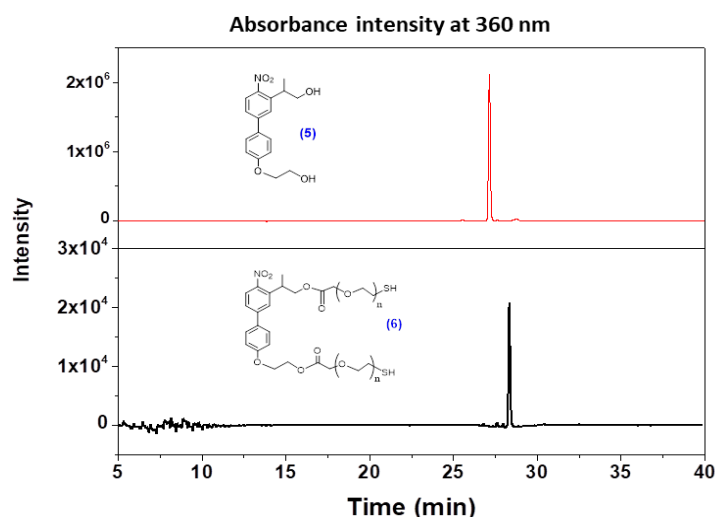


Figure 2.9 Analytical RP-HPLC chromatograms of PMNB(E-PEG_n-SH)₂ vs. intermediate PMNB(OH)₂.

PMNB(E-EG₁₂-N₃)₂, (7)

The azide-functionalized PMNB crosslinker was obtained in two-step, as opposed to -SH or -MS groups that required 3 and 5 steps, respectively. The introduction of terminal azide groups for conjugation was considered advantageous since -N₃ group is biorthogonal to many other functional groups and this facilitates upscaling. PMNB(E-EG₁₂-N₃)₂ was synthesized by esterification of PMNB(OH)₂ with COOH-PEG₁₂-N₃ using DMAP as base and DCC as coupling agent (**Figure 2.8**). The product was obtained in 71% yield and was soluble in water at a concentration of 10 wt%. The purity of the compound was 94% according to analytical HPLC chromatography, and the corresponding signal appeared at

Chapter 2

retention time 32 min (**Figure 2.10**). Mass spectrometry analysis confirmed the chemical structure of the product with a $[M+NH_4]^+$ peak at $m/z = 1585.8$ (**Appendix**). The 1H -NMR spectrum showed an intense and broad multiplet at 3.50-3.66 ppm (93 H) corresponding to the methylene protons of the PEG chain (**Appendix**).

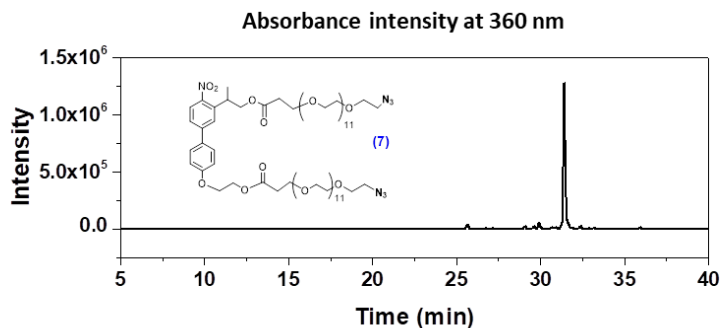


Figure 2.10 Analytical RP-HPLC chromatograms of PMNB(E-EG₁₂-N₃)₂

PMNB(E-EG₁₃-Ox-MS)₂, (8)

The synthesis of PMNB(E-EG₁₃-Ox-MS)₂, (**8**) required 4 steps (**Figure 2.8&11**) since the hetero-bifunctional PEG carrying -MS and -COOH groups is not commercially available. The MS-PEG₁₃-COOH intermediate was prepared in 3 steps according to previously reported protocols.^{31, 32, 41, 42} The synthesis started by N-acylation of 4-(5-(methylsulfonyl)-1,3,4-oxadiazol-2-yl)aniline with Boc-Gly-OH using isobutyl chloroformate in a one-pot reaction. A protected amine group was necessary to avoid reaction between amine and isobutyl chloroformate, and thus **9** was chemoselectively obtained in good yield (73%). The reaction product was confirmed by mass spectrometry ($m/z=419.0$ for $[M+Na]^+$) and the appearance of new signals from the aromatic ring (7.91-8.10 ppm, 4 H) and methyl protons (3.63 ppm, 3 H) corresponding to the -SO₂Me group in the 1H -NMR spectrum (**Appendix**). After Boc-cleavage in acidic conditions, the free amine of **10** was obtained and coupled to the NHS group of NHS-PEG₁₃-COOH. Compounds **10** and **11** were obtained in 67 and 52% yield, respectively. Compound **10** was identified by the $m/z = 297.1$ ($[M+H]^+$) and the disappearance of the signal corresponding to the -Boc group (1.43 ppm) in the 1H -NMR spectrum (**Appendix**). It should be noted that **10** showed low stability and decomposed in < 1 day. Therefore, compound **10** was always freshly prepared before use. Compound **11** was identified by the $[M+NH_4]^+$ signal at $m/z = 986.4$ in the mass spectrum (**Appendix**) and by the appearance of the methylene protons of the PEG chain (3.48 -3.8 ppm) in the 1H -NMR spectrum (**Appendix**). The final compound **8** was obtained by esterification of PMNB(OH)₂ with **11**. HPLC chromatography was used to purify compound **11**. The product was characterized by mass and NMR analysis. 1H -NMR analysis showed the protons from PEG spacer (3.50-3.66 ppm, 96H), the aromatic protons from the biphenyl unit (7.02-7.64 ppm, 7H) and the protons from the arylmethylsulfone group (7.84-8.06 ppm, 8H and 3.48 ppm, 6H). Mass spectrometry analysis confirmed the chemical structure of the product with a $[M+2NH_4]^{2+}$ peak at $m/z = 1127.50$ (**Appendix**). The corresponding integrals matched expected values and confirmed the identity of the product. However, the determination of the purity of the compound by HPLC chromatography proved difficult (**Figure 2.12**). Multiple peaks were observed with similar retention times in analytical HPLC after

purification, presumably due to the presence of some impurities. Of note, dialysis method was also performed, but failed to purify the compound, presumably due to the low molecular weight (~2 kDa) of the linker, which was limited by the pore size distribution of commercial dialysis membrane.

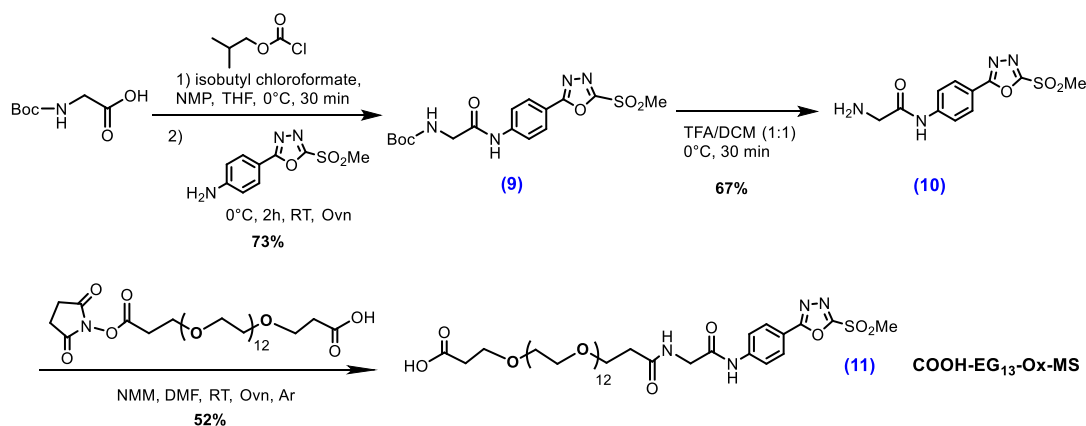


Figure 2.11 Synthesis route for compound 11.

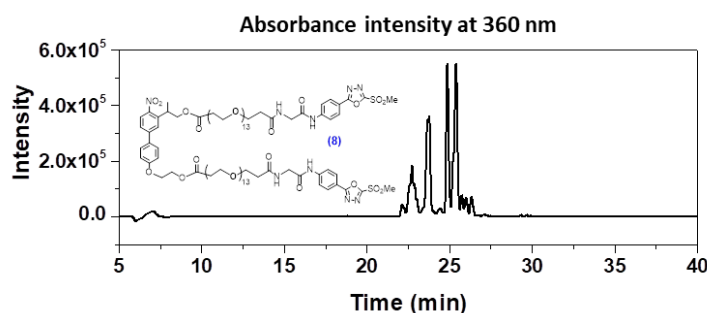


Figure 2.12 Analytical RP-HPLC chromatograms of PMNB(E-EG₁₃-Ox-MS)₂ before HPLC purification

2.3.2 Synthesis of control crosslinker

NB-E-(EG_n-N₃)₂ (13)

NB-E-(EG_n-N₃)₂ was synthesized in two steps (Figure 2.13) by sequentially introducing EG-N₃ arms to commercially available 4-[4-(1-hydroxyethyl)-2-methoxy-5-nitrophenoxy] butyric acid. The first reaction involved the amidation of the carboxylic group with NH₂-PEG₁₀-N₃ to obtain OH-NB-EG₁₀-N₃, **12** at yield of 90%. The reaction product was confirmed by the [M+H]⁺ peak in the mass spectrum at m/z = 808.4, and by the appearance of the methylene protons from PEG spacer (3.56 -3.66 ppm, 84H) in the ¹H-NMR spectrum (Appendix). HPLC analysis showed a new peak at retention time of 26 min (Figure 2.14). The final product NB-E-(PEG_n-N₃)₂, **13** was obtained by the esterification of **12** with COOH-PEG₁₂-N₃ at yield of 88 %. The mass analysis showed the [M+2NH₄]²⁺ signal of the expected product at m/z = 734.3. This control crosslinker has similar molar mass compared to PMNB(E-EG₁₂-N₃)₂ but a bit lower than PMNB(E-PEG_n-SH)₂ and PMNB(E-EG₁₃-Ox-MS)₂. The similar molecular weight between crosslinkers to be used for the formation of a polymer network analogues typically enables the obtention of materials with similar mechanical response, and thus allows direct comparison. The

Chapter 2

$^1\text{H-NMR}$ spectrum (**Appendix**) showed new signals at 2.61 ppm and 3.38 ppm corresponding to methylene protons of $\text{COOH-PEG}_{12}\text{-N}_3$. HPLC analysis showed a new peak at retention time of 27.5 min (**Figure 2.14**). A purity of 93% was determined by HPLC chromatography. $\text{NB-E-(PEG}_n\text{-N}_3)_2$ was soluble in PBS at 10 wt% concentration.

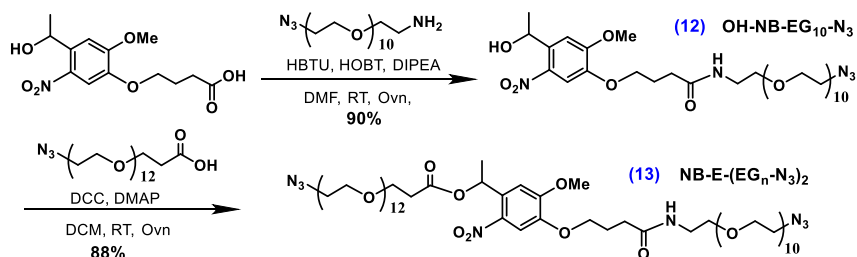


Figure 2.13 Synthesis route for $\text{NB-E-(EG}_n\text{-N}_3)_2$

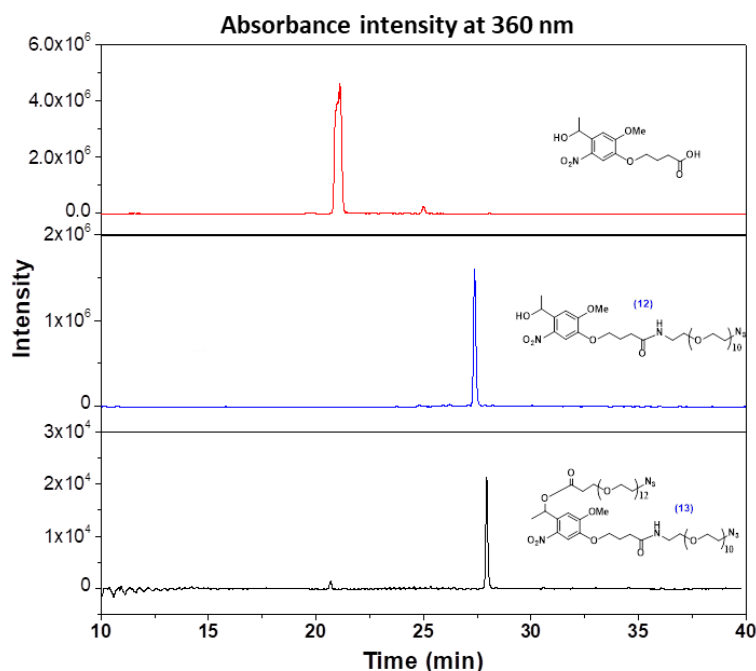


Figure 2.14 Analytical RP-HPLC chromatograms of $\text{NB-E-(EG}_n\text{-N}_3)_2$ vs. 4-[4-(1-hydroxyethyl)-2-methoxy-5-nitrophenoxy] butyric acid and $\text{OH-NB-EG}_{10}\text{-N}_3$

2.3.3 Synthesis of PMNB carbamate crosslinkers

$\text{PMNB(C-EG}_{11}\text{-Tz-MS)}_2$ (25)

In order to obtain carbamate bonds, 4-nitrophenyl chloroformate was used to activate the hydroxyl groups of compound **5** in the presence of base (triethylamine, Et_3N). The intermediate **14** was obtained at high yield of 83% and its chemical structure was confirmed by $^1\text{H-NMR}$ and mass analysis after HPLC purification. The analytical HPLC chromatogram (**Appendix**) showed a new peak at retention time 37 min. Mass analysis (**Appendix**) showed $[\text{M}+\text{NH}_4]^+$ signal at $m/z = 665.2$. The $^1\text{H-NMR}$ (**Appendix**) spectrum showed new signals corresponding to aromatic protons from the nitrophenyl unit (8.22-8.31 ppm, 4H and 7.28-7.42 ppm, 4H). Worth noting, compound **14** showed good stability

as solid up to 1 month under storage at -20°C . Compound **14** was reacted with amine-substituted hetero-bifunctional PEG(NH_2 -PEG $_n$ -X). In addition, for coupling with star PEGs, X= -SH or -MS were considered as terminal groups (Figure 2.15).

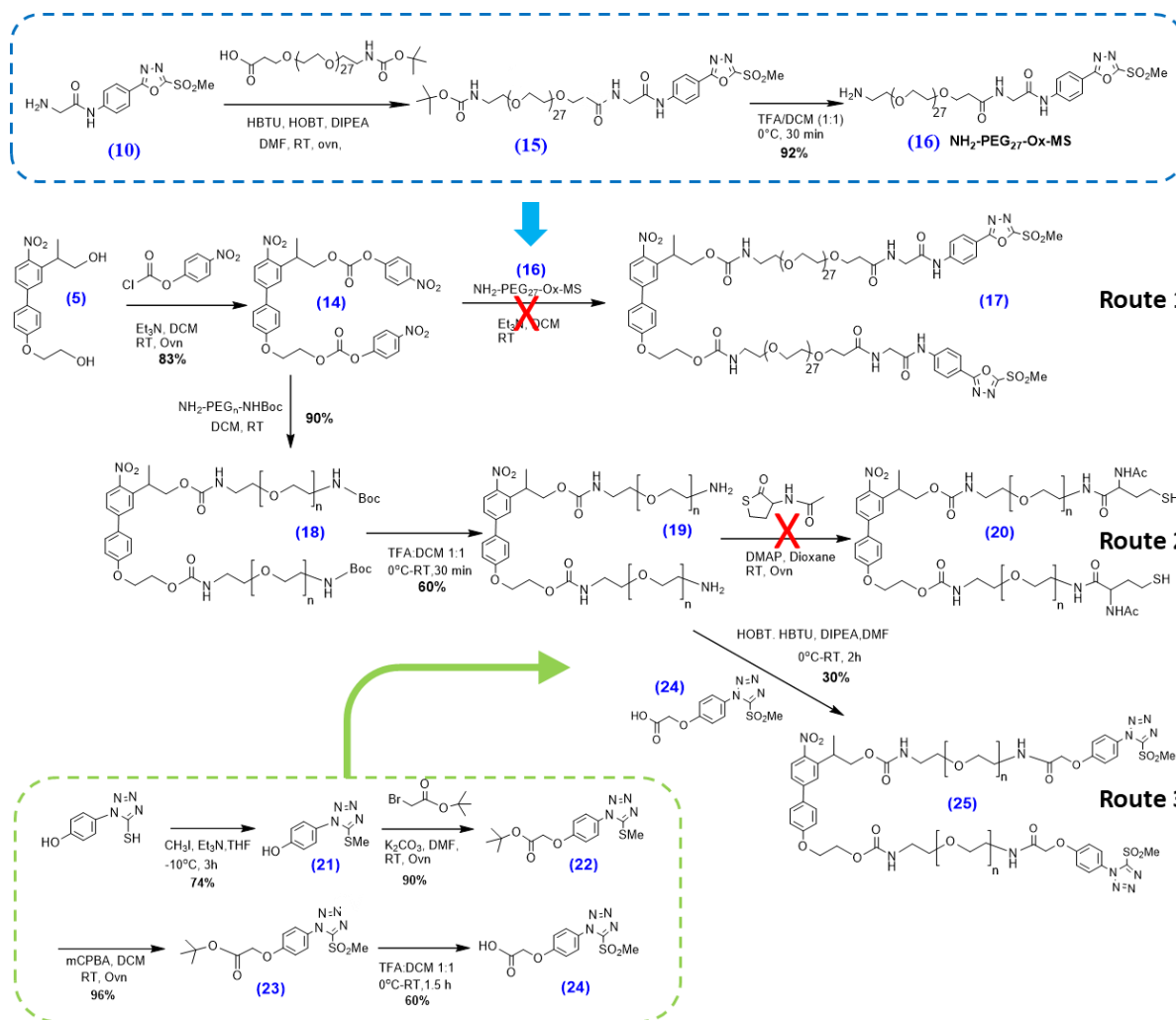
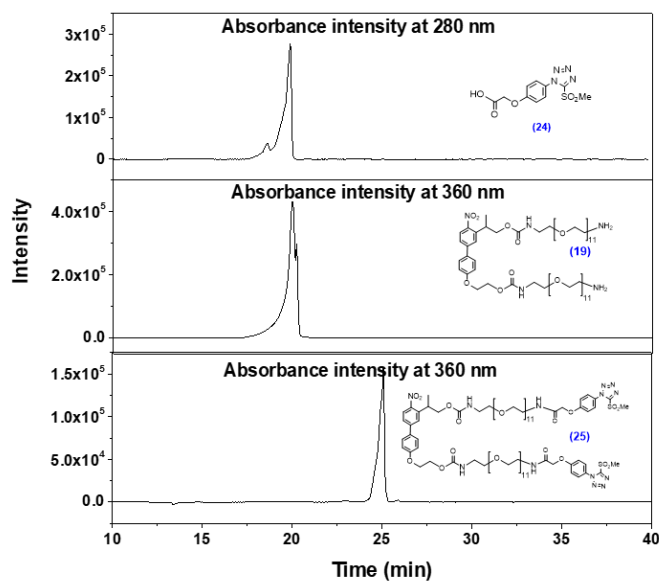
A first route to PMNB carbamate crosslinker, **17** was performed by reacting **14** and NH_2 -PEG $_{27}$ -Ox-MS, **16**. Compound **16** was obtained in a 3-step procedure starting from **10**. The $-\text{NH}_2$ group of **10** was coupled with free $-\text{COOH}$ group of COOH -PEG $_{27}$ -NHBoc to obtain **15**. The mass analysis (Appendix) showed the $[\text{M}+2\text{NH}_4]^{2+}$ signal of the expected product at $m/z = 867.9$. The purification of the **15** by HPLC chromatography proved challenging since some impurities remained. Therefore, compound **15** was used for the next step without further purification. The deprotection of -Boc groups of **15** to free $-\text{NH}_2$ groups was achieved using TFA/DCM to afford **16** with a purity of 92% after HPLC separation. Compound **16** was identified by mass spectrometry ($[\text{M}+\text{NH}_4]^{2+}$, $m/z = 809.4$ m/z) and the appearance of $-\text{NH}_2$ group signal at 3.15 ppm (2H). Aminolysis of nitrophenyl carbonate of **14** to obtain **17** was firstly performed without base at room temperature. The reactants remained unreacted even after 24 h, as evidenced by HPLC. We hypothesized that the long and flexible PEG chain of **16** are folded, therefore, the free $-\text{NH}_2$ are hindered and not available for coupling. To overcome this, the reaction temperature was increased to 40°C and reaction was conducted overnight, however no success was observed from HPLC. Moreover, a base (Et_3N) was added to promote the conversion of reaction.⁴³ However, the increased reaction rate also leads to various side products which might due to the hydrolysis of -MS group. No relevant mass corresponding to the expected compound was detected from mass analysis. No further attempts to optimize this reaction condition were conducted.

A second route was carried out. Compound **18** was synthesized under milder condition (no base and heating were needed) by reacting **14** with a shorter $-\text{NH}_2$ functionalized PEG in which the second $-\text{NH}_2$ is protected by -Boc group. The product was obtained with 90% yield since the compound **14** hydrolyzed to small extent during reaction. This reaction was proved successful by mass spectrometry ($m/z=846.9$ for $[\text{M}+2\text{NH}_4]^{2+}$) and the appearance of new signals from -Boc group (1.42 ppm, 18H) and methylene protons from PEG spacer (3.46 -3.64 ppm, 88H) in the ^1H -NMR spectrum (Appendix). The deprotection of -Boc to get free amine groups was achieved using TFA/DCM to afford, **19** in yield (60%) and purity (>98%) after HPLC separation. Compound **19** was identified by mass spectrometry ($[\text{M}+2\text{H}]^{2+}$ 729.9 m/z) and by the disappearance of the -Boc group signal at 1.42 ppm (18H) and appearance of $-\text{NH}_2$ group signal at 3.10 ppm (4H). Synthesis of compound **20** was attempted by reacting **19** with 2-acetamido-4-mercaptopbutyric acid- γ -thiolactone based on thiolactone chemistry. However, a low degree of thiolation of the crosslinker was achieved with excess thiolactone compound vs. $-\text{NH}_2$ groups, while excess $-\text{NH}_2$ vs. thiolactone compound are typically used in the literature to ensure the high thiolation degree.⁴⁴ No further attempts to optimize thiolation condition were carried out in this thesis.

Based on the second route, converting $-\text{NH}_2$ into other functional group (e.g. -MS group) would be an attractive alternative for later coupling with star PEGs carrying thiol groups. A small linker compound containing $-\text{Tz}$ -MS and $-\text{COOH}$ groups was envisioned as suitable for coupling with **19**. Compound **24** was synthesized in a 4-step procedure starting from commercial 1-(4-Hydroxyphenyl)-5-mercaptopotrazole. The first reaction involves the methylation of the -SH group with methyl iodide

Chapter 2

(CH₃I) to obtain **21** at yield of 74%. The reaction product was confirmed by the [M+H]⁺ peak in the mass spectrum at m/z = 209.0, and the appearance of protons from methyl group (2.79 ppm, 3H) in the ¹H-NMR spectrum (**Appendix**). Etherification of **21** with tert-butyl bromoacetate at room temperature rendered **22** with a purity of 90% after extraction, which was confirmed by ¹H-NMR spectrum (**Appendix**). Compound **22** was used in the next step without further purification. The -SMe group of **22** was oxidized by meta-Chloroperoxybenzoic acid (mCPBA) to give **23** in high yield after HPLC purification (96%). Reaction was monitored by mass analysis since the starting compound and product were eluting together in TLC and HPLC. The reaction product was confirmed by mass analysis (m/z=372.1 for [M+NH₄]⁺) and the appearance of the signals corresponding to the -SO₂Me (3.63 ppm, 3H) in ¹H NMR. The acidic cleavage of tert butyl group to give -COOH was achieved using TFA/DCM to afford **24** in a moderate yield (60%) after HPLC separation. The reaction product was confirmed by mass spectrometry ([M+ NH₄]⁺ at m/z = 316.0) and by the disappearance of the tert butyl group signal at 1.47 ppm (9H). Of note is that compound **24** showed good stability as solid up to 2 weeks under storage at -20°C (confirmed by NMR analysis). PMNB carbamate crosslinker PMNB(C-EG₁₁-Tz-MS)₂, **25** was synthesized by reacting **19** and **24** via coupling reaction using HBTU and HOBT as coupling agents. This reaction was completed in 2 hours at room temperature, as monitored by HPLC. HPLC analysis showed a new peak at retention time of 25 min (**Figure 2.16**). A purity of 95% was determined by HPLC chromatography. ¹H-NMR analysis showed the protons from PEG spacer (3.40-3.67 ppm, 88H) and the aromatic protons from (7.02-7.64 ppm, 7H). The protons from the methylsulfone group (6H, expected at around 3.6 ppm) could not be identified since the peaks were overlapped with PEG core signal in ¹H-NMR spectrum. Therefore, the appearance of signal corresponding to -SO₂Me (44.35 ppm) in ¹³C-NMR analysis was used to confirm the product. Mass spectrometry analysis confirmed the chemical structure of the product with a [M+2NH₄]²⁺ peak at m/z = 1027.0 (**Appendix**). To ensure solubility, OEG arms with n=15 were also attached to it to yield PMNB(C-EG₁₅-Tz-MS)₂ by following same synthetic route.

Figure 2.15 Different synthesis routes for PMNB(C-EG_n-Tz-MS)₂Figure 2.16 Analytical RP-HPLC chromatograms of PMNB(C-EG₁₁-Tz-MS)₂ vs. compound 19 and compound 24

Chapter 2

PMNB(C-EG_n-Ox-MS)₂, (28)

A small linker compound containing –Ox-MS and –COOH groups was first synthesized for further coupling with **19**. Compound **27** was synthesized in a 2-step procedure starting from commercial tert-butyl malonate and 4-(5-(methylsulfonyl)-1,3,4-oxadiazol-2-yl)aniline (**Figure 2.17**). The first reaction involves the coupling of carboxylic acid with amine groups using HBTU and HOBT as coupling agents to obtain **26** at relatively low yield (30%). The reaction product was confirmed by the [M+H]⁺ peak in the mass spectrum at m/z = 382.2, and the appearance of protons from methyl group (3.64 ppm, 3H), aromatic ring (7.9-8.1 ppm, 4H) and tert butyl group (1.46 ppm, 9H) in the ¹H-NMR spectrum (**Appendix**). The acidic cleavage of tert butyl group to give –COOH was achieved using TFA/DCM to afford **27** in a moderate yield (68%) after HPLC separation. The reaction product was confirmed by mass spectrometry ([M+NH₄]⁺ at m/z = 343.2) and by the disappearance of the tert butyl group signal at 1.46 ppm (9H). Worth noting, compound **27** showed good stability as solid up to 2 months under storage at -20°C. PMNB(C-EG₁₅-Ox-MS)₂, **28** was synthesized by reacting **19** and **27** using HBTU and HOBT as coupling agents in a yield of 71% (**Figure 2.17**). ¹H-NMR analysis showed the protons from PEG spacer (3.52-3.65 ppm, 121H) and the aromatic protons from (7.01-8.08 ppm, 15H). The mass analysis (**Appendix**) showed the [M+2NH₄]²⁺ signal of the expected product at m/z = 1230.0. To ensure solubility, OEG arms with n=23 were also attached to it, to yield PMNB(C-EG₁₅-Ox-MS)₂ by following same synthetic route.

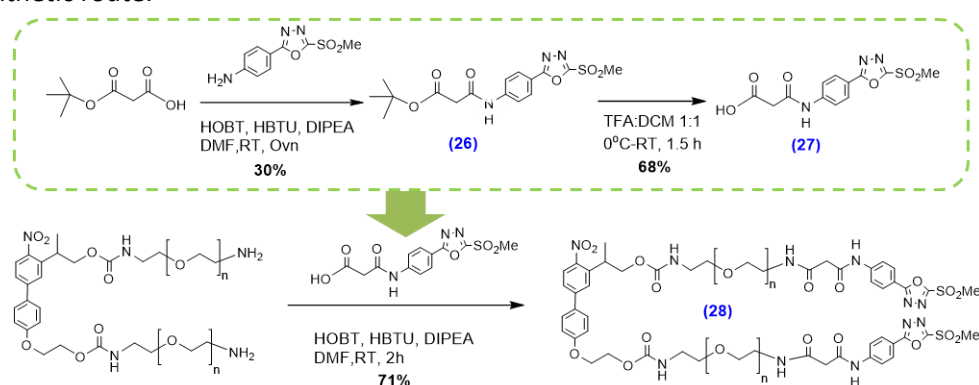


Figure 2.17 Synthesis routes for PMNB(C-EG_n-Ox-MS)₂

2.4 Synthesis of star PEG-hydrogel precursors

Star PEGs (20 kDa) functionalized with -Ox-MS and -DBCO terminal groups were obtained by derivatization of commercially available star PEGs with reactive end groups. A high degree of substitution degree of PEG macromers is necessary to achieve high crosslinking degree and thus to build stable and predictable hydrogel networks. Therefore, one-step reactions -with expected high yield were selected for PEG modification, in order to have end-group functionalization degrees close to 100%. Purification of the derivatized star PEGs was performed by dialysis.

Star PEG-Ox-MS

Star PEG-Ox-MS was synthesized by terminal group modification of star PEG-COONHS with the arylmethylsulfone precursor, 2-amino-N-(4-(5-(methyl sulfonyl)-1,3,4-oxadiazol-2-yl) phenyl) acetamide, following a reported protocol (**Figure 2.18**).³² The NHS activated carboxylic acid reacted

with the free amine in the presence of NMM as a base. The crude was dialyzed against water/acetone. $^1\text{H-NMR}$ analysis confirmed the coupling of the MS group by the appearance of the methyl sulfone protons as a singlet at 3.48 ppm (3H) and the protons of the phenyl-oxadiazole ring at 7.83-8.08 ppm (4H). The substitution degree was estimated by end-group determination from the integrals of the $^1\text{H-NMR}$ spectrum (**Figure 2.19**). The integral of the PEG core (3.5-3.6 ppm) was set to 440H and related to the integral of the protons of the phenyl-oxadiazole ring (7.83-8.08 ppm, 4H). A functionalization degree of >88% was obtained, which is at the reasonable range of functionalization. The Star PEG-Ox-MS polymer was obtained in a 200 mg scale and showed long-term stability over 6 months under storage at -20°C .

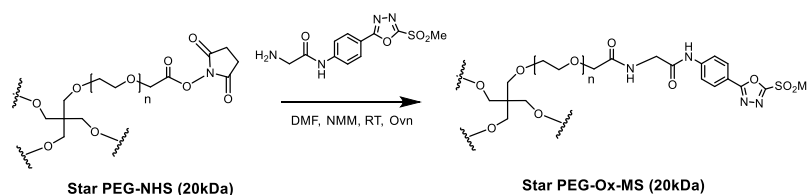


Figure 2.18 Synthesis route for star PEG-Ox-MS

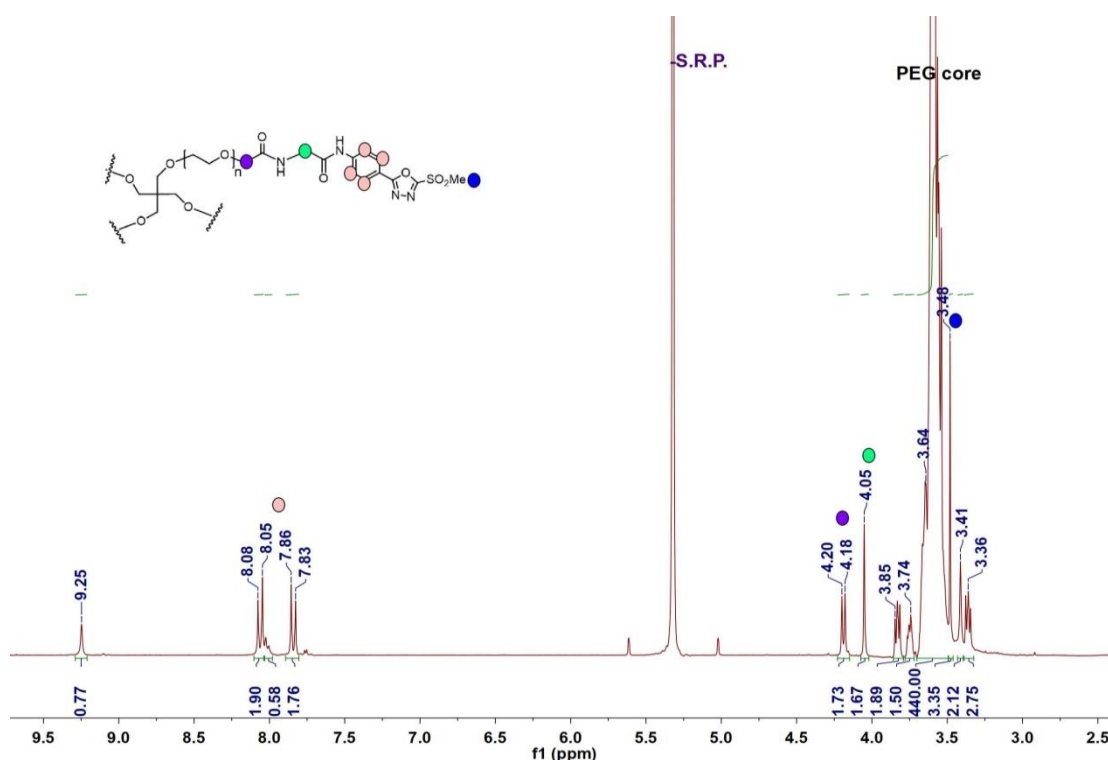


Figure 2.19 $^1\text{H-NMR}$ of star PEG-Ox-MS

Star PEG-DBCO

Star PEG-DBCO was first synthesized by reacting star PEG-COONHS and DBCO-NH₂ in the presence of a base (NMM). However, a polymer with low substitution degree was obtained. A second condition was studied: star PEG-DBCO was synthesized by reacting star PEG-COOH and DBCO amine in presence of coupling agents (HOBT and HBTU) and a base (DIPEA). A high substitution degree was obtained but with low reproducibility even in high excess molar ratio of DBCO-NH₂ to star PEG-COOH (4:1) and long

Chapter 2

reaction time (up to 72 hours). Therefore, a third condition was selected according to previously reported protocols (**Figure 2.20**).⁴⁵ Star PEG-DBCO was synthesized by reacting star PEG-NH₂ with DBCO-COONHS in the presence of Et₃N. In order to maximize reaction conversion, the reaction was also tested in the presence of NMM. The reaction in Et₃N rendered higher conversion values (92%) than NMM (50%). Based on reported mechanism (**Figure 2.21**), a zwitterionic intermediate is generated from NHS ester and primary or secondary amines, which is followed by a rate-determining breakdown to afford amide product by two concurrent pathways, a noncatalyzed pathway, k'_1 , and a general-base catalyzed pathway, k'_2 . During aminolysis, a base is used to deprotonate the amine to get the final product. In this reaction, the use of NMM as a weaker base (pKa: 7.38) than TEA (pKa: 10.9) resulted in a lower substitution degree. We hypothesized that a stronger base is required efficiently promote the reaction.

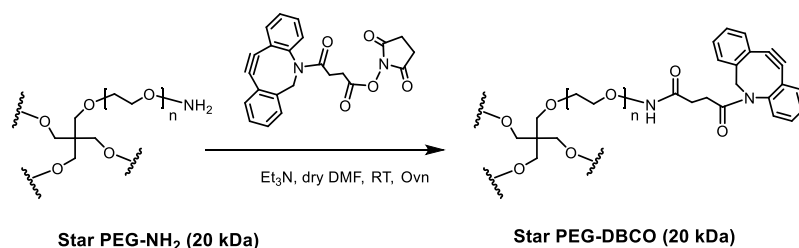


Figure 2.20 Synthesis route for star PEG-DBCO

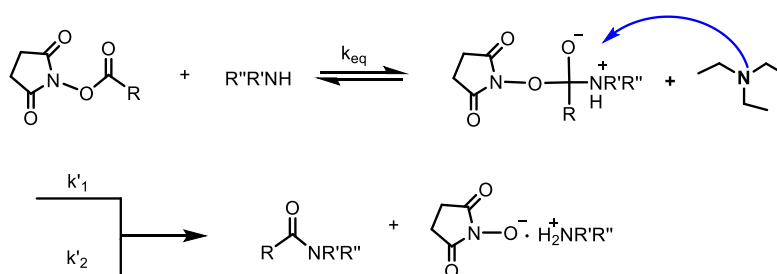


Figure 2.21 Mechanism of the aminolysis of -NHS ester to form amide bonds

The chemical structure of the product after dialysis was confirmed by the appearance of signals corresponding to the aromatic protons (7.25-7.67 ppm, 8H) and methylene protons (5.14 ppm) of the cyclooctyne ring in the ¹H-NMR spectrum (**Figure 2.22**). The substitution degree was calculated by the ratio of the methylene proton signal from cyclooctyne ring to the methylene signal of the PEG chain. The star PEG-DBCO polymer was obtained in a 200 mg scale. This reaction is considered a robust approach for preparation of DBCO substituted PEG polymers. However, star PEG-DBCO showed poor stability and signs of decomposition during 2-3 weeks of storage at -20°C under argon atmosphere. This was confirmed by ¹H-NMR by the progressive disappearance of the -CH₂ proton signal from DBCO ring. Therefore, the star PEG-DBCO polymer was always freshly prepared before use for hydrogels.

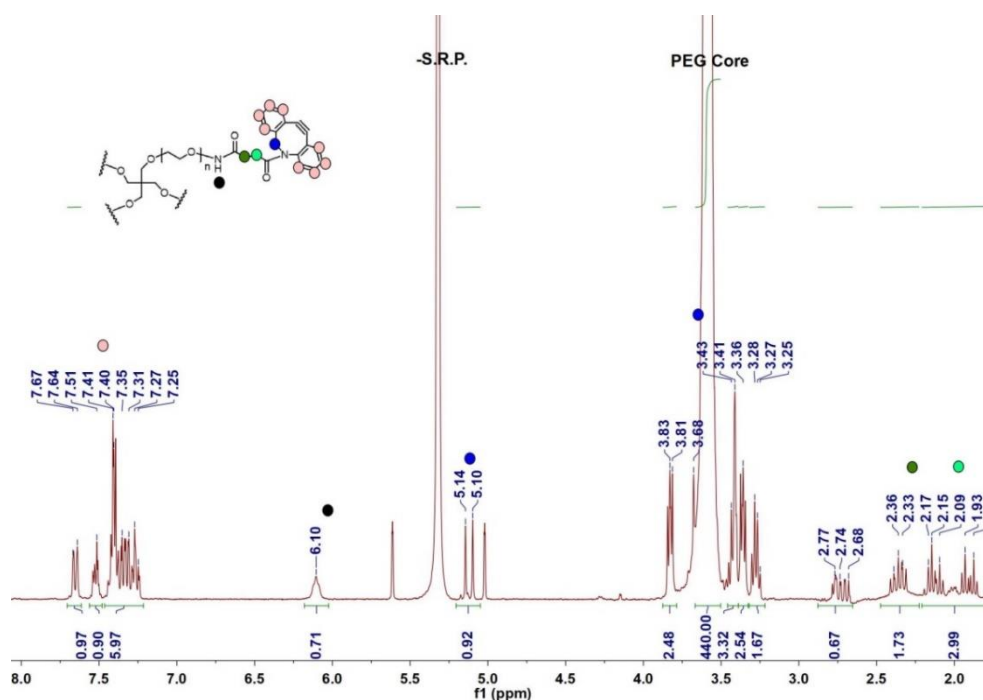


Figure 2.22 $^1\text{H-NMR}$ of star PEG-DBCO

2.5 Photochemical properties of $\text{PMNB}(\text{E-PEG}_n\text{-SH})_2$ and $\text{NB-E}(\text{EG}_n\text{-N}_3)_2$

The photolysis of $\text{PMNB}(\text{E-PEG}_n\text{-SH})_2$ (**6**) and $\text{NB-E}(\text{EG}_n\text{-N}_3)_2$ (**13**) at different light exposure conditions (365 and 420 nm and increasing exposure times) was monitored by UV/Vis spectroscopy of irradiated solutions, and analyzed quantitatively by HPLC. Light of 365 or 420 nm was used in the studies, since these are more convenient wavelengths to minimize phototoxicity in the cell studies. Typical irradiation conditions, such as 365 nm light, Irradiance = $5\text{--}20 \text{ mW cm}^{-2}$, $t = 2\text{--}20 \text{ min}$ (total dose $5\text{--}10 \text{ J cm}^{-2}$)^{46, 47} or 420 nm, irradiance 1.55 mW cm^{-2} , $t = 6\text{--}12 \text{ h}$ (total dose $29\text{--}63 \text{ J cm}^{-2}$) have been demonstrated cytocompatible to the cells.⁴⁸ The changes in the absorbance bands of the UV spectra and a decay of the integral of the HPLC signal as a function of irradiation time (to follow reaction conversion) were monitored to quantify the kinetics of the 1P photolysis reaction in order to have a comparison for reported chromophores and would be useful for the 1P-induced cellular applications.

$\text{PMNB}(\text{E-PEG}_n\text{-SH})_2$

The UV/Vis spectrum of $\text{PMNB}(\text{E-PEG}_n\text{-SH})_2$ (**Figure 2.23**) showed an absorption maximum at $\lambda_{\text{max}} = 317 \text{ nm}$. Upon irradiation at 365 nm, the intensity of this band decreased, and two new maxima appeared at 390 nm and 520 nm, already after 10 s of exposure. The intensity of the band at 520 nm decreased after 40 s exposure, suggesting that it could correspond to the formation and consumption of a photolysis intermediate. The intensity of the band at 390 nm increased until 90 s. Clear isosbestic points were observed at $\lambda = 303 \text{ nm}$ and 365 nm , suggesting that the photolysis reaction occurs through a single pathway without side reactions. No further changes were observed in the spectrum after 2 min of irradiation. ESI-MS analysis of the irradiated solution at 60 s corroborated the expected photolysis products: *o*-nitrostyrene ($m/z = 776.23$ for $[\text{M}+2\text{NH}_4]^{2+}$) and $\text{COOH-PEG}_n\text{-SH}$ ($m/z = 1073.30$ for $[\text{M}+\text{H}]^+$).

Chapter 2

Similar changes were also observed after exposure at 420 nm: the initial absorbance band at 315 nm gradually diminished while absorbance bands appeared at 390 nm and 520 nm. Isosbestic points were observed at 303 nm and 365 nm. These similarities indicate that the same photolysis mechanism is taking place at both wavelengths. However, 4 min of irradiation was needed for the complete photocleavage of PMNB(E-PEG_n-SH)₂, which is longer than at 365 nm, presumably due to the lower absorbance at 420 nm. ESI-MS analysis of an irradiated aliquot (t= 90 s) corroborated the expected photolysis product: *o*-nitrostyrene product ($m/z = 732.89$ for $[M+2NH_4]^{2+}$) and COOH-PEG_n-SH ($m/z = 1073.30$ for $[M+H]^+$).

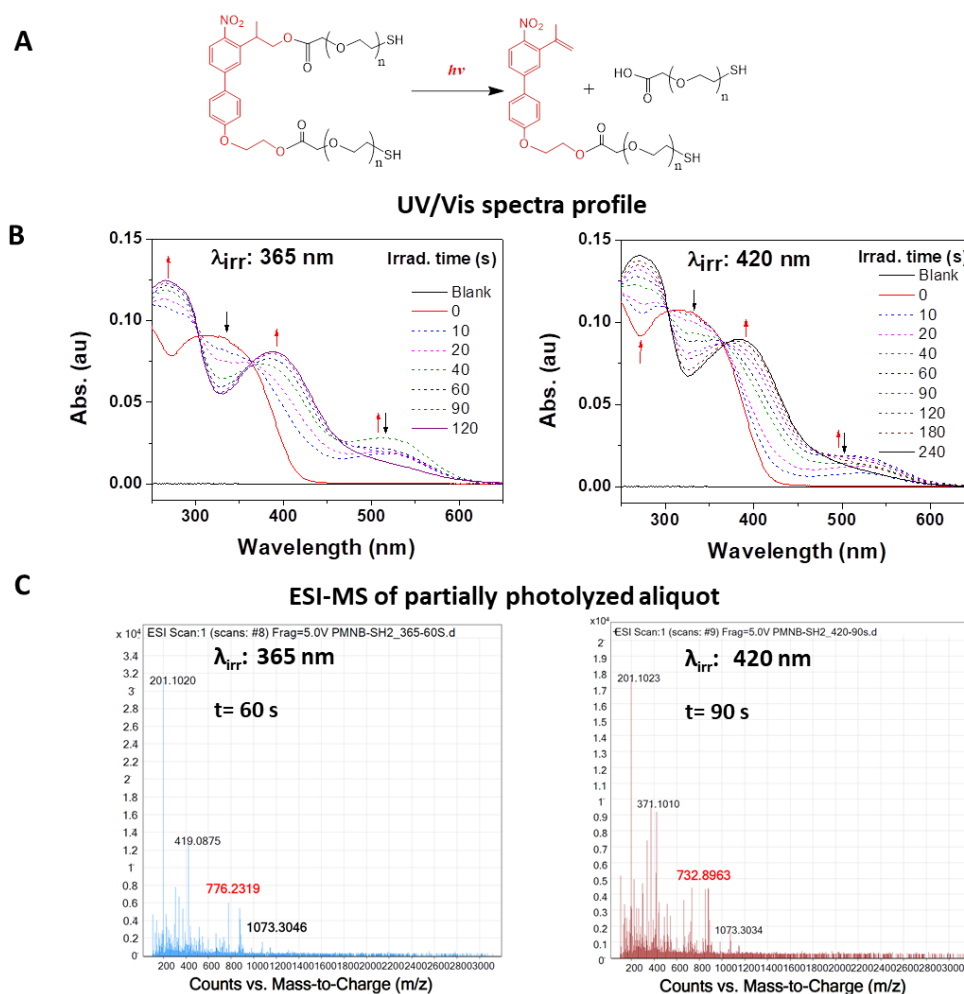


Figure 2.23 (A) Photochemical reaction expected for PMNB(E-PEG_n-SH)₂ in solution. (B) UV/Vis spectra evolution of PMNB(E-PEG_n-SH)₂ solution during photolysis (0.10 μ M, ACN/H₂O (1:1)). (C) ESI-MS analysis of photolyzed solution. Conditions: Irradiation wavelength = 360 nm and 420 nm, irradiance = 1.2 mW cm⁻².

The kinetics of the photolysis reaction was quantified by analyzing the consumption of the starting compound during irradiation by analytical HPLC (**Figure 2.24A and Appendix**). In the HPLC analysis, the starting crosslinker showed retention time at 28 min. It should be noted that the COOH-PEG_n-SH signal cannot be detected in HPLC. After illumination for 10 seconds, HPLC analysis showed a decay in PMNB(E-PEG_n-SH)₂ signal at 28 min and the parallel appearance of new signals at 26 min and 31 min. The signal at 31 min decreased over time, whereas the signal at 26 min continuously increased. Additional peaks were also observed at longer exposure times, suggesting the formation of byproducts

during photolysis as consequence of side reactions, probably the reaction between styrene-like side product and –SH groups, or the self-polymerization reactions proposed in the literature for styrene.⁴⁹ We did not further characterize fragmentation mechanism in this chapter.

The photolysis of PMNB(E-PEG_n-SH)₂ was faster at 365 nm than at 420 nm (**Figure 2.24B**): 93% of PMNB(E-PEG_n-SH)₂ was consumed in 2 min of irradiation at 365 nm, while 4 min were required when irradiating at 420 nm. A 90% photolysis conversion for PMNB-glutamate under 364 nm illumination was reported by Bolze et al.¹⁷ However, a direct comparison is not possible since the concentrations used for the studies were different.

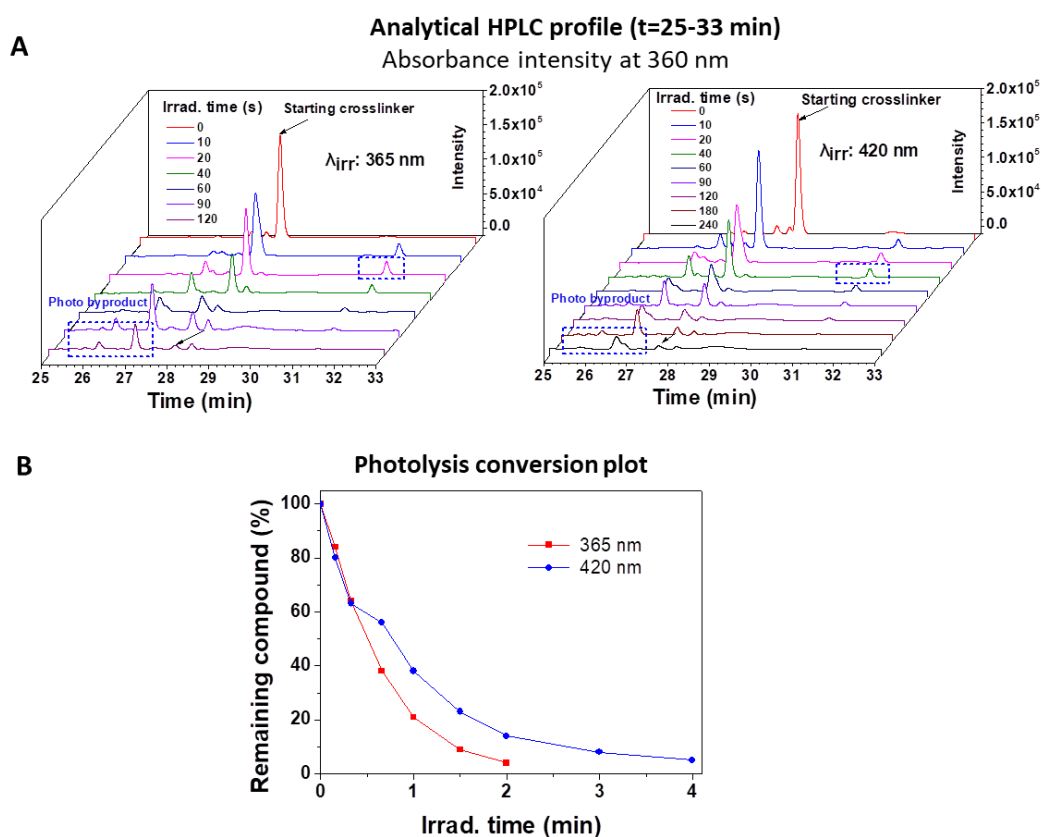


Figure 2.24 (A) Analytical HPLC profile of PMNB(E-PEG_n-SH)₂ aliquots before and after irradiation. **(B)** Comparison of photolysis conversion as function of exposure time for PMNB(E-PEG_n-SH)₂ solution at different irradiation wavelength quantified by analytical HPLC. Conditions: Irradiation wavelength = 360 nm and 420 nm, irradiance = 1.2 mW cm⁻².

The photolysis studies were also performed for PMNB(E-EG₁₂-N₃)₂ in solution. PMNB(E-EG₁₂-N₃)₂ showed similar photolysis efficiency both at 365 nm and 420 nm. These data are presented in **Appendix**.

NB-E-(EG_n-N₃)₂

The photolysis kinetics of NB based ester crosslinker was also studied. The UV/Vis spectrum of NB-E-(EG_n-N₃)₂ (**Figure 2.25**) showed an intense band at λ_{\max} = 300 nm which gradually decreased during exposure at 365 nm. New bands appeared at 270 nm and 360 nm with increasing intensity during exposure.⁵⁰ Clear isosbestic points at 288 nm and 320 nm were observed. ESI-MS analysis of an

Chapter 2

irradiated sample ($t = 15$ min) corroborated the expected photolysis product: *o*-nitroso ketone ($m/z = 807.4$ for $M+NH_4$) and $COOH-PEG_n-N_3$ ($m/z = 661.4$ for $M+NH_4$). Similar changes were observed during exposure at 420 nm, though in this case the intensity of the band at 360 nm increased until 15 min irradiation and then decreased. These changes are possibly associated with different photochemical side reactions of byproducts which were not reported in the literature and were not investigated here any further. ESI-MS analysis of an irradiated aliquot ($t=10$ min) corroborated the expected *o*-nitroso ketone and $COOH-PEG_n-N_3$ photolysis products.

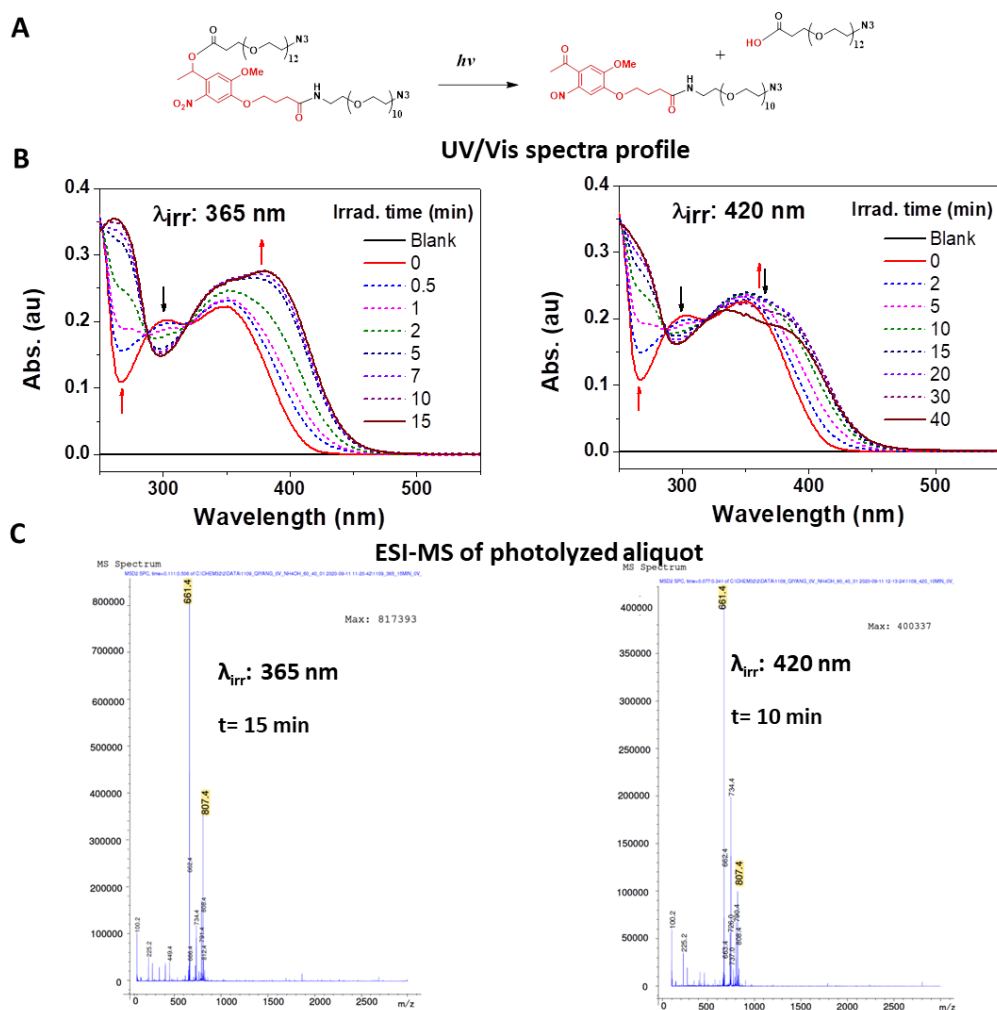


Figure 2.25 (A) Photochemical reaction expected for NB-E-(EG_n-N₃)₂ in solution. (B) UV/Vis spectra evolution of NB-E-(EG_n-N₃)₂ solution during photolysis (0.10 μ M, ACN/H₂O (1:1)). (C) ESI-MS analysis of photolyzed solution. Conditions: Irradiation wavelength = 360 nm and 420 nm, irradiance = 1.2 $mW\ cm^{-2}$.

The kinetics of the photolysis reaction was quantified by analyzing the consumption of the starting compound during irradiation by analytical HPLC (Figure 2.26A and Appendix). In the HPLC analysis, NB-E-(EG_n-N₃)₂ showed retention time at 26 min. After 1 minutes of illumination, HPLC analysis showed diminished NB-E-(EG_n-N₃)₂ signal at 26 min and the parallel appearance of new signals at 22 min. The signal at 26 min decreased over time, whereas the signal at 22 min increased and then decreased. Also, new peaks were also observed with longer exposure times. Same photolysis effect was observed as for 2-(4,5-dimethoxy-2-nitrophenyl)-propyl (DMNPP) (other NB derivatives) as

reported by Specht et.al.⁵¹ where only partial amount (60%) of photoproduct (benzoic acid) was detected, effect that was caused by alternative photolysis pathways.

NB-E-(EG_n-N₃)₂ showed higher photolysis conversion at 365 nm than at 420 nm under same illumination doses (**Figure 2.26B**). These results are also consistent with the lower absorbance at 420 nm in UV/Vis studies. NB-E-(EG_n-N₃)₂ consumed 99% in 15 min of irradiation under 365 nm while at 420 nm a similar consumption was observed after 40 min exposure. Interestingly, analytical HPLC chromatograms showed other signals of low intensity corresponding to other photolysis products, indicating a cleaner photolysis than for PMNB.

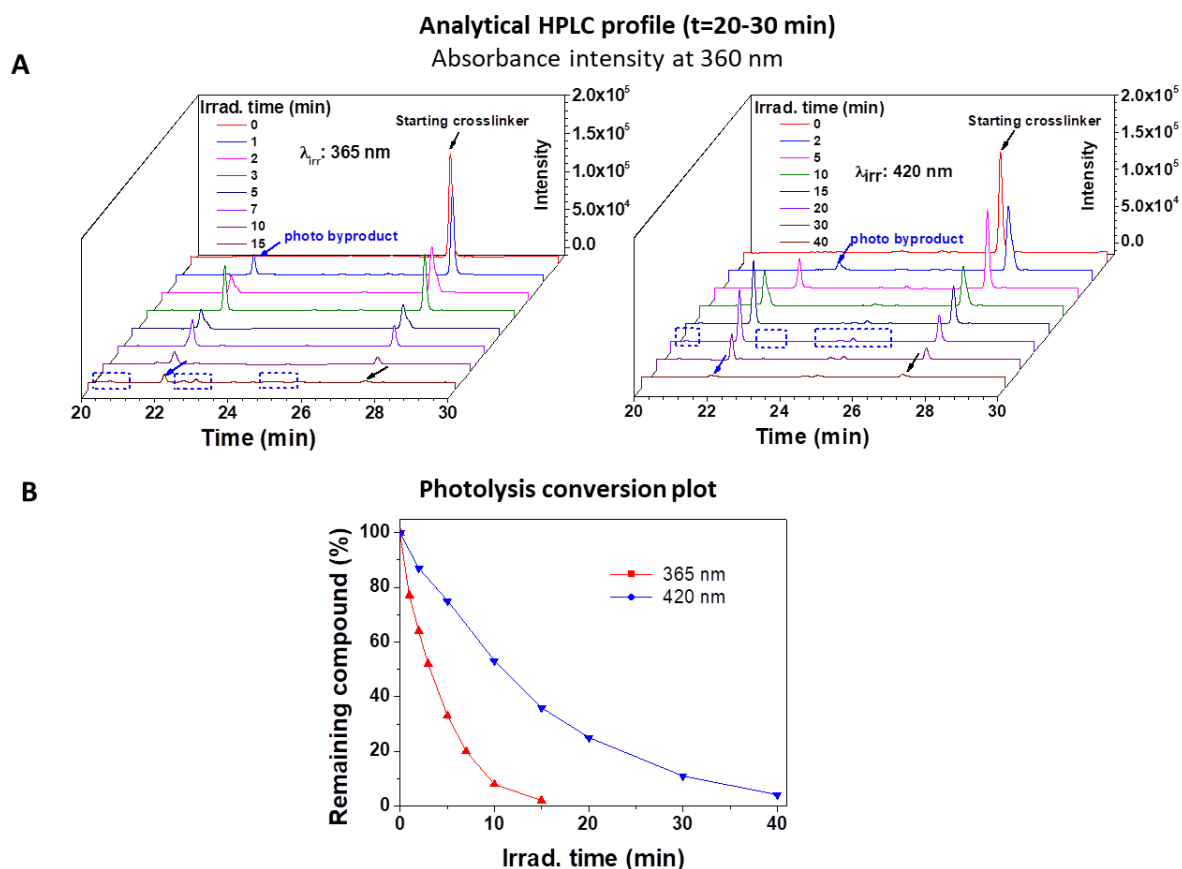


Figure 2.26 (A) Analytical HPLC profile of NB-E-(EG_n-N₃)₂ aliquots before and after irradiation. (B) Comparison of photolysis conversion as function of exposure time for NB-E-(EG_n-N₃)₂ solution at different irradiation wavelength quantified by analytical HPLC. Conditions: Irradiation wavelength = 360 nm and 420 nm, irradiance = 1.2 mW cm⁻².

According to the HPLC analysis of photolysis kinetics, the photocleavage of PMNB(E-PEG_n-SH)₂ was 7-times more efficient than NB-E-(EG_n-N₃)₂ after irradiation at 365 nm and 420 nm (**Figure 2.27A**). After 2 min of irradiation, a photolysis yield of 93% and 79% was obtained for PMNB(E-PEG_n-SH)₂, whereas 36% and 13% was obtained for NB-E-(EG_n-N₃)₂ at 365 nm and 420 nm, respectively. These results confirm that and extended conjugation of the π -system in *o*-nitrophenylethyl systems improves photo-efficiency in comparison to the *o*-nitrobenzyl ester systems.

Chapter 2

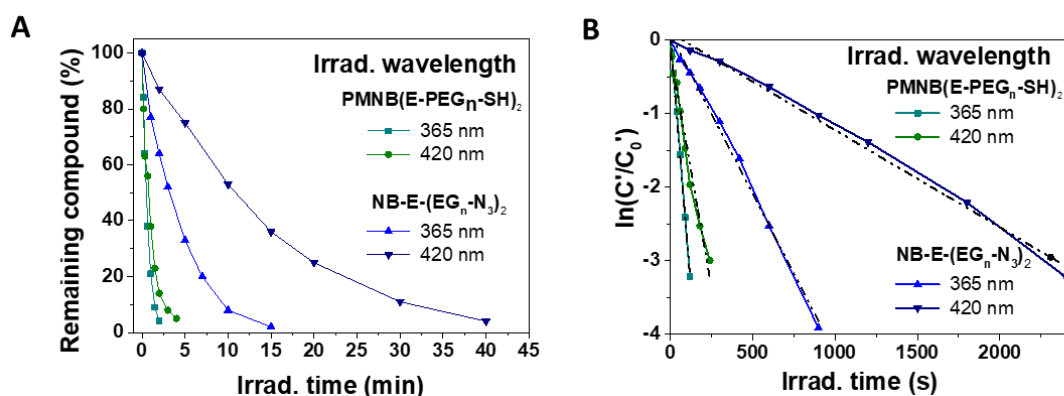


Figure 2.27 (A) Comparison of photolysis efficiency of NB-E-(EG_n-N₃)₂ and PMNB(E-PEG_n-SH)₂. (B) photodegradation kinetic curve fits for crosslinkers in solution: plotted from (A). Conditions: $\lambda = 365$ nm and 420 nm, $I_0 = 1.2$ mW cm⁻².

In order to calculate the photodegradation rate constant, it was assumed that the photolysis reaction followed a first-order kinetic law.¹

$$C'(t) = C'_0 e^{-k_{obs} t}$$

Where C' is the concentration of crosslinker at a given time, C'_0 is the initial concentration; t is the time of exposure. From this equation, the photodegradation rate constant can be obtained from the slope of the natural log of the normalized conversion versus exposure time as follows:

$$\ln \frac{C'}{C'_0} = -k_{obs} t$$

This plot is represented in **Figure 2.27B**. The first order rate constant obtained is listed in **Table 2.3**.⁶ For PMNB(E-PEG_n-SH)₂, a value of $27.3 \times 10^{-3} \text{ s}^{-1}$ was obtained at 365 nm, whereas a 2-fold smaller value of $12.75 \times 10^{-3} \text{ s}^{-1}$ was obtained at 420 nm. As a comparison, for NB-E-(EG_n-N₃)₂, a value of $4.34 \times 10^{-3} \text{ s}^{-1}$ and $1.32 \times 10^{-3} \text{ s}^{-1}$ were obtained at 365 nm and 420 nm, respectively.

Table 2.3. Comparison of photolysis kinetics values of PMNB(E-PEG_n-SH)₂ and NB-E-(PEG_n-N₃)₂ obtained at irradiation wavelengths of 365 and 420 nm.

Chromophore	365 nm		420 nm	
	Photodegradation rate constant k_{obs} [s ⁻¹]	k_{obs}/I_0 [cm ² s ⁻¹ mW ⁻¹] ⁽¹⁾	Photodegradation rate constant k_{obs} [s ⁻¹]	k_{obs}/I_0 [cm ² s ⁻¹ mW ⁻¹] ⁽¹⁾
PMNB(E-PEG _n -SH) ₂	27.3 (x10 ⁻³)	22.8 (x10 ⁻³)	12.75 (x10 ⁻³)	10.63 (x10 ⁻³)
NB-E-(EG _n -N ₃) ₂	4.34 (x10 ⁻³)	3.6 (x10 ⁻³)	1.32 (x10 ⁻³)	1.1 (x10 ⁻³)

⁽¹⁾ The apparent kinetic constant of cleavage normalized to the light intensity (k_{obs}/I_0). $I_0 = 1.2$ mW cm⁻².

The results for NB-E-(EG_n-N₃)₂ in the present study are consistent with previous reports, where a value of $3.3 \times 10^{-3} \text{ s}^{-1}$ upon 365 nm was informed, whereas the value upon 420 nm was unfortunately not informed.⁵² Based on these results, PMNB based ester crosslinker with conjugated biphenyl structure is demonstrated to be more efficient than NB based ester crosslinker upon one-photon illumination in solution.

2.6 Hydrolytic stability of PMNB ester and carbamate crosslinkers

The stability of PMNB ester $\text{PMNB}(\text{E-PEG}_n\text{-SH})_2$ and carbamate $\text{PMNB}(\text{C-EG}_{15}\text{-Tz-MS})_2$ macromers in PBS buffer at room temperature was analyzed by mass spec and HPLC. The solutions were prepared in the same concentration in an amber vial and protected from light at room temperature for 3 days. The fresh prepared solution ($t=0$ h) showed retention time at 28 min (**Figure 2.28A**). $\text{PMNB}(\text{E-PEG}_n\text{-SH})_2$ solution at day 2 showed a significantly diminished signal at 28 min and only 29% concentration remained. For a comparison, 95% remaining concentration of $\text{PMNB}(\text{C-EG}_{15}\text{-Tz-MS})_2$ solution was observed at day 3. These results were complemented with mass analysis (**Figure 2.28B**). ESI-MS analysis of $\text{PMNB}(\text{E-PEG}_n\text{-SH})_2$ solution ($t=$ day 2) corroborated the expected hydrolyzed product: HO- $\text{PMNB-E-PEG}_n\text{-SH}$ ($m/z = 1471.8$ for $[\text{M}+\text{Na}]^+$) and $\text{COOH-PEG}_n\text{-SH}$ ($m/z = 1171.6$ for $[\text{M}+\text{Na}]^+$). No related masses of hydrolyzed compounds were found for $\text{PMNB}(\text{C-EG}_{15}\text{-Tz-MS})_2$ solution ($t=$ day 3). All these results indicate a much lower hydrolytic stability of ester vs. carbamate labile bond.

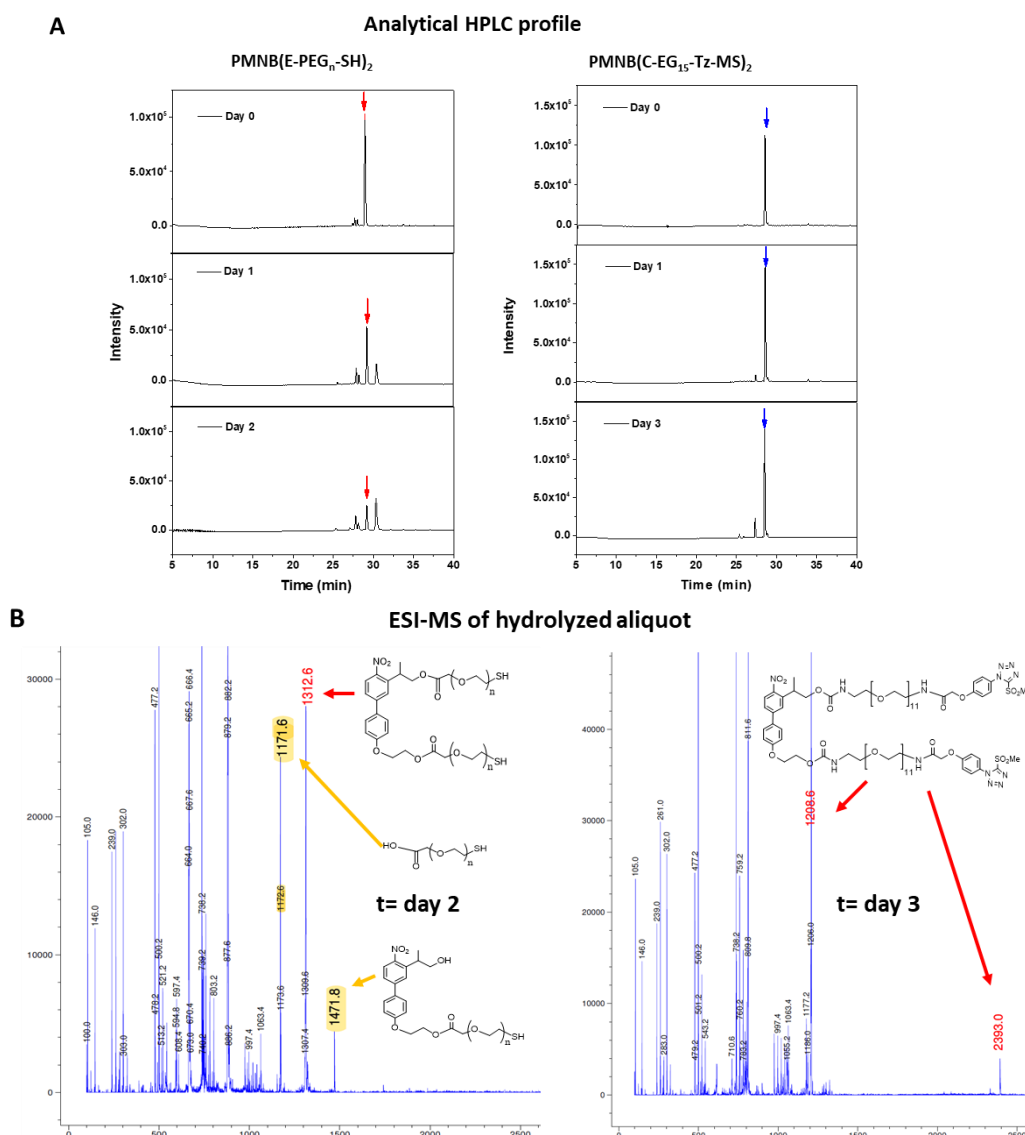


Figure 2.28 (A) Analytical HPLC profile of $\text{PMNB}(\text{E-PEG}_n\text{-SH})_2$ and $\text{PMNB}(\text{C-EG}_{15}\text{-Tz-MS})_2$ aliquots during hydrolysis. Conditions: $0.10 \mu\text{M}$ in PBS buffer at room temperature. Absorbance intensity at 360 nm. **(B)** ESI-MS analysis of hydrolyzed solutions.

Chapter 2

2.7 Conclusion

Three photodegradable ester crosslinkers based on PMNB chromophore, bearing different functional end groups (-MS, -SH or -N₃) were successfully synthesized. The PMNB(E-PEG_n-SH)₂ and PMNB(E-EG₁₂-N₃)₂ were obtained in only 1 step and from the key intermediate PMNB(OH)₂. PMNB(E-EG₁₂-N₃)₂ was synthesized at >50 mg-scale, favored by the only small excess of spacer (1.5-fold) needed. In contrast, the synthesis of PMNB(E-PEG_n-SH)₂ required big excess of SH-PEG_n-COOH spacer (>10-fold) and this fact limited the synthesis scale to < 50 mg, due to the high cost of the PEG spacer. Higher synthetic effort (3 more synthetic steps) was needed for synthesis of PMNB(E-EG₁₃-Ox-MS)₂ since the COOH-PEG₁₃-MS spacer is not commercially available. All these crosslinkers presented good solubility in aqueous solvents. To compare the effect of linkage chemistry between the OEG chains and the PMNB chromophore on the hydrolytic stability of the linker, PMNB(C-EG_n-Tz-MS)₂ and PMNB(C-EG_n-Ox-MS)₂ with carbamate labile bonds were also synthesized via multiple steps at ~ 50-100 mg scale. A considerably longer OEG arm with n > 15 was needed to ensure good aqueous solubility due to the bulky hydrophobic structure of -Tz-MS and -Ox-MS groups. The different solubility of PMNB-based crosslinkers highlighting the importance of how the hydrophilicity of terminal functional groups affecting the solubility, of which needs to be carefully considered. The functional end-groups allow flexibility in the selection of the crosslinking reaction in presence of cells. Two additional control crosslinkers were designed and successfully synthesized. First, a NB-based ester crosslinker, NB-E-(EG_n-N₃)₂ with -N₃ groups was successfully synthesized at 85 mg scale, in 2 synthesis steps with a high overall yield of 87%. This NB-based crosslinker will be used as benchmark to PMNB ester system. Second, a non-photodegradable control crosslinker, PEG(C-Tz-MS)₂ for PMNB carbamate crosslinker (of similar length) was synthesized in a 5 steps procedure with an overall yield of 18%.

Star PEG macromer precursors with -MS and -DBCO functional end groups at high substitution degree were successfully obtained. The star PEG-Ox-MS precursor was obtained in 4 synthesis steps at 200 mg scale, showed long-term stability under storage (6 months) and presented good solubility in aqueous solvents. The star PEG-DBCO precursor was obtained in 1 synthesis step from commercial compounds at 200 mg scale and with high substitution degree. In this case, the reaction conditions were optimized for star PEG-DBCO synthesis. The star PEG-DBCO precursor presented good solubility in aqueous solvents, however it showed poor stability under storage (< 3 weeks). Compared to star PEG-Ox-MS, the poorer stability of star PEG-DBCO is expected to limit its use in practical applications.

The one-photon photolysis efficiency of crosslinkers with ester labile bonds in aqueous solution was studied and compared. PMNB(E-PEG_n-SH)₂ crosslinker showed higher photolysis efficiency than NB-E-(EG_n-N₃)₂ under light exposure at 365 nm and 420 nm. The high 1P efficiency of PMNB-based crosslinker is promising for further cell studies to reduce the photodamage.

The hydrolytic stability of PMNB ester vs. carbamate labile bonds was studied. PMNB(C-EG_n-Tz-MS)₂ showed significantly higher hydrolytic stability than PMNB(E-PEG_n-SH)₂ in aqueous solutions, which is good for better understanding the hydrolysis behavior of different linking groups, thus utilized to design the degradable hydrogels in different time scale for applications. Moreover, the high hydrolytic stability of PMNB carbamate crosslinker makes it a good candidate for long term cell experiments.

The crosslinkers and PEG macromers described in this Chapter were used to fabricate derived PEG hydrogels and their properties were characterized, as shown in the coming Chapters.

2.8 References

1. DeForest, C. A.; Anseth, K. S., Cytocompatible click-based hydrogels with dynamically tunable properties through orthogonal photoconjugation and photocleavage reactions. *Nature chemistry* **2011**, *3* (12), 925-31.
2. Kloxin, A. M.; Kasko, A. M.; Salinas, C. N.; Anseth, K. S., Photodegradable hydrogels for dynamic tuning of physical and chemical properties. *Science* **2009**, *324* (5923), 59-63.
3. Luo, Y.; Shoichet, M. S., A photolabile hydrogel for guided three-dimensional cell growth and migration. *Nature Materials* **2004**, *3* (4), 249-253.
4. Barhoumi, A.; Liu, Q.; Kohane, D. S., Ultraviolet light-mediated drug delivery: Principles, applications, and challenges. *J Control Release* **2015**, *219*, 31-42.
5. Chan, A.; Orme, R. P.; Fricker, R. A.; Roach, P., Remote and local control of stimuli responsive materials for therapeutic applications. *Advanced Drug Delivery Reviews* **2013**, *65* (4), 497-514.
6. LeValley, P. J.; Neelapapu, R.; Sutherland, B. P.; Dasgupta, S.; Kloxin, C. J.; Kloxin, A. M., Photolabile Linkers: Exploiting Labile Bond Chemistry to Control Mode and Rate of Hydrogel Degradation and Protein Release. *Journal of the American Chemical Society* **2020**, *142* (10), 4671-4679.
7. Tibbitt, M. W.; Kloxin, A. M.; Sawicki, L. A.; Anseth, K. S., Mechanical Properties and Degradation of Chain and Step-Polymerized Photodegradable Hydrogels. *Macromolecules* **2013**, *46* (7), 2785-2792.
8. Arakawa, C. K.; Badeau, B. A.; Zheng, Y.; DeForest, C. A., Multicellular Vascularized Engineered Tissues through User-Programmable Biomaterial Photodegradation. *Adv Mater* **2017**, *29* (37).
9. Yanagawa, F.; Sugiura, S.; Takagi, T.; Sumaru, K.; Camci-Unal, G.; Patel, A.; Khademhosseini, A.; Kanamori, T., Activated-ester-type photocleavable crosslinker for preparation of photodegradable hydrogels using a two-component mixing reaction. *Adv Healthc Mater* **2015**, *4* (2), 246-54.
10. Lunzer, M.; Shi, L.; Andriotis, O. G.; Gruber, P.; Markovic, M.; Thurner, P. J.; Ossipov, D.; Liska, R.; Ovsianikov, A., A Modular Approach to Sensitized Two-Photon Patterning of Photodegradable Hydrogels. *Angewandte Chemie (International ed. in English)* **2018**, *57* (46), 15122-15127.
11. Azagarsamy, M. A.; McKinnon, D. D.; Alge, D. L.; Anseth, K. S., Coumarin-Based Photodegradable Hydrogel: Design, Synthesis, Gelation, and Degradation Kinetics. *ACS Macro Letters* **2014**, *3* (6), 515-519.
12. Yavitt, F. M.; Brown, T. E.; Hushka, E. A.; Brown, M. E.; Gjorevski, N.; Dempsey, P. J.; Lutolf, M. P.; Anseth, K. S., The Effect of Thiol Structure on Allyl Sulfide Photodegradable Hydrogels and their Application as a Degradable Scaffold for Organoid Passaging. *Adv Mater* **2020**, *32* (30), e1905366.
13. Rapp, T. L.; DeForest, C. A., Visible Light-Responsive Dynamic Biomaterials: Going Deeper and Triggering More. *Adv Healthc Mater* **2020**, *9* (7), e1901553.
14. Krivenkov, V.; Samokhvalov, P.; Dyagileva, D.; Karaulov, A.; Nabiev, I., Determination of the Single-Exciton Two-Photon Absorption Cross Sections of Semiconductor Nanocrystals through the Measurement of Saturation of Their Two-Photon-Excited Photoluminescence. *ACS Photonics* **2020**, *7*

Chapter 2

(3), 831-836.

15. Klán, P.; Šolomek, T.; Bochet, C. G.; Blanc, A.; Givens, R.; Rubina, M.; Popik, V.; Kostikov, A.; Wirz, J., Photoremovable Protecting Groups in Chemistry and Biology: Reaction Mechanisms and Efficacy. *Chemical Reviews* **2013**, *113* (1), 119-191.
16. Šolomek, T.; Mercier, S.; Bally, T.; Bochet, C. G., Photolysis of ortho-nitrobenzyl derivatives: the importance of the leaving group. *Photochemical & Photobiological Sciences* **2012**, *11* (3), 548-555.
17. Gug, S.; Charon, S.; Specht, A.; Alarcon, K.; Ogden, D.; Zietz, B.; Léonard, J.; Haacke, S.; Bolze, F.; Nicoud, J. F.; Goeldner, M., Photolabile glutamate protecting group with high one- and two-photon uncaging efficiencies. *Chembiochem* **2008**, *9* (8), 1303-7.
18. Donato, L.; Mouro, A.; Davenport, C. M.; Herbivo, C.; Warther, D.; Leonard, J.; Bolze, F.; Nicoud, J. F.; Kramer, R. H.; Goeldner, M.; Specht, A., Water-soluble, donor-acceptor biphenyl derivatives in the 2-(o-nitrophenyl)propyl series: highly efficient two-photon uncaging of the neurotransmitter gamma-aminobutyric acid at $\lambda = 800$ nm. *Angewandte Chemie (International ed. in English)* **2012**, *51* (8), 1840-3.
19. Garcia-Fernandez, L.; Herbivo, C.; Arranz, V. S.; Warther, D.; Donato, L.; Specht, A.; del Campo, A., Dual photosensitive polymers with wavelength-selective photoresponse. *Adv Mater* **2014**, *26* (29), 5012-7.
20. Farrukh, A.; Paez, J. I.; del Campo, A., 4D Biomaterials for Light-Guided Angiogenesis. *Adv Funct Mater* **2019**, *29* (6), 1807734.
21. Gug, S.; Bolze, F.; Specht, A.; Bourgoigne, C.; Goeldner, M.; Nicoud, J. F., Molecular engineering of photoremovable protecting groups for two-photon uncaging. *Angewandte Chemie (International ed. in English)* **2008**, *47* (49), 9525-9.
22. Aujard, I.; Benbrahim, C.; Gouget, M.; Ruel, O.; Baudin, J. B.; Neveu, P.; Jullien, L., o-nitrobenzyl photolabile protecting groups with red-shifted absorption: syntheses and uncaging cross-sections for one- and two-photon excitation. *Chemistry* **2006**, *12* (26), 6865-79.
23. Weinstain, R.; Slanina, T.; Kand, D.; Klán, P., Visible-to-NIR-Light Activated Release: From Small Molecules to Nanomaterials. *Chemical Reviews* **2020**, *120* (24), 13135-13272.
24. Takaoka, K.; Tatsu, Y.; Yumoto, N.; Nakajima, T.; Shimamoto, K., Synthesis and photoreactivity of caged blockers for glutamate transporters. *Bioorganic & Medicinal Chemistry Letters* **2003**, *13* (5), 965-970.
25. Walbert, S.; Pfeleiderer, W.; Steiner, U. E., Photolabile protecting groups for nucleosides: Mechanistic studies of the 2-(2-nitrophenyl)ethyl group. *Helv Chim Acta* **2001**, *84* (6), 1601-1611.
26. Barltrop, J. A.; Schofield, P., Photosensitive Protecting Groups. *Tetrahedron Letters* **1962**, *3* (16), 697-699.
27. Hasan, A.; Stengele, K.-P.; Giegrich, H.; Cornwell, P.; Isham, K. R.; Sachleben, R. A.; Pfeleiderer, W.; Foote, R. S., Photolabile protecting groups for nucleosides: Synthesis and photodeprotection rates. *Tetrahedron* **1997**, *53* (12), 4247-4264.
28. Specht, A.; Bolze, F.; Donato, L.; Herbivo, C.; Charon, S.; Warther, D.; Gug, S.; Nicoud, J. F.; Goeldner, M., The donor-acceptor biphenyl platform: a versatile chromophore for the engineering of highly efficient two-photon sensitive photoremovable protecting groups. *Photochemical & photobiological sciences : Official journal of the European Photochemistry Association and the*

European Society for Photobiology **2012**, *11* (3), 578-86.

29. Hadjichristidis, N.; Pitsikalis, M.; Iatrou, H.; Driva, P.; Sakellariou, G.; Chatzichristidi, M., 6.03 - Polymers with Star-Related Structures: Synthesis, Properties, and Applications. In *Polymer Science: A Comprehensive Reference*, Matyjaszewski, K.; Möller, M., Eds. Elsevier: Amsterdam, 2012; pp 29-111.
30. Phelps, E. A.; Enemchukwu, N. O.; Fiore, V. F.; Sy, J. C.; Murthy, N.; Sulchek, T. A.; Barker, T. H.; Garcia, A. J., Maleimide cross-linked bioactive PEG hydrogel exhibits improved reaction kinetics and cross-linking for cell encapsulation and in situ delivery. *Adv Mater* **2012**, *24* (1), 64-70, 2.
31. Farrukh, A.; Paez, J. I.; Salierno, M.; del Campo, A., Bioconjugating Thiols to Poly(acrylamide) Gels for Cell Culture Using Methylsulfonyl Co-monomers. *Angewandte Chemie (International ed. in English)* **2016**, *55* (6), 2092-6.
32. Paez, J. I.; Farrukh, A.; Valbuena-Mendoza, R.; Włodarczyk-Biegun, M. K.; del Campo, A., Thiol-Methylsulfone-Based Hydrogels for 3D Cell Encapsulation. *ACS Applied Materials & Interfaces* **2020**, *12* (7), 8062-8072.
33. Paez, J. I.; de Miguel-Jiménez, A.; Valbuena-Mendoza, R.; Rathore, A.; Jin, M.; Gläser, A.; Pearson, S.; del Campo, A., Thiol-Methylsulfone-Based Hydrogels for Cell Encapsulation: Reactivity Optimization of Aryl-Methylsulfone Substrate for Fine-Tunable Gelation Rate and Improved Stability. *Biomacromolecules* **2021**.
34. Lin, C.-C., Recent advances in crosslinking chemistry of biomimetic poly(ethylene glycol) hydrogels. *RSC Advances* **2015**, *5* (50), 39844-39853.
35. Kirschner, C. M.; Anseth, K. S., In situ control of cell substrate microtopographies using photolabile hydrogels. *Small* **2013**, *9* (4), 578-84.
36. Claassen, C.; Claassen, M. H.; Gohl, F.; Tovar, G. E. M.; Borchers, K.; Southan, A., Photoinduced Cleavage and Hydrolysis of o-Nitrobenzyl Linker and Covalent Linker Immobilization in Gelatin Methacryloyl Hydrogels. *Macromol Biosci* **2018**, *18* (9), e1800104.
37. Reichmanis, E.; Gooden, R.; Wilkins, C. W.; Schonhorn, H., A study of the photochemical response of o-nitrobenzyl cholate derivatives in P(MMA-MAA) matrices. *Journal of Polymer Science: Polymer Chemistry Edition* **1983**, *21* (4), 1075-1083.
38. Reichmanis, E.; Smith, B. C.; Gooden, R., O-nitrobenzyl photochemistry: Solution vs. solid-state behavior. *Journal of Polymer Science: Polymer Chemistry Edition* **1985**, *23* (1), 1-8.
39. Baldwin, A. D.; Kiick, K. L., Reversible maleimide-thiol adducts yield glutathione-sensitive poly(ethylene glycol)-heparin hydrogels. *Polymer Chemistry* **2013**, *4* (1), 133-143.
40. Nie, T.; Baldwin, A.; Yamaguchi, N.; Kiick, K. L., Production of heparin-functionalized hydrogels for the development of responsive and controlled growth factor delivery systems. *Journal of Controlled Release* **2007**, *122* (3), 287-296.
41. Zhao, X.; Lv, G.; Peng, Y.; Liu, Q.; Li, X.; Wang, S.; Li, K.; Qiu, L.; Lin, J., Targeted Delivery of an Activatable Fluorescent Probe for the Detection of Furin Activity in Living Cells. *ChemBiochem* **2018**, *19* (10), 1060-1065.
42. Zheng, Z.; Li, G.; Wu, C.; Zhang, M.; Zhao, Y.; Liang, G., Intracellular synthesis of d-aminoluciferin for bioluminescence generation. *Chemical Communications* **2017**, *53* (25), 3567-3570.
43. Takeda, K.; Akagi, Y.; Saiki, A.; Tsukahara, T.; Ogura, H., Convenient Methods for Syntheses of Active Carbamates, Ureas and Nitrosoureas Using N,N'-disuccinimido Carbonate (DSC). *Tetrahedron*

Chapter 2

Letters **1983**, 24 (42), 4569-4572.

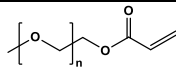
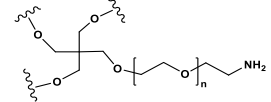
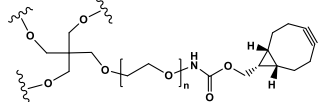
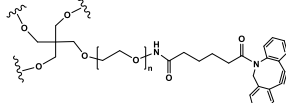
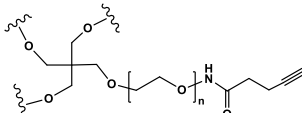
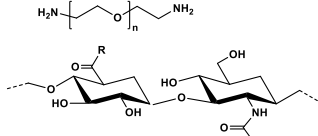
44. Espeel, P.; Du Prez, F. E., One-pot multi-step reactions based on thiolactone chemistry: A powerful synthetic tool in polymer science. *European Polymer Journal* **2015**, 62, 247-272.
45. Zhan, H.; de Jong, H.; Löwik, D. W. P. M., Comparison of Bioorthogonally Cross-Linked Hydrogels for in Situ Cell Encapsulation. *ACS Applied Bio Materials* **2019**, 2 (7), 2862-2871.
46. Maeda, K., Analysis of Ultraviolet Radiation Wavelengths Causing Hardening and Reduced Elasticity of Collagen Gels In Vitro. **2018**, 5 (1), 14.
47. Wong, D. Y.; Ranganath, T.; Kasko, A. M., Low-Dose, Long-Wave UV Light Does Not Affect Gene Expression of Human Mesenchymal Stem Cells. *PLoS One* **2015**, 10 (9), e0139307-e0139307.
48. Youn, H. Y.; Chou, B. R.; Cullen, A. P.; Sivak, J. G., Effects of 400 nm, 420 nm, and 435.8 nm radiations on cultured human retinal pigment epithelial cells. *Journal of photochemistry and photobiology. B, Biology* **2009**, 95 (1), 64-70.
49. Takahashi, T.; Ikejiri, Y.; Himori, S.; Gotoh, H., Polymerization inhibition mechanism of 1,4-naphthoquinone by experimentation and DFT calculations. *Polymer Journal* **2019**, 51 (9), 929-934.
50. Alvarez, M.; Best, A.; Pradhan-Kadam, S.; Koynov, K.; Jonas, U.; Kreiter, M., Single-Photon and Two-Photon Induced Photocleavage for Monolayers of an Alkyltriethoxysilane with a Photoprotected Carboxylic Ester. *Advanced Materials* **2008**, 20 (23), 4563-4567.
51. Specht, A.; Thomann, J. S.; Alarcon, K.; Wittayanan, W.; Ogden, D.; Furuta, T.; Kurakawa, Y.; Goeldner, M., New photoremovable protecting groups for carboxylic acids with high photolytic efficiencies at near-UV irradiation. Application to the photocontrolled release of L-glutamate. *Chembiochem* **2006**, 7 (11), 1690-5.
52. Griffin, D. R.; Kasko, A. M., Photodegradable Macromers and Hydrogels for Live Cell Encapsulation and Release. *Journal of the American Chemical Society* **2012**, 134 (31), 13103-13107.

Chapter 3: Synthesis and physicochemical properties of photodegradable PEG-hydrogels

3.1 Introduction

Photodegradable hydrogels allow dynamic and user-defined degradation of the network structure by controlled light exposure.^{1,2} Such materials are attractive for biomedical applications including drug delivery and tissue engineering.³ Photodegradable hydrogels for cell encapsulation have used hyaluronic acid (HA),⁴ polyethylene glycol (PEG)^{1, 5, 6} and gelatin⁷ as polymeric backbones, as summarized in **Table 3.1**.

Table 3.1 Main polymeric backbones and crosslinking approaches for fabrication of photodegradable hydrogels.

Polymeric backbones	Structures	Crosslinking approaches	Cell applications	
			In situ 3D cell encapsulation	Cellular response upon 1P or 2P exposure
PEGA ⁸		Free-radical polymerization	x	1P-induced cell migration
Star PEG-amine Or Gelatin ⁷		Amine-NHS ester coupling chemistry	x	1P-induced cell migration
Star PEG-BCN ⁹		SPAAC	x	Endothelialized 3D vascular networks after 2P degradation
Star PEG-DBC ¹⁰		SPAAC	√	2P induced cell migration
Star PEG alkyne ²		CuAAC	x	x
PEG diamine and HA ⁴		Michael-type thiol-ene addition	√	2P induced cell migration

In one of the first reported degradable hydrogels, Anseth and coworkers synthesized hydrogels by using PEG monoacrylate (PEGA) with a total 15 wt% macromer *o*NB-based photodegradable crosslinker: PEGA 10 mol% : 90 mol%) in water and 0.3 M redox initiator AP via redox-initiated free radical polymerization. HT1080 fibrosarcoma cells were encapsulated in the hydrogels with 100 nM fibronectin and cell migration into the eroded channels (UV light at 365nm, 10 mW cm⁻² for 20 min) was observed over 2 days. However, no 2P-induced cell migration was studied due to the high irradiation dose needed for hydrogel degradation.⁸ In another work, Sugiura and coworkers synthesized activated-ester-type *o*NB-based photocleavable crosslinker and prepared hydrogels by

Chapter 3

using star PEG amine or gelatin via amine-NHS ester coupling chemistry in a high concentrated buffer system (in 10 mM phthalic acid buffer (pH 4.0) with 0.14 M NaCl, PBS and 0.3 M HEPES buffer (pH 7.0)). HUVECs were cultured on the hydrogels and present high viability after illumination ($>2.0 \text{ J cm}^{-2}$ at 365 nm). However, in situ 3D cell encapsulation was not studied which might be due to the use of the high buffer concentration. Moreover, the amine-NHS ester coupling has a significant dependence on pH which can also limit the alternation for hydrogel composites for cell applications.¹¹ More recently, Ovsianikov and coworkers reported a high 2P degradation efficient PEG-HA based hydrogels (PEG-HA-SH) in presence of P2CK photosensitizer with 12.5 wt% total macromer content via Michael-type thiol-ene addition. 3D spheroids were encapsulated in the hydrogels and exhibit good biocompatibility under the encapsulation conditions. Cell migration was observed into predetermined channels in a high spatiotemporal controlled manner upon 2P excitation.⁴ Despite the progress for utilized crosslinking and degradation approaches for cell studies, in situ 3D cell encapsulation in hydrogels with tunable kinetics under physiological conditions and high 2P efficient hydrogel degradation remains a challenge.

Therefore, in this Chapter, 2P photodegradable PMNB-based crosslinkers and PEG macromers synthesized in Chapter 2 are used to prepare 2P-degradable PEG hydrogels. The crosslinking kinetics and photochemical properties of photodegradable gels are evaluated. Crosslinking kinetics, final mechanical strength and 1P degradation of PMNB-based PEG hydrogels (PMNB hydrogels) are characterized by photo-rheology. Patterned degradation of derived gels is demonstrated with 2P illumination in a laser scanning microscope (LSM) and using a NanoScribe system. A PMNB-based benchmark gel and a control non-degradable gel are prepared for benchmarking with reported systems. PMNB-based hydrogels described in this chapter allow modulation of the mechanical properties at low illumination doses. Hydrogel formulations and hydrolytic stability are also adjusted for cell encapsulation and light-triggered migration. Finally, the possibility of encapsulating living cells in these materials is tested.

3.2 Synthesis of hydrogels

4-arm star PEG-Ox-MS and PEG-DBCO precursors (20 kDa) and the photocleavable crosslinkers synthesized in **Chapter 2 (Figure 2.4)** were used to prepare hydrogels. Non-photodegradable hydrogels were also synthesized for control experiments. Five different hydrogel variants were prepared, as shown in **Figure 3.2**, using the thiol-MS or SPAAC crosslinking.

In reported literature, PEG polymer concentrations between 2.5 wt% and 10 wt% have been demonstrated to provide hydrogels with mechanical properties within a physiologically relevant range (i.e., elastic moduli ranging from 0.03 to 6 kPa).¹² For this reason, hydrogels with polymer content between 5.7 and 6.5 wt% were prepared. For this purpose, precursor solutions freshly prepared were mixed at (1:1) molar ratio of functional groups (MS:thiol or DBCO:N₃) and in equal volume. Precursor solutions presented low viscosity and allowed mixing of the two components to obtain homogeneous reactive mixtures after vortexing and centrifuging to remove bubbles.

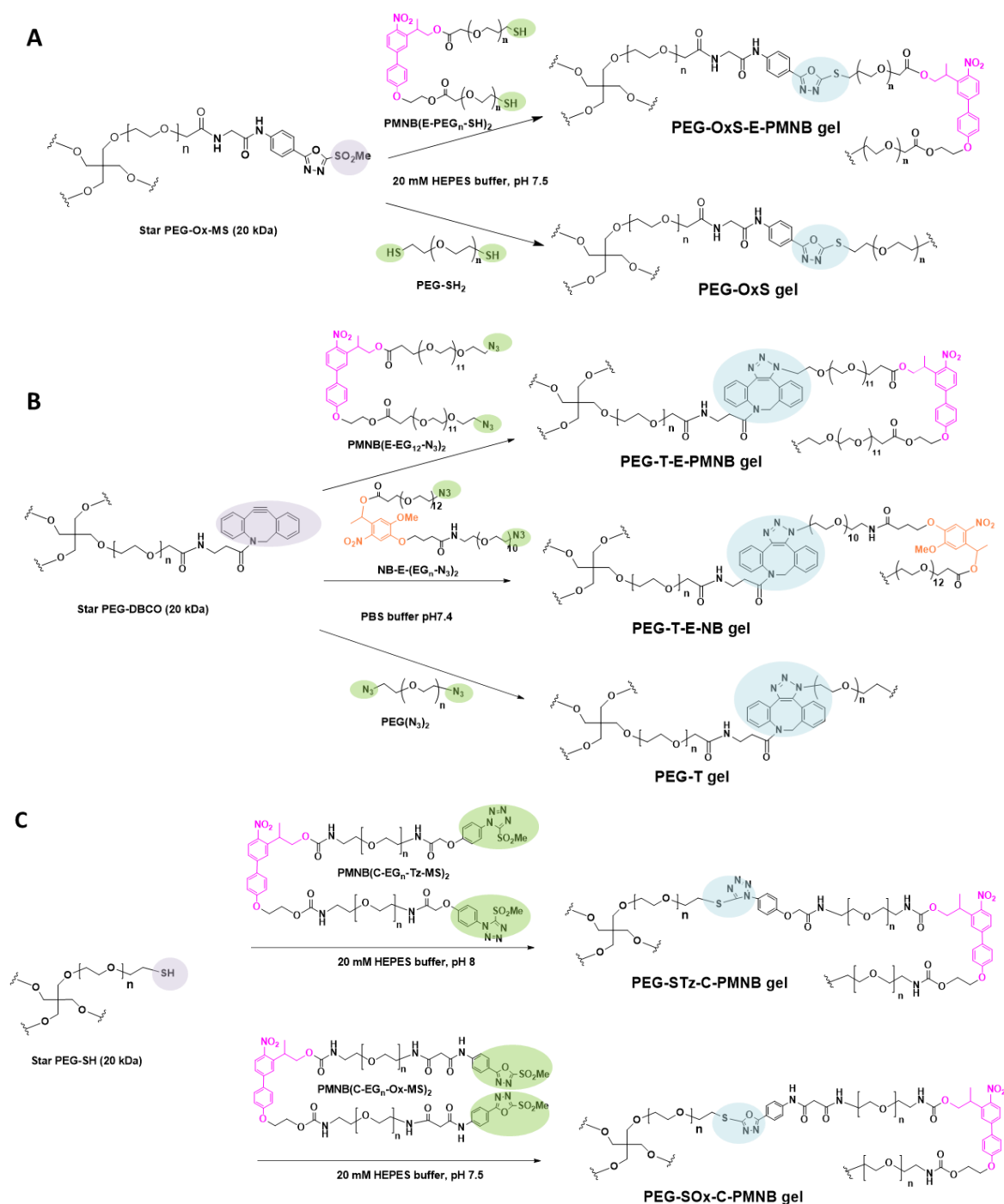


Figure 3.2 Hydrogels developed in this work based on thiol-MS **(A)** **(C)** or SPAAC crosslinking **(B)**. **(A)** Photodegradable hydrogel (PEG-OxS-E-PMNB hydrogel) with ester labile bonds and non-photodegradable control gel (PEG-OxS hydrogel) preparation by crosslinking of star PEG-MS with PMNB(E-PEG_n-SH)₂ or PEG-SH₂. **(B)** Photodegradable hydrogel with ester labile bonds (PEG-T-E-PMNB hydrogel), benchmark gel (PEG-T-E-NB hydrogel) and non-photodegradable control hydrogel (PEG-T hydrogel) preparation by crosslinking of star PEG-DBCO with PMNB(E-EG₁₂-N₃)₂, NB-E-(EG_n-N₃)₂ or PEG(N₃)₂. **(C)** Photodegradable hydrogel (PEG-STz-C-PMNB hydrogel and PEG-SOx-C-PMNB hydrogel) with carbamate labile bonds by crosslinking of star PEG-SH with PMNB(C-EG_n-Tz-MS)₂ or PMNB(C-EG_n-Ox-MS)₂.

Hydrogels synthesized by thiol-MS crosslinking were prepared in 20 mM HEPES buffer, pH 7.5/8 and at room temperature.¹³ These conditions were selected to obtain high conversion and an intermediate

Chapter 3

crosslinking speed in order to ensure the homogeneous distribution for 3D cell encapsulation and high cell cytocompatibility. Hydrogels including PEG-OxS-E-PMNB hydrogels, PEG-OxS hydrogels, PEG-STz-C-PMNB hydrogels and PEG-SOx-C-PMNB hydrogels were prepared under these conditions. The reaction between the thiol and arylmethylsulfonyl groups is a nucleophilic aromatic substitution (**Figure 3.3**), where the nucleophilic thiolate attacks the electrophilic aromatic ring at the position substituted by the MS group, followed by a release of methanesulfinate anion as leaving group (pK_a 2.3).¹³⁻¹⁶

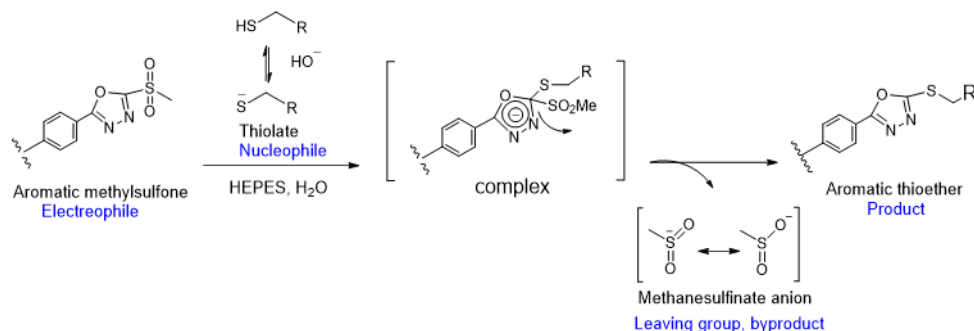


Figure 3.3 Mechanism of thiol-MS reaction particularized for the Ox-MS substrate.

Hydrogels synthesized by SPPAC reaction of DBCO and N₃ terminated precursors were prepared in PBS buffer, pH 7.4 and at room temperature. These conditions were selected to achieve for high conversion and intermediate gelation speed. The reaction between the azide and DBCO groups is following a 1,3-dipolar cycloaddition reaction, affording a highly stable 1,2,3-triazole linkage (**Figure 3.4**). SPAAC click chemistry have been widely used in cell studies due to high specificity (chemical orthogonality to many biological processes), high stability and high yield.¹⁷ Variants were obtained by reaction of star PEG-DBCO with PMNB(E-EG₁₂-N₃)₂, or PEG(N₃)₂ (non-degradable control) and NB-E-(EG_n-N₃)₂.

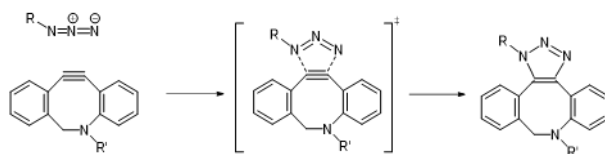


Figure 3.4 Mechanism of N₃-DBCO click reaction.

An important parameter for cell encapsulation is the gelation time. This time was measured by pipetting method for the described hydrogels, and is defined as the time from the time point of mixing the two precursors until pipetting of the mixture was no longer possible. For cell encapsulation experiments, a gelation time between seconds to minutes is considered appropriate, since it enables the homogenization of precursor solutions and leads to fewer network defects. For thiol-MS crosslinking chemistry, the gelation time is dependent on the pH due to the deprotonation of -SH group ($pK_a \sim 8$).¹⁸ In order to optimize crosslinking time for PEG-OxS-E-PMNB hydrogels, HEPES buffer of varying pH (7.5-8) and concentration (10-20 mM) were studied. The concentration increase from 10 mM to 20 mM allowed speeding up the gelation process from 5 h to 3 s. The pH decrease from 8 to 7.5 allowed slowing down the gelation process from 3 s to 30 s. **Table 3.1** shows the estimated gelation times for PEG-OxS-E-PMNB hydrogels. For PEG-OxS hydrogel, a shorted gelation time ~ 10 s

was obtained when same conditions were used (HEPES buffer, pH 7.5, 20 mM), which is probably due to the higher flexibility of PEG-SH₂ chains that allows them to interact with binding sites more efficiently.

Table 3.1 Preparation conditions for PEG-OxS-E-PMNB hydrogels formulations and gelation times estimated by a macroscopic test.

Polymer concentration [wt %]	HEPES Buffer pH and Concentration	Temperature	Gelation time*
6.3%	pH 8, 10 mM	25 °C	~ 5 h
6.3%	pH 8, 20 mM	25 °C	~ 3 s
6.3%	pH 7.5, 20 mM	25 °C	~ 30 s

* Gelation time was taken from the time point of mixing the two precursors until pipetting of the mixture was no longer possible.

The gelation kinetics of MS-hydrogels can also be influenced by factors like temperature or buffer concentration, in addition to pH and the type of MS substrate. For thiol and Ox-MS coupling, the pH range between 6.6 and 8, the temperature range 40-50 °C and the polymer concentration range 1.3 to 10 wt% allow formation of gels within a range of gelation times between 3 s - 4 mins, 7 - 30 s and 2 - 18 s respectively.¹⁹ For thiol and Tz-MS coupling, a longer gelation time ranged from 36 s to 1.9 h was obtained under same conditions due to the lower electrophilicity of -Tz group. Faster gelation rate ($k_{obs} \times 10^4 \text{ Pa s}^{-1}$: 2.05 ± 0.42 to 10.1 ± 2.0) was reported in the literature by increasing buffer concentration (10, 20, or 50 mM concentration of HEPES).²⁰ Different parameters, including encapsulation medium (HEPES buffer (20 mM)) and pH (7.5-8), were studied in this Thesis for the adjustment of gelation rate.

For PEG-STz-C-PMNB and PEG-SOx-C-PMNB hydrogels, a reducing agent (tris(2-carboxyethyl)phosphine, TCEP) is required to break disulfide bond formation between free -SH groups of the star PEG-SH precursor. An equimolar ratio of TCEP in respect to thiol groups was used (i.e., TCEP:SH 1:1). For PEG-SOx-C-PMNB hydrogels, a similar gelation time was obtained ~ 30 s as for PEG-OxS-E-PMNB hydrogels under same conditions (HEPES buffer, pH 7.5, 20 mM). For PEG-STz-C-PMNB hydrogels, A longer gelation time was obtained, around ~ 15 min, in HEPES buffer (pH 7.5, 20 mM) due to the lower electrophilicity of the Tz ring and the restricted solubility properties of PMNB(C-EG₁₅-Tz-MS)₂. Gelation time was shorted to ~ 7 min was when using higher pH (HEPES buffer, pH 8, 20 mM) in order to avoid sedimentation of the embedded cells.

For SPAAC coupling between -N₃ and -DBCO groups, the relation time ranged from 50-90 s in PBS buffer (pH 7.4), which is a comfortable range to enable homogenization of precursor solutions before the gelation is achieved. Similar gelation time was observed for SPAAC crosslinking chemistry as reported by Anseth et.al.^{10, 21} **Table 3.2** shows the estimated gelation times (tube inversion method) after optimization for different PEG hydrogels.

Chapter 3

Table 3.2 Preparation conditions for different PEG hydrogels formulations and gelation times estimated by a macroscopic test.

Hydrogel	MS:SH molar ratio	DBCO:N ₃ molar ratio	Final polymer conc. [wt%]	Solvent	Gelation time [s]*
PEG-OxS-E-PMNB	1:1	-	6.3%	20 mM HEPES, pH 7.5	~30 s
PEG-OxS	1:1	-	6.5%	20 mM HEPES, pH 7.5	~10 s
PEG-T-E-PMNB	-	1:1	5.8%	PBS buffer, pH 7.4	~50 s
PEG-T-E-NB	-	1:1	5.7%	PBS buffer, pH 7.4	~60 s
PEG-T	-	1:1	6%	PBS buffer, pH 7.4	~90 s
PEG-STz-C-PMNB	1:1	-	6 wt%	20 mM HEPES, pH 8 + TCEP [#]	~7 min 10 s
PEG-SOx-C-PMNB	1:1	-	5.25 wt%	20 mM HEPES, pH 7.5 +TCEP [#]	~30 s

* Gelation time was taken from the time point of mixing the two precursors until pipetting of the mixture was no longer possible.

[#] TCEP was added in a 1:1 molar ratio to -SH groups of star PEG-SH.

3.3 Characterization of crosslinking kinetics and mechanical properties of the hydrogels by rheology

In order to monitor the gelation kinetics of the hydrogels and to quantify their mechanical properties, shear oscillatory rheology experiments were performed during crosslinking. In oscillatory time sweep experiments, the storage (G') and loss (G'') moduli were tracked as function of time. The gelation time in this method is defined as the time where the cross-over of G' and G'' curves occurs. The plateau value of G' was taken as the final stiffness of the hydrogel. Precursor mixtures were prepared directly on the plates of a rotational rheometer and mixed with pipet for a few seconds. A 12 mm diameter top plate was lowered to set an initial gap of 250 μm and the area surrounding the sample was sealed with silicone oil to prevent dehydration during measurement. The time sweep measurement was immediately conducted at controlled temperature of 25°C (using a Peltier element), strain of 1% and frequency of 1 Hz. These values are within the linear viscoelastic range of the sample. A time about 90 s was needed for setting in-situ rheology experiments, after which data collection started. The shear storage and loss moduli were tracked during 60 min. Of note, star PEGs and OEG crosslinkers (> 90%) with high substitution degree of end-functionalized groups (> 88%) were used.

The time sweep curves of the different gels are shown in **Figure 3.5** and relevant parameters are summarized in **Table 3.3**. An increase in G' was observed during the first minutes in most samples, indicating that the hydrogel stiffens as the crosslinking reaction progresses. In all samples the gelation point ($G' > G''$) was achieved before the start of the measurement, i.e. within the first 90 s, and therefore the crossover point is not visible in the curves. This is in agreement with the macroscopic

observations (Table 3.2). Gelation is completed within 5-7 minutes, as indicated by a steady state value reached by G' .

The crosslinking rate varied with the type of the crosslinker and crosslinking conditions. PEG-OxS-E-PMNB hydrogels showed slower crosslinking rate than PEG-OxS hydrogels, which might be explained by a restricted conformational mobility of the spacer in the former due to the rigid biphenyl structure. This could make the terminal -SH less accessible to be incorporated into the network structure of the star PEGs. Hydrogels crosslinked with DBCO- N_3 showed a faster gelation than thiol-MS systems, these results are also consistent with reported data.^{13, 22}

The final G' values of the crosslinked hydrogels were also dependent on the type of crosslinker and crosslinking reaction. G' of PEG-OxS hydrogels was 8 times bigger than of PEG-OxS-E-PMNB hydrogels, which might due to the high flexibility of SH groups of linear PEG-SH₂.

In DBCO- N_3 crosslinked hydrogels smaller differences of G' were observed between the three variants, though a small trend PEG-T hydrogels > PEG-T-E-NB hydrogels \approx PEG-T-E-PMNB hydrogels was still noticed. This can be explained by the 1) higher flexibility of PEG linker than NB and PMNB crosslinker structure that allows more efficient coupling to DBCO groups, and 2) higher rigidity of the biphenyl structure of PMNB in relation to NB structure.

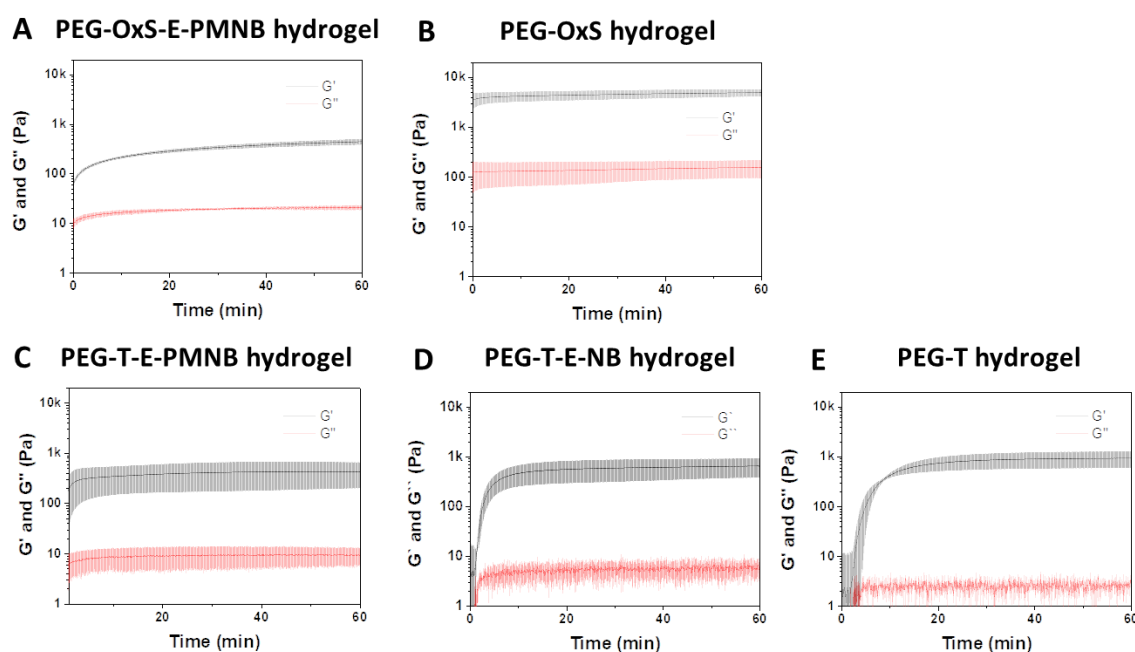


Figure 3.5 Rheological time sweep curves showing the curing kinetics and final mechanical strength of different PEG-based gels: PEG-OxS-E-PMNB hydrogel (A), PEG-OxS hydrogel (B), PEG-T-E-PMNB hydrogel (C), PEG-T-E-NB hydrogel (D) and PEG-T hydrogel (E). Hydrogel composition: star, 20 kDa PEG macromers, 5.7-6.5 wt% final polymer content, in 20 mM HEPES pH 7.5 (A-B) or PBS pH 7.4 (C-D).

Chapter 3

Table 3.3 Shear storage modulus (G') for different PEG hydrogel formulations at 30 and 60 min curing.

Hydrogel	G' (Pa) at t= 30 min	G' (Pa) at t= 60 min
PEG-OxS-E-PMNB	338±29	444±55
PEG-OxS	4494±871	4883±750
PEG-T-E-PMNB	410±235	427±223
PEG-T-E-NB	589±272	629±277
PEG-T	848±289	926±324

In summary, hydrogels with shear modulus values ranging from 0.4 to 5 kPa were prepared using close-to-physiological conditions at room temperature. Good mixing and homogenization of precursor solutions was possible in all cases, in spite of the fact that the gelation time, defined as the crossover point of G' and G'' in the rheology curves, was < 90 s in all cases. Gelation kinetics mediated by thiol-MS coupling was slower than in DBCO- N_3 crosslinked hydrogels.

The polymer concentration is known to affect the gelation rate, but this factor was not further studied in this Thesis. For later cell studies, cell medium instead of PBS might be used for gel formation and cell encapsulation, and this could also affect the gelation. However, in a macroscopic test similar gelation time was observed for PEG-OxS-E-PMNB hydrogel (6.3 wt%) and PEG-SOx-C-PMNB hydrogel (5.25 wt%) preincubated with cyclo[RGDfC] (1/8 or 1/6) when using a mixture of cell culture medium and HEPES buffer. Finally, coupling of cell adhesive ligands to the network before gelation might also affect gelation kinetics. In fact, incorporation of RGD domains in crosslinked hydrogels resulted in longer gelation times and lower storage modulus as consequence of the lower effective crosslinking degree.²³

3.4 Study of hydrolytic stability of the hydrogels

Hydrolytic stability of hydrogels in culture is an important parameter that influences cellular response and the life time of the cell culture itself. In this work, we aimed at fabricating photo-tunable hydrogels which degradability can be regulated by light exposure on demand. Ideally, these materials should be hydrolytically stable to allow the user direct control of the materials degradation rate at will. However, from the chemical structure of the crosslinkers used in this work (ester vs. carbamate linkages) the possibility of hydrolytic degradation cannot be excluded. Therefore, the stability of the hydrogels was studied in cell culture medium and 37 °C. Degradation is expected to decrease the crosslinking degree and to result in increased swelling and final dissolution of the network.

Hydrogels were incubated in cell culture medium at 37 °C in the dark, and the degradation of the hydrogel over time was monitored. For these experiments, hydrogels modified with 1-2 mM concentration of the cell-adhesive peptide RGDfX were used, as needed for the later cell experiments. **Table 3.4** shows the hydrolytic behavior of different hydrogels. PEG-OxS-E-PMNB hydrogels, with a

polymer concentration from 6.3 to 9.4 wt%, fully degraded in 12 h. The hydrolysis of the ester bond is supposed responsible for the degradation.^{24, 25} In an attempt to extend the stability, hydrogels with a mixture of degradable PMNB(E-PEG_n-SH)₂ crosslinker and non-degradable PEG-SH₂ crosslinker were studied. No significant improvement of stability (<2 days) was observed. The hydrogels with carbamate labile bonds PEG-STz-C-PMNB (4.83 – 6 wt%) and PEG-SOx-C-PMNB (4.0 - 5.25 wt%) presented higher stability and remained intact for more than 2 months. This behavior is similar to that of nondegradable control hydrogels PEG-OxS. In summary, the chemical identity of the linker bonds between PMNB chromophore and PEG spacer affected the hydrolytic stability of the hydrogels. PEG-STz-C-PMNB and PEG-SOx-C-PMNB hydrogels with carbamate labile bond exhibited stability for > 2 months, suggesting their utility for long term cell studies. Note that this degradation might be accelerated in the presence of living cells because the cells can secrete proteases which can participate in multi proteolytic activities, thus leading to hydrogel degradation.

Table 3.4 Hydrolytic stability of hydrogels with different crosslinker

Hydrogel	Crosslinker	Polymer Concentration (wt%)	RGD amount (RGD:-MS molar ratio)	RGD concentration	Stability
PEG-OxS-E-PMNB	PMNB(E-PEG _n -SH) ₂	6.3%	1/8	1.25 mM	< 12 h
		9.4%	-	-	< 12 h
	PMNB(E-PEG _n -SH) ₂ :PEG-SH ₂ 1:1	6.3%	-	-	< 2 days
		9.4%	-	-	< 2 days
		12.6%	-	-	< 2 days
PEG-OxS	PEG-SH ₂	6.3%	-	-	> 2 months
		5.25 wt%	1/6	1.34 mM	> 2 months
		4.6 wt%	1/6	1.18 mM	> 2 months
PEG-STz-C-PMNB	PMNB(C-EG ₁₅ -Tz-MS) ₂	6.2 wt%	1/6	1.67 mM	> 2 months
		4.83 wt%	1/6	1.33 mM	> 2 months
PEG-SOx-C-PMNB	PMNB(C-EG ₂₃ -Ox-MS) ₂	5.25 wt%	1/6	1.33 mM	> 2 months
		4.6 wt%	1/6	1.17 mM	> 2 months
		4.0 wt%	1/6	1 mM	> 2 months

3.5 Study of hydrogel photodegradation with UV/Vis light by rheology

3.5.1 1P degradation of hydrogel at UV/Vis

The photo-degradation of the hydrogels during illumination was monitored in a rheology experiment. The evolution of G' upon exposure to UV light at increasing time was recorded. Cleavage of the photolabile bonds within the polymer backbone breaks the network structure and this should lead to a decrease of G' with the irradiation time.¹

Chapter 3

For these experiments, a rheometer with a parallel plate geometry and a transparent lower plate was used. An illumination source (Omniculture s2000, filter $\lambda = 365$ nm) was connected to the rheometer and the irradiance was adjusted by output power. The sample was allowed to cure in the dark for 30 - 120 min until reaching a stable G' value. Afterwards, the lamp was switched on and the sample was irradiated for other 120 min while the measurement continued. The irradiation dose used for the photodegradation experiments is calculated as:

$$\text{Irradiation dose} = \frac{\text{Irradiance}}{1000} \times \text{time}$$

Where irradiation dose is defined in J cm^{-2} , irradiance in mW cm^{-2} and time in s.

PEG-OxS-E-PMNB and PEG-OxS hydrogels

Figure 3.6 shows the evolution of the shear and loss modulus of PEG-OxS-E-PMNB and PEG-OxS hydrogels as a function of illumination time. In PEG-OxS-E-PMNB hydrogels, a progressive decay of G' and G'' was observed during illumination, indicating a softening of the network, presumably as a consequence of the photocleavage of the PMNB group (**Figure 3.6A**). Initial $G' \sim 600$ Pa decreased by 50% and 90% after 5.5 and 18 min exposure at 20 mW cm^{-2} . The degradation of the network was confirmed by the fluid appearance of the irradiated sample after completion of the study. In the control hydrogel PEG-OxS, no changes in G' or G'' with exposure were observed. This result confirmed that the decay observed in PEG-OxS-E-PMNB hydrogels is solely associated with the presence of the photocleavable PMNB group.

The rate and extent of hydrogel photodegradation was dependent on the irradiance of the lamp. PEG-OxS-E-PMNB hydrogels with initial $G' \sim 600$ Pa showed a 50% drop in G' when irradiated for 5.5, 6 or 9.5 min at 20 , 10 or 5 mW cm^{-2} , and a $>90\%$ drop after 18, 20 and 40 min exposure, respectively. These results demonstrate that PEG-OxS-E-PMNB hydrogels allow controlled photodegradation by regulating the exposure dose. Moreover, the irradiation dose used for degrading PEG-OxS-E-PMNB hydrogels is in the range for cytocompatible cell encapsulation ($5\text{--}10 \text{ J cm}^{-2}$).^{26, 27} According to the reported literature, typically irradiation conditions which have proved under cytocompatible range are $\lambda = 365$ nm, Irradiance = $5\text{--}20 \text{ mW cm}^{-2}$, $t = 2\text{--}20$ min; total dose $5\text{--}10 \text{ J cm}^{-2}$.^{28, 29} For PEG-OxS-E-PMNB hydrogels, a same corresponding irradiation dose of 12 J cm^{-2} was required at irradiance of 5 and 10 mW cm^{-2} due to different irradiation time, while a higher irradiation dose of 21.6 J cm^{-2} was required at irradiance of 20 mW cm^{-2} . According to these results, irradiation dose required for fully degradation of PEG-OxS-E-PMNB hydrogels is above the cytocompatible range, which might need to be carefully used according to the different degradation degree for 1P degradation of hydrogels in presence of cells.

The G' and G'' curves of PEG-OxS-E-PMNB showed a fast drop (in seconds) when irradiation started, but the curve returned almost to the initial value within one minute. A similar behavior was reported for disulfide-crosslinked hydrogels, which can cleave and reform upon UV exposure due to thiol-disulfide exchange.³⁰ Thiol-disulfide exchange can be initiated by light via the thiol-centered mechanism. A nucleophile thiolate anion (RS^-) attacks the sulfur atoms of the disulfide to give a new disulfide bond and a new free thiolate is released.³¹ This leads to the hypothesis that the PEG-OxS-E-

PMNB hydrogels could present thiol-disulfide exchange. Light exposure would induce the conformational changes of polymer chain, thus the hindered $-SH$ groups are exposed. The self-reaction of the thiol groups of the crosslinker would form disulfide bonds and undergo thiol-disulfide exchange. On the other side, there are also disulfide bonds formed during hydrogel preparation, which can also undergo thiol-disulfide exchange. After illumination, cleavage of the disulfide groups and the formation of new bonds (i.e. reconfiguration) could lead to the sudden changes in G' and G'' . For PEG-OxS hydrogels, no sudden change was observed upon illumination, which might be due to a higher conversion because more $-SH$ groups reacted with MS groups (due to higher mobility of PEG-SH₂ crosslinker). Upon illumination with varying exposure doses, PEG-OxS control hydrogels didn't shown any sign of degradation, as expected from the absence of cleavable chromophores. A slightly variable G' value was observed which might also be due to the thiol-disulfide exchange (**Figure 3.6B**). The side photolytic reactions can lead to unpredicted change of G' and uncontrolled degradation degree, therefore a longer irradiation time was needed, resulting a poor precision over degradation accuracy and higher irradiation doses may cause reduced cytocompatibility to the further cell experiments.

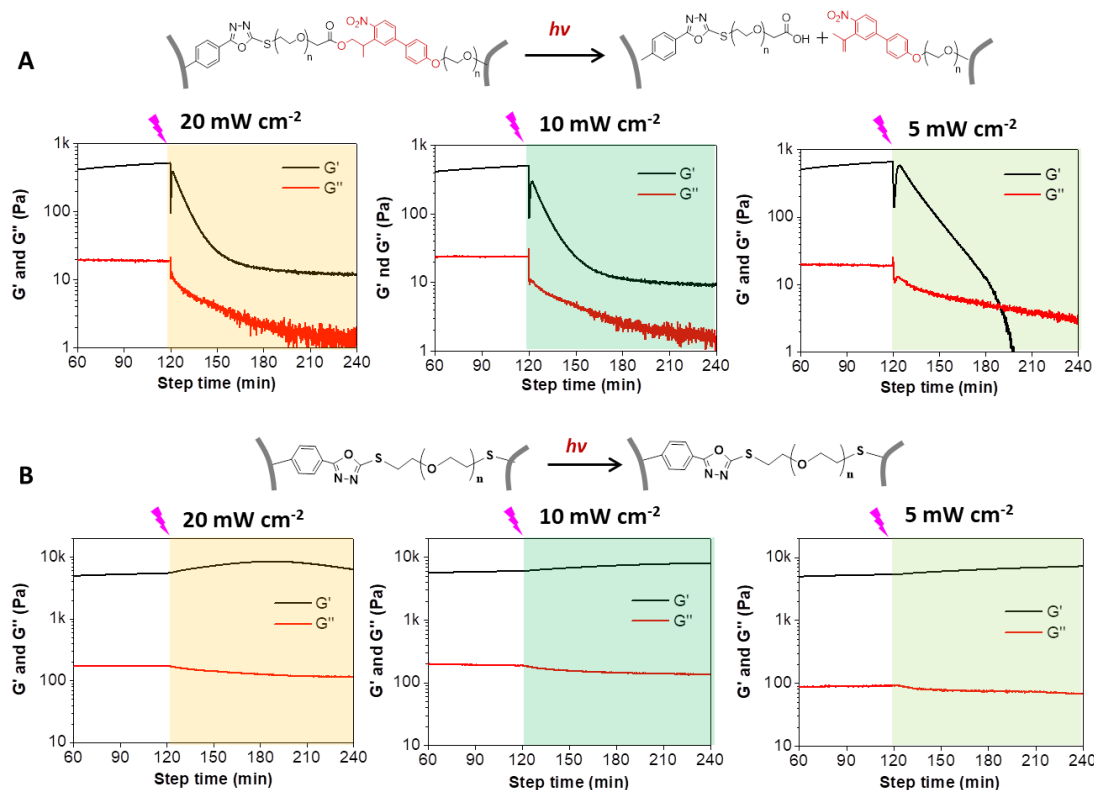


Figure 3.6 Evolution of the shear and loss modulus of PEG-OxS-E-PMNB (**A**) and PEG-OxS (**B**) hydrogels during illumination at different irradiance values. Colored regions in the plots indicate the illumination time. PEG-OxS-E-PMNB and PEG-OxS hydrogels composition: 20 kDa, star PEG-MS, 6.3-6.5 wt% polymer content, 20 mM HEPES (pH 7.5). Conditions for illumination: $\lambda=365$ nm, irradiance = 5, 10 or 20 mW cm⁻².

In summary, these results demonstrate that the network structure of PEG-OxS-E-PMNB hydrogels can be degraded by light illumination, and that the degradation rate and extent can be modulated by tuning the light dose.

PEG-T-E-PMNB and PEG-T hydrogels

Chapter 3

Figure 3.7 shows the evolution of the shear and loss modulus of PEG-T-E-PMNB and PEG-T hydrogels as a function of illumination time. PEG-T-E-PMNB hydrogel of initial $G' \sim 166$ Pa showed a 60% drop of G' followed by a jump to 462 Pa within the first seconds of light exposure. A progressive increase of G' to 678 Pa was observed in the following 60 minutes of exposure, indicative of an increase in the crosslinking degree of the network. No signs of the expected softening, i.e. degradation, were observed during 120 min illumination (**Figure 3.7A**). The hydrogel sample after irradiation was brownish and maintained a gel character in visual inspection. The stiffening of the hydrogel upon illumination was unexpected, and contrasted with the softening observed in the PEG-OxS-E-PMNB hydrogel in the previous experiments (**Figure 3.6**). These two systems differ in the type of crosslinking. The irradiation seems to trigger unexpected side reactions that lead to additional crosslinking of the network instead of depolymerization. The phototriggered stiffening could be consequence of i) cycloaddition reactions between unpolymerized DBCO groups or ii) cross-reaction between triazole groups with the nitrostyrene photolysis product. Ethyl azide groups are not expected to contribute to the observed stiffening, since photoinitiators and catalyst are needed for photoactivated cycloaddition reactions between ethyl azide and alkyne groups.³²

To test these hypotheses, a number of control experiments were performed. To test the possibility of cycloadditions between unpolymerized DBCO groups, control experiments with PEG-T hydrogels were performed. No changes in G' or G'' were observed upon exposure. However, it is important to highlight that PEG-T hydrogels showed higher G' final values and, therefore, a higher crosslinking degree is expected or, in other words, no free DBCO groups would be available for additional cycloadditions (**Figure 3.7B**). These results with PEG-T hydrogels are, therefore, not conclusive. Photorheology measurements of a solution of PEG-DBCO precursor were performed (**Figure 3.7C**). A slow increase of G' and G'' was observed. A gelation point was achieved after 70 min exposure, and a gel with $G' \sim 805$ Pa formed after 120 min. This result indicates that light exposure might induce cycloaddition reactions between unpolymerized DBCO groups, but this might not be a major reason for the photo-triggered stiffening of PEG-OxS-E-PMNB hydrogel since a time delay was observed. Note that photoreaction of DBCO groups in the presence of a photoinitiator in SPAAC hydrogels has also been reported by other authors.^{22, 33} This effect could be avoided by blocking of unreacted DBCO groups via incubation with a short N_3 compound before illumination. In order to test this possibility, PEG-T-E-PMNB hydrogels were incubated with O-(2-Azidoethyl)-O'-methyl-triethylene glycol in order to react remaining free DBCO groups after gel formation prior to light exposure (**Appendix**).³⁴ In the subsequent rheology experiment, G' (68 Pa) increased to 508 Pa within the first minutes, and gradually decreased during the following 90 minutes the initial value (**Figure 3.7D**). This result indicates that the observed photo-stiffening of PEG-T-E-PMNB hydrogels is not caused by unreacted cyclooctynes.

Based on these results, the unexpected photo-stiffening of PEG-T-E-PMNB hydrogel is attributed to a light-promoted reaction between nitrostyrene photoproduct and other groups in the polymer chain, presumably the triazole group. These features hinder the application of the PEG-T-E-PMNB hydrogel and, therefore, this system was not studied further in this **Thesis**.

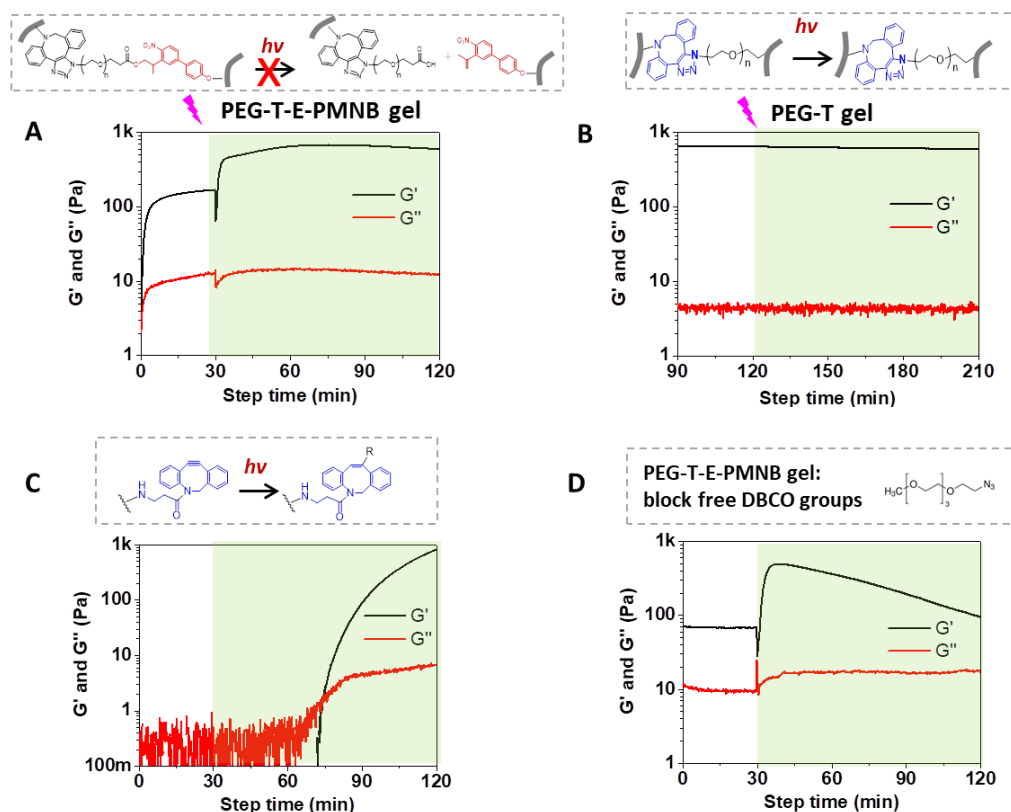


Figure 3.7 Behavior of PEG-T-E-PMNB and PEG-T hydrogels upon light exposure, as followed by in situ rheology. Colored regions in the plots indicate illumination. **(A)** PEG-T-E-PMNB hydrogels. **(B)** PEG-T hydrogels. **(C)** Star PEG-DBCO precursor only upon light illumination. **(D)** PEG-T-E-PMNB hydrogels with prior blocking of free DBCO groups via reaction with a monofunctional PEG- N_3 spacer. Hydrogel composition (A,B,D): 20 kDa star PEG-DBCO, 5.8-6.0 wt% polymer content, in PBS buffer pH 7.4. Composition in (C): 5 wt% polymer content in PBS buffer pH 7.4. Conditions for illumination: $\lambda=365$ nm, 5 mW cm^{-2} .

Comparison of photodegradation of PEG-OxS-E-PMNB and PEG-T-E-NB hydrogels

In order to compare the photodegradation efficiency of PMNB-based hydrogels with the benchmark NB-based hydrogels, similar rheology studies were performed with PEG-T-E-NB hydrogel (**Figure 3.8A**). Light illumination of the PEG-T-E-NB hydrogel led to rapid decrease of G' , indicative of an efficient photolysis of the NB photocleavable group and consequent softening of gels. A 50% decay of G' was observed at 0.25 min (at 20 mW cm^{-2}). Photodegradation rate was regulated by light dose. Upon illumination at irradiance = 20 , 10 and 5 mW cm^{-2} , a drop of $> 90\%$ of G' was observed in 6.4 min, 3 min and 1 min, respectively.

Corresponding irradiation dose of 1.92 J cm^{-2} , 1.8 J cm^{-2} and 1.2 J cm^{-2} was required at irradiance of 5 - 120 mW cm^{-2} . Control experiments with PEG(N_3) $_2$ (**Figure 3.8B**) showed no changes in G' or G'' , confirming that the degradation of PEG-T-E-NB gels is due to the presence of NB group. The photolysis product of PEG-T-E-NB hydrogels is a *o*-nitrosoketone group that does not seem to interfere with the photodegradation, as observed in PEG-T-E-PMNB hydrogels (**Figure 3.9**). This is an apparent advantage of the NB system vs. the PMNB hydrogel in the context of 1P degradation.

Chapter 3

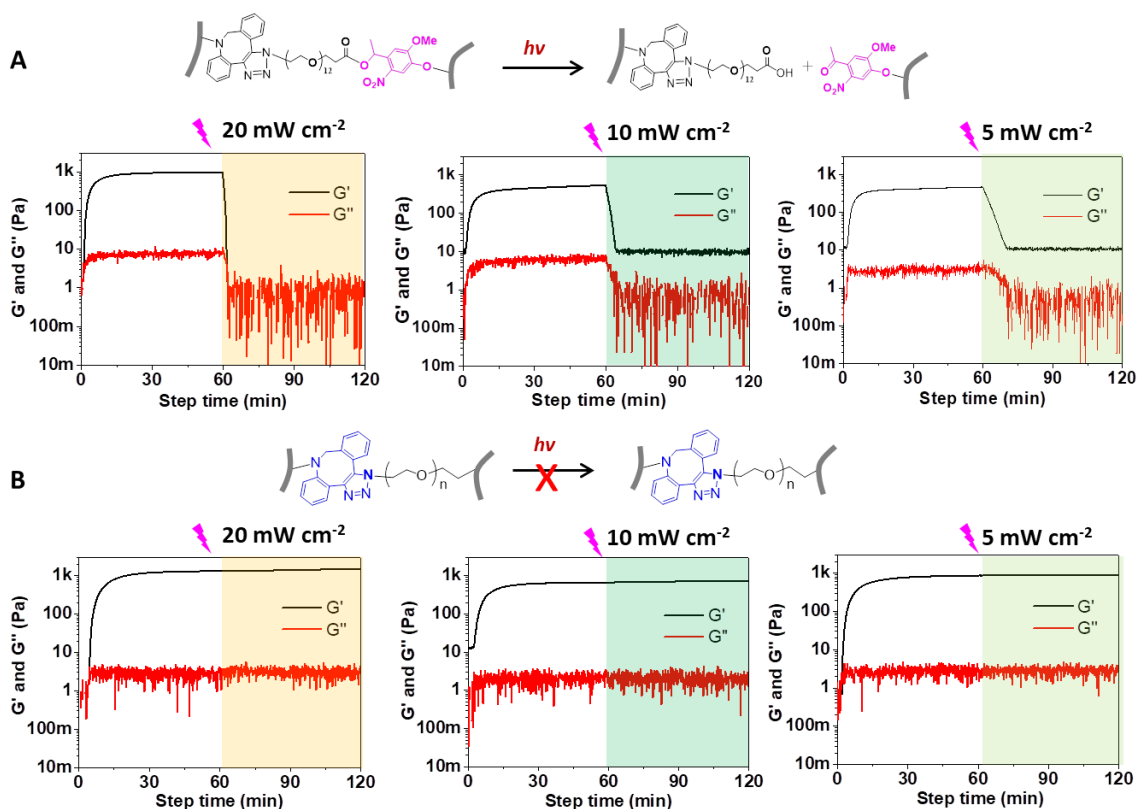


Figure 3.8 Behavior of PEG-T-E-NB and PEG-T hydrogels upon light exposure by in situ rheology. Colored regions in the plots indicate illumination. **(A)** Photodegradation kinetics of PEG-T-E-NB hydrogels upon different illumination dose. **(B)** Control PEG-T hydrogels. Gel composition: 20 kDa star PEG-DBCO, 5.7-6.0 wt% polymer content, PBS buffer pH 7.4. Conditions for illumination: $\lambda=365$ nm, 5 mW cm^{-2} , 10 mW cm^{-2} or 20 mW cm^{-2} .

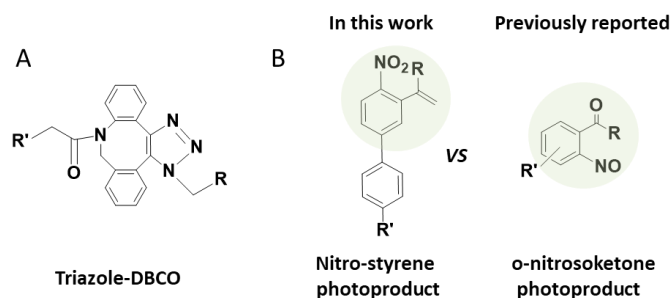


Figure 3.9 Chemical structures of **(A)** triazole-DBCO, and **(B)** photoproducts of PMNB and *o*NB photolysis: *o*-nitro styrene vs. *o*-nitrosoketone.

In order to compare the photodegradation efficiency of the PMNB and *o*NB-based hydrogels, the rheological curves of PEG-OxS-E-PMNB and PEG-T-E-NB hydrogels measured at different irradiances were normalized and merged in one graph (**Figure 3.8A**). Note that both hydrogels showed G' values of 444 ± 55 Pa and 629 ± 277 Pa after crosslinking. PEG-T-E-NB hydrogels showed a faster photodegradation efficiency than PEG-OxS-E-PMNB hydrogels. Moreover, all the hydrogels showed dose-dependent degradation. Longer exposure time (> 25 min) was needed for PEG-OxS-E-PMNB hydrogels, while < 7 min were used for PEG-T-E-NB hydrogels. Corresponding irradiation doses of PEG-T-E-NB hydrogels (1.2 - 1.92 J cm^{-2}) were significantly lower than PEG-OxS-E-PMNB hydrogels (12 - 21.6

J cm⁻²). These results indicate a higher suitability of NB-based photodegradable hydrogels in the applications of encapsulated cells excited by 1P.

The kinetic parameters of the photolysis reaction were extracted from these curves by assuming that the photolysis reaction occurs with a first-order kinetics, and fitting the rheological curve to a first-order degradation model, where the first order rate constant (k_{obs}) that can be expressed as:^{10, 28, 33}

$$G'(t) = G'_0 e^{-k_{obs} t}$$

Where G' is the shear storage modulus at a given time, G'_0 is the initial shear storage modulus, and t is the time of exposure. From the integral of this equation:

$$\ln \left(\frac{G'}{G'_0} \right) = -k_{obs} t$$

By plotting $\ln(G'/G'_0)$ as a function of time and after linear fitting, the value of k_{obs} can be obtained from the slope. To avoid interference of other photolysis processes, only the 90% to 50% of initial G'_0 was selected for calculation of the rate constant.³⁵ Of note, in the rheological data from PEG-OxS-E-PMNB hydrogels, the initial jump was not considered for this calculation.

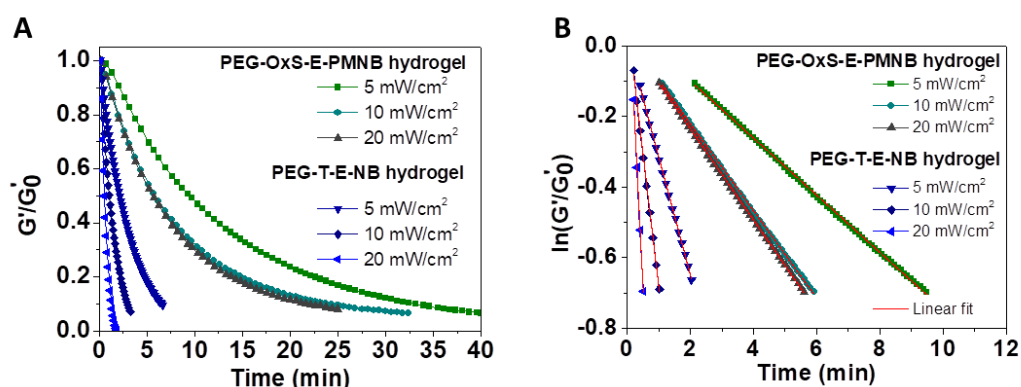


Figure 3.10 (A) Comparison of photodegradation efficiency of PEG-OxS-E-PMNB hydrogels and PEG-T-E-NB hydrogels. **(B)** Photodegradation kinetic curve fits for PEG-OxS-E-PMNB hydrogels and PEG-T-E-NB hydrogels. Gel composition: 20 kDa, star PEG, 5.7-6.3 wt% polymer content, PBS buffer pH 7.4 or 20 mM HEPES buffer pH 7.5. Conditions for illumination: $\lambda=365$ nm, 5-20 mW cm⁻².

The photo-softening curves of PEG-OxS-E-PMNB gels and PEG-T-E-NB hydrogels fit well to the first-order approximation (**Figure 3.10**). **Table 3.5** shows the values of the value of k_{obs} and also the calculated apparent kinetic constants of the photodegradation process normalized by the light intensity (k_{obs}/I_0). The photodegradation rate constants obtained for PEG-OxS-E-PMNB hydrogels ranged from 1.36 to $2.16 \times 10^{-3} \text{ s}^{-1}$, and for PEG-T-E-NB hydrogels from 5.6 to $28.8 \times 10^{-3} \text{ s}^{-1}$. The 5- to 10-fold slower photodegradation rate obtained for PEG-OxS-E-PMNB gels vs. PEG-T-E-NB hydrogels is surprising taking into account that contrary trend in these parameters were observed in the photocleavage studies of the PMNB and NB crosslinkers in solution (followed by HPLC and UV/Vis spectra) (see **Chapter 2, Table 2.3**). We attribute the lower photo-efficiency of PMNB gels obtained from rheology data to the occurrence of photo-triggered polymerization reactions in parallel to the

Chapter 3

photolysis process. Our results showed that these could be reactions involving disulfide and free –SH groups in the network.

Table 3.5 Photodegradation rate comparison of crosslinkers and hydrogels upon 365 nm light irradiation.

Chromophore	Hydrogel	
	Photodegradation rate k_{obs} [s^{-1}] ⁽¹⁾	k_{obs}/I_0 [$cm^2s^{-1}mW^{-1}$] ⁽¹⁾
PMNB	1.36-2.16 ($\times 10^{-3}$)	0.1-0.28 ($\times 10^{-3}$)
oNB	5.6-28.8 ($\times 10^{-3}$)	1.12-1.44 ($\times 10^{-3}$)

⁽¹⁾ The apparent kinetic constant of cleavage normalized to the light intensity (k_{obs}/I_0). $I_0 = 5-20$ mW cm^{-2} .

In conclusion, both the nature of the photocleavable group and the nature of the crosslinking groups used in the network affected the photodegradation of the hydrogels. PEG-T-E-NB hydrogels showed a faster photodegradation rate than PEG-OxS-E-PMNB hydrogels, while PEG-OxS and PEG-T hydrogels did not photodegrade due to the unexpected occurrence of light-induced side reactions of the photolysis byproduct. These results indicate that the photo-efficiency of PEG-OxS-E-PMNB hydrogels is lower than the efficiency of PEG-T-E-NB hydrogels that might limit the applications of encapsulated cells excited by 1P.

3.5.2 2P degradation of PEG-OxS-E-PMNB hydrogels

In order to visualize the spatially defined photodegradation after 2P excitation, exposure experiments were performed using a 3D laser scanning microscope (LSM). An LSM equipped with a Ti-Sapphire pulse laser operating at 740 nm was used to scan small volumes at defined exposure doses. A resolution (lateral resolution: 872 nm, axial resolution: 2.18 μm) at 740 nm can be achieved with a 10x objective (NA:0.3), which was calculated according to the two-photon-modified Abbe's diffraction formula.³⁶

For the visualization of the degraded sites, a previously reported method was followed.⁴ Hydrogels were immersed in a solution of fluorescein-dextran (FITC-dextran, 1 mg mL^{-1}) with an average molecular weight of approximately 2000 kDa. This molecule cannot diffuse into the crosslinked hydrogel and remains in the surrounding solution. The illumination of hydrogel close to the hydrogel surface cleaves the network chains, increases the mesh size at the illuminated regions and allows diffusion of the fluorescent dextran and reveals the illuminated pattern by fluorescence imaging in 3D using a confocal microscope.

PEG-OxS-E-PMNB vs. PEG-T-E-NB hydrogels

Defined volumes of PEG-OxS-E-PMNB hydrogels swollen in dextran solution (1 mg mL^{-1} in PBS) were illuminated at 740 nm with a Ti-Sapphire pulsed laser. Rectangular prisms of 150x50x52.6 μm^3 were scanned inside the hydrogel, with the laser starting scanning from the hydrogel surface (**Figure 3.11A**). A series of prisms scanned with increasing light doses were achieved by varying the laser power

between 1 and 3%, the scan speed between 628 and 19.6 $\mu\text{s } \mu\text{m}^{-1}$, and the number of scans. The sample was then imaged to detect fluorescence of the dextran diffusing into the scanned volumes. **Figure 3.11B** shows the obtained images. A fluorescent pattern appeared, with similar dimensions to the scanned pattern. The fluorescence intensity in the scanned volumes increased with the illumination dose, indicating a dose-dependent diffusion of the FITC-dextran and, consequently, a light-regulated degradation of the hydrogel. The threshold dose for the appearance of fluorescence was observed at 1% power intensity and scanning speed $> 314 \mu\text{s } \mu\text{m}^{-1}$, at 2% power intensity and speed $> 39.2 \mu\text{s } \mu\text{m}^{-1}$, and at 3% power intensity and speed $> 19.6 \mu\text{s } \mu\text{m}^{-1}$. A gradient in intensity from the edge of the hydrogel to the interior volume was observed in each prism, indicating that diffusion of the fluorescent dextran into the degraded hydrogel is more hindered inside the hydrogel. Similar scanning experiments were performed on control PEG-OxS hydrogels. No fluorescence was detected after illumination, in agreement with the lack of photosensitivity of these hydrogels (**Figure 3.11B**). These results demonstrate that PEG-OxS-E-PMNB hydrogels photodegrade by two-photon exposure by photocleavage of the PMNB group intercalated in the network structure. The z-stack images shown in **Figure 3.12A** demonstrate the fluorescent intensity in the z dimension and demonstrate the 3D resolution that can be achieved by 2P photodegradation. The illuminated volumes maintained the same shape at low irradiation doses (laser power intensity $< 2\%$), whereas higher doses, i.e. more extensive degradation, resulted in small shape changes as consequence of the increased swelling of the exposed regions.

Similar experiments were performed with PEG-T-E-NB hydrogels. Significantly higher irradiation doses were needed to observe fluorescent patterns (**Figure 3.11B&12B**). Fluorescence was only visible at laser power intensity $> 2\%$ using scanning speeds $< 628 \mu\text{s } \mu\text{m}^{-1}$. At laser power intensity $> 3\%$, scanning speeds $< 314 \mu\text{s } \mu\text{m}^{-1}$ were required. Similar scanning experiments were also performed on control hydrogels PEG-T and no fluorescence was detected after illumination (**Figure 3.11B**).

Notably, at same doses used (i.e. intensity:1%, scanning speeds: 628 $\mu\text{s } \mu\text{m}^{-1}$), a higher degradation degree was observed in PEG-OxS-E-PMNB hydrogel than PEG-T-E-NB, signed by a higher fluorescence signal in the irradiation region. These proof-of-concept 2P degradation experiments demonstrated a significantly lower 2P degradation efficiency of PEG-T-E-NB vs. PEG-OxS-E-PMNB hydrogels, indicating a higher 2P efficiency of PMNB compared to the oNB within the hydrogel networks. They proof the validity of the hypothesis of this **Thesis**, and are in good agreement with the lower 2P cross-section of oNB vs. PMNB group (**Chapter 2, Table 2.2**).^{37, 38}

Chapter 3

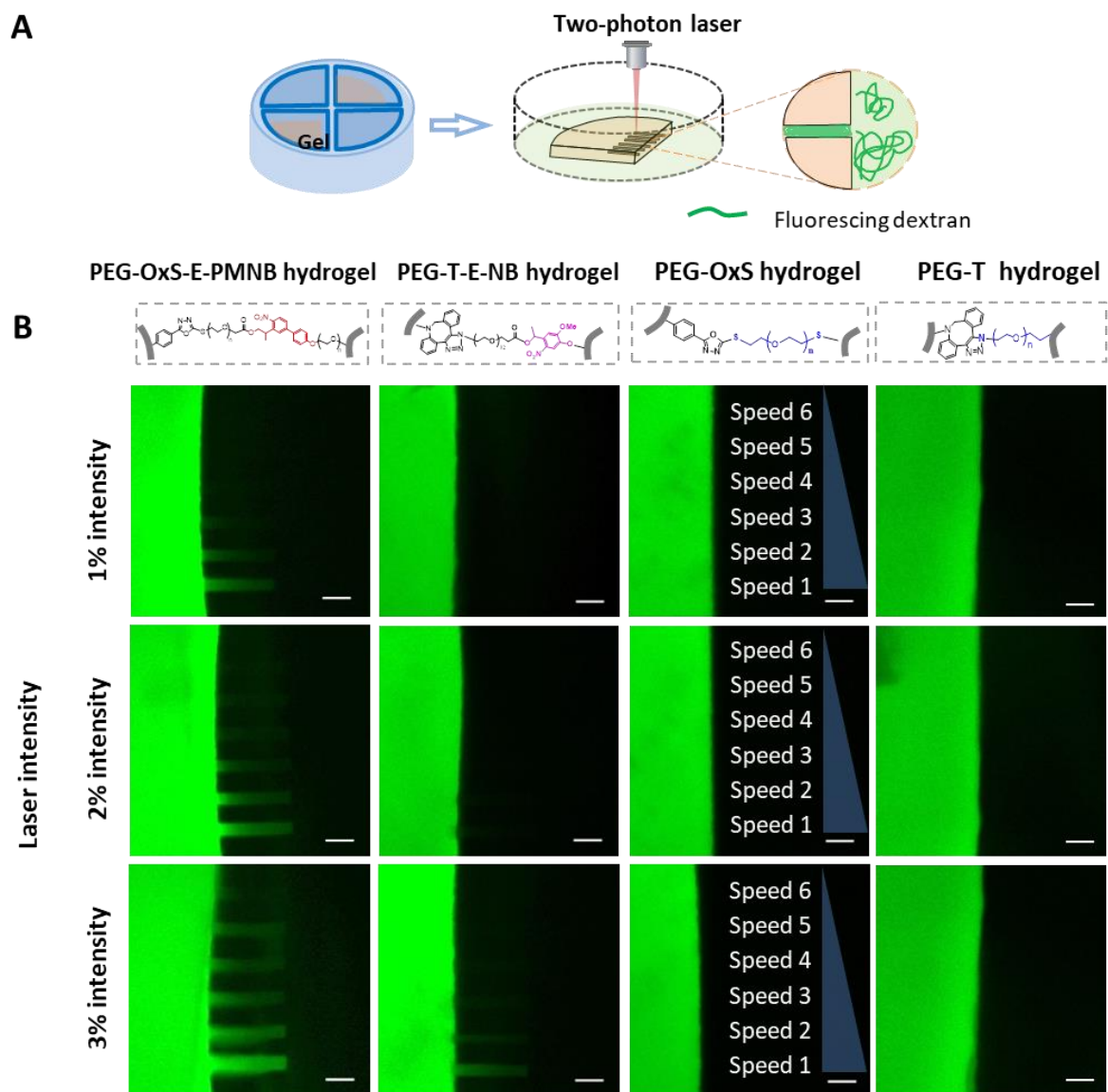


Figure 3.11 Photopatterning of the different gels by 2P excitation upon illumination with a 740 nm laser. **(A)** Scheme of hydrogel preparation, micro-channel fabrication with a 2P laser and visualization of exposed volume by soaking in a solution of FITC-dextran. Illuminated volumes present lower crosslinking degree (i.e. softening), are infiltrated by FITC-dextran and show increased localized fluorescence. **(B)** Confocal microscopy images displaying orthogonal cross-sections (x,y-plane) of micro-channels fabricated at varying irradiation dose over the different hydrogels. Scale bars= 100 μm . Conditions for illumination: 740 nm, 1-3% power intensity, speed: 628 - 19.6 $\mu\text{s } \mu\text{m}^{-1}$, scan 1, interval at z-direction: 6.57 μm . Hydrogel composition: 20 kDa, star PEG, 5.7-6.3 wt% polymer content, PBS buffer pH 7.4 or 20 mM HEPES buffer pH 7.5.

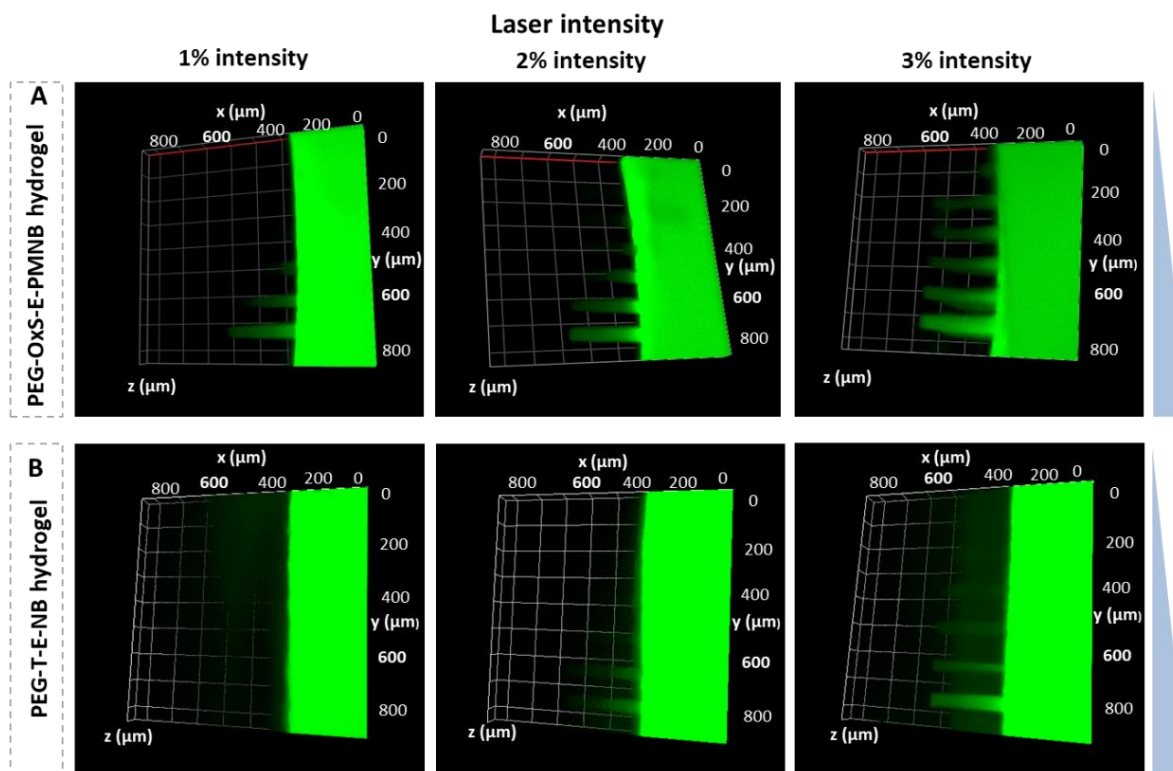


Figure 3.12 Confocal images with z-stack of 3D hydrogel patterning at different 2P illumination doses. **(A)** PEG-OxS-E-PMNB hydrogels **(B)** PEG-T-E-NB hydrogels. Conditions for illumination: 740 nm, 1-3% power intensity, speed: 1-6 ($628 - 19.6 \mu\text{m}^{-1}$), scan 1, interval at z-direction: $6.57 \mu\text{m}$. Hydrogel composition: 20 kDa, star PEG, 5.7-6.3 wt% polymer content, PBS buffer pH 7.4 or 20 mM HEPES buffer pH 7.5.

In an additional experiment, the local degradation of PEG-OxS-E-PMNB hydrogels was visualized using a different strategy. In this case, the fluorophore Alexa Fluor 555 maleimide was covalently coupled to the PEG-OxS-E-PMNB network by adding it to the polymerization mixture. The maleimide group of the fluorophore is covalently bound to $-\text{SH}$ groups of $\text{PMNB}(\text{E-PEG}_n\text{-SH})_2$ (1/8 -Mal to $-\text{SH}$ groups). Light exposure is expected to cleave the PMNB group and also the fluorophore from the network and, in consequence, a loss of fluorescence is expected in the irradiated volumes.

The scanning laser was used to write different 3D patterns within the hydrogels with a thickness of $52.6 \mu\text{m}$ (**Figure 3.13A**). Fluorescence imaging of the exposed areas reflected a local decrease of fluorescence signal (**Figure 3.13B**). Similar scanning experiments were performed on control PEG-OxS hydrogels. No fluorescence decrease was detected after illumination, confirming the decrease of fluorescence is not caused by photo bleaching (**Figure 3.13C**). This experiment demonstrates the 3D resolution of the activation process using two-photon irradiation inside the hydrogels.

At this point, it is important to compare the illumination conditions used in these experiments with acceptable illumination doses for living cells. Reported data in the group have used the same scanning laser at $\lambda=740 \text{ nm}$, power intensity 95% and speed $170 \mu\text{m}^{-1}$ to activate caged peptide to induce the HUVECs migrated towards the activated area.³⁹ The exposure conditions for degradation of NB based

Chapter 3

hydrogels in other groups were $\lambda = 860 \text{ nm}$, power $350 \text{ mW } \mu\text{m}^{-2}$, speed $1.27 \mu\text{s } \mu\text{m}^{-2}$ to direct 3D cell motility within 3D patterned hydrogels.²¹ But it should be noted here, no direct illumination on the cells was performed in these reported studies. The illumination doses used in this chapter for the degradation of PEG-OxS-E-PMNB hydrogels are considerably lower. The exposure dose is expected to be compatible with encapsulated living cells and not cause photodamage and associated loss of function of the cells due to the lower dose used compared to oNB systems.

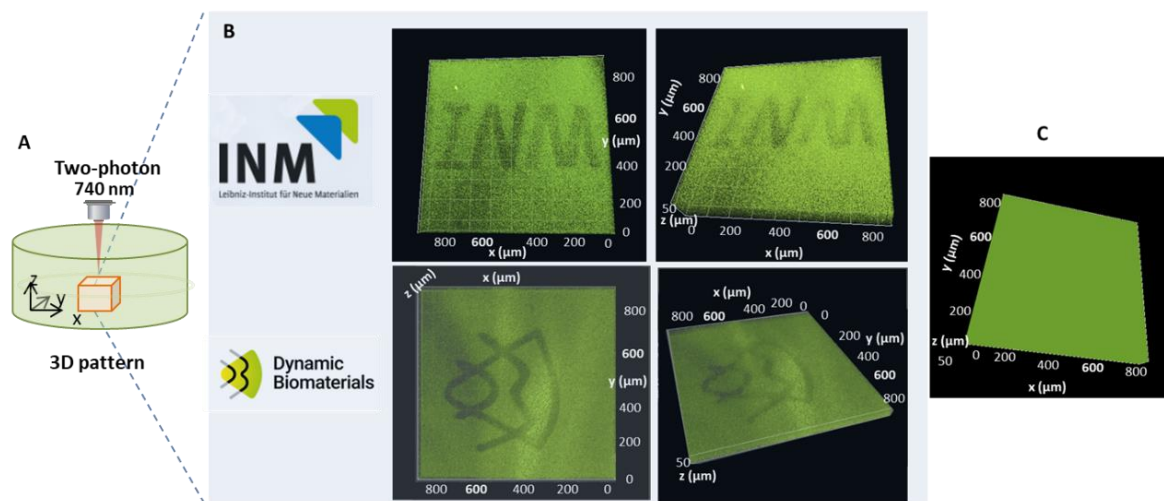


Figure 3.13 Confocal images with z-stack showing 3D patterning of fluorescently labeled hydrogels. **(A)** Scheme of 3D patterning of hydrogel with a 2P laser, **(B)** PEG-OxS-E-PMNB hydrogels, **(C)** PEG-OxS hydrogels. Gel composition: 20 kDa, star PEG-MS, 6.3-6.5 wt% polymer content, 20 mM HEPES buffer pH 7.5, labeled with 0.15 mM Alexa Fluor 555. Conditions for illumination: 740 nm, 2% power, speed $19.6 \mu\text{s } \mu\text{m}^{-1}$, interval at z-direction: $6.57 \mu\text{m}$.

PEG-SOx-C-PMNB and PEG-STz-C-PMNB hydrogels

Similar photodegradation experiments were also performed with PEG-STz-C-PMNB and PEG-SOx-C-PMNB hydrogels. For PEG-STz-C-PMNB hydrogels, a pattern was observed in the illumination region but no increase of bright field signal was detected, indicative of absent of photodegradation and an occurrence of photoinduced side reactions (**Figure 3.14A-B**). We hypothesized that the photo-triggered reaction could be consequence of reactions of i) light induced thiol-ene reactions between the unreacted thiol groups and the nitrostyrene photolysis product or ii) cross-reaction between tetrazole groups with the nitrostyrene photolysis product. To test the first hypothesis, PEG-STz-C-PMNB hydrogels were incubated with the Mal-PEG-OMe (5kDa) in order to react the remaining free -SH groups after hydrogel formation (**Appendix**). However, a similar effect was observed (**Figure 3.14C**), suggesting that the free -SH groups were not involved in this additional crosslinking. In consideration of the second hypothesis, it should be noted that the light induced nitrile imine mediated tetrazole-ene cycloaddition (NITEC) has been reported on the literature, where the tetrazole groups can be activated by light illumination to form a highly reactive nitrile imine intermediate, which in turn reacted with unsaturated alkene groups via 1,3-dipolar cycloaddition reaction.^{40, 41} These results demonstrate that PEG-STz-C-PMNB hydrogels are not a good scaffold for 2P degradation. For PEG-

SOx-C-PMNB hydrogels, a similar degradation was observed as PEG-OxS-E-PMNB hydrogels with dose dependent (Figure 3.15).

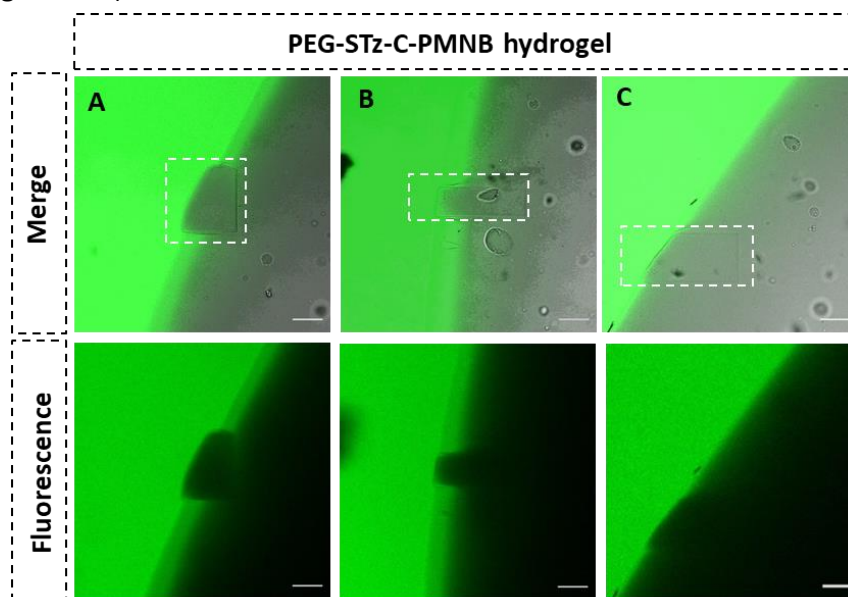


Figure 3.14 Photopatterning of PEG-STz-C-PMNB hydrogels (A-C) and PEG-SOx-C-PMNB hydrogels (D) by 2P excitation upon illumination with a 740 nm laser. Scale bars= 50 μm . Conditions for illumination: (A,C) 2% power, speed: $157 \mu\text{s} \mu\text{m}^{-1}$, scan 1, interval at z-direction: 6.57 μm . (B) 1% power, speed: $39.2 \mu\text{s} \mu\text{m}^{-1}$, scan 1, interval at z-direction: 6.57 μm . (D) 2% power, speed: $39.2\text{-}628 \mu\text{s} \mu\text{m}^{-1}$, scan 1, interval at z-direction: 6.57 μm .

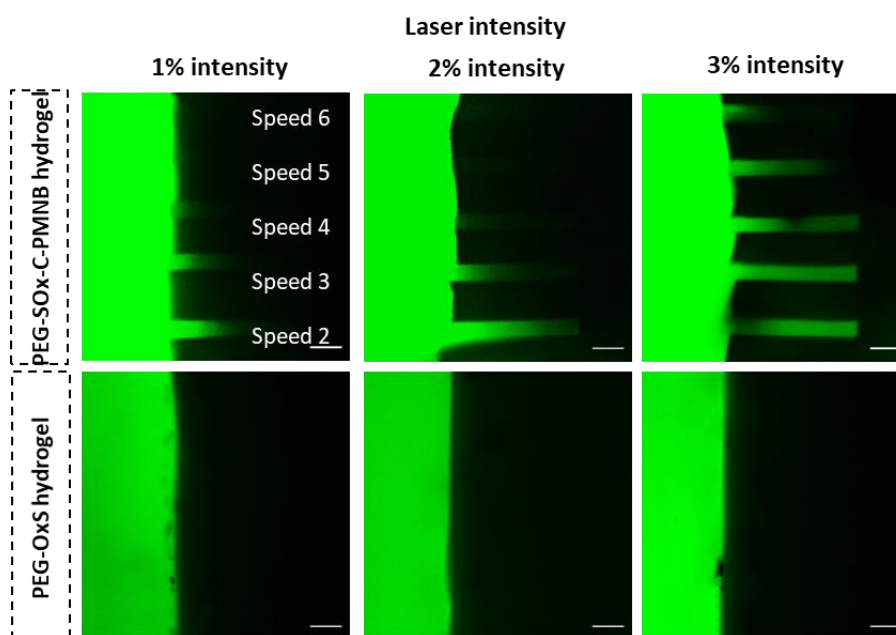


Figure 3.15 Photopatterning of PEG-SOx-C-PMNB and PEG-OxS hydrogels by 2P excitation upon illumination at 740 nm with varying irradiation dose. Scale bars= 50 μm . Conditions for illumination: 740 nm, 1-3% power intensity, speed: 2-6 ($314 - 19.6 \mu\text{s} \mu\text{m}^{-1}$), scan 1, interval at z-direction: 6.57 μm . Hydrogel composition: 20 kDa, star PEG-SH, 5.25 wt% polymer content, 20 mM HEPES buffer pH 7.5 with TCEP.

Chapter 3

Scanned patterns in the hydrogel using the Nanoscribe®

In order to test the possibility of micropatterning PEG-OxS-E-PMNB hydrogels at high speed, an ultrafast multi-photon lithography (MPL) equipment was used to scan more complex patterns with higher spatial resolution.⁴² The software of this equipment makes it easier for users to fabricate complex patterns in a straightforward process from CAD model. The equipment allows fast scanning speed can be achieved (≥ 100 mm/s) compared to a normal confocal microscope (e.g. LSM880: $628 \mu\text{m}^{-1}$).^{43,44} A resolution (latera resolution: 348 nm, axial resolution: $1.2 \mu\text{m}$) at 780 nm can be achieved with the following setting: 25x objective with oil immersion (NA:0.8).^{36,45}

PEG-OxS-E-PMNB hydrogel samples, prepared in a mold and attached to a glass slide (**Figure 3.16A**), were scanned with the MPL (**Figure 3.16B**). The scanning parameters were optimized by changing the speed ($5\text{-}100 \text{ mm s}^{-1}$) and laser power ($5\text{-}25 \text{ mW}$) while scanning cuboids of volume $50 \times 75 \times 100 \mu\text{m}^3$ with the 780 nm laser (**Figure 3.16C**). 2P degradation of the PEG-OxS-E-PMNB hydrogels was visible at a laser power of 10 mW and writing speeds up to 100 mm/s, which is the highest writing speed limit of Nanoscribe. The degradation could also be observed at a power of 5 mW with a writing speed $< 25 \text{ mm/s}$. Importantly, the patterning of multiple cuboids (25 cuboids, total volume: $9.375 \times 10^6 \mu\text{m}^3$) in the MPL required 30 min in PEG-OxS-E-PMNB hydrogels. Similar patterned volumes required $> 3 \text{ h}$ at the laser scanning microscope.

In comparison, the PEG-T-E-NB hydrogels required a higher power ($15\text{-}25 \text{ mW}$) and lower writing speeds ($5\text{-}15 \text{ mm s}^{-1}$) to reveal a pattern (**Figure 3.16C**). These results were also consistent with the results obtained from LSM: PEG-OxS-E-PMNB hydrogel can be efficiently degraded upon two-photon illumination and showed faster degradation rate than PEG-T-E-NB hydrogels. No photodegradation was observed in control PEG-OxS hydrogels (**Figure 3.16C**). These experiments defined the working window for the patterning of PEG-OxS-E-PMNB hydrogels and PEG-T-E-NB hydrogels in the MPL equipment.

To demonstrate the possibility to pattern complex 3D geometries by MPL, a 3D pattern mimicking branched blood vessels was scanned in the PEG-OxS-E-PMNB hydrogel (**Figure 3.16D**). This pattern took 30 min when using a power of 10 mW and a writing speed of 50 mm s^{-1} .

In summary, PEG-OxS-E-PMNB hydrogels were efficiently photodegraded and photopatterned with a two-photon scanning laser using a conventional two photon laser scanning microscope for cell imaging, or a Nanoscribe® equipment designed for complex two-photon lithographic processes. The PEG-OxS-E-PMNB hydrogels show significantly higher photodegradation efficiency than the PEG-T-E-NB hydrogels when the photolysis is performed using two-photon excitation. The degradation rate and extent of degradation can be modulated with the illumination dose. Visualization of hydrogel degradation was successfully achieved by fluorescence microscopy using hydrogel-conjugated fluorophores or diffusible fluorescent dextran polymers with high spatial resolution.

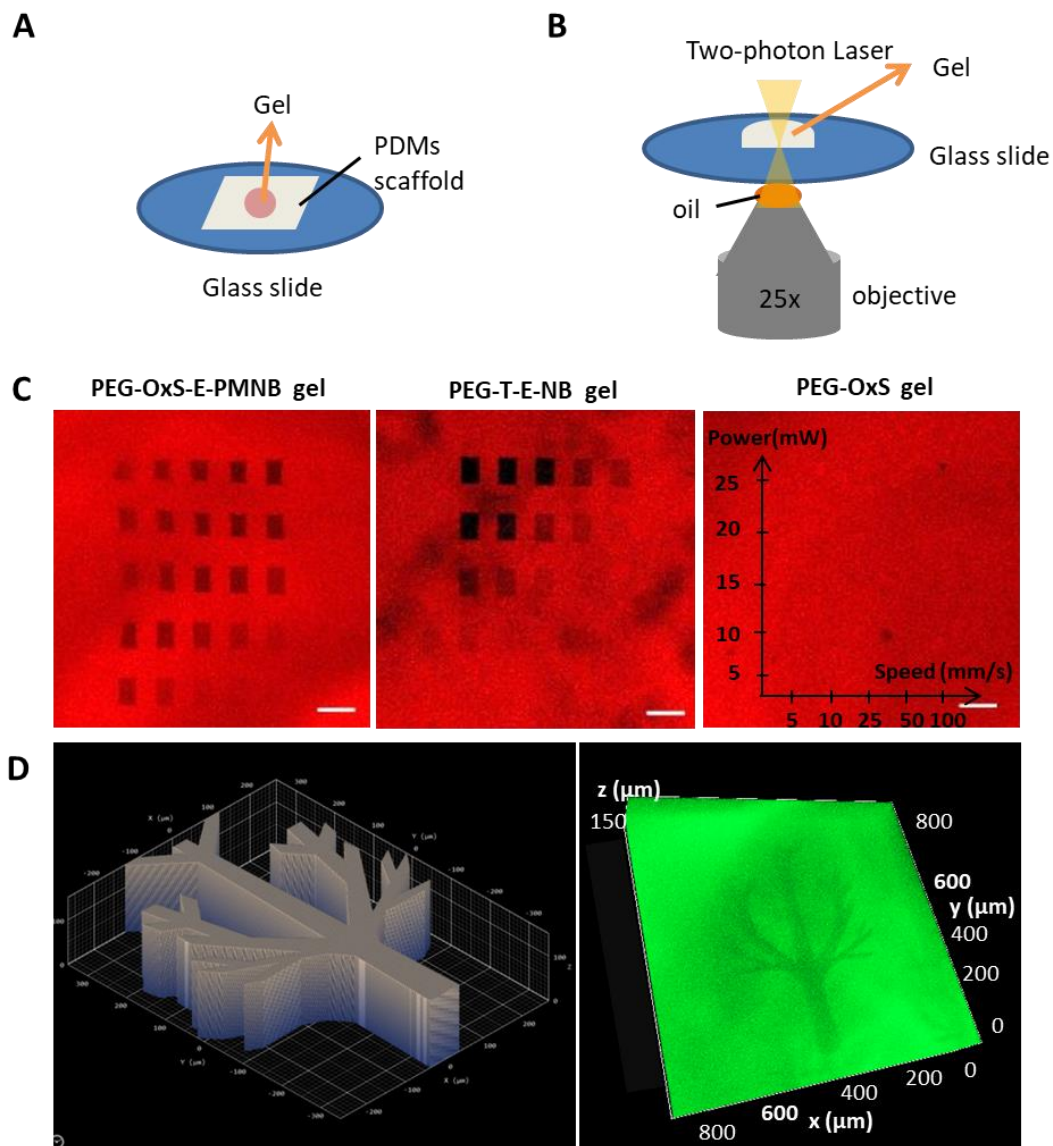


Figure 3.16 2P degradation of gels at the Nanoscribe. **(A)** Schematics of gel preparation on pre-functionalized glass slides and **(B)** placing the sample of multi-photon lithography. **(C)** Optimization of light exposure conditions for the different hydrogels. Speed and power sweep were conducted by multi-photon lithography. Conditions for processing: 780 nm, laser power: 5-25 mW, writing speed: 5-100 mm s⁻¹. Scale bars= 100 μm. **(D)** Fabrication of artificial blood vessels with a total dimension of 700 μm x 500 μm x 150 μm on PEG-OxS-E-PMNB hydrogels. Programmed 3D structure (left) and results obtained (right). Conditions for processing: laser power: 10 mW, writing speed: 50 mm s⁻¹, interval at z-direction: 1 μm.

3.6 Cytocompatibility of photodegradable hydrogels and application for dynamic cell culture

PEG-OxS-E-PMNB, and PEG-SOx-C-PMNB hydrogels were tested as matrix for 3D cell encapsulation and for dynamic cell culture. Different cell assays were performed in collaboration with Rocío Valbuena, a PhD student in the group.

Chapter 3

To support cell culture, PEG hydrogels need to be functionalized with cell adhesive peptides. For this purpose, the polymer content of 6.3 wt% and 5.25 wt% were selected for PEG-OxS-E-PMNB and PEG-SOx-C-PMNB hydrogels (5-10 wt% PEG hydrogels are typically used to encapsulate cells^{20, 46}) and the RGD peptide concentration in the range of 1.25 -2 mM (1/8 – 1/4 to -SH or -MS groups) were selected (1-2 mM are typically used to encapsulate cells)^{46, 47}. In addition, hydrogels for 3D cell culture need to be degradable to provide cells the ability to remodel the synthetic matrix and create their own. In this Thesis, such degradation functionality is included by the photodegradable crosslinker. However, for control experiments, GCRDVPMSMRGGDRCG (VPM) peptides (degraded by matrix metalloproteinases (MMP)) were used as enzymatically degradable crosslinkers to support degradation.⁴⁸

The cytocompatibility of thiol-methylsulfone-based hydrogels have been explored and reported for the 3D cell encapsulation application and the cells remained high viability (>90%) at day 6, proving the cytocompatibility of thiol-methylsulfone-based hydrogels.¹⁹ Therefore, PEG-OxS-E-PMNB, and PEG-SOx-C-PMNB hydrogels are expected to exhibit good cytocompatibility and further cytocompatibility tests will be carried out, which are not described in this Thesis.

Light-guided cell migration in photodegradable hydrogels

We tested the possibility to photodegrade PEG-OxS-E-PMNB, and PEG-SOx-C-PMNB hydrogels in the presence of cells by light exposure, and the ability of the embedded cells to migrate into the exposed areas. HUVEC spheroids were used for the migration assay. After spheroid encapsulation, regions around the spheroid were scanned and the migration of the cells from the spheroids into the degraded areas was monitored.

Spheroids of HUVEC (1000 cells/spheroid) stained with green cell tracker were encapsulated in PEG-OxS-E-PMNB (6.3 wt%) hydrogel biofunctionalized with 1.25 mM cyclo[RGDfC] peptide (see details in the **Appendix**). Encapsulated spheroids showed their typical cobblestone morphology, which was analyzed by the 3D reconstruction using Z-stack images, and had an average diameter of 153.7 ± 6.4 μm . After 1.5 h encapsulation in the hydrogels, prisms-shaped channels (z: 24.9 μm) with increasing exposure dose (740 nm, power:2%, scan speed: 314 $\mu\text{s} \mu\text{m}^{-1}$, scan number: 1-32) were scanned around the spheroids (Figure 3.17). After three hours, cells were imaged by fluorescence microscopy. Initial migration of cells out of the spheroid into the scanned channels was observed (**Figure 3.17**). PEG-OxS-E-PMNB hydrogels degraded completely within 12 h and, therefore, photoinduced migration could not be monitored. No migration was observed in negative control hydrogels with no degradation units (PEG-OxS hydrogels).

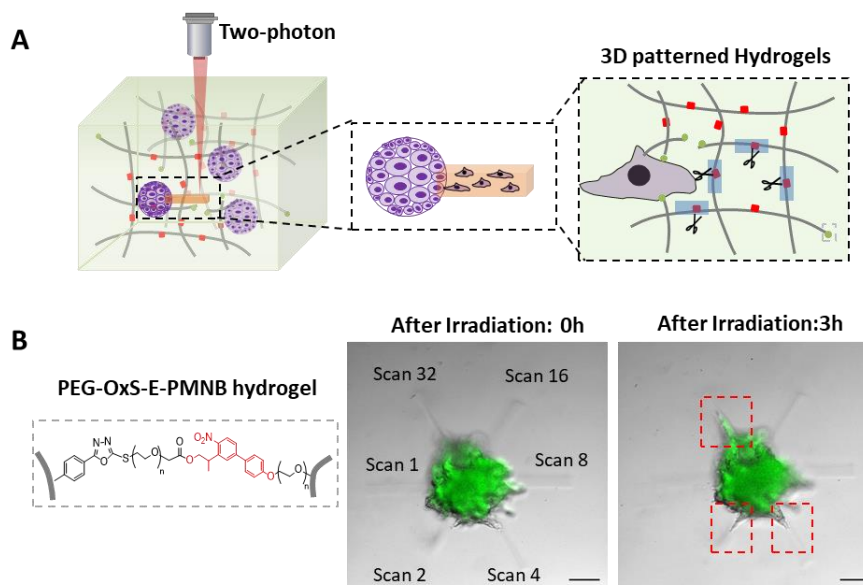


Figure 3.17 Schematics of HUVEC spheroids encapsulated in PEG-OxS-E-PMNB hydrogels (6.3 wt%, 1.25 mM cyclo[RGDfC] peptide). **(A)** and demonstration of light-triggered cell migration along the micro 3D channels after 2P light illumination; **(B)**. Irradiation conditions: 740 nm, power:2%, scan speed: $314 \mu\text{s} \mu\text{m}^{-1}$, scan number: 1-32. Scale bars= 50 μm .

To overcome the fast degradation, PEG-SOx-C-PMNB system was then used for encapsulation. In this system, the ester groups are replaced by more stable carbamate groups. HUVEC spheroids (500 cells/spheroid) were encapsulated in PEG-OxS-E-PMNB (5.25 wt%) hydrogels functionalized with 2 mM cyclo[RGDfK(Mal)] peptide with an average diameter of $135.3 \pm 8.2 \mu\text{m}$. After 1.5 h encapsulation, a volume surrounding half of the spheroid was scanned ($107.9 \times 132.8 \times 39.45 \mu\text{m}^3$). After 1 d of culture, cells migrated into the irradiated area and migration continued up to day 3. No migration was observed into the non-irradiated area (**Figure 3.18A**). Control experiments were performed with PEG-OxS hydrogels (nondegradable, negative control) and hydrogels crosslinked with enzymatically degradable VPM peptide as crosslinker (enzyme degradable, positive control). In the negative control, no migration was observed after exposure (**Figure 3.18B**). In the positive control, migration of cells was observed already at day 1 and became more visible at day 3 (**Figure 3.18C**). However, cells stopped migration after day 3. A live/dead assay (see **Appendix**) conducted at day 3 indicated low cell viability in all the hydrogels (including positive and negative control hydrogels) (**Figure 3.19**). The low viability of cells may explain the failure of cell migration after 3 days, indicating the need of further optimization of the system, including e.g., the protocol of spheroids preparation and the steps of culture conditions. Of note, the illumination experiments was not performed for positive hydrogels.

Collectively, these preliminary results demonstrate the possibility to regulate hydrogel degradation and consequently cellular migration in 2P photodegradable PEG-SOx-C-PMNB hydrogels in a 3D-regulated manner. Future studies to optimize this system for light-guided bulk migration and angiogenesis are planned. Compared to the reported 2P degradable hydrogels (e.g., oNB-based hydrogels),^{4, 8, 35} PEG-SOx-C-PMNB hydrogels not only enabled a more efficient degradation upon 2P excitation but also maintained high hydrolytic stability in the cell culture conditions. Such 2P degradable hydrogels are potentially interesting for studies such as their usage as angiogenesis

Chapter 3

scaffold, for the study of isolated cell functions and cellular response to the changes in their mechanical environment.

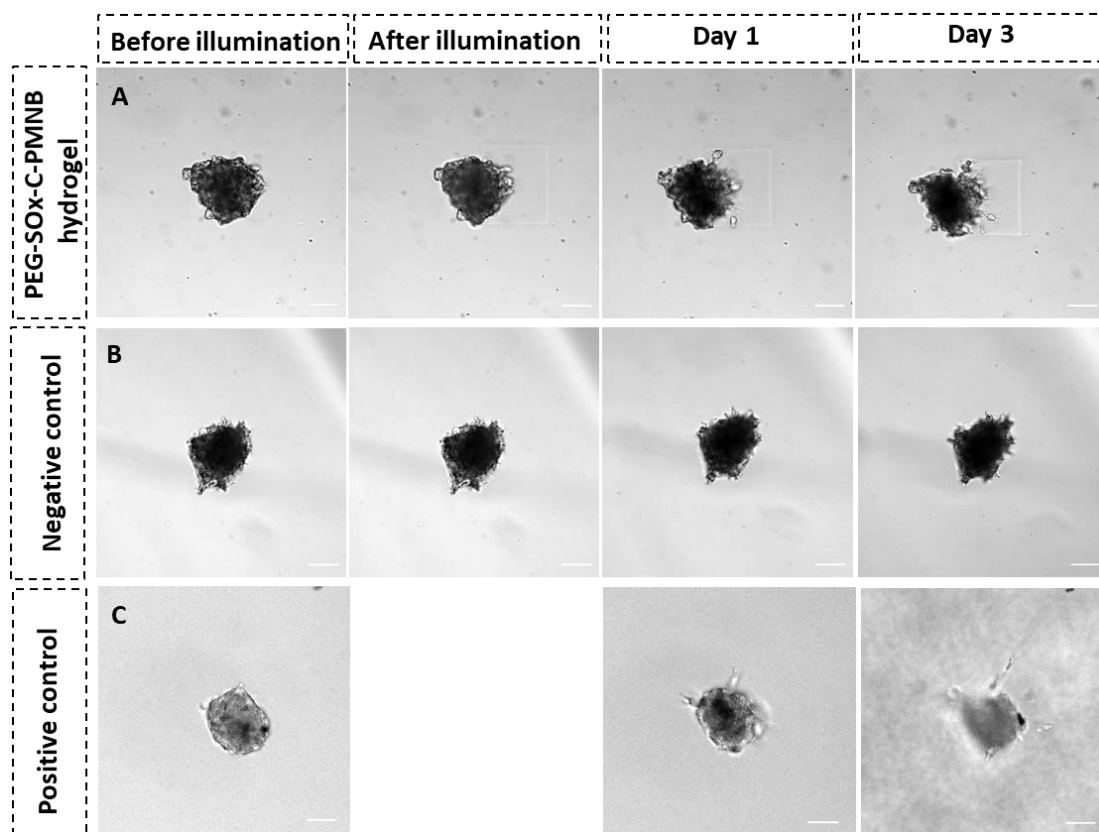


Figure 3.18 Light-triggered cell migration from HUVEC spheroids in PEG-SOx-C-PMNB hydrogels (A), negative control (B) and positive control hydrogels (C). Irradiation conditions: 740 nm, power:3%, scan speed: $314 \mu\text{s} \mu\text{m}^{-1}$, scan number: 4. Scale bars= 50 μm . Final polymer composition (5.25 wt%): 20 kDa, 10 wt% star PEG, 2 mM cyclo[RGDfK(Mal)] or cyclo[RGDfC] peptide, 20 mM HEPES buffer, pH 7.5.

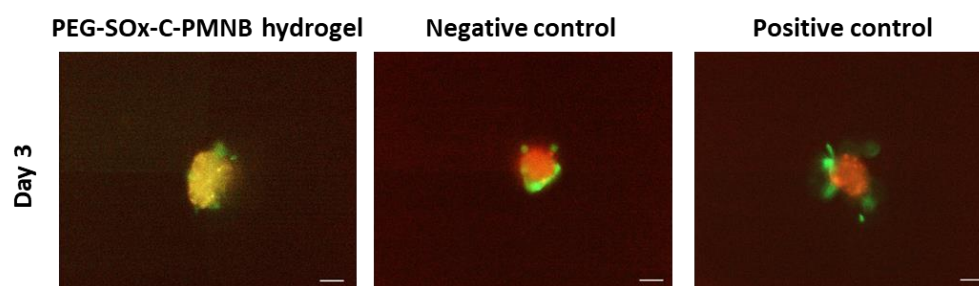


Figure 3.19 Live (green)/Dead (orange) assay of HUVEC spheroids in PEG-SOx-C-PMNB hydrogels, negative control and positive control hydrogels over 3 days of culture. Scale bars= 50 μm .

3.7 Conclusions

In this chapter, different photodegradable PEG-based hydrogels were synthesized and their physicochemical properties were characterized. Gelation time of PMNB-based hydrogels was achieved in a range of seconds to minutes under physiological conditions, which allowed comfortable

homogenization of precursor solutions and homogeneous distribution of embedded cells in the 3D cell encapsulation process.

PEG-OxS-E-PMNB and PEG-T-E-NB hydrogels were photodegradable upon illumination in the UV range. In opposition to the results of photolysis efficiency shown in **Chapter 2** (PMNB > NB), the degradation rate of the derived hydrogels followed the trend: PEG-T-E-NB hydrogel > PEG-OxS-E-PMNB hydrogel. This is attributed to reconfiguration in the PEG-OxS-E-PMNB network induced by UV exposure, as well to the occurrence of side reactions. Surprisingly, PEG-T-E-PMNB hydrogel did not show softening but stiffening upon light illumination. This is contrary to the photolysis of PEG-T-E-PMNB crosslinker in solution. This unexpected effect was attributed to parallel side reactions between the nitro-styrene photolysis product and triazole groups.

The hydrolytic stability of hydrogels depended on the nature of the photolabile linking group (ester vs. carbamate). PEG-OxS-E-PMNB hydrogel with ester labile groups presented low stability (< 12 h) in cell culture conditions, while PEG-STz-C-PMNB and PEG-SOx-C-PMNB hydrogels with carbamate labile groups were stable for more than 2 months. This stability range is advantageous for long culture studies.

The degradation of the hydrogels under 2P excitation was investigated. 3D patterns with spatial resolution with micrometer resolution (lateral resolution <1 μm and axial resolution $\geq 1.2 \mu\text{m}$) were scanned in the hydrogels using a LSM (740 nm) and a NanoScribe (780 nm). Visualization of the degradation step was achieved based on diffusivity of different fluorescent reporters. PEG-OxS-E-PMNB and PEG-T-E-NB hydrogels could be photodegraded after 2P excitation. The degradation rate followed the trend: PEG-OxS-E-PMNB hydrogel > PEG-T-E-NB hydrogel. This trend is reverse to that found in 1P-based photodegradation by rheology because of the higher 2P cross section of PMNB chromophore and also indicates the absence of side photolytic reactions (e.g., thiol-disulfide exchange) upon 2P illumination. Controlled degradation was achieved by regulating the scanning parameters. PEG-OxS-E-PMNB and PEG-SOx-C-PMNB hydrogel could be degraded at lower illumination doses, which is advantageous for a possible use as photodegradable matrix for cell encapsulation. PEG-STz-C-PMNB hydrogels underwent parallel polymerization reactions during illumination, indicating that the -Tz-MS and -SH coupling is not suitable for their integration in light induced degradation applications.

PEG-OxS-E-PMNB and PEG-SOx-C-PMNB hydrogels can support 3D cell encapsulation. Using controlled 2P exposure, spatial photodegradation patterns could be scanned and used to initially guide cell migration in PEG-OxS-E-PMNB hydrogels. However, the low hydrolytic stability limited the long-term cell studies. Cell migration and direct illumination of spheroids were also demonstrated for PEG-SOx-C-PMNB hydrogels, in this case with higher hydrolytic stability. These materials deserve further investigation as matrices for 3D cell culture with light-regulated spatiotemporal control.

2P photodegradable hydrogel (PEG-SOx-C-PMNB hydrogel) is demonstrated as a suitable scaffold for 3D cell encapsulation and potentially as efficient 2P degradable material to guide cell migration and angiogenesis.

Chapter 3

3.8 References

1. Kloxin, A. M.; Tibbitt, M. W.; Kasko, A. M.; Fairbairn, J. A.; Anseth, K. S., Tunable hydrogels for external manipulation of cellular microenvironments through controlled photodegradation. *Adv Mater* **2010**, *22* (1), 61-6.
2. Azagarsamy, M. A.; McKinnon, D. D.; Alge, D. L.; Anseth, K. S., Coumarin-Based Photodegradable Hydrogel: Design, Synthesis, Gelation, and Degradation Kinetics. *ACS Macro Letters* **2014**, *3* (6), 515-519.
3. Slaughter, B. V.; Khurshid, S. S.; Fisher, O. Z.; Khademhosseini, A.; Peppas, N. A., Hydrogels in Regenerative Medicine. **2009**, *21* (32-33), 3307-3329.
4. Lunzer, M.; Shi, L.; Andriotis, O. G.; Gruber, P.; Markovic, M.; Thurner, P. J.; Ossipov, D.; Liska, R.; Ovsianikov, A., A Modular Approach to Sensitized Two-Photon Patterning of Photodegradable Hydrogels. *Angewandte Chemie (International ed. in English)* **2018**, *57* (46), 15122-15127.
5. Tibbitt, M. W.; Kloxin, A. M.; Sawicki, L. A.; Anseth, K. S., Mechanical Properties and Degradation of Chain and Step-Polymerized Photodegradable Hydrogels. *Macromolecules* **2013**, *46* (7), 2785-2792.
6. Zhao, D.; Tang, Q.; Zhou, Q.; Peng, K.; Yang, H.; Zhang, X., A photo-degradable injectable self-healing hydrogel based on star poly(ethylene glycol)-b-polypeptide as a potential pharmaceuticals delivery carrier. *Soft Matter* **2018**, *14* (36), 7420-7428.
7. Yanagawa, F.; Sugiura, S.; Takagi, T.; Sumaru, K.; Camci-Unal, G.; Patel, A.; Khademhosseini, A.; Kanamori, T., Activated-Ester-Type Photocleavable Crosslinker for Preparation of Photodegradable Hydrogels Using a Two-Component Mixing Reaction. *Adv Healthc Mater* **2015**, *4* (2), 246-254.
8. Kloxin, A. M.; Kasko, A. M.; Salinas, C. N.; Anseth, K. S., Photodegradable hydrogels for dynamic tuning of physical and chemical properties. *Science* **2009**, *324* (5923), 59-63.
9. Arakawa, C. K.; Badeau, B. A.; Zheng, Y.; DeForest, C. A., Multicellular Vascularized Engineered Tissues through User-Programmable Biomaterial Photodegradation. *Adv Mater* **2017**, *29* (37), 1703156.
10. McKinnon, D. D.; Brown, T. E.; Kyburz, K. A.; Kiyotake, E.; Anseth, K. S., Design and Characterization of a Synthetically Accessible, Photodegradable Hydrogel for User-Directed Formation of Neural Networks. *Biomacromolecules* **2014**, *15* (7), 2808-2816.
11. Yanagawa, F.; Sugiura, S.; Takagi, T.; Sumaru, K.; Camci-Unal, G.; Patel, A.; Khademhosseini, A.; Kanamori, T., Activated-ester-type photocleavable crosslinker for preparation of photodegradable hydrogels using a two-component mixing reaction. *Adv Healthc Mater* **2015**, *4* (2), 246-54.
12. Engler, A. J.; Sen, S.; Sweeney, H. L.; Discher, D. E., Matrix Elasticity Directs Stem Cell Lineage Specification. *Cell* **2006**, *126* (4), 677-689.
13. Paez, J. I.; Farrukh, A.; Valbuena-Mendoza, R.; Włodarczyk-Biegun, M. K.; Del Campo, A., Thiol-Methylsulfone-Based Hydrogels for 3D Cell Encapsulation. *ACS Appl Mater Interfaces* **2020**, *12* (7), 8062-8072.
14. Wudl, F.; Lightner, D. A.; Cram, D. J., Methanesulfinic acid and its properties. *Journal of the American Chemical Society* **1967**, *89* (16), 4099-4101.
15. Zhang, D.; Devarie-Baez, N. O.; Li, Q.; Lancaster, J. R.; Xian, M., Methylsulfonyl Benzothiazole (MSBT): A Selective Protein Thiol Blocking Reagent. *Organic Letters* **2012**, *14* (13), 3396-3399.
16. Toda, N.; Asano, S.; Barbas, C. F., 3rd, Rapid, stable, chemoselective labeling of thiols with

Julia-Kocieński-like reagents: a serum-stable alternative to maleimide-based protein conjugation. *Angewandte Chemie (International ed. in English)* **2013**, *52* (48), 12592-6.

17. Svatunek, D.; Houszka, N.; Hamlin, T. A.; Bickelhaupt, F. M.; Mikula, H., Chemoselectivity of Tertiary Azides in Strain-Promoted Alkyne-Azide Cycloadditions. *Chemistry* **2019**, *25* (3), 754-758.

18. Stenzel, M. H., Bioconjugation Using Thiols: Old Chemistry Rediscovered to Connect Polymers with Nature's Building Blocks. *ACS Macro Letters* **2013**, *2* (1), 14-18.

19. Paez, J. I.; Farrukh, A.; Valbuena-Mendoza, R.; Włodarczyk-Biegun, M. K.; del Campo, A., Thiol-Methylsulfone-Based Hydrogels for 3D Cell Encapsulation. *ACS Applied Materials & Interfaces* **2020**, *12* (7), 8062-8072.

20. Paez, J. I.; de Miguel-Jiménez, A.; Valbuena-Mendoza, R.; Rathore, A.; Jin, M.; Gläser, A.; Pearson, S.; del Campo, A., Thiol-Methylsulfone-Based Hydrogels for Cell Encapsulation: Reactivity Optimization of Aryl-Methylsulfone Substrate for Fine-Tunable Gelation Rate and Improved Stability. *Biomacromolecules* **2021**.

21. DeForest, C. A.; Anseth, K. S., Cytocompatible click-based hydrogels with dynamically tunable properties through orthogonal photoconjugation and photocleavage reactions. *Nature Chemistry* **2011**, *3* (12), 925-931.

22. Brown, T. E.; Silver, J. S.; Worrell, B. T.; Marozas, I. A.; Yavitt, F. M.; Günay, K. A.; Bowman, C. N.; Anseth, K. S., Secondary Photocrosslinking of Click Hydrogels To Probe Myoblast Mechanotransduction in Three Dimensions. *Journal of the American Chemical Society* **2018**, *140* (37), 11585-11588.

23. Hasturk, O.; Jordan, K. E.; Choi, J.; Kaplan, D. L., Enzymatically crosslinked silk and silk-gelatin hydrogels with tunable gelation kinetics, mechanical properties and bioactivity for cell culture and encapsulation. *Biomaterials* **2020**, *232*, 119720-119720.

24. Kharkar, P. M.; Kiick, K. L.; Kloxin, A. M., Design of thiol- and light-sensitive degradable hydrogels using Michael-type addition reactions. *Polymer Chemistry* **2015**, *6* (31), 5565-5574.

25. Claaßen, C.; Claaßen, M. H.; Gohl, F.; Tovar, G. E. M.; Borchers, K.; Southan, A., Photoinduced Cleavage and Hydrolysis of o-Nitrobenzyl Linker and Covalent Linker Immobilization in Gelatin Methacryloyl Hydrogels. *Macromol Biosci* **2018**, *18* (9), e1800104.

26. Maeda, K., Analysis of Ultraviolet Radiation Wavelengths Causing Hardening and Reduced Elasticity of Collagen Gels In Vitro. **2018**, *5* (1), 14.

27. Wong, D. Y.; Ranganath, T.; Kasko, A. M., Low-Dose, Long-Wave UV Light Does Not Affect Gene Expression of Human Mesenchymal Stem Cells. *PLoS One* **2015**, *10* (9), e0139307-e0139307.

28. LeValley, P. J.; Neelarapu, R.; Sutherland, B. P.; Dasgupta, S.; Kloxin, C. J.; Kloxin, A. M., Photolabile Linkers: Exploiting Labile Bond Chemistry to Control Mode and Rate of Hydrogel Degradation and Protein Release. *Journal of the American Chemical Society* **2020**, *142* (10), 4671-4679.

29. Truong, V. X.; Li, F.; Forsythe, J. S., Photolabile Hydrogels Responsive to Broad Spectrum Visible Light for Selective Cell Release. *ACS Applied Materials & Interfaces* **2017**, *9* (38), 32441-32445.

30. Fairbanks, B. D.; Singh, S. P.; Bowman, C. N.; Anseth, K. S., Photodegradable, Photoadaptable Hydrogels via Radical-Mediated Disulfide Fragmentation Reaction. *Macromolecules* **2011**, *44* (8), 2444-2450.

31. Bach, R. D.; Dmitrenko, O.; Thorpe, C., Mechanism of Thiolate–Disulfide Interchange Reactions

Chapter 3

in Biochemistry. *The Journal of Organic Chemistry* **2008**, *73* (1), 12-21.

32. Chen, R. T.; Marchesan, S.; Evans, R. A.; Styan, K. E.; Such, G. K.; Postma, A.; McLean, K. M.; Muir, B. W.; Caruso, F., Photoinitiated Alkyne–Azide Click and Radical Cross-Linking Reactions for the Patterning of PEG Hydrogels. *Biomacromolecules* **2012**, *13* (3), 889-895.
33. DeForest, C. A.; Anseth, K. S., Cytocompatible click-based hydrogels with dynamically tunable properties through orthogonal photoconjugation and photocleavage reactions. *Nature chemistry* **2011**, *3* (12), 925-31.
34. Zheng, Y.; Han, M. K. L.; Zhao, R.; Blass, J.; Zhang, J.; Zhou, D. W.; Colard-Itté, J.-R.; Dattler, D.; Hoth, M.; García, A. J.; Qu, B.; Bennewitz, R.; Giuseppone, N.; del Campo, A., Optoregulated force application to cellular receptors using molecular motors. *bioRxiv* **2020**, 2020.03.31.015198.
35. Griffin, D. R.; Kasko, A. M., Photodegradable Macromers and Hydrogels for Live Cell Encapsulation and Release. *Journal of the American Chemical Society* **2012**, *134* (31), 13103-13107.
36. Fischer, J.; Wegener, M., Three-dimensional optical laser lithography beyond the diffraction limit. *Laser & Photonics Reviews* **2013**, *7* (1), 22-44.
37. Aujard, I.; Benbrahim, C.; Gouget, M.; Ruel, O.; Baudin, J. B.; Neveu, P.; Jullien, L., o-nitrobenzyl photolabile protecting groups with red-shifted absorption: syntheses and uncaging cross-sections for one- and two-photon excitation. *Chemistry* **2006**, *12* (26), 6865-79.
38. Klán, P.; Šolomek, T.; Bochet, C. G.; Blanc, A.; Givens, R.; Rubina, M.; Popik, V.; Kostikov, A.; Wirz, J., Photoremovable Protecting Groups in Chemistry and Biology: Reaction Mechanisms and Efficacy. *Chemical Reviews* **2013**, *113* (1), 119-191.
39. Farrukh, A.; Paez, J. I.; del Campo, A., 4D Biomaterials for Light-Guided Angiogenesis. *Adv Funct Mater* **2019**, *29* (6), 1807734.
40. Majek, M.; Jacobi von Wangelin, A., Metal-free carbonylations by photoredox catalysis. *Angewandte Chemie (International ed. in English)* **2015**, *54* (7), 2270-4.
41. Blasco, E.; Sugawara, Y.; Lederhose, P.; Blinco, J. P.; Kelterer, A. M.; Barner-Kowollik, C., Understanding Reactivity Patterns in Light-Induced Nitrile Imine Mediated Tetrazole-Ene Cycloadditions. *Chemphotochem* **2017**, *1* (5), 159-163.
42. Stampf, J. u.; Liska, R.; Ovsianikov, A., Multiphoton lithography : techniques, materials and applications. **2017**.
43. Batchelor, R.; Messer, T.; Hippler, M.; Wegener, M.; Barner-Kowollik, C.; Blasco, E., Two in One: Light as a Tool for 3D Printing and Erasing at the Microscale. *Adv Mater* **2019**, *31* (40), e1904085.
44. Qin, X. H.; Wang, X.; Rottmar, M.; Nelson, B. J.; Maniura-Weber, K., Near-Infrared Light-Sensitive Polyvinyl Alcohol Hydrogel Photoresist for Spatiotemporal Control of Cell-Instructive 3D Microenvironments. *Adv Mater* **2018**, *30* (10), 1705564.
45. Fragal, V. H.; Catori, D. M.; Fragal, E. H.; Garcia, F. P.; Nakamura, C. V.; Rubira, A. F.; Silva, R., Two-dimensional thermoresponsive sub-microporous substrate for accelerated cell tissue growth and facile detachment. *Journal of Colloid and Interface Science* **2019**, *547*, 78-86.
46. Villiou, M.; Paez, J. I.; del Campo, A., Photodegradable Hydrogels for Cell Encapsulation and Tissue Adhesion. *ACS Applied Materials & Interfaces* **2020**, *12* (34), 37862-37872.
47. Lee, T. T.; García, J. R.; Paez, J. I.; Singh, A.; Phelps, E. A.; Weis, S.; Shafiq, Z.; Shekaran, A.; del Campo, A.; García, A. J., Light-triggered in vivo activation of adhesive peptides regulates cell

adhesion, inflammation and vascularization of biomaterials. *Nature Materials* **2015**, *14* (3), 352-360.

48. Foster, G. A.; Headen, D. M.; González-García, C.; Salmerón-Sánchez, M.; Shirwan, H.; García, A. J., Protease-degradable microgels for protein delivery for vascularization. *Biomaterials* **2017**, *113*, 170-175.

Chapter 3

Chapter 4: Synthesis of two-photon activatable cell adhesive peptide

4.1 Introduction

The interaction of cells with synthetic hydrogels is usually mediated by coupling cell adhesive molecules in the synthetic material. These can be adhesive proteins from the extracellular matrix (fibronectin, collagen, laminin, etc) or short peptidomimetics derived from them (e.g., RGD, GFOGER or IKVAV). The cell adhesive molecules can be recognized by specific adhesive receptors at the cell membrane, typically integrins, and mediate the formation of adhesive complexes between the cell and the material. Among cell adhesive peptides, RGD variants and in particular the cyclic RGDfX (cRGDfX) pentapeptide, is commonly used as it can be recognized by different integrins.

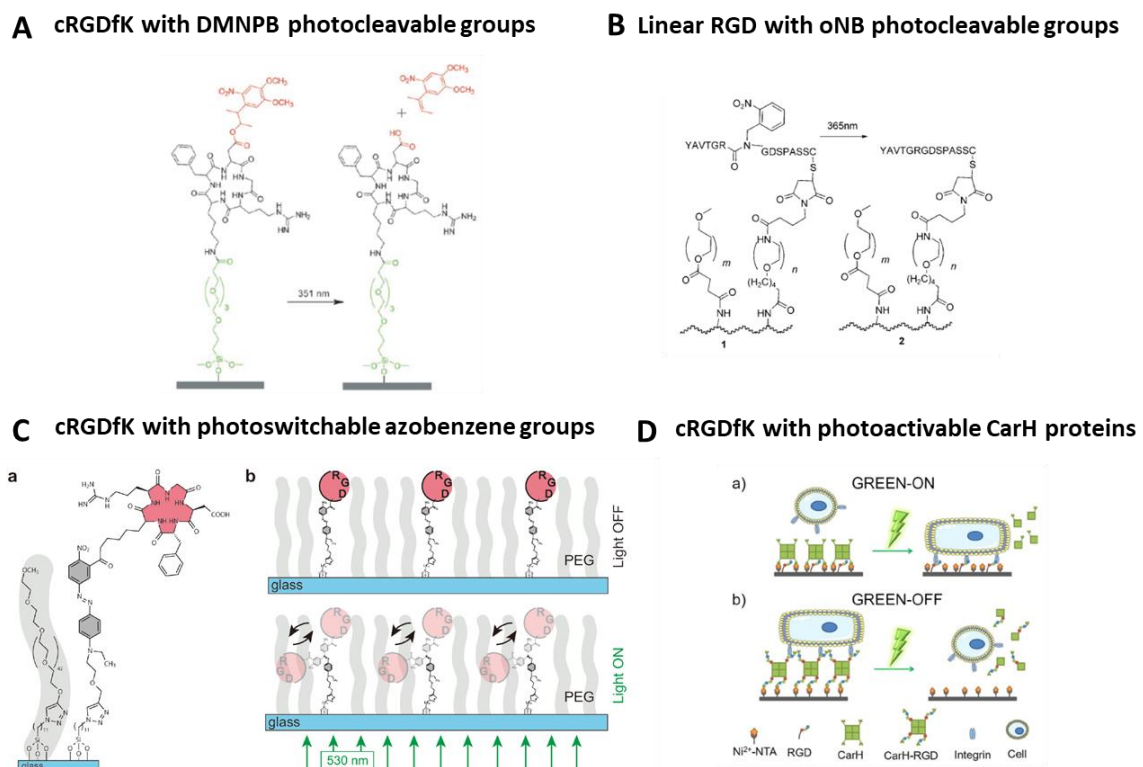


Figure 4.1 Light-responsive variants of RGD peptide with different photoactivatable groups. **(A)** Phototriggering of cRGDfK with DMNPB photocleavable group at 350 nm.¹ **(B)** Phototriggering of linear RGD peptide with oNB photocleavable groups at 365 nm.² **(C)** Phototriggering of cRGDfK with photoswitchable azobenzene groups at 530 nm.³ **(D)** Phototriggering of cRGDfK with photoactivatable CarH proteins groups upon green light exposure.⁴

In order to regulate the adhesive interaction between cells and materials, photoresponsive molecular designs have been developed based on modification of the adhesive molecules with photocleavable groups^{1, 5} or photoswitches,^{4, 6} or the use of photoswitchable adhesive proteins.^{7, 8} The del Campo's group reported a photoactivatable variant of the cRGDfK peptide where the COOH group of the Asp side chain was modified with a 3-(4,5-Dimethoxy-2-nitro phenyl)-2-butyl ester (DMNPB) photocleavable group ($\lambda_{\max} = 346$ nm, $\epsilon_{\max} = 4100$ M⁻¹cm⁻¹) (**Figure 4.1A**). The aspartate was selected as site for modification since it anchors a bivalent cation within the RGD-integrin binding site. The presence of the DMNPB chromophore inhibited the bioactivity of the cRGDfK peptide. Activity was restored by irradiation at 351 nm and photomodulated cell adhesion was demonstrated on 2D

Chapter 4

surfaces with spatio-temporal resolution. Photo-regulated cell attachment was also achieved using a photoactivatable variant of the linear peptide YAVTGRGDSPASS after exposure at 365 nm (**Figure 4.1B**).² In this case the *o*-nitrobenzyl (*o*NB) photocleavable group was intercalated at the amide bond between the Gly and Arg residues, which was proved as a critical site for biological activity.³ Besides photocleavable groups, azobenzene photoswitches were also used to link the cRGDfK to a materials surface and change the orientation of the peptide at the surface for binding to the membrane integrins (**Figure 4.1C**).⁴ The Wegner's group also reported spatiotemporal control of cell adhesions by a green light responsive protein CarH to change the availability of adhesive ligands at the surface (**Figure 4.1D**). CarH forms a tetramer in the dark and dissociates into its monomers upon green light exposure.⁸

The described approaches allow manipulation of cell-materials adhesive interactions in 2D. In order to regulate these interactions in 3D, 2P excitation can be used. For this purpose longer wavelengths, which are less phototoxic for cells and allow higher penetration into tissues, can be used.¹ In this direction, the Stevens's group (**Figure 4.2A**) developed a photoactivatable cell penetrating peptide containing hepta-arginine (R7), hepta-glutamic acid (E) sequences with an intercalated *o*NB photoremovable group. These peptide could be cleaved by exposure to 740 nm light of a femtosecond laser.⁹ However, *o*NB groups have a low two-photon absorption cross section ($\delta = 0.015\text{--}0.065\text{ GM at }750\text{ nm}$), therefore, they are not ideal for two-photon activation. The group of Specht¹⁰ reported a family of *o*-nitrophenylethyl based photoremovable groups with higher two-photon absorption cross-section than *o*NB groups. Among them, the 3-(2-propyl)-4'-methoxy-4-nitro-biphenyl (PMNB) group, with a two-photon cross-section of 3.2 GM at 740 nm, was used by del Campo to modify the RGD peptide. The c[RGD(PMNB)fC] peptide could be activated with coherent pulsed laser light ($\lambda = 740\text{ nm}$, power = 2320 mW cm^{-2} and scan speed = $170\text{ }\mu\text{s }\mu\text{m}^{-1}$) (**Figure 4.2B**). Compared to DMNPB ($\delta = 0.17\text{ GM at }720\text{ nm for DMNPB-glutamate}$),¹¹ PMNB can be activated at lower doses. Cell studies demonstrated that the exposure dose was acceptable for activating the cell adhesive peptide in regions around the cells, but caused phototoxicity when used for direct illumination of living cells.¹² More efficient chromophores are needed to allow photoactivation processes in 3D hydrogels requiring direct exposure of cells.

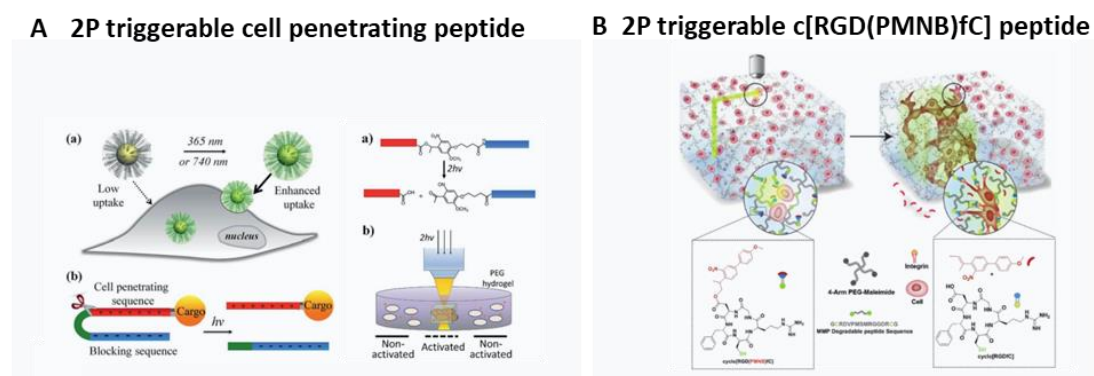


Figure 4.2 2P-induced cellular responses mediated by photo-triggerable ligands. **(A)** 2P light-activated cellular uptake of cargos via a structural transition of photo-caged peptide (antifouling ligand transitions to a cell-penetrating peptide upon irradiation).⁹ **(B)** 2P light-induced cell angiogenesis based on a two-photon activatable cRGDFc peptide, c[RGD(PMNB)fC]. (Irradiation conditions: 740 nm laser at $170\text{ }\mu\text{s }\mu\text{m}^{-1}$ scanning rate, 95% intensity).¹²

In the design of more effective photoremovable groups for 2P activation, two structural effects are important: (i) the length of the π -conjugated system, and (ii) the alternation of push-pull effect by an electron-donating substituent (D) and an electron-withdrawing substituent (A) at either ends of a molecule with dipolar character (D- π -A). The (*o*-nitrobiphenylacetylene)propyl family, with an intercalated alkynyl group that extends the conjugation length, and different electron-donating moiety at para position, is an interesting example.

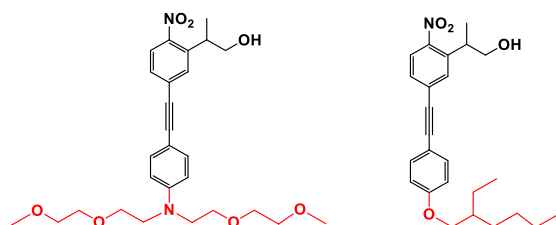


Figure 4.3. Structure of reported (*o*-nitrobiphenylacetylene)propyl family groups

A few examples (**Figure 4.3**) of photoactivatable molecules have been reported with dialkylamino or ethylhexyloxy group.¹³ The Hamburger's group studied the structure-2P property relationship between the (*o*-nitrobiphenyl)propyl chromophore and the (*o*-nitrobiphenylacetylene)propyl chromophore with a ethylhexyloxy group at para position. The 2P uncaging cross section of π -extended (*o*-nitrobiphenylacetylene)propyl protected fluorene monomers (25.8 ± 3.2 GM at 690 nm) was ~ 1.8 -fold higher than (*o*-nitrobiphenyl)propyl chromophore (14.0 ± 3.7 GM at 690 nm).

The Wombacher's group used this system to prepare a photoactivatable derivative of the phytohormone gibberellic acid (**Figure 4.4A**). Efficient translocation of far-red-fluorescent protein mPlum-GID1 to the mitochondria was observed within seconds (20-160 s) at 800 nm and at 80 mW.¹⁴ The photolysis efficiency of this compound at 800 nm was 1.8-fold higher than (2-(4'-bis(2-methoxyethoxy)ethyl)amino)-4-nitro-[1,1'-biphenyl]-3-yl)propan-1-ol (EANBP), i.e. the chromophore lacking the intercalated alkynyl group (**Figure 4.4B**). The -NR₂ group in para-position led to a bathochromic shift of λ_{max} to ~ 400 nm. This allowed 2P activation to occur at 800 nm, a wavelength range with reduced tissue scattering effects.¹⁴ The NR₂ group also increased the water solubility of the molecule.

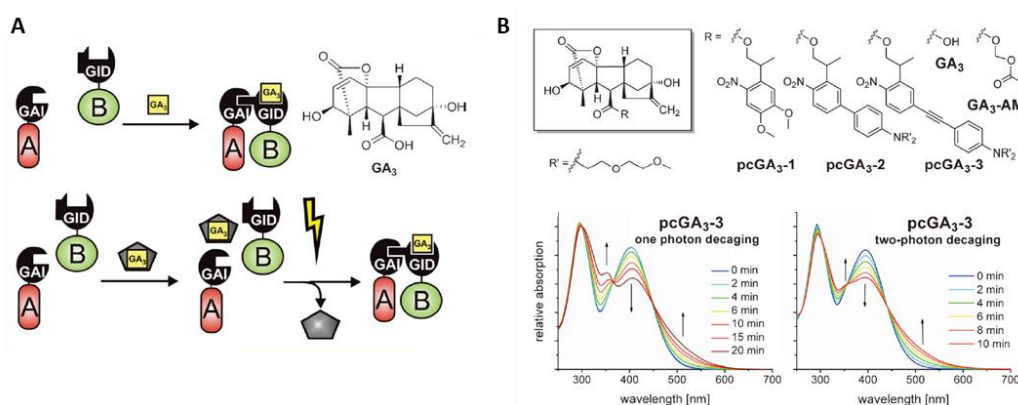


Figure 4.4 2P light-induced protein dimerization based on different phototriggerable chromophores of gibberellic acid (GA). **(A)** General scheme of photo-induced protein dimerization of the GA₃-receptor GID1 and GAI. **(B)** Chemical structures of photo-caged GA₃-derivatives with *o*NB, *o*-nitrophenylethyl and (*o*-nitrobiphenylacetylene)propyl based groups and photolysis studies upon 1P and 2P illumination. (1P Irradiation conditions: 412 nm, in phosphate buffer pH 7.4 with 3 vol% DMSO. 2P Irradiation conditions: 800 nm. In phosphate buffer pH 7.4 and acetonitrile 1:1 vol%).¹⁴

Chapter 4

The extension of the conjugation with an internal alkynyl group proved to be a valuable alternative to improve 2P absorption (**Table 4.1**). Additionally, the strong electron donating group NR₂ (e.g. dialkylamino group) in para-position significantly increased chromophore solubility and bathochromic shift.¹⁴ Despite these advantages, the presence of NR₂ group might result in overall lower hydrolytic stability of the compound, as reported for nitrobiphenyl derivatives (**Table 4.2**).^{12, 15, 16} One alternative to the NR₂ group is the use of a -OMe group, which has been demonstrated to result in higher hydrolytic stability in aqueous solution over one month of incubation in PBS buffer at room temperature. In view of these evidences, it appeared feasible to combine the properties of (o-nitrobiphenylacetylene)propyl system with the -OMe electron donating group, in order to synthesize a novel 2P active chromophore with high 2P properties and good hydrolytic stabilities.

Table 4.1 Comparison of (o-nitrobiphenyl)propyl family chromophore properties with an intercalated alkynyl group.¹³

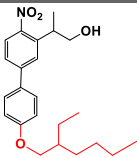
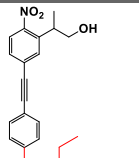
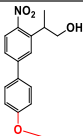
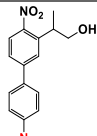
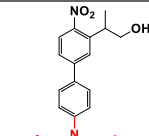
	2-(4'-((2-ethylhexyl)oxy)-4-nitro-[1,1'-biphenyl]-3-yl)propan-1-ol	2-(5-((4-((2-ethylhexyl)oxy)phenyl)ethynyl)-2-nitrophenyl)propan-1-ol
Structure		
2P uncaging cross-section	690 nm (14.0 ± 3.7 GM)	690 nm (25.8 ± 3.2 GM)

Table 4.2 Comparison of Nitrobiphenyl chromophore properties in terms of different electron-donating groups at para-position.^{12, 15, 16}

	3-(2-propyl)-4'-methoxy-4-nitro-biphenyl (PMNB)	2-(4'-(dimethylamino)-4-nitro-[1,1'-biphenyl]-3-yl)propan-1-ol (ANBP)	2-(4'-amino-4-nitro-[1,1'-biphenyl]-3-yl)propan-1-ol (HANBP)
Structure			
2P properties	740 nm (3.2 GM), 800 nm (0.45 GM). 9% quantum yield	800 nm (11 GM), 15% quantum yield	800 nm (11 GM), 15% quantum yield
Hydrolytic stability* in PBS (pH 7.4) at r.t	Stable for more than one month	63% cleavage in one week	58% cleavage in one week

*Chromophore attached to carboxylic side group of cRGDFC.

4.2 Molecular design of two-photon activatable RGD cell adhesive peptides

The molecular design of the 2P photoactivatable cRGD peptide followed previous work in the group and specified in the previous section.^{12, 17} The photocleavable group should be introduced at the COOH group of the Asp residue of the cRGDFX by forming an ester bond. Moreover, X could be a Cys or a Lys-N₃ rest, to be used for anchoring to the hydrogels synthesized in this Thesis. The -SH group of Cys and

the $-N_3$ group of Lys- N_3 are suitable for covalent binding to $-Mal$, $-MS$ or $-DBCO$ functionalized hydrogel precursors, as shown in **Figure 4.5**.

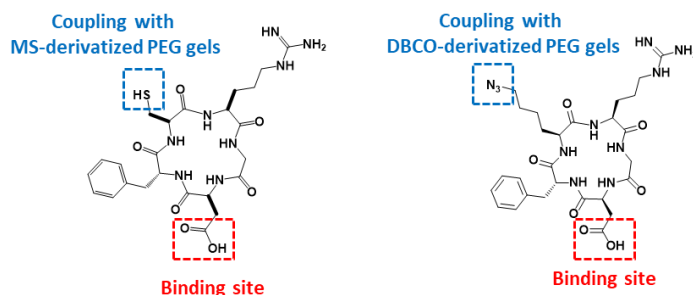


Figure 4.5 Chemical structure of cRGDFc and c[RGDFk- N_3].

4.3 Synthesis of cyclo[RGD(PNEP)fx]

4.3.1 Synthesis PNEP-Asp

The introduction of the PNEP group at the COOH side group of Asp required the synthesis of the precursor 2-(5-((4-methoxyphenyl)ethynyl)-2-nitrophenyl)propan-1-ol (PENP-OH) to react with commercially available Fmoc-Asp.¹⁷ PENP was synthesized following a previously described 6-step procedure (**Figure 4.6**).^{14,16} Briefly, the synthesis started from 2-(5-bromo-2-nitrophenyl)propan-1-ol, **a**, obtained by the reduction of **2** using DIBAL-H as reducing agent in a moderate yield (53%). The reaction product was confirmed by the appearance of the signals corresponding to the methylene carbon (3.78 ppm, 2H) and methine carbon (3.55 ppm, 1H) in ¹H NMR. The product **2** was obtained as described in **Section 2.3.1, Chapter 2**. Compound **c** was obtained in a one-pot reaction with two steps. First, compound **b** was obtained by reaction of 4-Iodoanisole with trimethylsilylacetylene by Sonogashira coupling using PdCl₂(PPh₃)₄ as catalyst. Then, the deprotection of trimethylsilyl group of **b** was performed using potassium carbonate in methanol and dichloromethane. This procedure afforded compound **c** in 89% yield. The success of the reaction was confirmed by the appearance of a singlet at 2.99 ppm (1H) that corresponds to the -CH from ethynyl group in ¹H-NMR. Compound **c** is labile and decomposed in < 3 days. Therefore, compound **c** was always freshly prepared before use. Reaction of **a** and **c** via Sonogashira coupling for 24 h at 50°C afforded compound **d** with a yield of 67%. The product was identified by mass spectrometry ([M+H]⁺ 312.2 m/z) and by the disappearance of the methine group signal at 2.99 ppm (1H) in ¹H-NMR. ¹³C-NMR confirmed the carbon signals from alkynyl group at 86.61 ppm and 93.60 ppm. However, the carbon signal from anisole that connected to the alkynyl carbon-carbon triple bond was missing from the ¹³C-NMR spectrum (CPD). Therefore, attached proton test (APT) NMR was used to distinguish between carbon atoms with even or odd number of attached hydrogens. The spectrum showed a negative signal from the quaternary carbon from anisole overlaid with a positive signal from the aromatic methines at 114.19 ppm, indicating the success of reaction. This spectroscopic evidence confirmed the successful synthesis of PENP-OH for coupling to Asp.

Fmoc-Asp with a tert-butyl protected alpha carboxylic unit was subsequently reacted with **d** to afford **e** using DMAP and DCC for ester coupling in 57% yield. ¹H-NMR analysis showed the protons from aromatic rings from PENP and Fmoc protecting group (6.87-7.78 ppm, 15H), the protons from methoxy

Chapter 4

group (1.36-1.39 ppm, 3H) and the protons from tert butyl group (1.41-1.35 ppm, 9H). Mass spectrometry analysis confirmed the chemical structure of the product with a $[M+Na]^+$ peak at $m/z = 727.40$. Deprotection of tert-butyl ester was first carried out in TFA:DCM (1:1) at room temperature for 1 h. However, formation of several side products was observed by analytical HPLC and **f** was obtained at very low yield (<10%). Attempts to optimize the reaction by using a lower reaction temperature (0°C) improved the yield to 36%, as confirmed by quantitative HPLC (**Figure 4.7**). Importantly, it is presumed that TFA-mediated decomposition during purification may be responsible for the low yield since no photolysis byproduct was detected during the course of the reaction. Therefore, TFA was removed from HPLC solvent (typically 0.1% TFA is added as eluents) in order to minimize the decomposition. After purification, the reaction product was confirmed by mass analysis ($m/z=649.2$ for $[M+H]^+$) and the disappearance of the signals corresponding to the tert-butyl group (1.41-1.35 ppm, 9H) in 1H NMR. NMR and mass analysis data for each intermediate are presented in **Appendix**.

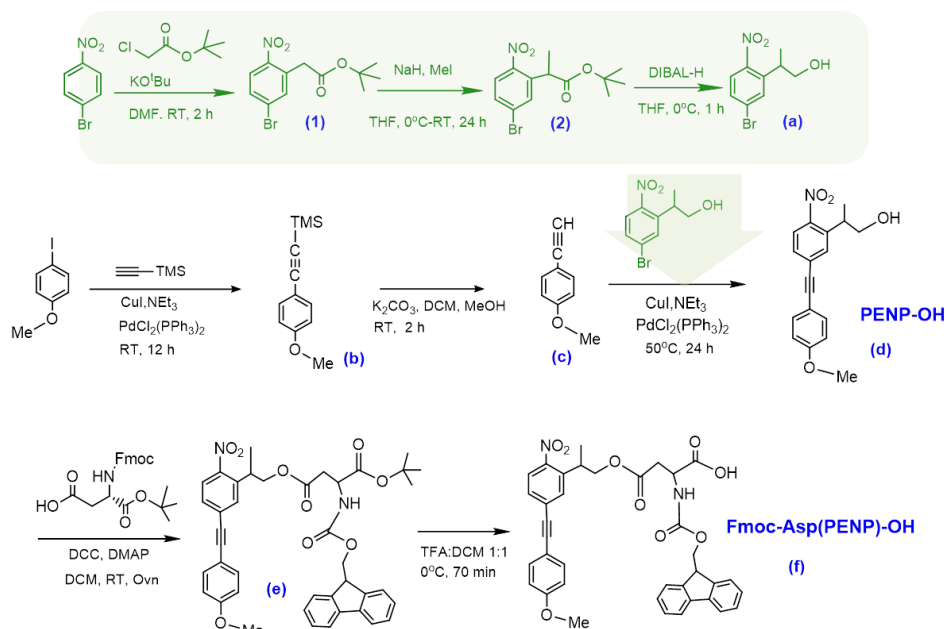


Figure 4.6 Synthesis route for Fmoc-Asp(PENP)-OH

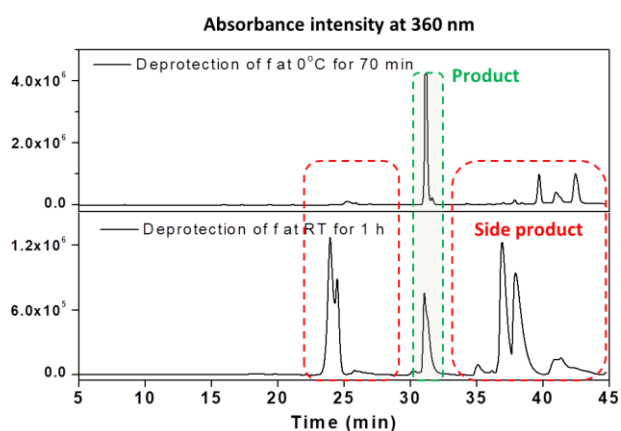


Figure 4.7 Synthesis evolution of Fmoc-Asp(PENP)-OH followed by RP-HPLC at different temperatures.

4.3.2 Stability study of Fmoc-Asp(PENP)-OH

The stability of **f** in regular conditions used in solid phase peptide synthesis (SPPS) was tested. In case of hydrolytic instability in acidic media, the ester group could be prone to hydrolysis in water media to form PENP-OH and Fmoc-Asp-OH, as shown in **Figure 4.8**.

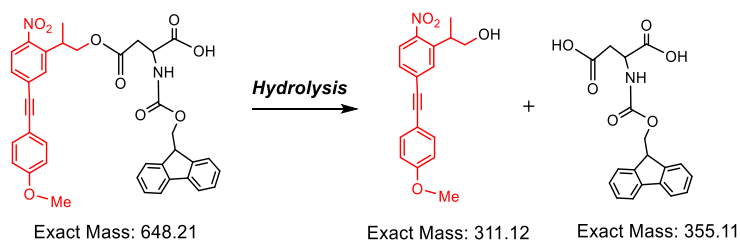


Figure 4.8 Hydrolysis reaction expected for Fmoc-Asp(PENP)-OH

Stability tests in mild acidic conditions (TFE/AcOH/DCM 1:3:6) and strong acidic conditions (TFA/DCM/TIS 4:1:20) commonly used in SPPS were performed (**Figure 4.9**). Decomposition of Fmoc-Asp(PENP)-OH was observed in 4 hours under strong acidic conditions, while no decomposition was observed under milder acidic conditions. The stability of the compound under more physiologically relevant conditions was then tested. In PBS buffer at pH 7.4, room temperature and in the dark, 90% of PENP aspartate decomposed in 72 h, as observed by analytical HPLC (**Figure 4.10**). The expected hydrolysis products, i.e. Asp and PENP-OH, could not be detected by mass spectrometry analysis. Therefore, the decomposition mechanism remains unknown at this point. The poor stability of Fmoc-Asp(PENP)-OH in aqueous environment limits the use of this chromophore for long-term cell studies. In comparison, the previously reported c[RGD(PMNb)fC] had shown higher hydrolytic stability: proven stable upon incubation in PBS at room temperature for more than one month.^{12, 15} Despite the observed poor hydrolytic stability of Fmoc-Asp(PENP)-OH compound, it was reasoned that its incorporation in the derived cRGD peptide could improve such degradability rate (for example, if the cyclic peptide structure provides steric shielding thus preventing significant hydrolysis at this position) and still remain valuable for cell biology experimentation. This hypothesis was tested in the next section.

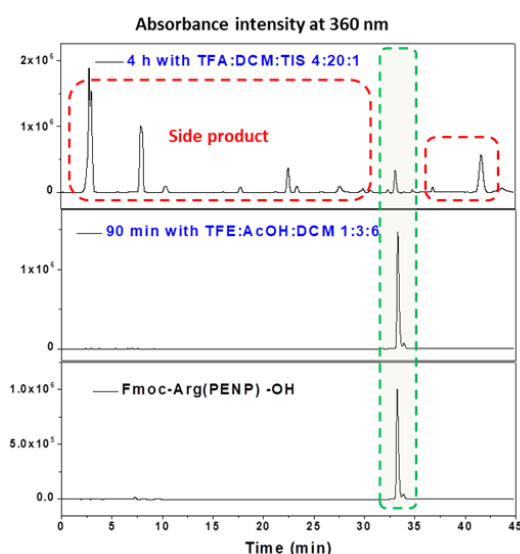


Figure 4.9 Stability study of Fmoc-Asp(PENP)-OH under acidic conditions of common use in SPPS followed by RP-HPLC.

Chapter 4

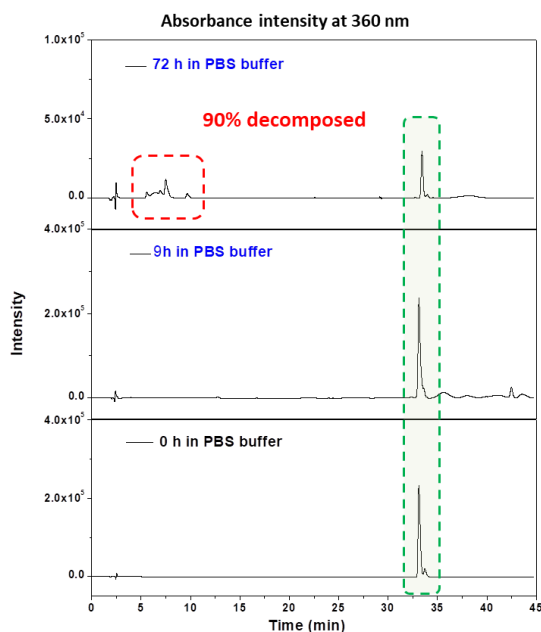


Figure 4.10 Stability of Fmoc-Asp(PENP)-OH in PBS buffer at room temperature followed by RP-HPLC.

4.3.3 Synthesis of c[RGD(PENP)fC] via solid phase peptide synthesis

The cyclic peptide, c[RGD(PENP)fC] (**Figure 4.11**) was synthesized manually by SPPS following established procedures in the group for the preparation of photoactivatable c[RGD(DMNPB)fC] peptide via substituting DMNPB-Asp by PENP-Asp.¹⁷ The SPPS started from H-Gly-2-Cl-Trt resin and the Fmoc-protected amino acids were added sequentially to the resin to build the linear peptide chain in the order: Arg(Pbf), Cys(Trt), D-Phe and Asp(PENP). HOBt, HBTU and DIPEA in DMF was used as coupling medium. The Fmoc-group was cleaved using 20% piperidine in DMF. PENP-Asp was coupled to the GRcf sequence at the last step to prevent decomposition of PENP chromophore decomposition reactions during the deprotection/coupling cycles. The success of the coupling reaction was confirmed by mass analysis after each coupling step. Taking into account the low stability observed for PENP-Asp in the previous section, the GRcfD(PENP) peptide was cleaved from the resin using mild acidic conditions, i.e. TFE/AcOH/DCM (1:3:6), to preserve the aspartate ester bond as well as Pbf and Trt protecting groups. Mass spectrometry analysis confirmed the chemical structure of the product with a $[M+H]^+$ peak at $m/z = 1384.5$. The cleaved linear peptide was used for the cyclisation step without further purification. The cyclisation reaction was performed using DPPA as coupling agent at high dilution (0.001 mM) in DMF in order to favor intramolecular vs. intermolecular couplings. The cyclic peptide was precipitated from the crude into water and purified by HPLC. The target cyclic peptide was confirmed by mass analysis ($m/z=1366.2$ for $[M+H]^+$) and a peak at retention time 44 min in the analytical HPLC chromatogram (**Appendix**). Cleavage of the -Trt and -Pbf protecting groups was first performed at acidic conditions using TFA/DCM/TIS (95/2.5/2.5) at room temperature. However, hydrolysis of the PENP was observed in parallel. Deprotection was also tested under milder acidic conditions (TFA/DCM/TIS 4/20/1, 0°C, 3.5-5 h). The deprotected peptide c[RGD(PENP)fC] was identified by mass analysis ($m/z=890.2$ for $[M+NH_4]^+$) and an HPLC peak at retention time 25 min (**Appendix**). However, c[RGD(PENP)fC] was obtained only at yield of 10% after optimization of the

deprotection conditions (~1.3 mg). The intercalation of alkyne spacer in PMNB system seems to lead to a decreased stability of the ester group, even when the -OMe group is used as substituent in the para-position. Note that c[RGD(DMNPB)fC] and c[RGD(PMNB)fC], which also contain a protected ester group, have been obtained in 36.5% and 54% yield.^{12, 17}

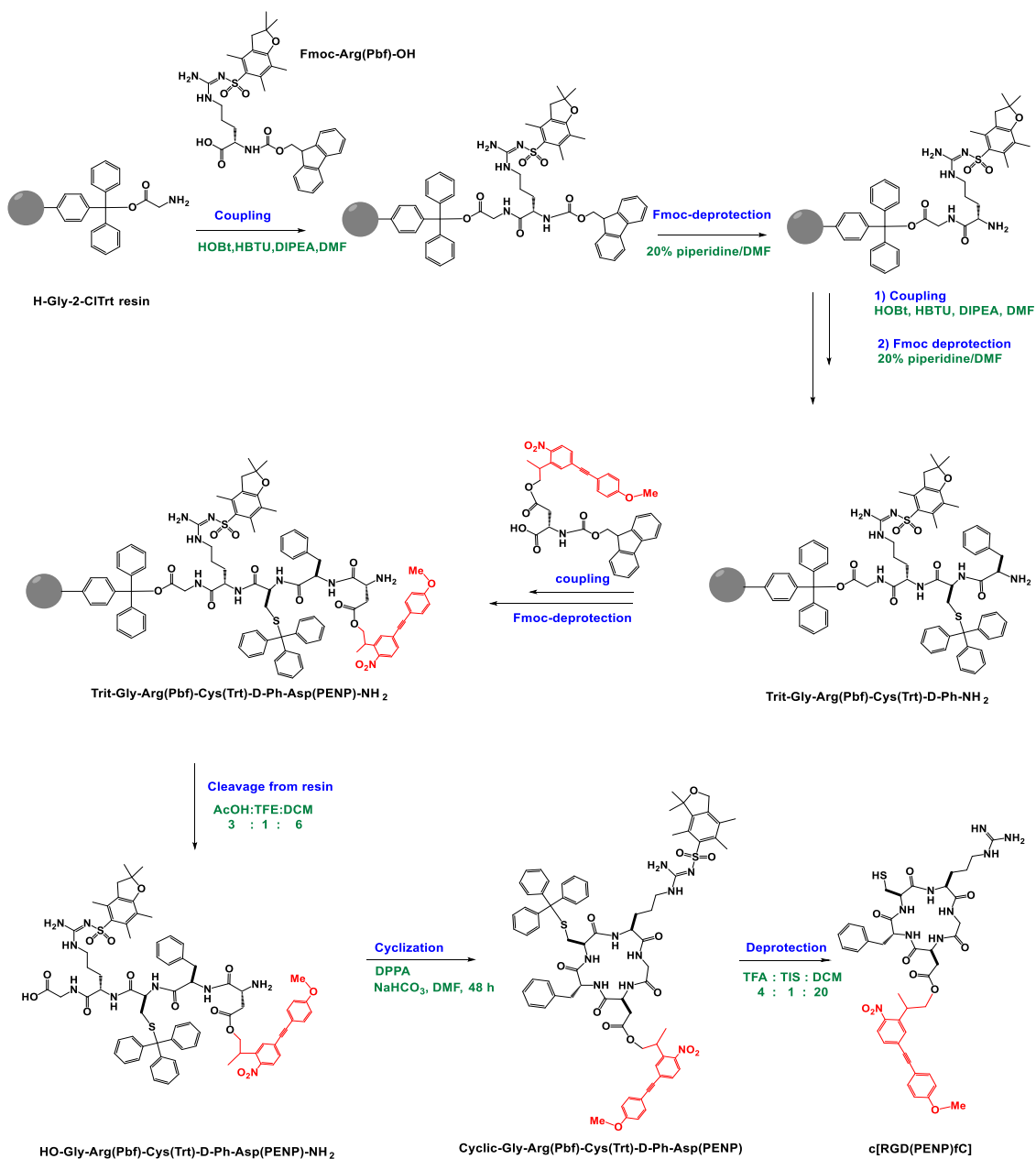


Figure 4.11 Synthesis route of c[RGD(PENP)fC] by SPPS.

In order to have enough amount of target compound for physicochemical characterization and subsequent use in cell biology experiments, a last attempt to obtain the PENP derivatized RGD in higher yield was made. In this case, we attempted the synthesis of the peptide c[RGD(PENP)fK-N₃] in one step by direct reaction of commercial c[RGDfK-N₃] with PENP-OH (**Figure 4.12**). This one-step route was expected to provide an alternative pathway to the synthesis of photoactivatable c[RGD(PENP)fK-N₃] through lower synthetic effort while avoiding the last acidic deprotection step needed in the previous synthetic design. Moreover, the target compound was designed to present a lateral -N₃ group,

Chapter 4

to allow covalent coupling to DBCO-functionalized hydrogel precursors via Strain-promoted azide-alkyne cycloaddition (SPAAC). The synthesis of c[RGD(PENP)fK-N₃] was performed under Steglich esterification conditions using DMAP and DCC to mediate ester coupling. After HPLC purification, the targeted peptide was obtained in ~30% yield and identified by mass spectrometry analysis ([M+H]⁺ peak at m/z = 923.20) and a HPLC peak at retention time 33 min (**Appendix**). This result is an improvement vs. the previous synthetic approach, which had only afforded 10% of pure compound (<1 mg).

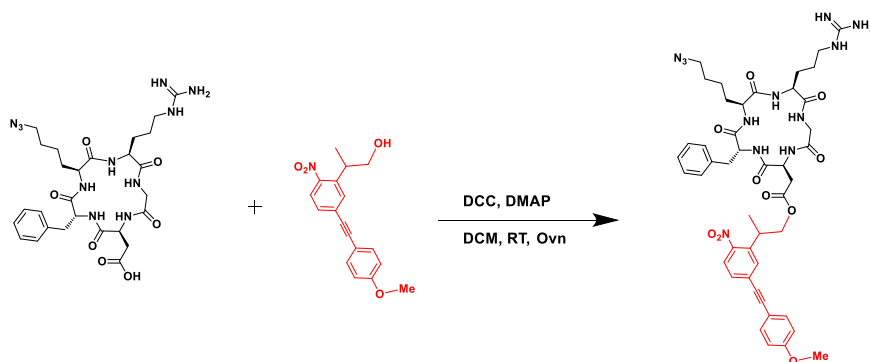


Figure 4.12 Synthesis route of c[RGD(PENP)fK-N₃]

4.4 Photochemical properties of Fmoc-Asp(PENP)-OH in solution

Figure 4.13B shows the UV/Vis spectrum of Fmoc-Asp(PENP)-OH, with an absorption maximum at 390 nm that tails up to 550 nm ($\pi \rightarrow \pi^*$). Compared to c[RGD(PMNB)fC] ($\lambda_{\text{max}} = 317$ nm),¹² the extension of the conjugated system leads to a 80 nm red-shift of λ_{max} . This is an advantageous property for the use of this system in experiments with living cells, since visible light can be employed for the photoactivation reaction.

The photolysis of 2-nitro-2-phenethyl esters is described in the literature to follow a β -elimination pathway, signed by the release of a COOH group and formation of a 4-((4-methoxyphenyl)ethynyl)-1-nitro-2-(prop-1-en-2-yl)benzene as photo by-product (**Figure 4.13A**).^{13, 15} The photolysis of Fmoc-Asp(PENP)-OH was expected to follow the same pathway. To test this hypothesis, photolysis studies were performed by UV/Vis spectroscopy and mass spec analysis of 0.2 mM Fmoc-Asp(PENP)-OH solutions in H₂O/DMSO (4:1) after irradiation at 420 nm at increasing exposure times. Upon irradiation, the intensity of the band at 390 nm decreased and a new peak with increasing intensity appeared at 450 nm. No clear isosbestic points were observed, suggesting that the photolysis reaction does not occur through a single pathway and side reactions might happen in parallel. ESI-MS analysis (**Figure 4.13C**) of the irradiated solution at 3 min corroborated the expected photolysis products: 4-((4-methoxyphenyl)ethynyl)-1-nitro-2-(prop-1-en-2-yl)benzene (m/z = 294.0 for [M+H]⁺) and Fmoc-Asp-OH (m/z = 378.2 for [M+Na]⁺).

The photolysis reaction was also monitored by analytical HPLC. The consumption of Fmoc-Asp(PENP)-OH during irradiation was quantified (**Figure 4.13D**). Before irradiation, Fmoc-Asp(PENP)-OH appeared at a retention time of 34 min at 360 nm channel while Fmoc-Asp appeared at 5 min in the 210 nm channel. After illumination, the Fmoc-Asp(PENP)-OH signal at 34 min decreased in intensity, and a

major signal appeared at 31 min corresponding to 4-((4-methoxyphenyl)ethynyl)-1-nitro-2-(prop-1-en-2-yl)benzene and a number of other signals appeared at other retention times. These could be reaction side products. Fmoc-Asp(PENP)-OH was consumed 95% upon 1 min of irradiation and full consumption was observed after 3 min of exposure. The Fmoc-Asp peak at 5 min in the 210 nm channel was observed after 3 minutes exposure. These results indicate the high photo-efficiency of (*o*-nitrobiphenylacetylene)propyl systems.

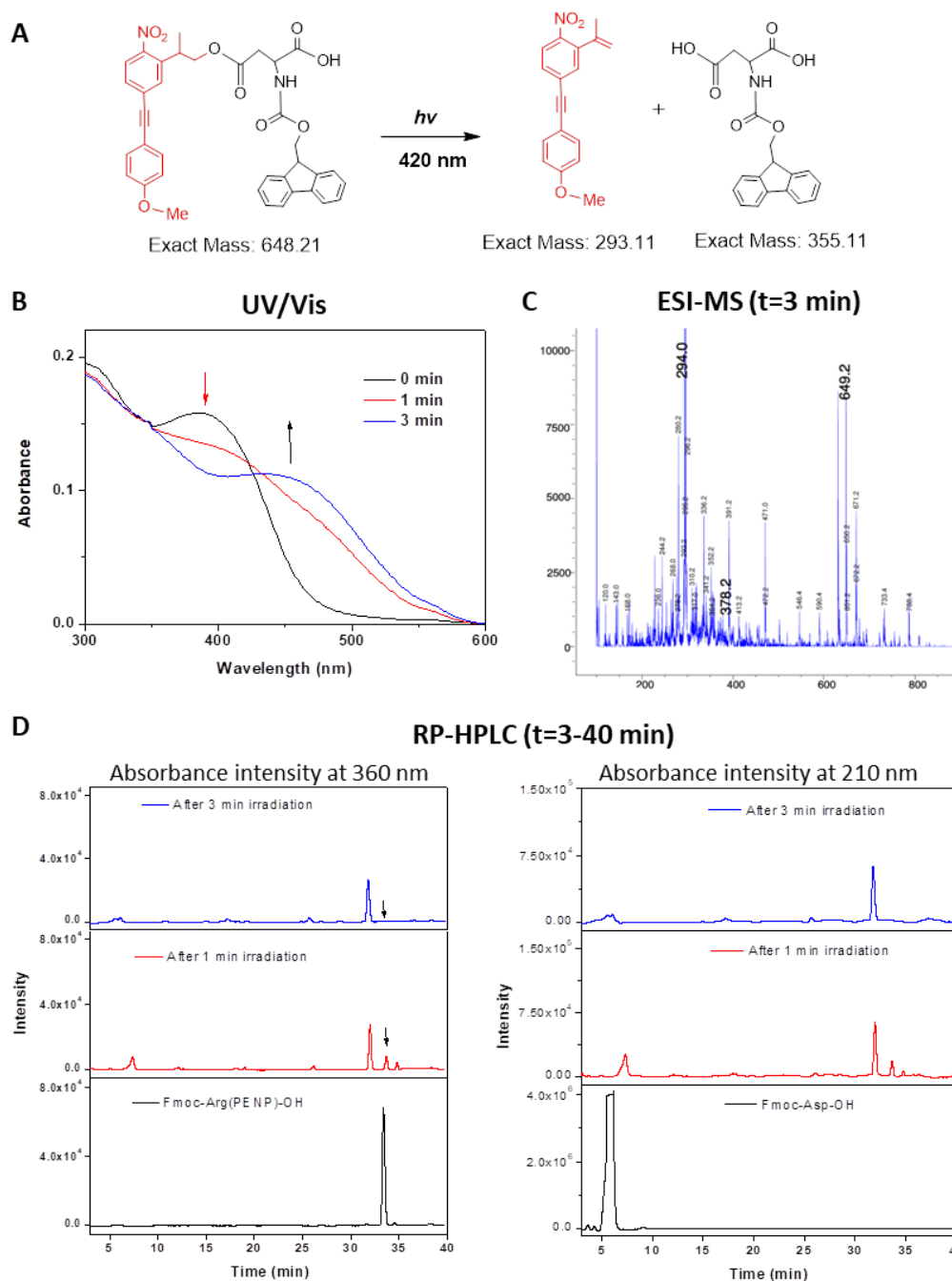


Figure 4.13 (A) Photochemical reaction expected for Fmoc-Asp(PENP)-OH in solution. (B) UV/Vis spectra evolution of Fmoc-Asp(PENP)-OH solution during photolysis (0.2 mM, H₂O/DMSO (4:1)). Conditions: Irradiation wavelength = 420 nm, irradiance = 1.2 mW cm⁻². (C) ESI-MS analysis of photolyzed solution. (D) Analytical HPLC profile of Fmoc-Asp(PENP)-OH aliquots before and after irradiation, $\lambda_{\text{detection}} = 210$ nm and 360 nm. Method: 50B-95B, 40 min.

4.5 Photochemical properties of c[RGD(PENP)fK-N₃] in solution

The expected photolysis reaction of c[RGD(PENP)fK-N₃] is shown in **Figure 4.14A**. c[RGDfK-N₃] and 4-((4-methoxyphenyl)ethynyl)-1-nitro-2-(prop-1-en-2-yl) benzene are the expected photolysis products. The UV/Vis spectrum of c[RGD(PENP)fK-N₃] showed an absorption maximum at 400 nm (**Figure 4.14B**), which decreased in intensity when irradiated at 420 nm while a new band appeared at ~450 nm. No clear isosbestic points were observed, suggesting that the photolysis reaction occurs through multiple pathways, as observed for Fmoc-PENP. ESI-MS analysis (**Figure 4.14C**) of the irradiated solution at 1 min corroborated the expected photolysis products: 4-((4-methoxyphenyl)ethynyl) -1-nitro-2- (prop-1-en-2-yl) benzene ($m/z = 294.0$ for $[M+H]^+$) and cRGDfK-N₃ ($m/z = 630.4$ for $[M+H]^+$).

HPLC analysis of the irradiated samples showed the peak corresponding to c[RGD(PENP)fK-N₃] at retention time 33 min (254 and 360 nm channel) and c[RGDfK-N₃] at 31 min (254 nm channel) (**Figure 4.14D**). Upon illumination, the intensity of the signal at 33 min decreased while a major signal with increasing intensity appeared at 31 min. c[RGD(PENP)fK-N₃] was consumed in 95% in 1 min of irradiation and full consumption of was observed after 5 min exposure. Compared to the photolysis reaction of Fmoc-Asp(PENP), the photolysis process of c[RGD(PENP)fK-N₃] seems cleaner (i.e., fewer peaks of byproducts observed in the chromatogram profile). One possible explanation for this result is the absence of a free -COOH group in the cyclic peptide.

To conclude, the bridging alkyne spacer has a beneficial effect of bathochromic shift (~ 80 nm) into 400 nm. An irradiation dose of 0.216 J cm⁻² and 0.36 J cm⁻² were required for Fmoc-Asp(PENP)-OH and c[RGD(PENP)fK-N₃] at 420 nm at irradiance of 1.2 mW cm⁻², while a doses of 6.48 J cm⁻² and 2.16 J cm⁻² were needed for c[RGD(DMNPB)fC] and c[RGD(PMNB)fC] at 365 nm at irradiance of 1.2 mW cm⁻². These results indicate a higher photo-efficiency of PENP caged compounds compared with reported DMNPB- and PMNB-caged compounds under 1P excitation. The bathochromic shift at ~ 400 nm (2P activation at ~800 nm) enabled the utilization of cytocompatibility doses with reduced phototoxic and less tissue scattering effect.¹⁸

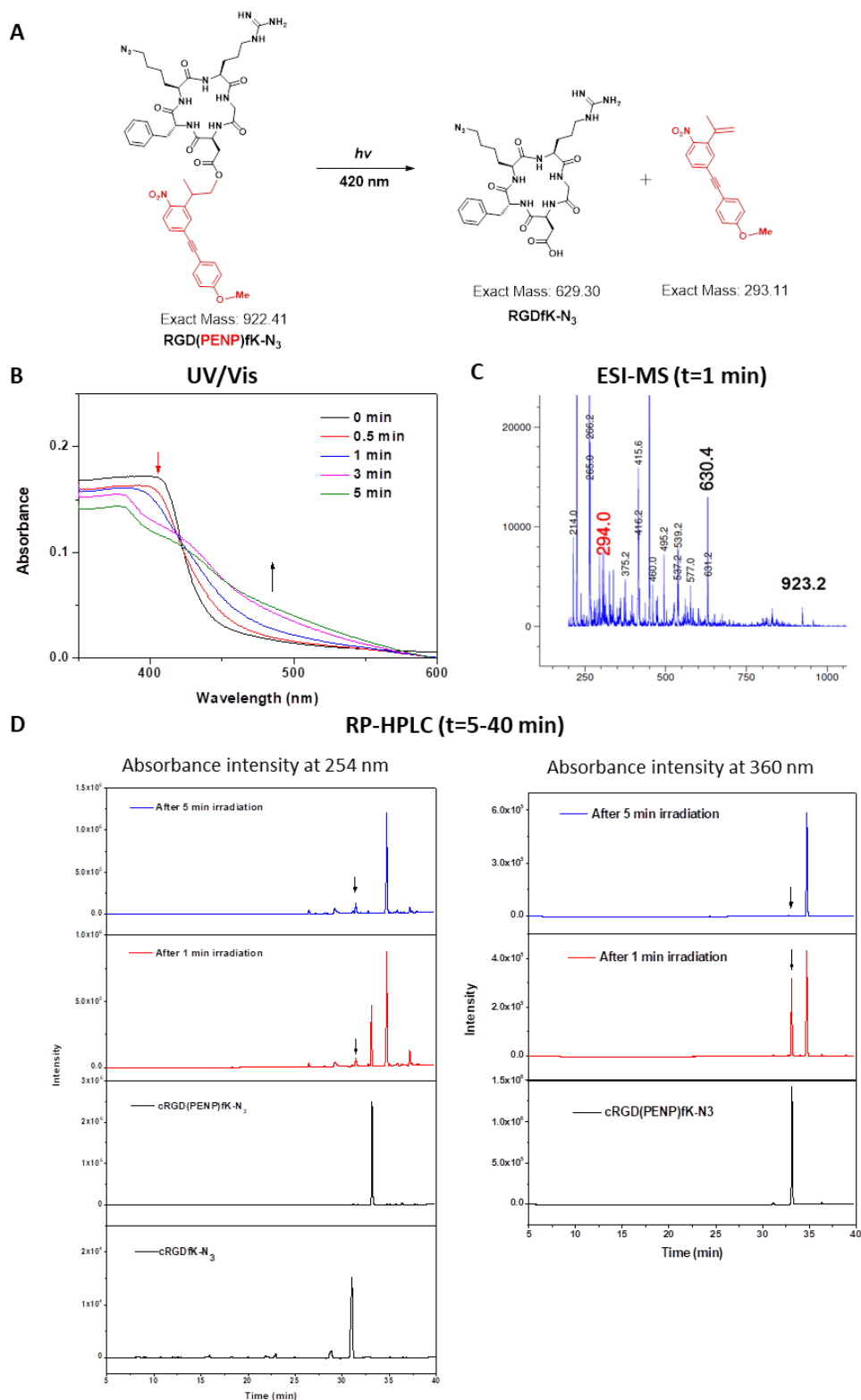


Figure 4.14 (A) Photochemical reaction expected for c[RGD(PENP)fK-N₃] in solution. (B) UV/Vis spectral evolution of c[RGD(PENP)fK-N₃] during photolysis (0.2 mM solution, H₂O). Conditions: Irradiation wavelength = 420 nm, irradiance = 1.2 mW cm⁻². (C) ESI-MS analysis of photolyzed solution. (D) Analytical HPLC profile of c[RGD(PENP)fK-N₃] before and after irradiation, $\lambda_{\text{detection}} = 254$ nm and 360 nm. Method: 5B-95B, 40 min.

Chapter 4

4.6 Discussion

The 2P sensitive chromophore (PENP) with an intercalated alkyne spacer in the biphenyl system and with a methoxy group in para-position was synthesized at reasonable scale ~200 mg. The PENP-OH derivative was synthesized in 6 steps with an overall yield of 18%. PENP Asp was successfully synthesized in 2 steps with a rather low overall yield of 21%. The stability of Fmoc-Asp(PENP)-OH was investigated under the conditions used in SPPS. Fmoc-Asp(PENP)-OH showed low stability under strong acidic conditions. Meanwhile, Fmoc-Asp(PENP)-OH decomposed in neutral PBS buffer in 3 days. Compared with the reported PMNB groups from our previous studies,¹⁰ the lower stability of PENP chromophore might be due to the intercalated alkyne spacer which is an unsaturated triple bond and can go through a variety of addition reactions, e.g. hydrogenation and halogen addition. c[RGD(PENP)fC] was successfully synthesized manually by solid phase peptide synthesis (SPPS) with a very low overall yield due to the low stability of PENP under strong acidic conditions. Optimization of conditions for the deprotection of protecting groups was carried out by altering the ratio of acid, reaction temperature and reaction time. The best condition found was TFA/DCM/TIS (4:20:1) at 0°C for 3.5-5 h to afford a yield ~10%. To avoid decomposition under strong acidic conditions of PENP aspartate, c[RGD(PENP)fK-N₃] was successfully synthesized via a one-step route with an improved yield~30%.

Also, other highly conjugated chromophores, e.g. coumarin^{19, 20} quinoline^{21, 22} and BODIPY derivatives²³ can be structural alternatives to PENP to improve stability and retain high two-photon absorption cross-section. Although the low hydrolytic stability of PENP limits the application of long-term cell studies, it would be useful for those applications that need simultaneous release or sequential hydrolysis. Such applications go beyond the scope of this work.

4.7 Reference

1. Petersen, S.; Alonso, J. M.; Specht, A.; Duodu, P.; Goeldner, M.; del Campo, A., Phototriggering of cell adhesion by caged cyclic RGD peptides. *Angewandte Chemie (International ed. in English)* **2008**, *47* (17), 3192-5.
2. Ohmuro-Matsuyama, Y.; Tatsu, Y., Photocontrolled cell adhesion on a surface functionalized with a caged arginine-glycine-aspartate peptide. *Angewandte Chemie (International ed. in English)* **2008**, *47* (39), 7527-9.
3. Dechantsreiter, M. A.; Planker, E.; Mathä, B.; Lohof, E.; Hölzemann, G.; Jonczyk, A.; Goodman, S. L.; Kessler, H., N-Methylated Cyclic RGD Peptides as Highly Active and Selective α V β 3 Integrin Antagonists. *Journal of Medicinal Chemistry* **1999**, *42* (16), 3033-3040.
4. Kadem, L. F.; Suana, K. G.; Holz, M.; Wang, W.; Westerhaus, H.; Herges, R.; Selhuber-Unkel, C., High-Frequency Mechanostimulation of Cell Adhesion. *Angewandte Chemie (International ed. in English)* **2017**, *56* (1), 225-229.
5. Lee, T. T.; García, J. R.; Paez, J. I.; Singh, A.; Phelps, E. A.; Weis, S.; Shafiq, Z.; Shekaran, A.; del Campo, A.; García, A. J., Light-triggered in vivo activation of adhesive peptides regulates cell adhesion, inflammation and vascularization of biomaterials. *Nature Materials* **2015**, *14* (3), 352-360.

6. Kadem, L. F.; Holz, M.; Suana, K. G.; Li, Q.; Lamprecht, C.; Herges, R.; Selhuber-Unkel, C., Rapid Reversible Photoswitching of Integrin-Mediated Adhesion at the Single-Cell Level. *Adv Mater* **2016**, *28* (9), 1799-802.
7. Ricken, J.; Medda, R.; Wegner, S. V., Photo-ECM: A Blue Light Photoswitchable Synthetic Extracellular Matrix Protein for Reversible Control over Cell-Matrix Adhesion. *Adv Biosyst* **2019**, *3* (3), e1800302.
8. Xu, D.; Ricken, J.; Wegner, S. V., Turning Cell Adhesions ON or OFF with High Spatiotemporal Precision Using the Green Light Responsive Protein CarH. *Chemistry* **2020**, *26* (44), 9859-9863.
9. Lin, Y.; Mazo, M. M.; Skaalure, S. C.; Thomas, M. R.; Schultz, S. R.; Stevens, M. M., Activatable cell-biomaterial interfacing with photo-caged peptides. *Chemical Science* **2019**, *10* (4), 1158-1167.
10. Specht, A.; Bolze, F.; Donato, L.; Herbivo, C.; Charon, S.; Warther, D.; Gug, S.; Nicoud, J. F.; Goeldner, M., The donor-acceptor biphenyl platform: a versatile chromophore for the engineering of highly efficient two-photon sensitive photoremovable protecting groups. *Photochemical & photobiological sciences : Official journal of the European Photochemistry Association and the European Society for Photobiology* **2012**, *11* (3), 578-86.
11. Specht, A.; Thomann, J. S.; Alarcon, K.; Wittayanan, W.; Ogden, D.; Furuta, T.; Kurakawa, Y.; Goeldner, M., New photoremovable protecting groups for carboxylic acids with high photolytic efficiencies at near-UV irradiation. Application to the photocontrolled release of L-glutamate. *ChemBiochem* **2006**, *7* (11), 1690-5.
12. Farrukh, A.; Paez, J. I.; del Campo, A., 4D Biomaterials for Light-Guided Angiogenesis. *Adv Funct Mater* **2019**, *29* (6), 1807734.
13. Schelkle, K. M.; Becht, S.; Faraji, S.; Petzoldt, M.; Mullen, K.; Buckup, T.; Dreuw, A.; Motzkus, M.; Hamburger, M., Emission turn-on and solubility turn-off in conjugated polymers: one- and two-photon-induced removal of fluorescence-quenching solubilizing groups. *Macromolecular rapid communications* **2015**, *36* (1), 31-7.
14. Schelkle, K. M.; Griesbaum, T.; Ollech, D.; Becht, S.; Buckup, T.; Hamburger, M.; Wombacher, R., Light-induced protein dimerization by one- and two-photon activation of gibberellic acid derivatives in living cells. *Angewandte Chemie (International ed. in English)* **2015**, *54* (9), 2825-9.
15. Donato, L.; Mouro, A.; Davenport, C. M.; Herbivo, C.; Warther, D.; Léonard, J.; Bolze, F.; Nicoud, J.-F.; Kramer, R. H.; Goeldner, M.; Specht, A., Water-soluble, donor-acceptor biphenyl derivatives in the 2-(o-nitrophenyl)propyl series: highly efficient two-photon uncaging of the neurotransmitter γ -aminobutyric acid at $\lambda = 800$ nm. *Angewandte Chemie (International ed. in English)* **2012**, *51* (8), 1840-1843.
16. Garcia-Fernandez, L.; Herbivo, C.; Arranz, V. S.; Warther, D.; Donato, L.; Specht, A.; del Campo, A., Dual photosensitive polymers with wavelength-selective photoresponse. *Adv Mater* **2014**, *26* (29), 5012-7.
17. Wirkner, M.; Weis, S.; San Miguel, V.; Álvarez, M.; Gropeanu, R. A.; Salierno, M.; Sartoris, A.; Unger, R. E.; Kirkpatrick, C. J.; del Campo, A., Photoactivatable caged cyclic RGD peptide for triggering integrin binding and cell adhesion to surfaces. *ChemBiochem* **2011**, *12* (17), 2623-9.
18. Pawlicki, M.; Collins, H. A.; Denning, R. G.; Anderson, H. L., Two-photon absorption and the design of two-photon dyes. *Angewandte Chemie (International ed. in English)* **2009**, *48* (18), 3244-66.

Chapter 4

19. Li, X.; Zhao, Y.; Wang, T.; Shi, M.; Wu, F., Coumarin derivatives with enhanced two-photon absorption cross-sections. *Dyes and Pigments* **2007**, *74* (1), 108-112.
20. Weinstain, R.; Slanina, T.; Kand, D.; Klán, P., Visible-to-NIR-Light Activated Release: From Small Molecules to Nanomaterials. *Chemical Reviews* **2020**, *120* (24), 13135-13272.
21. Davis, M. J.; Kragor, C. H.; Reddie, K. G.; Wilson, H. C.; Zhu, Y.; Dore, T. M., Substituent Effects on the Sensitivity of a Quinoline Photoremovable Protecting Group to One- and Two-Photon Excitation. *The Journal of Organic Chemistry* **2009**, *74* (4), 1721-1729.
22. Tran, C.; Gallavardin, T.; Petit, M.; Slimi, R.; Dhimane, H.; Blanchard-Desce, M.; Acher, F. C.; Ogden, D.; Dalko, P. I., Two-Photon "Caging" Groups: Effect of Position Isomery on the Photorelease Properties of Aminoquinoline-Derived Photolabile Protecting Groups. *Organic Letters* **2015**, *17* (3), 402-405.
23. Zhang, X.; Xiao, Y.; Qi, J.; Qu, J.; Kim, B.; Yue, X.; Belfield, K. D., Long-Wavelength, Photostable, Two-Photon Excitable BODIPY Fluorophores Readily Modifiable for Molecular Probes. *The Journal of Organic Chemistry* **2013**, *78* (18), 9153-9160.

Conclusions & Outlook

In this PhD thesis, 2P-degradable hydrogels were developed, applied for cell encapsulation and tested for light-guided 3D cell migration. The hydrogels were obtained by the thiol-MS coupling reaction of PMNB-based 2P-activable crosslinkers and star PEGs in buffer at physiological pH. The gelation conditions are compatible with the in situ encapsulation of living cells. Crosslinkers with different photolabile groups and length of hydrophilic spacers were developed to improve the hydrolytic stability and water solubility of the system. The resulting hydrogels efficiently degraded upon 2P exposure. The opened space within the gel triggered migration of cells towards the light exposed sites. This work contributes to the field of photodegradable hydrogels with an in-depth study of structure–property relationship. The developed hydrogels showed improved stability and 2P cleavage efficiency in comparison to previously reported materials, which highlights the possibilities for spatial-temporal controlled photodegradation in 3D cellular applications to study cellular behaviour.

Additionally, a 2P-activable RGD peptidomimetics was synthesized. A π -extended chromophore was attached to the Asp rest to temporarily block the bioactivity site and enabled further 2P light activation. However, the low stability of obtained photoactivatable peptide limits the further long-term cellular applications.

The following are the major conclusions of this work:

1. 2P-cleavable crosslinkers based on bifunctional-PMNB chromophores with ester and carbamate labile groups and terminated with -SH, -Tz-MS and -Ox-MS groups can be synthesized in reasonable yields to be used as model hydrogel matrices for in vitro cell studies. The incorporation of the PMNB group and the arylmethyl end-groups reduces the water solubility of the crosslinkers, which was improved in this Thesis by further increasing the length of the hydrophilic PEG spacer. The linkage of the photolabile group to the PEG chain influences the hydrolytic stability of the network, and a change of an ester by a carbamate was needed to enable longer term cell culture experiments. As demonstrated in **Chapter 2**, the new PMNB-based crosslinker proved to be advantageous vs. the previously reported oNB analogue in terms of photoefficiency upon light exposure at 365 nm and 420 nm in solution.
2. The reactivity of the crosslinking groups (reaction yield and kinetics) profoundly affects the suitability of a hydrogel system for cell encapsulation. In this work, the thiol-MS system was successfully used for this purpose, and new macromers terminated in the Ox group were developed and crosslinked with thiolated macromers within minutes time scale. PMNB(C-EG_n-Ox-MS)₂ crosslinker proved to be the best choice to prepare hydrogels with high hydrolytic stability and highly efficient and chemoselective photocleavage. Preliminary cell studies revealed the potential of these hydrogels as 3D scaffold to light-guide cell migration in a spatial temporal manner, and open the door to more complex biological studies in the future.

Conclusions & Outlook

3. As shown in **Chapter 4**, extending the length of the π -conjugated unit in a PMNB-based chromophore is beneficial from the point view of 2P-photoefficiency. However, this advantage could not be exploited for the synthesis of 2P-photoactivatable peptides in the expected extent due to the chemical lability of this group and its incompatibility with reaction conditions used for SPPS. The relationship between structure to properties needs to be reconsidered for next-generation designs of advanced peptidomimetics and derived triggerable materials.

In the following, a reflection on the encountered limitations in this doctoral work and an outlook on future developments in this field are provided.

1. The chemical approach of this Thesis is demonstrated as a powerful method to engineer hydrogel formation and degradation. The crosslinkers can be synthesized in 50-100 mg scale which is enough to support many rounds of preliminary cell migration experiments replication but the synthesized approach (e.g. the Suzuki coupling and the coupling conditions for aromatic amine and carboxylic acid), should be implemented for a bigger-scale manufacturing of crosslinkers for further applications.
2. Although PMNB group exhibits a high 2P efficiency, the nitrostyrene photolysis byproduct is a strong active species, which was found to be involved in many side reactions during light exposure, thus leading to lower control of material response upon illumination. Therefore, the selection and utilization of other highly efficient chromophores, with "cleaner" photolysis mechanisms, could be an alternative for future research towards engineering photoresponsive hydrogels. For example, BODIPY-based chromophores could be investigated using a similar approach, and compared to the results found here for PMNB groups. Additionally, it was encountered that the somewhat rigid biphenyl structure of PMNB moiety limits the mobility of PEG spacer, which might lead to a lower crosslinking conversion and thus to materials with lower mechanical strength than anticipated. Further studies should be conducted to investigate the effect of hindered mobility of PMNB-containing spacers on the crosslinking conversion, and how can this be optimized, e.g., by incorporating diverse flanking spacers (such as PEGs of different length).
3. Although thiol-MS coupling chemistry and SPAAC chemistry were proved as great chemical approaches for hydrogel formation (i.e., crosslinking), the selection of -MS (e.g. -Tz-MS, -Ox-MS) and cycloalkyne reactive groups should be carefully considered to avoid further side reactions at subsequent time points of the biomaterial. For example, the use of -Tz-MS reactive group towards thiols via thiol-MS coupling chemistry proved excellent for the crosslinking step, but afterward proved non-optimal during the light exposure step, because side reactions involving the thioether-Tz with photoproducts of PMNB, unexpectedly lead to hydrogel stiffening instead of softening. It is hypothesized that -Tz-MS is not chemically orthogonal to the photoproduct of PMNB upon light exposure. Future research should be

Conclusions & Outlook

performed to identify appropriate crosslinking chemistries that are also orthogonal to other relevant chromophores during light exposure, to anticipate possible crosstalk. This will enable higher control over engineered hydrogel properties.

4. Preliminary cell migration experiments indicated that PEG-SO_x-C-PMNB hydrogel is a good candidate to enable 4D manipulation of synthetic cellular microenvironments with high spatial resolution (at least within the first 3 days of culture), however the platform has not been fully exploited yet. Future research should be performed to optimize the photoactivation conditions and culture parameters for better understanding the system in more detail. For example, optimization of the concentration of cell-adhesive cue RGD for triggering the migration of HUVECs is needed; as well as to solve the problem of low cell viability found after 3 days culture. Additionally, co-culturing HUVECs with other cell type such as human dermal fibroblasts (HDF) could help to stabilize HUVECs, leading in the future to a more reliable platform to investigate the angiogenesis process. Finally, the knowledge gained for HUVECs/angiogenesis study could be applied to investigate other cell biology questions. In this regard, this platform offers the possibility of studying other cellular behaviours like cell differentiation.

Conclusions & Outlook

Appendix

Appendix	Section
Materials and instrumentation	Section 5.1
Chapter 2	Section 5.2
Chapter 3	Section 5.3
Chapter 4	Section 5.4

5.1 Materials and instrumentation

Most of chemicals were purchased from Sigma Aldrich Chemie GmbH (Steinheim, Germany) or Alfa Aesar (Kandel, Germany). Alexa Fluor 555 C2 maleimide was obtained from ThermoFisher (Dreieich, Germany). SH-PEG_n-SH (3 kDa) was purchased from Iris Biotech GmbH (Marktredwitz, Germany). NH₂-PEG_n-NHBoc (n=9, 15 or 23) were purchased from BroadPharm (San Diego, USA). Star PEG-COONHS (20 kDa), star PEG-COOH (20 kDa), star PEG-SH (20kDa) and star PEG-NH₂ (20 kDa) were purchased from JenKem Technology USA Inc. (Plano, USA).

Buffer solutions were freshly prepared. 20 mM HEPES buffers (pH 7.5 and pH 8) and phosphate-buffer saline buffer (PBS) (pH 7.4) were used, unless otherwise stated.

Microwave reactions were performed on an Anton Paar Multiwave PRO. Thin layer chromatography (TLC) plates (ALUGRAM® SIL G/UV254) and silica gel for column chromatography (60 Å pore size, 63-200 µm particle size) were obtained from Macherey-Nagel (Düren, Germany). TLC plates were observed under 254 or 365 nm light. HPLC analysis and purification of the compounds were performed with a HPLC JASCO 4000 (Japan) equipped with diode array, UV-Vis detector and fraction collector. Reprosil C18 columns were used for semi-preparative (250 × 25 mm) and analytical (250 × 25 mm) runs. Solvent gradients using a combination of the following eluents were used: solvent A (MilliQ water + 0.1% TFA) and solvent B (95% ACN/5% MilliQ water + 0.1% TFA), typically over 40 or 45 min duration.

Solution ¹H-NMR and ¹³C-NMR spectra were recorded using a Bruker Avance 300 MHz or a Bruker Avance III UltraShield 500 MHz at 25°C. Chemical shifts are reported in parts per million (ppm) using the residual non-deuterated signal of CD₂Cl₂ (δ_H = 5.32 ppm), CDCl₃ (δ_H = 7.26 ppm) or acetone-d₆ (δ_H = 2.05 ppm) as internal reference. The following abbreviations are used: s: singlet, d: doublet, dd: doublet of doublets, t: triplet, m: multiplet. Data was processed and analyzed using the software MestReNova.

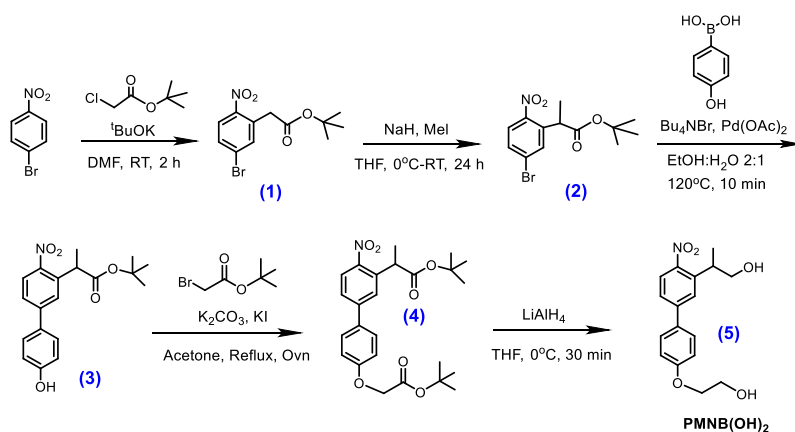
Electrospray ionization mass spectrometry (ESI-MS) was recorded using an Agilent Technologies 1260 Infinity Liquid Chromatography/Mass Selective Detector (LC/MSD) (Agilent Technologies, DE). Quadrupole Time-of-Flight (Q-TOF) was recorded using electrospray ionization with a 6545 Accurate-Mass Quadrupole Time-of-Flight (LC/Q-TOF-MS) (Agilent Technologies, DE). UV/Vis spectra were acquired in a Varian Cary 4000 UV/Vis spectrometer (Varian Inc. Palo Alto, USA).

Appendix

Photolysis experiments in solution were performed at 365 nm or 420 nm with a LUMOS 43 lamp (100 W, 1.2 mW cm⁻²) (Atlas Photonics, Switzerland).

5.2 Chapter 2

5.2.1 Synthesis of PMNB ester crosslinkers



Compounds **1-5** were synthesized according to previously reported protocols,¹ with some modifications applied, as detailed in following sections.

(1) *Tert-butyl 2-(5-bromo-2-nitrophenyl)acetate*

1-Bromo-4-nitrobenzene (1 eq., 4.95 mmol, 1 g) and *tert*-butyl chloroacetate (1.5 eq., 7.43 mmol, 1.12 g) were dissolved in dry DMF (15 mL) under argon. Then the mixture was slowly added to a stirred solution of *t*-BuOK (6 eq., 29.7 mmol, 3.33 g) in dry DMF (15 mL) and purged with argon. The reaction was stirred for 2 h at room temperature, then 5% HCl solution (15 mL) was added dropwise at 0°C. The reaction mixture was extracted with ethyl acetate (2×100 mL) and washed with brine. The organic layer was dried over Na₂SO₄, evaporated under vacuum and the crude product was purified by silica gel column chromatography (10 % ethyl acetate/*n*-hexane) to obtain a pale yellow solid (1.1 g, 70 % yield). The spectroscopic characterization data matched the values reported on the literature.

¹H-NMR (300 MHz, CDCl₃, δ [ppm]) = 7.99 (d, 1H, -CH Ar); 7.59 (dd, 1H, -CH Ar); 7.49 (d, 1H, -CH Ar); 3.91 (s, 2H, -CH₂); 1.44 (s, 9H, -C(CH₃)₃).

¹³C-NMR (75 MHz, CDCl₃, δ [ppm]) = 168.60; 147.85; 136.29; 132.50; 131.65; 128.32; 126.79; 82.35; 40.94; 28.09.

(2) *Tert-butyl 2-(5-bromo-2-nitrophenyl)propanoate*

Tert-butyl 2-(5-bromo-2-nitrophenyl)acetate (**1**) (1 eq., 3.17 mmol, 1 g) was dissolved in dry THF (15 mL) at 0°C and purged with nitrogen for 5 min. In the following order, MeI (9.5 eq., 30 mmol, 2 mL) and NaH (60% in suspension in oil, 3.2 eq., 10 mmol, 400 mg) were slowly added to the above solution at 0°C. The reaction was stirred at room temperature for 30 min and quenched with water. The reaction mixture was extracted with ethyl acetate (2 × 80 mL) and washed with brine. The organic layer was dried over MgSO₄, evaporated and the crude product was purified by silica gel column

chromatography (5% ethyl acetate/n-Hexane) to obtain a pale yellow solid (0.9 g, 86% yield). The spectroscopic characterization data matched the values reported on the literature.

$^1\text{H-NMR}$ (300 MHz, CDCl_3 , δ [ppm]) = 7.84 (d, 1H, -CH Ar); 7.63 (d, 1H, -CH Ar); 7.56 (dd, 1H, -CH Ar); 4.23 (m, 1H, -CH); 1.59 (d, 3H, $-\text{CH}_3$); 1.40 (s, 9H, $-\text{C}(\text{CH}_3)_3$).

$^{13}\text{C-NMR}$ (75 MHz, CDCl_3 , δ [ppm]) = 171.80; 148.00; 137.8; 132.95; 131.11; 128.12; 126.45; 81.98; 42.38; 27.96.

(3) *Tert-butyl 2-(4'-hydroxy-4-nitro-[1,1'-biphenyl]-3-yl)propanoate*

Tert-butyl-2-(5-bromo-2-nitrophenyl)propanoate (**2**) (1 eq., 1.21 mmol, 0.4 g), 4-hydroxyphenyl boronic acid (1.5 eq., 1.81 mmol, 0.25 g), K_2CO_3 (2.5 eq., 3.03 mmol, 0.42 g), Bu_4NBr (1 eq., 1.21 mmol, 0.39 g), and $\text{Pd}(\text{OAc})_2$ (1 mol-% catalyst) were dissolved in 15 mL (2:1) mixture of ethanol/ H_2O and purged with nitrogen for 10 min. The reaction mixture was heated under microwave conditions at 120 °C for 10 min. Water (100 mL) was added and the reaction mixture was extracted with ethyl acetate (2 x 100 mL). The combined organic phase was washed with brine; dried over Na_2SO_4 ; evaporated and the crude product was purified by silica gel column chromatography (20% ethyl acetate/n-hexane) to obtain the title compound (0.28 g, 50% yield). The spectroscopic characterization data matched the values reported on the literature.

ESI- MS^+ : 366.2 (M+Na), 709.2 (2M+Na).

$^1\text{H-NMR}$ (300 MHz, CDCl_3 , δ [ppm]) = 8.00-8.03 (d, 1H, -CH Ar); 7.60 (d, 1H, -CH Ar); 7.52-7.55 (dd, 1H, -CH Ar); 7.47-7.50 (d, 2H, -CH Ar); 6.91-6.94 (d, 2H, -CH Ar); 4.28-4.35 (m, 1H, -CH); 1.61-1.63 (d, 3H, $-\text{CH}_3$); 1.41 (s, 9H, $-\text{C}(\text{CH}_3)_3$).

$^{13}\text{C-NMR}$ (75 MHz, CDCl_3 , δ [ppm]) = 172.89; 156.66; 145.94; 136.49; 131.41; 128.90; 128.86; 127.72; 125.82; 125.75; 116.15; 81.76; 42.77; 28.04; 17.72.

(4) *Tert-butyl 2-(4'-(2-(tert-butoxy)-2-oxoethoxy)-4-nitro-[1,1'-biphenyl]-3-yl) propanoate*

Tert-butyl 2-(4'-hydroxy-4-nitro-[1,1'-biphenyl]-3-yl)propanoate (**c**) (1 eq., 0.58 mmol, 0.2 g), tert-butyl bromoacetate (2 eq., 1.16 mmol, 0.23 g), potassium carbonate (2 eq., 1.16 mmol, 0.16 g) and potassium iodide (0.1 eq., 0.058 mmol, 9.6 mg) were dissolved in 8 mL acetone under nitrogen atmosphere. The mixture was heated at reflux overnight under inert atmosphere, then poured into 20 mL water, and extracted with ethyl acetate (2 x 20 mL). The combined organic phase was washed with brine; dried over Na_2SO_4 ; evaporated and the crude product was purified by silica gel column chromatography (20% ethyl acetate/n-hexane) to obtain a pale yellow oil (0.15 g, 58% yield). The spectroscopic characterization data matched the values reported on the literature.

ESI- MS^+ : 480.2 (M+Na), 937.4 (2M+Na).

$^1\text{H-NMR}$ (300 MHz, CDCl_3 , δ [ppm]) = 7.99-8.02 (d, 1H, -CH Ar); 7.61 (d, 1H, -CH Ar); 7.53-7.55 (m, 3H, -CH Ar); 6.98-7.01 (d, 2H, -CH Ar); 4.57 (s, 2H, $-\text{CH}_2$); 4.27-4.34 (m, 1H, -CH); 1.60-1.62 (d, 3H, $-\text{CH}_3$); 1.50 (s, 9H, $-\text{C}(\text{CH}_3)_3$); 1.40 (s, 9H, $-\text{C}(\text{CH}_3)_3$).

$^{13}\text{C-NMR}$ (75 MHz, CDCl_3 , δ [ppm]) = 172.47; 167.84; 158.71; 147.48; 145.72; 136.60; 132.15; 128.68; 127.81; 125.78; 125.75; 115.28; 82.75; 81.51; 65.78; 42.68; 28.19; 28.00; 17.76.

Appendix

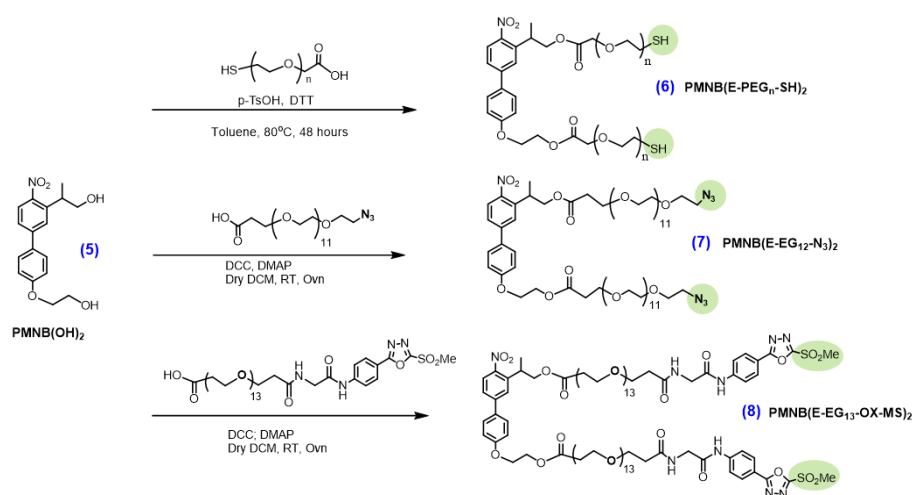
(5) 2-(4'-(2-hydroxyethoxy)-4-nitro-[1,1'-biphenyl]-3-yl)propan-1-ol

Tert-butyl 2-(4'-(2-(tert-butoxy)-2-oxoethoxy)-4-nitro-[1,1'-biphenyl]-3-yl)propanoate (**d**) (1 eq., 0.63 mmol, 0.2 g) was dissolved in 20 mL anhydrous THF at 0°C, and 2 mL of LiAlH₄ (1 M in THF) was carefully added dropwise to the solution with syringe under nitrogen atmosphere and the suspension was stirred for 30 min at 0°C. The reaction was quenched with water; dried over Na₂SO₄, filtered, evaporated, and purified by preparative HPLC (method: 30 B to 95 B, 360 nm, r.t.= 18 min) to obtain a pale yellow powder (156 mg, 75% yield) after freeze-drying. The spectroscopic characterization data matched the values reported on the literature.

ESI-MS⁺: 318.2 (M+H).

¹H-NMR (300 MHz, CDCl₃, δ [ppm]) = 7.85-7.88 (d, 1H, -CH Ar); 7.62 (d, 1H, -CH Ar); 7.49-7.56 (m, 3H, -CH Ar); 7.02-7.05 (d, 2H, -CH Ar); 4.14-4.15 (m, 2H, -CH₂O-); 3.99-4.02 (m, 2H, -CH₂); 3.84-3.87 (m, 2H, -CH₂); 3.63-3.70 (m, 1H, -CH); 1.37-1.40 (d, 3H, -CH₃).

¹³C-NMR (75 MHz, CDCl₃, δ [ppm]) = 159.42; 149.12; 145.49; 139.13; 132.10; 128.76; 126.44; 125.42; 125.23; 115.29; 69.50; 68.15; 61.58; 36.59; 17.76.



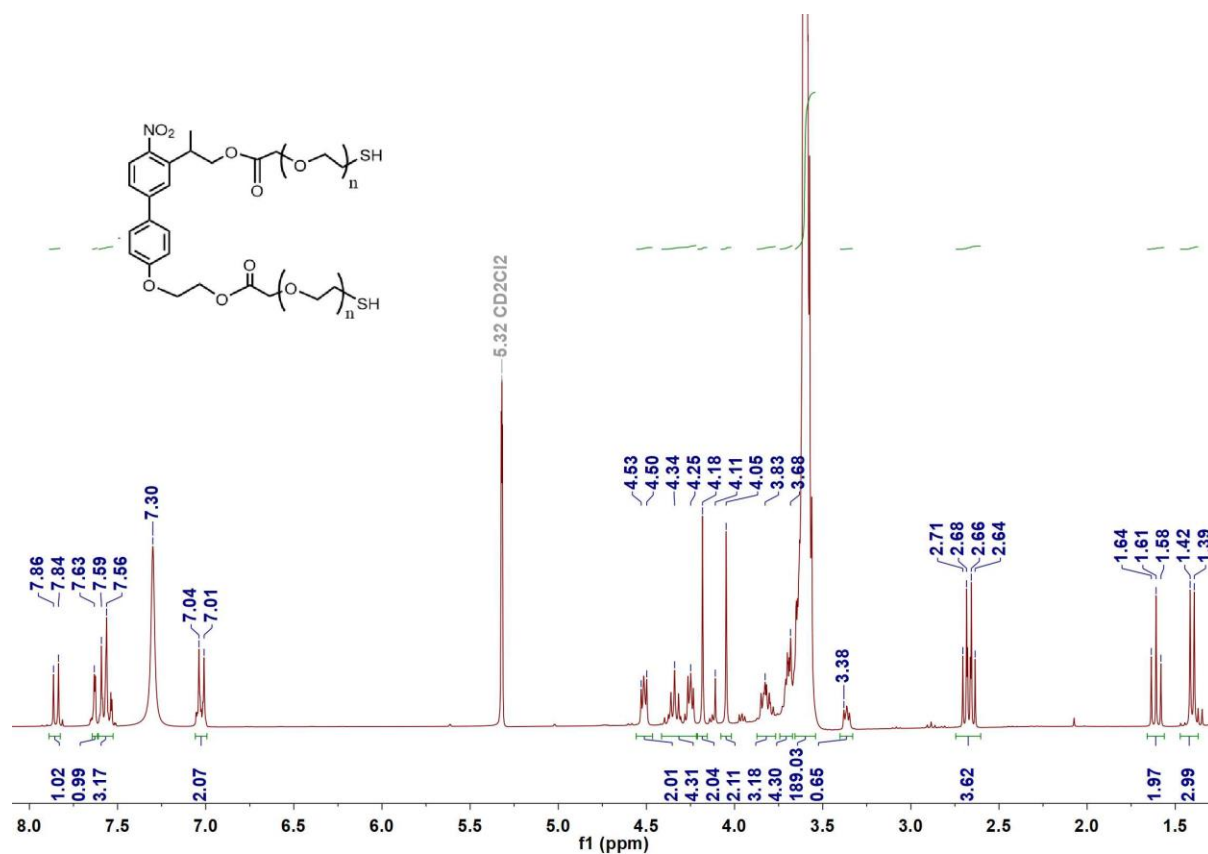
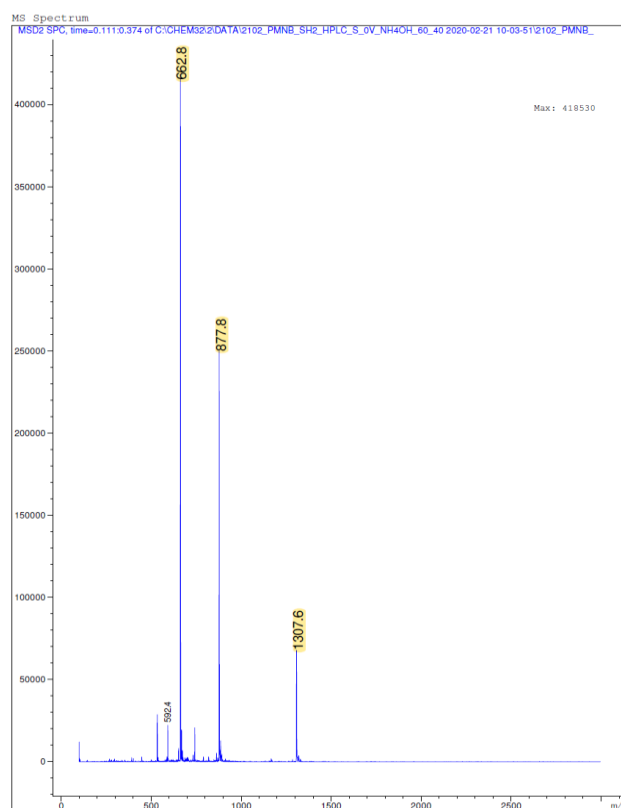
(6) PMNB(E-PEG_n-SH)₂

2-(4'-(2-hydroxyethoxy)-4-nitro-[1,1'-biphenyl]-3-yl)propan-1-ol (**5**) (1 eq., 0.032 mmol, 10 mg), 1 kDa COOH-PEG_n-SH (20 eq., 0.63 mmol, 0.63 g), p-TsOH (0.2 eq., 6 μmol, 1.2 mg), and DTT (0.5 eq., 16 μmol, 2.5 mg) were dissolved in 2.5 mL toluene under nitrogen stream. The mixture was heated at 80°C overnight under inert atmosphere. Toluene was removed under reduced pressure. The crude product was purified by prep HPLC (method: 20 B to 95 B, 360 nm, r.t.= 25 min) to obtain a pale yellow powder (57 mg, 70% yield) after freeze-drying.

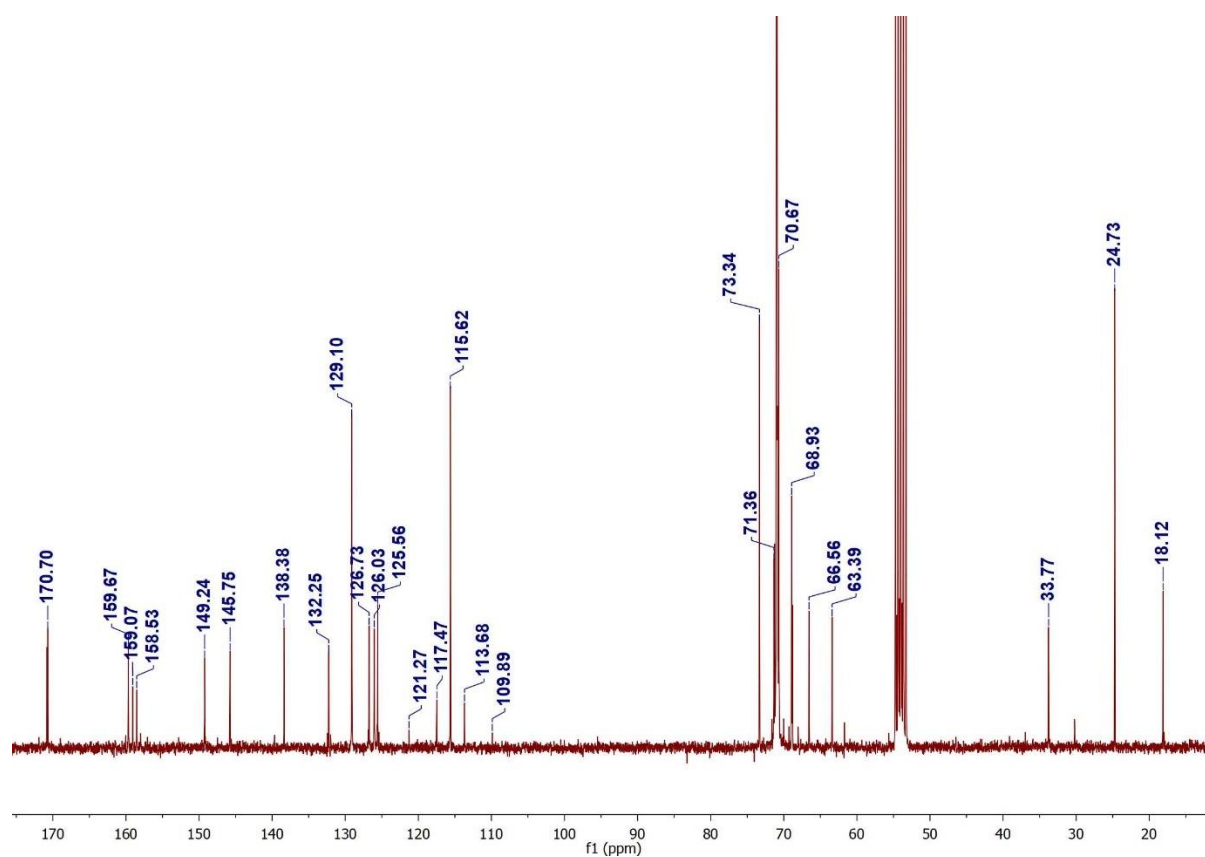
ESI-MS⁺: 662.4 (M+4NH₄)⁴, 877.2 (M+3NH₄)³, 1307.2 (M+2NH₄)².

¹H-NMR (300 MHz, CD₂Cl₂, δ [ppm]) = 7.84-7.86 (d, 1H, -CH Ar); 7.63 (d, 1H, -CH Ar); 7.56-7.59 (m, 3H, -CH Ar); 7.01-7.04 (d, 2H, -CH Ar); 4.50-4.53 (t, 2H, -CH₂); 4.31-4.36 (m, 2H, -CH₂); 4.23-4.27 (m, 2H, -CH₂); 4.18 (s, 2H, -CH₂CO); 4.05 (s, 2H, -CH₂CO); 3.58-3.68 (m, 193H, PEG chain and -CH); 2.68 (m, 4H, -CH₂S); 1.61 (t, 2H, -SH); 1.42 (d, 3H, -CH₃).

^{13}C -NMR (75 MHz, CD_2Cl_2 , δ [ppm]) = 170.70; 159.67; 159.07; 158.53; 149.24; 145.75; 138.38; 132.25; 129.10; 126.73; 126.03; 125.56; 121.27; 117.47; 115.62; 113.68; 109.89; 73.34; 71.36; 70.67; 68.93; 66.56; 63.39; 61.68; 33.77; 30.22; 24.73; 18.12.



Appendix



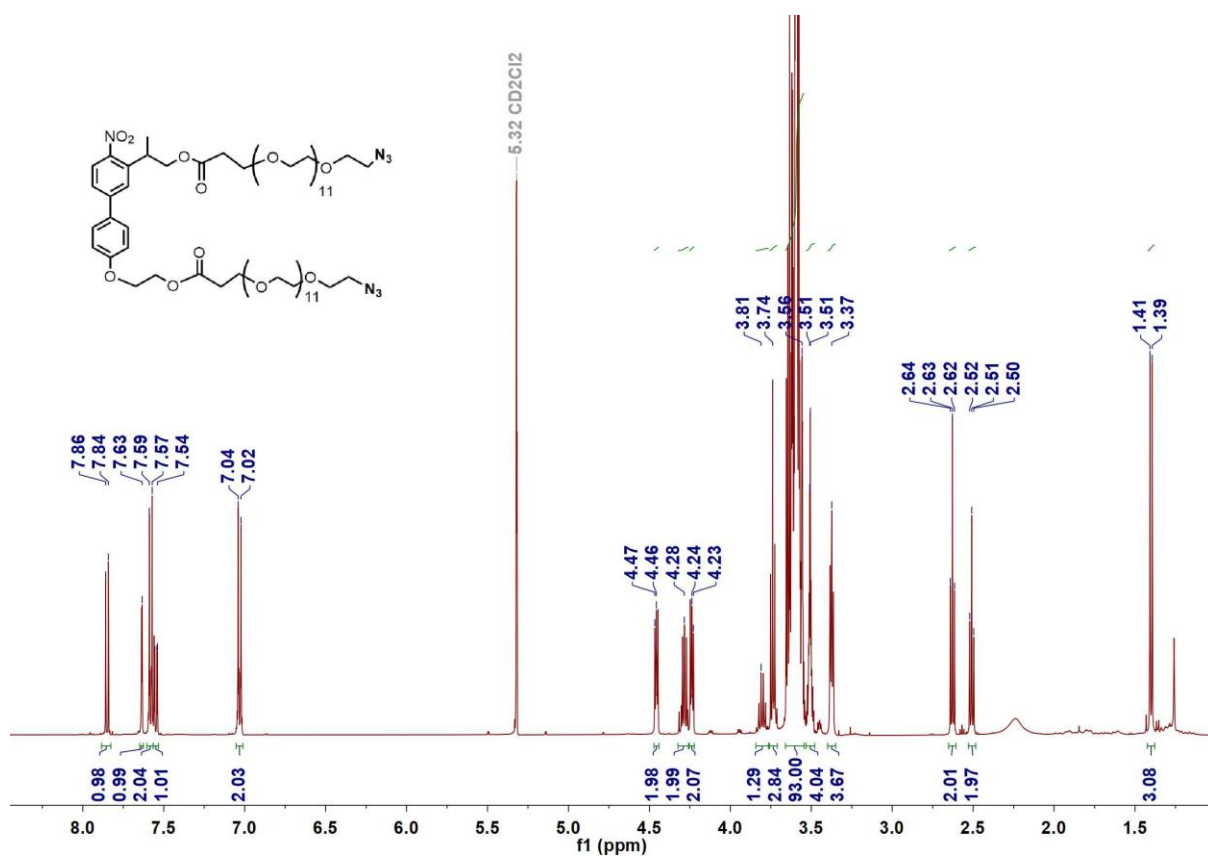
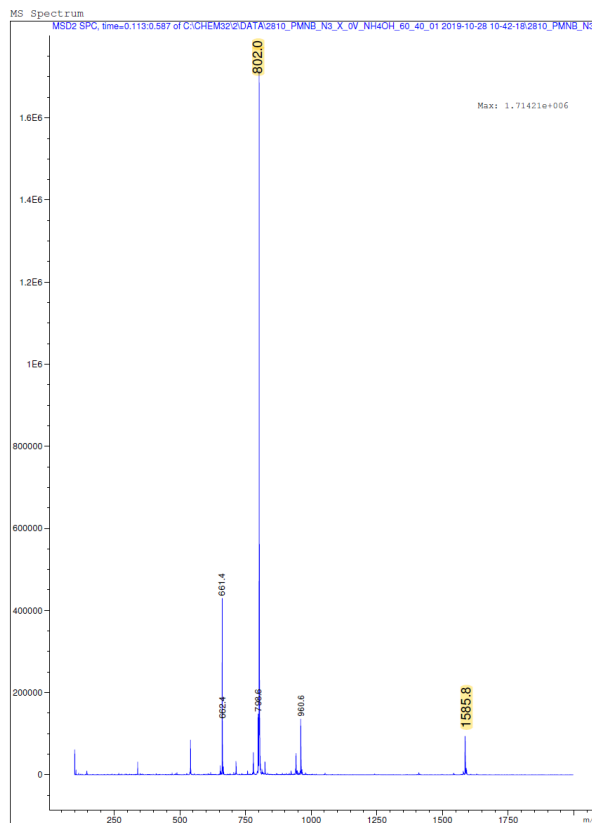
(7) *PMNB(E-EG₁₂-N₃)₂*

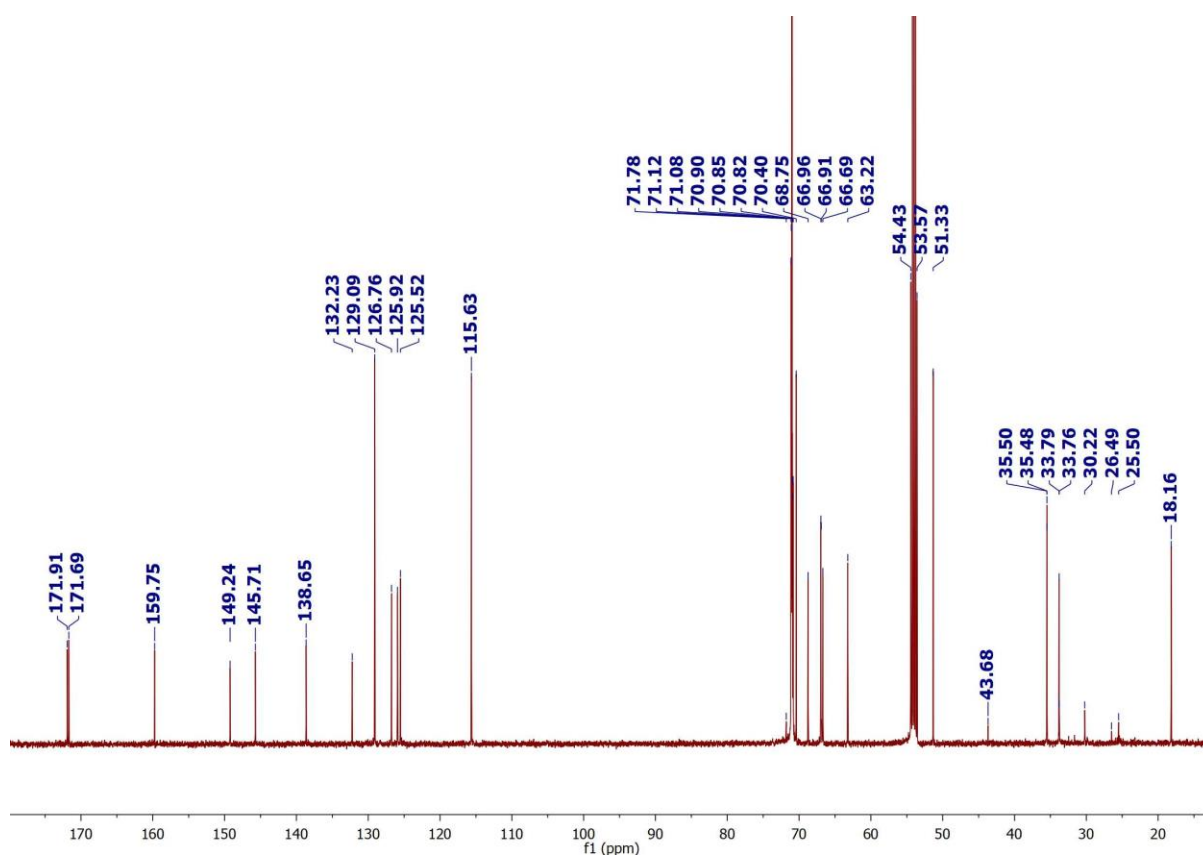
2-(4'-(2-hydroxyethoxy)-4-nitro-[1,1'-biphenyl]-3-yl)propan-1-ol (**5**) (1 eq., 0.032 mmol, 10 mg) was dissolved in 4 mL dry DCM under nitrogen atmosphere, and the following reagents were added in the specific order: COOH-PEG₁₂-N₃ (3 eq., 0.096 mmol, 61.8 mg), DCC (6 eq., 0.19 mmol, 39.6 mg) and DMAP (0.32 eq., 0.01 mmol, 1.25 mg). The mixture was stirred overnight under nitrogen atmosphere at room temperature. DCM was removed under nitrogen flow. The crude product was purified by prep HPLC (20 B to 95 B, 360 nm, rt = 29 min) to obtain a pale yellow oil (35 mg, 71% yield) after freeze-drying.

ESI-MS⁺: 802.0 (M+2NH₄)², 1585.8 (M+NH₄).

¹H-NMR (500 MHz, CD₂Cl₂, δ [ppm]) = 7.84-7.86 (d, 1H, -CH Ar); 7.64 (d, 1H, -CH Ar); 7.57-7.59 (d, 2H, -CH Ar); 7.54-7.56 (d, 1H, -CH Ar); 7.02-7.04 (d, 2H, -CH Ar); 4.46 (m, 2H, -CH₂O); 4.28 (m, 2H, -CH₂O); 4.24 (t, 2H, -CH₂O); 3.50-3.66 (m, 97H, PEG chain and -CH); 3.37 (t, 4H, -CH₂CO); 2.63 (t, 2H, -CH₂N₃); 2.51 (t, 2H, -CH₂N₃); 1.39-1.41 (d, 3H, -CH₃).

¹³C-NMR (125 MHz, CD₂Cl₂, δ [ppm]) = 171.91; 171.69; 159.75; 149.24; 145.71; 138.65; 132.22; 129.09; 126.76; 125.92; 125.52; 115.63; 71.78; 71.12; 71.08; 71.00; 70.98; 70.90; 70.85; 70.82; 70.40; 68.75; 66.96; 66.91; 66.69; 63.22; 51.33; 35.50; 35.48; 33.79; 33.76; 30.22; 26.49; 25.50; 18.16.

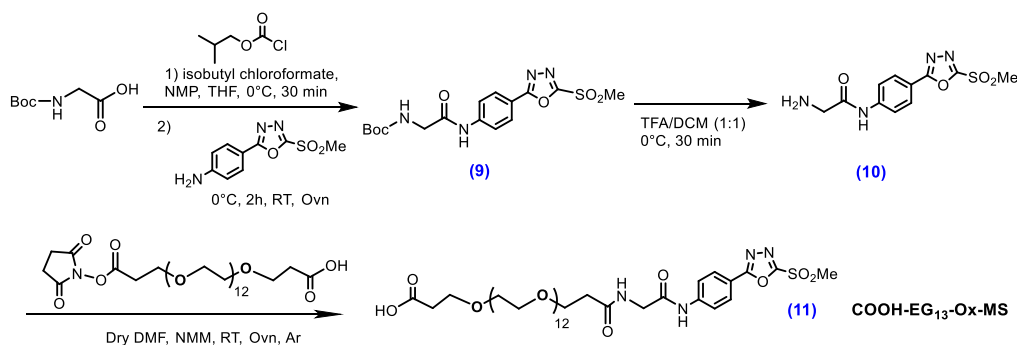




(8) $PMNB(E-EG_{13}-Ox-MS)_2$

2-(4'-(2-hydroxyethoxy)-4-nitro-[1,1'-biphenyl]-3-yl)propan-1-ol (**5**) (1 eq., 0.032 mmol, 10 mg) was dissolved in 4 mL dry DCM under nitrogen atmosphere, and the following reagents were added in the specific order: COOH-EG₁₃-Ox-MS (**11**) (3 eq., 0.096 mmol, 93 mg), DCC (6 eq., 0.19 mmol, 39.6 mg) and DMAP (0.32 eq., 0.01 mmol, 1.25 mg). The mixture was stirred overnight under nitrogen atmosphere at room temperature. DCM was removed under nitrogen flow. The crude product was purified by prep HPLC (20 B to 95 B, 360 nm, rt = 27 min) to obtain a pale yellow oil (14 mg, 20% yield) after freeze-drying.

ESI-MS⁺: 1127.5 (M+2NH₄)².



Compounds **9-10** were synthesized according to previously reported protocols,² as detailed in following sections.

(9) Tert-butyl (2-((4-(5-(methylsulfonyl)-1,3,4-oxadiazol-2-yl)phenyl)amino)-2-oxoethyl) carbamate

Boc-Gly-OH (1 eq., 16.7 mmol, 2.93 g) was dissolved in 50 mL dry THF/DMF (1:1) at 0 °C and purged with nitrogen for 5 min, and isobutyl chloroformate (1.25 eq., 22 mmol, 2.74 mL) was added to the solution. After 5 min of stirring, NMM (2.5 eq., 41.7 mmol, 4.6 mL) was added dropwise. The suspension was stirred for 30 minutes. A solution of 4-(5-(methylsulfonyl)-1,3,4-oxadiazol-2-yl)aniline (0.25 eq., 4.2 mmol, 1 g) in 13 mL dry THF/DMF (1:1) was added dropwise to the mixture and stirred for additional 2 h at 0 °C, then overnight at room temperature. Saturated NaHCO₃ (100 mL) was added and the reaction mixture was extracted with ethyl acetate (2 x 100 mL). The combined organic phase was washed with brine; dried over Na₂SO₄; evaporated and the crude product was purified by silica gel column chromatography (50% ethyl acetate/n-hexane) to obtain final product (4.83 g, 73% yield). The spectroscopic characterization data matched the values reported on the literature.

ESI-MS⁺: 419.0 (M+Na); 815.2 (2M+Na)².

¹H-NMR (300 MHz, CD₂Cl₂, δ [ppm]): 9.62 (s, 1H, -NH amide); 8.10 (pseudo-d, 2H, -CH Ar); 7.92 (pseudo-d, 2H, -CH Ar); 6.32 (t, 1H, -NH amide); 3.95 (d, 2H, -CH₂); 3.63 (s, 3H, -SO₂Me); 1.43 (s, 9H, -C(CH₃)₃).

¹³C-NMR (75 MHz, CD₂Cl₂, δ [ppm]) = 169.58; 166.93; 163.08; 156.98; 144.12; 129.35; 120.21; 117.99; 79.45; 45.31; 43.48; 28.53.

(10) 1.2.9 2-amino-N-(4-(5-(methylsulfonyl)-1,3,4-oxadiazol-2-yl)phenyl)acetamide

Tert-butyl (2-((4-(5-(methylsulfonyl)-1,3,4-oxadiazol-2-yl)phenyl)amino)-2-oxoethyl) carbamate (**9**) (300 mg) was dissolved in 4 mL TFA/dry DCM (1:1) at 0 °C under nitrogen atmosphere, then stirred at room temperature for 30 min. The reaction was followed by TLC (EtOAc) every 10 min. TFA and DCM were removed by nitrogen flow. The crude was purified with preparative HPLC (5B to 95B, 280 nm, rt = 18 min) to obtain a white solid (150 mg, 67% yield). The product was immediately coupled to the COOH-PEG_n-NHS polymer. The spectroscopic characterization data matched the values reported on the literature.

ESI-MS⁺: 297.1 (M+H), 593.2 (2M+H), 615.2 (2M+Na).

¹H-NMR (300 MHz, CD₂Cl₂, δ [ppm]) = 8.11 (d, 2H, -CH Ar); 7.93 (d, 2H, -CH Ar); 4.90 (s, 2H, -CH₂); 3.64 (s, 3H, -SO₂Me).

¹³C-NMR (75 MHz, CD₂Cl₂, δ [ppm]) = 166.86; 164.24; 163.15; 143.77; 129.31; 120.48; 118.48; 51.16; 43.52.

(11) COOH-EG₁₃-Ox-MS

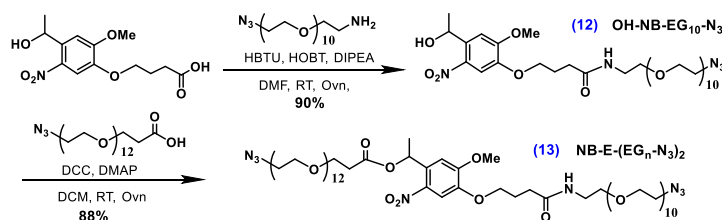
2-amino-N-(4-(5-(methylsulfonyl)-1,3,4-oxadiazol-2-yl)phenyl)acetamide (**2**) (3 eq., 0.5 mmol, 150 mg) was dissolved in dry DMF (15 mL) and NMM (30 eq., 5 mmol, 0.55 mL) was added. The solution was purged with nitrogen for 15 min. Linear COOH-PEG₁₃-NHS polymer (1 eq., 0.17 mmol, 126 mg) was dissolved in dry DMF (4 mL) and added to the mixture under nitrogen atmosphere. The reaction was allowed to proceed overnight at room temperature. The crude was purified with preparative HPLC (5B to 95B, 280 nm, rt = 24 min) to obtain a pale yellow solid (85 mg, 52% yield).

Appendix

ESI-MS⁺: 679.2 (M+NH₄)², 1341.4 (M+NH₄).

¹H-NMR (300 MHz, CD₂Cl₂, δ [ppm]) = 10.41 (s, -COOH); 9.19 (s, -NH); 8.05 (d, -CH Ar); 7.87 (d, -CH Ar); 6.25 (s, -NH); 4.22 (s, -OCH₂CO); 4.05 (d, -CH₂CO); 3.5-3.8 (m, PEG chain); 3.49 (s, -SO₂Me).

5.2.2 Synthesis of control crosslinker



(12) OH-NB-EG₁₀-N₃

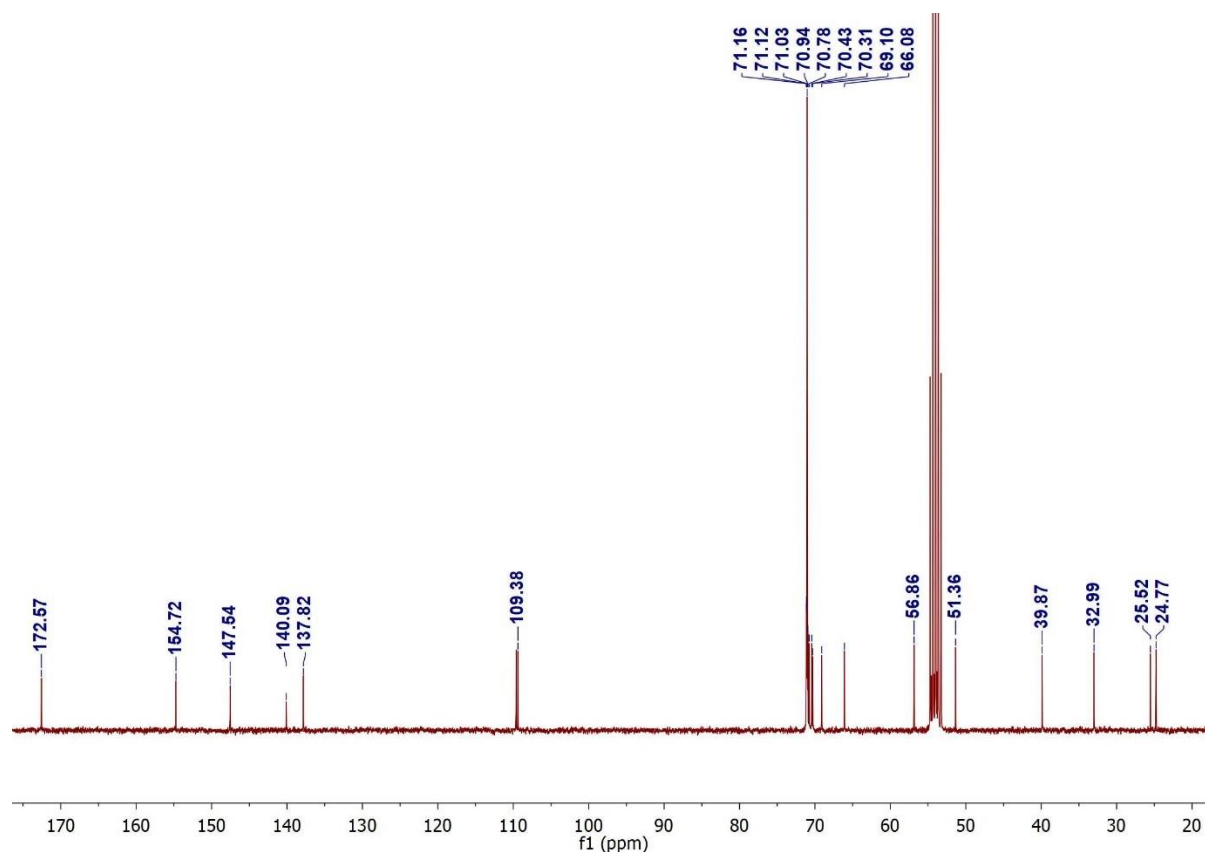
4-(4-(1-hydroxyethyl)-2-methoxy-5-nitrophenoxy)butanoic acid (1 eq., 0.17 mmol, 50 mg) was dissolved in dry DMF (1 mL) and purged with argon. The coupling mixture HBTU (1.2 eq., 0.2 mmol, 77 mg), HOBT (1.2 eq., 0.2 mmol, 28 mg), and DIPEA (5 eq., 0.85 mmol, 110 mg) was added and stirred for 5 min, then N₃-PEG₁₀-amine (1.5 eq., 0.25 mmol, 132 mg) in DMF (0.7 mL) was added. The reaction mixture was stirred at room temperature overnight, and purified by preparative HPLC (method: 20 B to 95 B, 360 nm, r.t.= 19 min) to obtain a pale yellow powder (120 mg, 90% yield) after freeze-drying.

ESI-MS⁺: 808.4 (M+H). 825.4 (M+NH₄).

¹H-NMR (300 MHz, CD₂Cl₂, δ [ppm]) = 7.54 (s, 1H, -CH Ar); 7.32 (s, 1H, -CH Ar); 6.30 (s, 1H, -NH); 5.47-5.53 (m, 1H, -CH); 4.05-4.09 (t, 2H, -CH₂ OAr); 3.96 (s, 3H, -OCH₃); 3.56-3.66 (m, 38H, PEG chain and -CH₂); 3.50-3.53 (m, 2H, -OCH₂); 3.36-3.43 (m, 4H, -COCH₂ and -CH₂); 2.35-2.40 (m, 2H, -CH₂); 2.07-2.16 (m, 2H, -CH₂N₃); 1.49-1.52 (d, 3H, -CH₃).

¹³C-NMR (75 MHz, CD₂Cl₂, δ [ppm]) = 172.57; 154.72; 147.54; 140.09; 137.82; 109.62; 109.38; 71.16; 71.12; 71.03; 70.94; 70.78; 70.43; 70.31; 69.10; 66.08; 56.86; 51.36; 39.87; 32.99; 25.52; 24.77.

Appendix



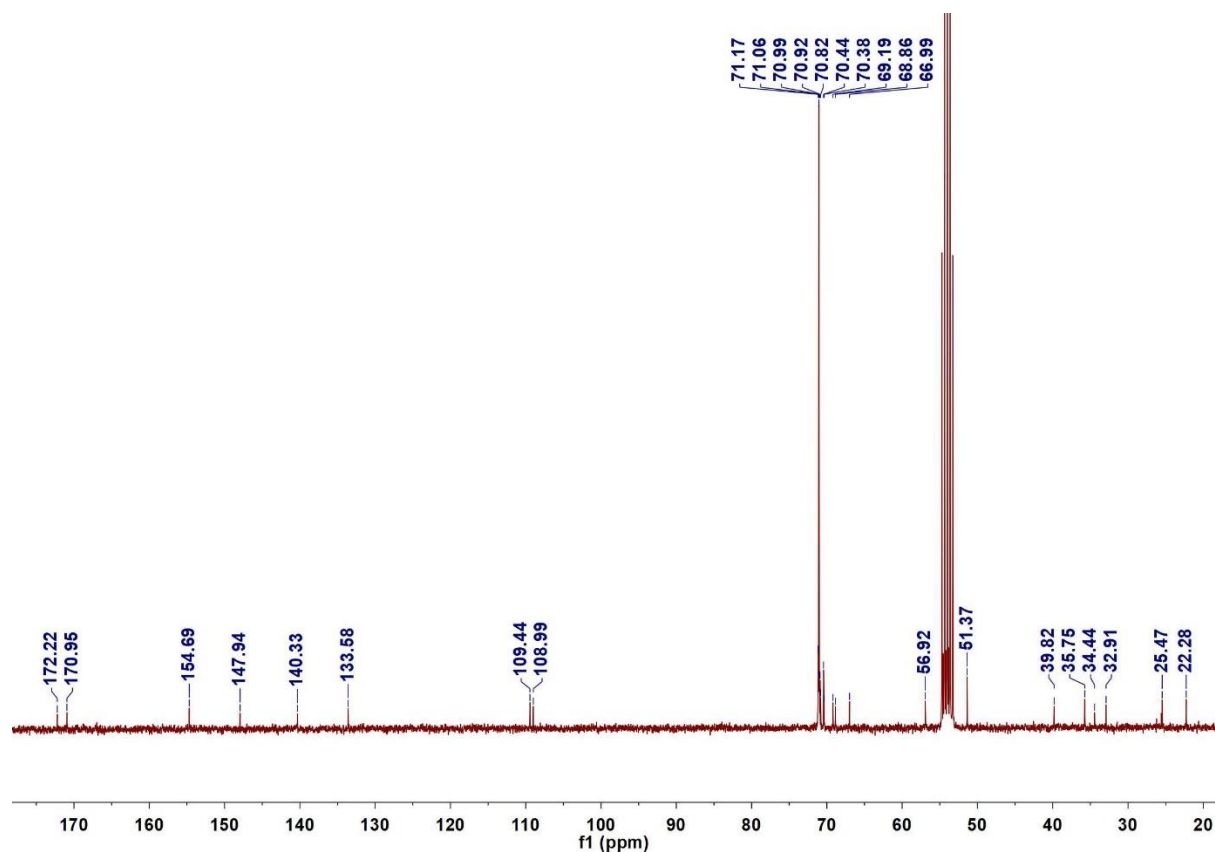
(13) NB-E-(EG_n-N₃)₂

OH-NB-EG₁₀-N₃ (**12**) (1 eq., 0.06 mmol, 50 mg) was dissolved in dry DCM (6 mL) under nitrogen atmosphere, and the following reagents were added in the specific order: COOH-PEG₁₂-N₃ (1.5 eq., 0.09 mmol, 60 mg), DCC (3 eq., 0.19 mmol, 39.6 mg) and DMAP (0.16 eq., 0.01 mmol, 1.25 mg). The mixture was stirred overnight under nitrogen atmosphere at room temperature. DCM was removed under nitrogen flow. The crude product was purified by prep HPLC (method: 20 B to 95 B, 360 nm, r.t. = 19 min) to obtain a pale yellow oil (85 mg, 88 % yield) after freeze-drying.

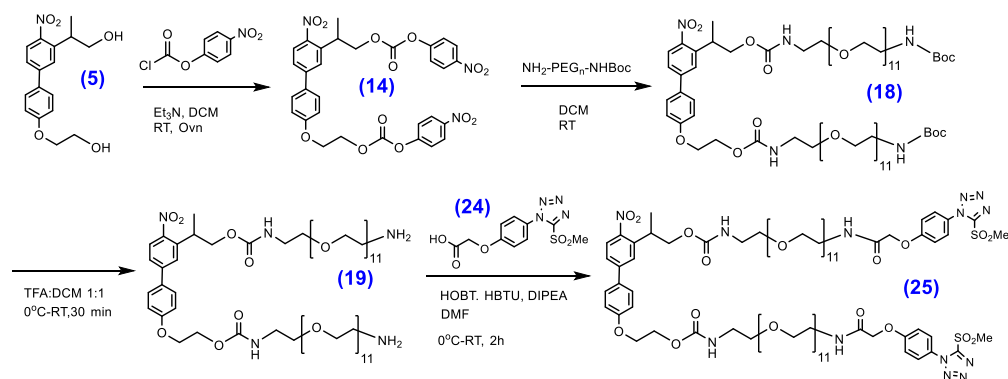
ESI-MS⁺: 734.3 (M+2NH₄)²

¹H-NMR (300 MHz, CD₂Cl₂, δ [ppm]) = 7.56 (s, 1H, -CH Ar); 7.04(s, 1H, -CH Ar); 6.38-6.44 (m, 1H, -CH); 6.30 (s, 1H, -NH); 4.06-4.10 (t, 2H, -CH₂ OAr); 3.94 (s, 3H, -OCH₃); 3.69-3.75 (m, 2H, -CH₂); 3.51-3.67 (m, 84H, PEG chain and -CH₂); 3.33-3.43 (m, 6H, -COCH₂ and -CH₂); 2.56-2.64 (m, 2H, -CH₂N₃); 2.34-2.38 (m, 2H, -CH₂); 2.07-2.16 (m, 2H, -CH₂N₃); 1.59-1.61 (d, 3H, -CH₃).

¹³C-NMR (75 MHz, CD₂Cl₂, δ [ppm]) = 172.22; 170.95; 154.69; 147.94; 140.33; 133.58; 109.44; 108.99; 71.17; 71.06; 70.99; 70.92; 70.82; 70.44; 70.38; 69.19; 69.94; 68.86; 66.99; 56.92; 51.37; 39.82; 35.75; 34.44; 32.91; 25.47; 22.28.



5.2.3 Synthesis of PMNB carbamate crosslinker



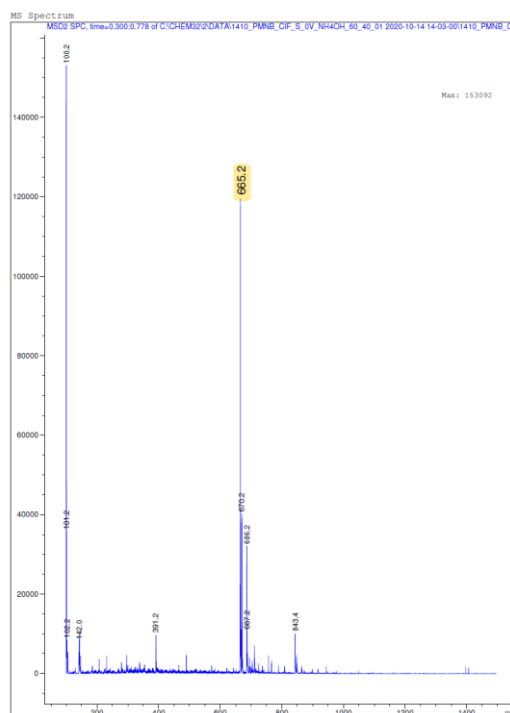
(14) 2-(4-nitro-4'-((2-(((4-nitrophenoxy)carbonyloxy)ethoxy)-[1,1'-biphenyl]-3-yl)propyl (4-nitrophenyl) carbonate

2-(4'-((2-hydroxyethoxy)-4-nitro-1,1'-biphenyl-3-yl)propan-1-ol (**5**) (1 eq., 0.137mmol, 43.6 mg) was dissolved in dry DCM (4.4 mL) at 0°C and purged with nitrogen for 5 min. In the following order, 4-nitrophenyl chloroformate (3 eq., 0.412 mmol, 82.9 mg) and EtN₃ were added to the above solution at 0°C. The reaction was stirred at room temperature for overnight. The solvents were removed under nitrogen steam to give a yellow slurry which was directly purified by prep HPLC (method: 20 B to 95

B, 360 nm, r.t. = 25 min) to obtain a pale yellow powder (54.5 mg, 83% yield) after freeze-drying. Notably, TFA was removed from solvent A and B for HPLC purification.

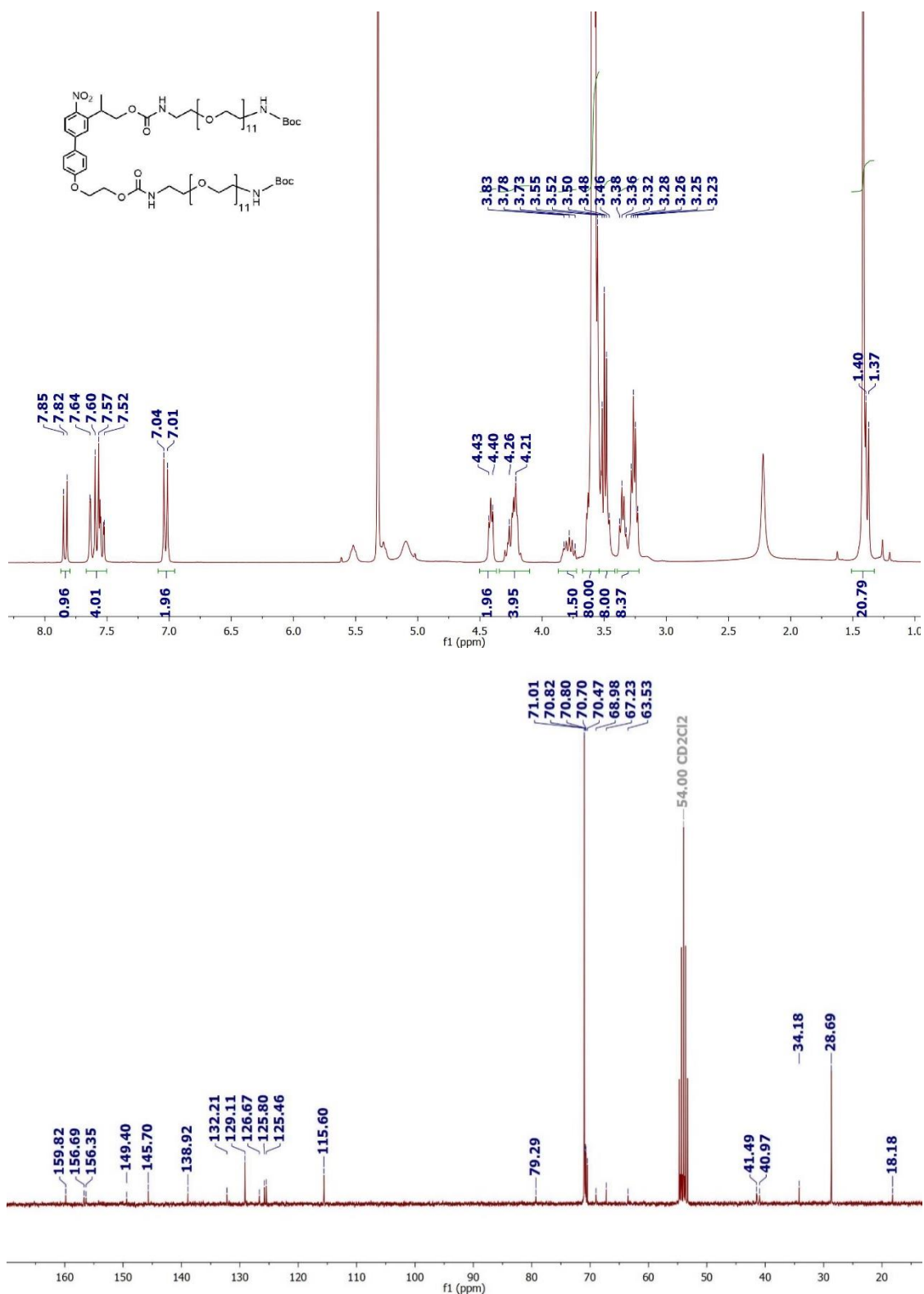
ESI-MS⁺: 665.2 (M+NH₄)

¹H-NMR (300 MHz, CDCl₃, δ [ppm]) = 8.28-8.31 (d, 2H, -CH Ar); 8.22-8.25 (d, 2H, -CH Ar); 7.92-7.95 (d, 1H, -CH Ar); 7.63 (d, 1H, -CH Ar); 7.55-7.58 (m, 3H, -CH Ar); 7.39-7.42 (d, 2H, -CH Ar); 7.28-7.31 (d, 2H, -CH Ar); 7.05-7.08 (d, 2H, -CH Ar); 4.67-4.70 (m, 2H, -CH₂O); 4.45-4.60 (m, 2H, -CH₂O); 4.34-4.37 (m, 2H, -CH₂O); 3.96-4.02 (m, 1H, -CH); 1.48-1.50 (d, 3H, -CH₃).



$^1\text{H-NMR}$ (300 MHz, CD_2Cl_2 , δ [ppm]) = 7.82-7.85 (d, 1H, -CH Ar); 7.52-7.64 (m, 4H, -CH Ar); 7.01-7.04 (d, 2H, -CH Ar); 4.40-4.43 (m, 2H, $-\text{CH}_2\text{O}$); 4.21-4.26 (m, 4H, $-\text{CH}_2\text{O}$); 3.73-3.83 (m, 1H, -CH); 3.46-3.64 (m, 88H, PEG chain); 3.23-3.38 (m, 8H, $-\text{CH}_2$); 1.42 (s, 18H, $-\text{C}(\text{CH}_3)_3$); 1.37-1.40 (d, 3H, $-\text{CH}_3$).

$^{13}\text{C-NMR}$ (75 MHz, CD_2Cl_2 , δ [ppm]) = 159.82; 156.69; 156.35; 149.40; 145.70; 138.92; 132.21; 129.11; 126.67; 125.8; 125.46; 115.60; 79.29; 71.01; 70.82; 70.80; 70.70; 70.47; 68.98; 67.23; 63.53; 41.49; 40.97; 34.18; 28.69; 18.18.



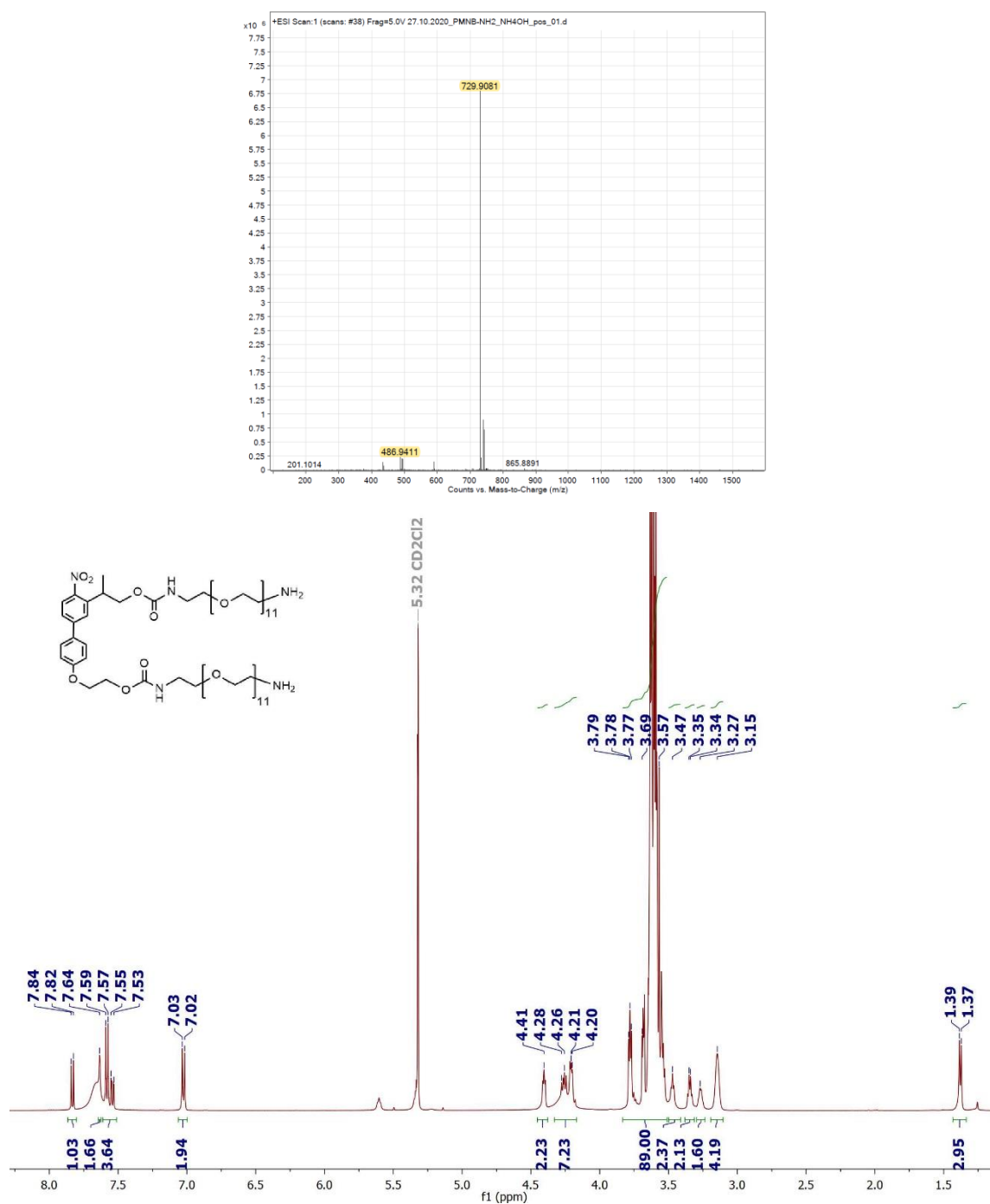
Appendix

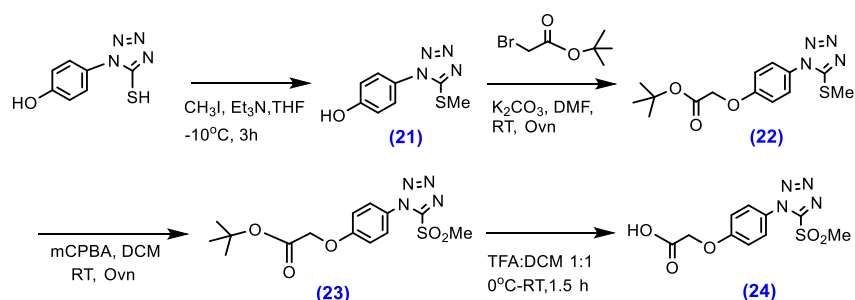
(19) PMNB(C-EG₁₁-NH₂)₂

PMNB(C-EG₁₁-NHBoc)₂ (**18**) (28 mg) was dissolved in 0.1 mL TFA/dry DCM (1:1) at 0 °C under nitrogen atmosphere, then stirred at room temperature for 30 min. TFA and DCM were removed by nitrogen flow. The crude was purified with preparative HPLC (5B to 95B, 280 nm, rt = 25 min) to obtain a pale yellow oil (14.8 mg, 60% yield).

ESI-MS⁺: 729.9 (M+2H)²⁺; 486.9 (M+3H)³⁺.

¹H-NMR (300 MHz, CD₂Cl₂, δ [ppm]) = 7.82-7.84 (d, 1H, -CH Ar); 7.53-7.64 (m, 4H, -CH Ar); 7.02-7.03 7.04 (d, 2H, -CH Ar); 4.28-4.41 (m, 2H, -CH₂O); 4.20-4.26 (m, 4H, -CH₂O); 3.57-3.79 (m, 89H, PEG chain and -CH); 3.15-3.35 (m, 8H, -CH₂); 1.37-1.39 (d, 3H, -CH₃).





Compounds **21** were synthesized according to previously reported protocols,³ as detailed in following sections.

(21) 4-(5-(methylthio)-1H-tetrazol-1-yl)phenol

4-(5-mercapto-1H-tetrazol-1-yl)phenol (1 eq., 5.13 mmol, 1 g) was dissolved in dry THF (22 mL) and cooled down to -10°C using a bath of dry ice in acetone. The following reagents were added: Et_3N (1.2 eq., 6.16 mmol, 0.86 mL) and CH_3I (1 eq., 5.13 mmol, 0.32 mL). The reaction was stirred for 3 h at -10°C , then quenched with 1 M HCl and allowed to reach room temperature. The organic phase was extracted with ethyl acetate; washed with brine; dried over MgSO_4 ; evaporated and the crude product was purified by silica gel column chromatography (45% ethyl acetate/n-hexane) to obtain a white solid (0.79 g, 74% yield). The spectroscopic characterization data matched the values reported on the literature.

ESI-MS⁺: 209.0 (M+H); 439.2 (2M+Na).

¹H-NMR (300 MHz, acetone- d_6 , δ [ppm]): 9.13 (s, 1H, -OH); 7.46 (d, 2H, -CH Ar); 7.08 (d, 2H, -CH Ar); 2.79 (s, 3H, -SMe).

¹³C-NMR (125 MHz, acetone- d_6 , δ [ppm]) = 160.00; 155.97; 126.97; 126.27; 117.12; 15.29.

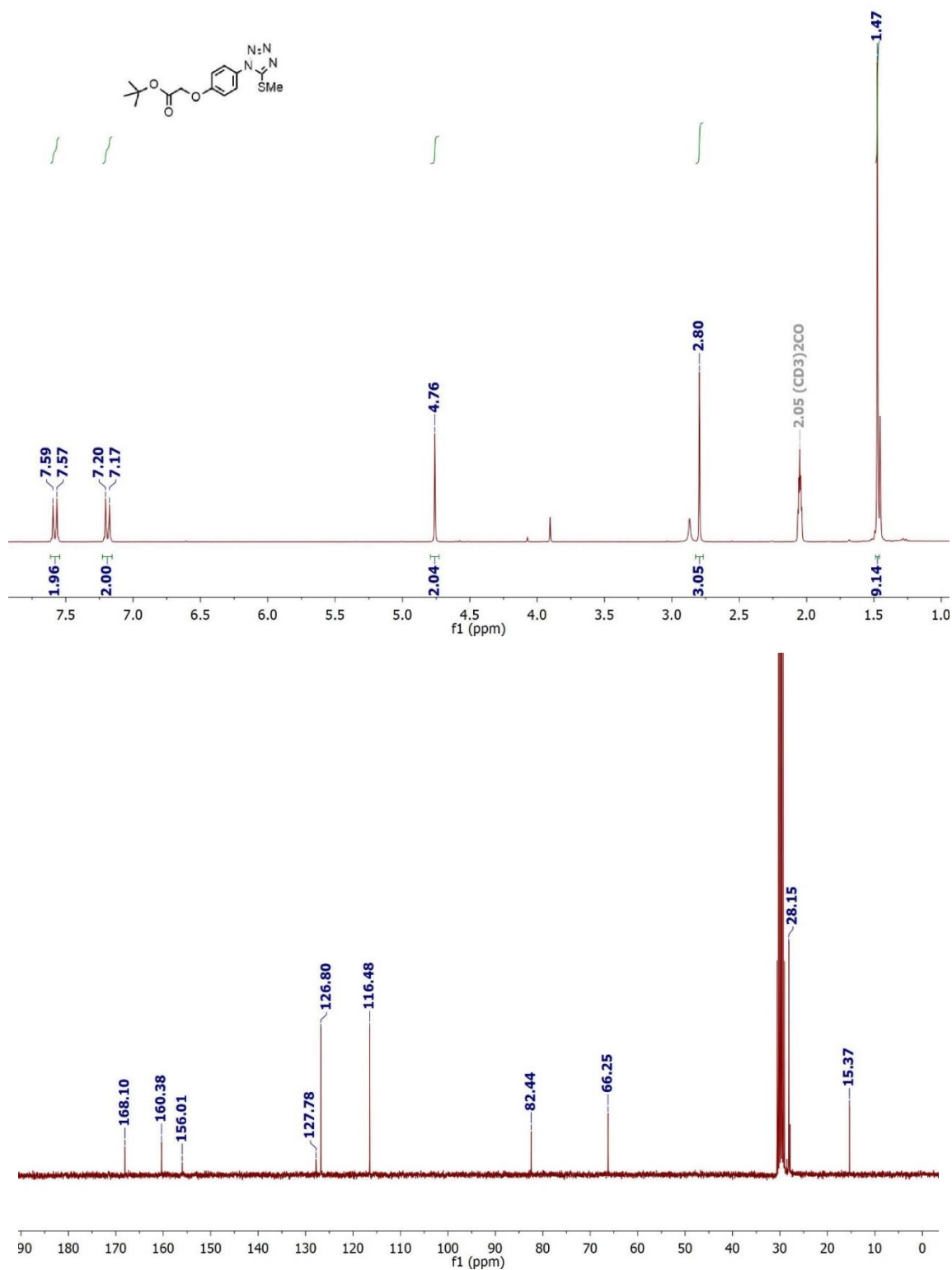
(22) Tert-butyl 2-(4-(5-(methylthio)-1H-tetrazol-1-yl)phenoxy)acetate

4-(5-(methylthio)-1H-tetrazol-1-yl)phenol (**21**) (1 eq., 0.38 mmol, 80 mg) was dissolved in dry DMF (2.5 mL), followed by addition of tert-butyl bromoacetate (2.2 eq., 0.84 mmol, 165 mg) and K_2CO_3 (5 eq., 1.9 mmol, 265 mg) under nitrogen atmosphere. The mixture was stirred overnight at room temperature. Reaction completion was confirmed by TLC. The mixture was extracted with ethyl acetate; washed with brine; dried over MgSO_4 ; evaporated and the crude product was obtained as a white powder (111.5 mg, 85% purity, 90% yield).

¹H-NMR (300 MHz, acetone- d_6 , δ [ppm]): 7.57-7.59 (d, 2H, -CH Ar); 7.17-7.20 (d, 2H, -CH Ar); 4.76 (s, 2H, -CH₂); 2.80 (s, 3H, -SMe); 1.42 (s, 9H, -C(CH₃)₃).

¹³C-NMR (75 MHz, acetone- d_6 , δ [ppm]) = 168.10; 160.38; 156.01; 127.78; 126.80; 116.48; 82.44; 66.25; 28.15; 15.37.

Appendix



(23) *Tert-butyl 2-(4-(5-(methylsulfonyl)-1H-tetrazol-1-yl)phenoxy)acetate*

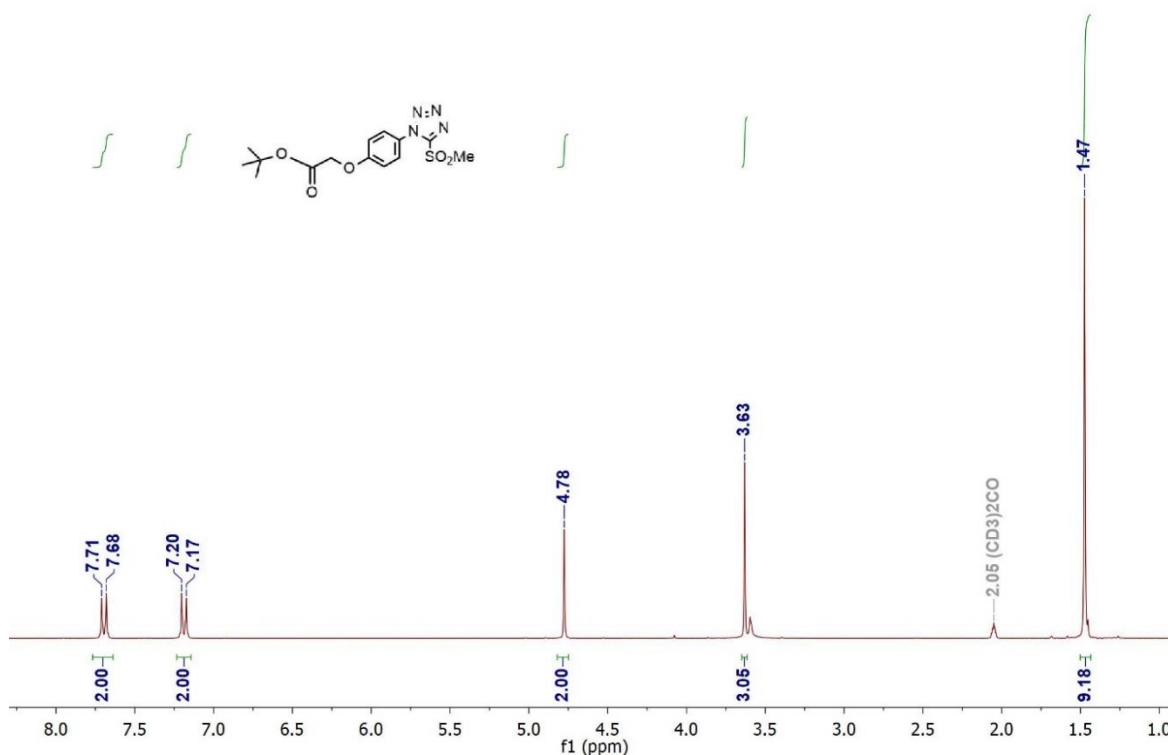
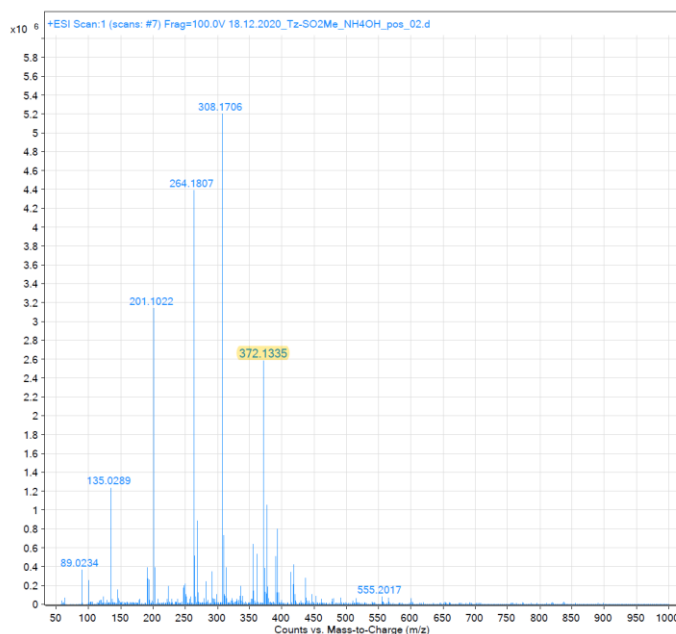
Tert-butyl 2-(4-(5-(methylthio)-1H-tetrazol-1-yl)phenoxy)acetate (**22**) (1 eq., 0.33 mmol, 106 mg) was dissolved in dry DCM (7.8 mL) and cooled down to 0°C, followed by addition of mCPBA (5 eq., 1.65 mmol, 320 mg). The mixture was stirred overnight at room temperature. Reaction completion was confirmed by mass analysis and ¹H-NMR since the similar elution were observed for starting reactant and product in TLC and analytical HPLC. The reaction mixture was then filtered, evaporated and

purified with preparative HPLC (20B to 95B, 280 nm, rt = 24 min) to obtain a pale pink powder (111.9 mg, 96% yield).

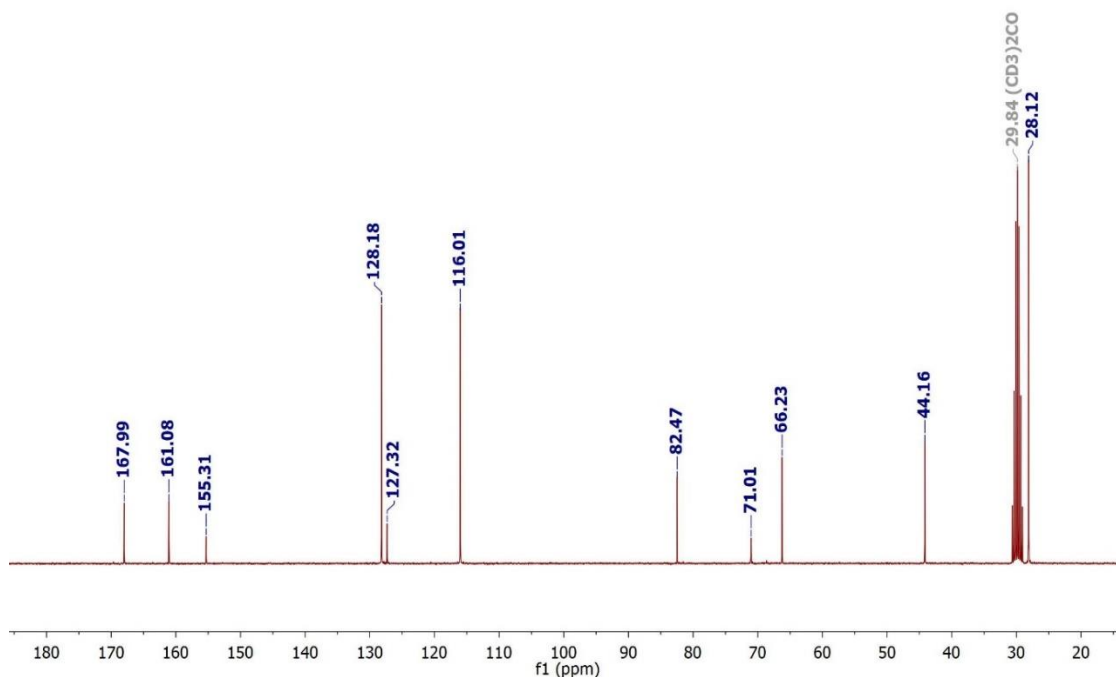
ESI-MS⁺: 372.1 (M+NH₄).

¹H-NMR (300 MHz, acetone-d₆, δ [ppm]): 7.68-7.71 (d, 2H, -CH Ar); 7.17-7.20 (d, 2H, -CH Ar); 4.78 (s, 2H, -CH₂); 3.63 (s, 3H, -SO₂Me); 1.47 (s, 9H, -C(CH₃)₃).

¹³C-NMR (75 MHz, acetone-d₆, δ [ppm]) = 167.99; 161.08; 155.31; 128.18; 127.32; 116.01; 82.47; 71.01; 66.23; 44.16; 28.12.



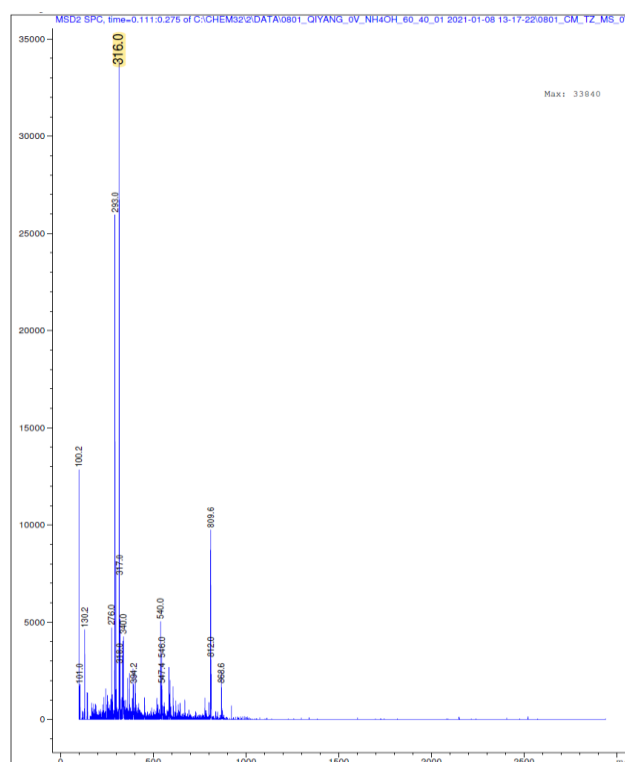
Appendix



(24) 2-(4-(5-(methylsulfonyl)-1H-tetrazol-1-yl)phenoxy)acetic acid

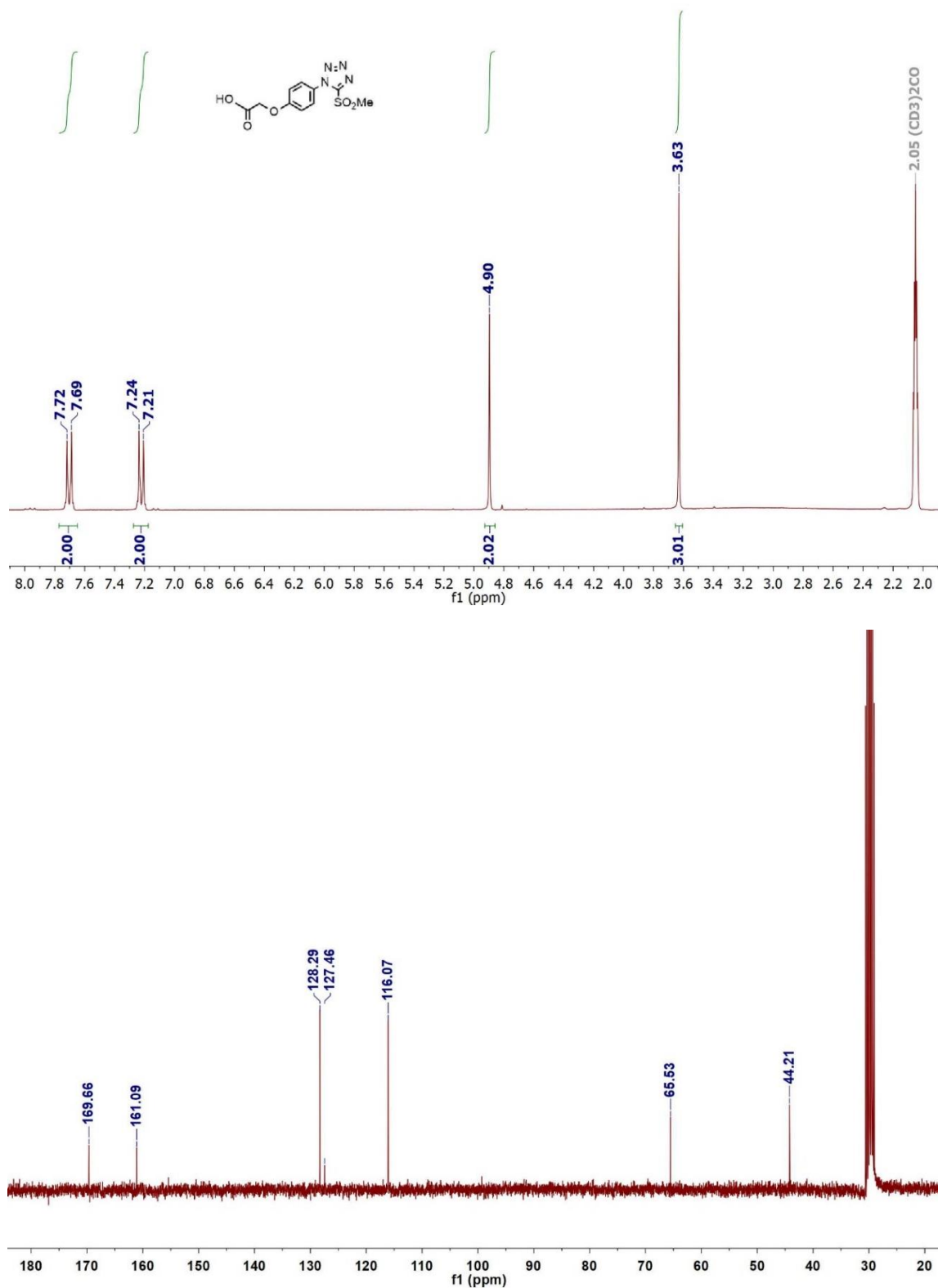
Tert-butyl 2-(4-(5-(methylsulfonyl)-1H-tetrazol-1-yl)phenoxy)acetate (**23**) (30 mg) was dissolved in 0.6 mL TFA/dry DCM (1:1) at 0 °C under nitrogen atmosphere, then stirred at room temperature for 1.5 h. Reaction completion was confirmed by TLC. TFA and DCM were removed by nitrogen flow. The crude was purified with preparative HPLC (5B to 95B, 280 nm, rt = 22 min) to obtain a pale yellow oil (15.2 mg, 60% yield).

ESI-MS⁺: 316.0 (M+NH₄).



$^1\text{H-NMR}$ (300 MHz, acetone- d_6 , δ [ppm]): 7.69-7.72 (d, 2H, -CH Ar); 7.21-7.24 (d, 2H, -CH Ar); 4.90 (s, 2H, -CH $_2$); 3.63 (s, 3H, -SO $_2$ Me).

$^{13}\text{C-NMR}$ (75 MHz, acetone- d_6 , δ [ppm]) = 169.66; 161.09; 128.29; 127.46; 116.07; 65.53; 44.21.



Appendix

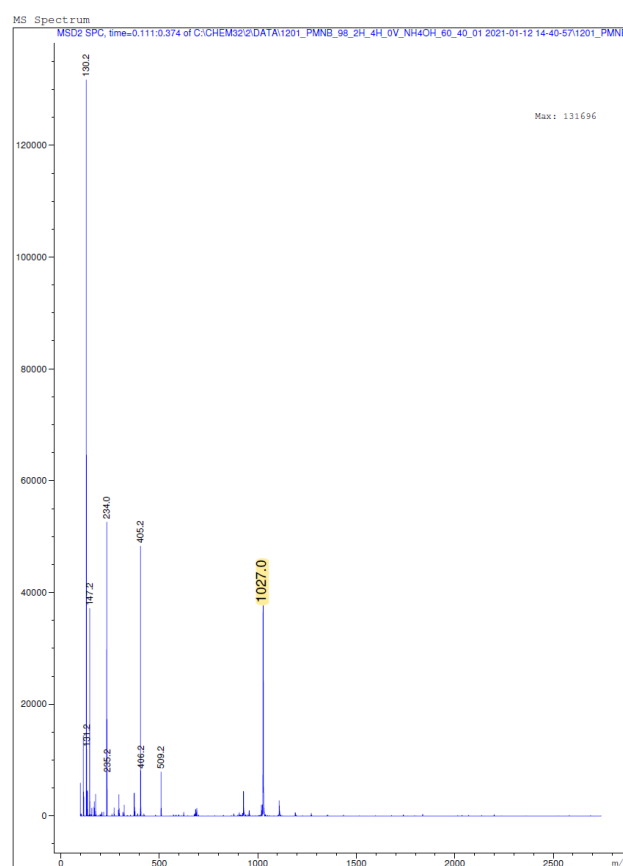
(25) PMNB(C-EG₁₁-Tz-MS)₂

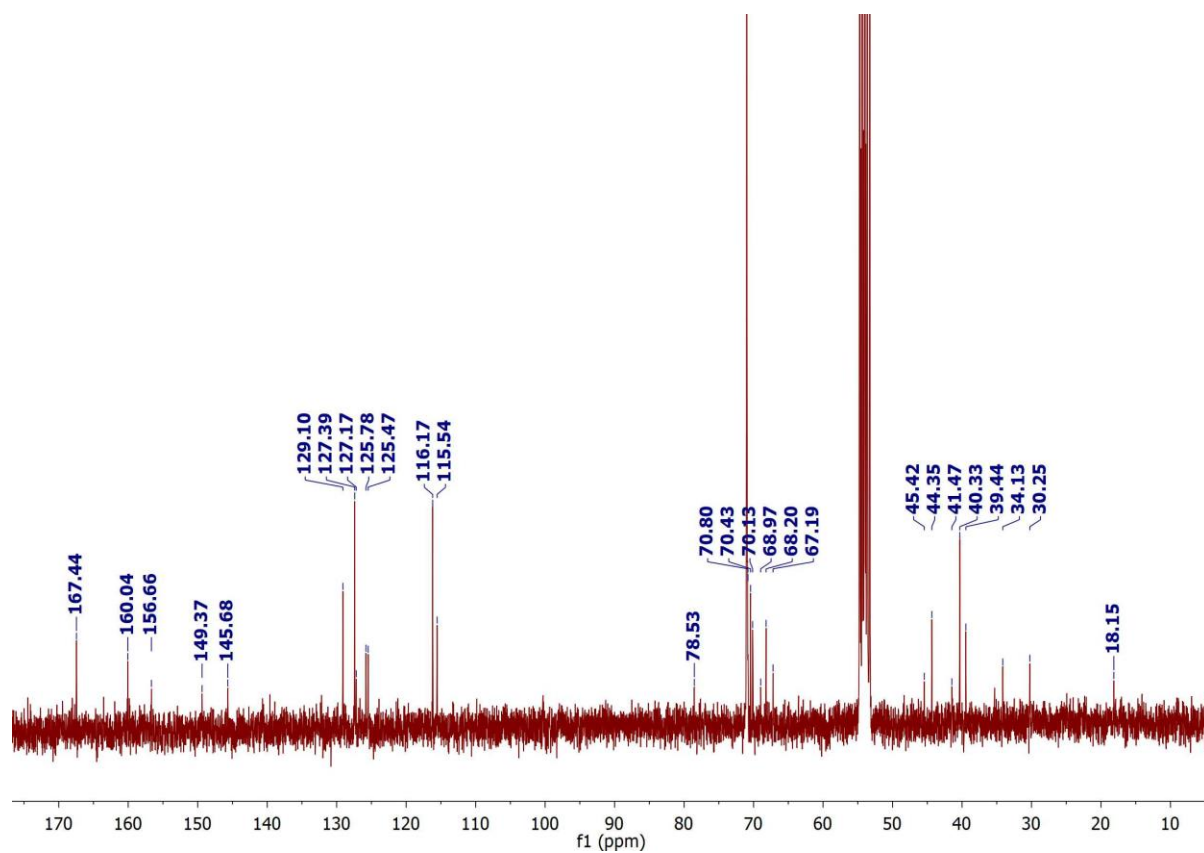
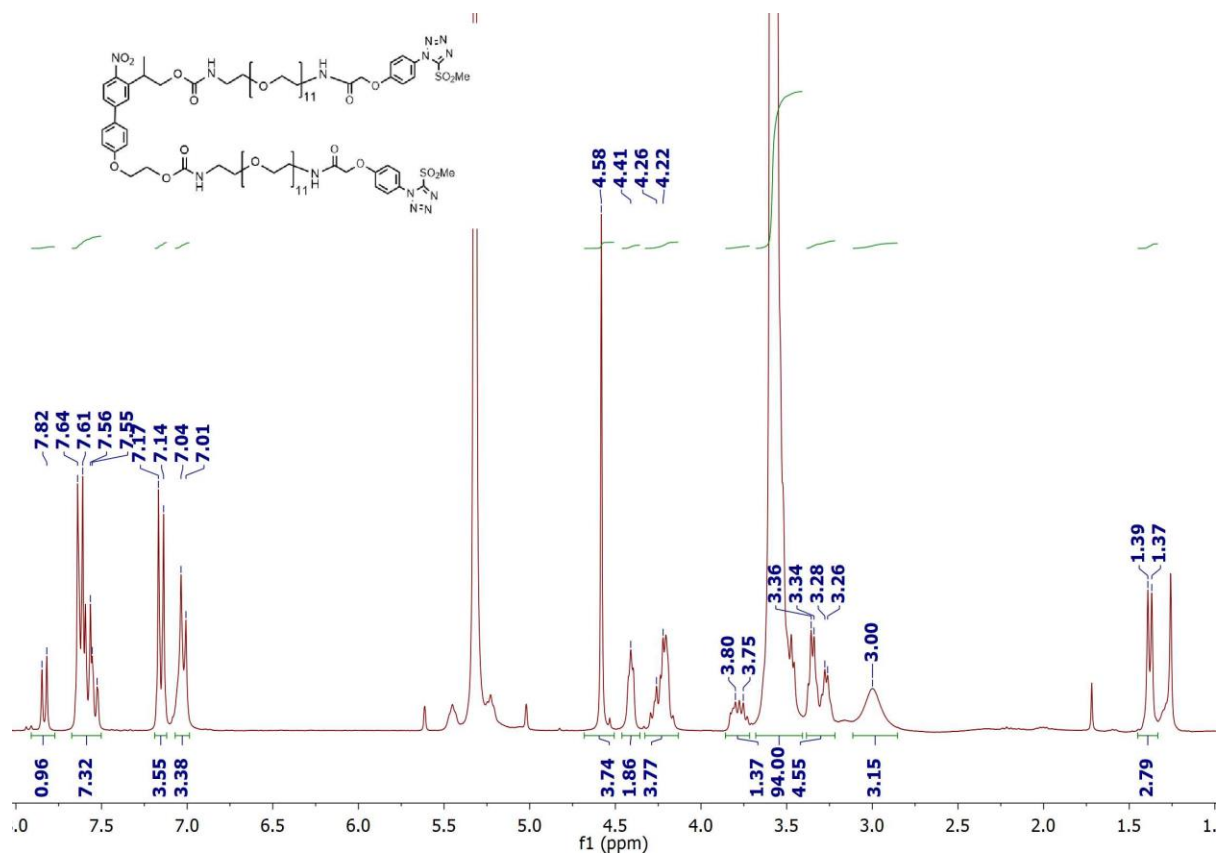
2-(4-(5-(methylsulfonyl)-1H-tetrazol-1-yl)phenoxy)acetic acid (**24**) (2.5 eq., 0.035mmol, 10.4 mg) was dissolved in DMF at room temperature and purged with nitrogen, followed by addition of HOBT (2.5 eq., 0.035 mmol, 4.7 mg), HBTU (2.5 eq., 0.035 mmol, 13.3 mg) and DIPEA (3 eq., 0.042 mmol, 7.3 μ L). After 5 min of stirring, PMNB(C-EG₁₁-NH₂)₂ (**19**) (1 eq., 0.014 mmol, 20 mg) was added. The reaction mixture was stirred for 2 h and DMF was removed by nitrogen flow. The crude was purified with preparative HPLC (5B to 95B, 360 nm, rt = 29 min) to obtain a pale yellow oil (21.4 mg, 81% yield).

ESI-MS⁺: 1027 (M+2NH₄)².

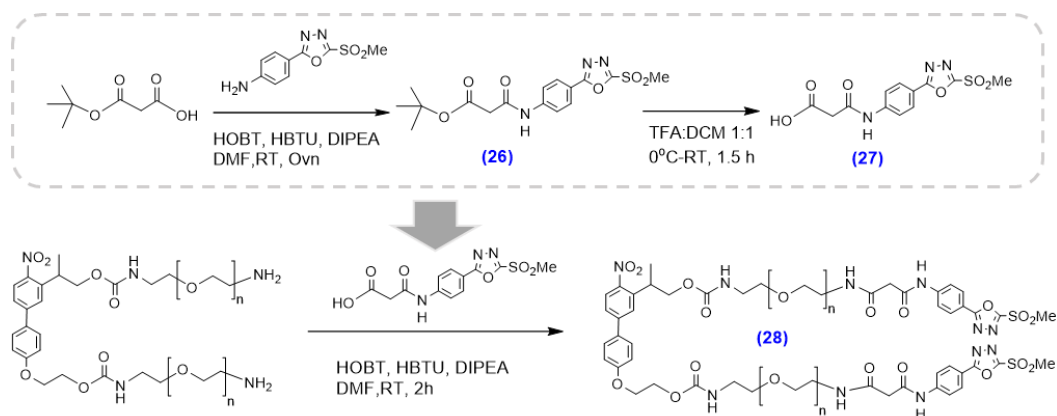
¹H-NMR (300 MHz, CD₂Cl₂, δ [ppm]) = 7.82-7.85 (d, 1H, -CH Ar); 7.53-7.61 (m, 7H, -CH Ar); 7.01-7.17 (m, 6H, -CH Ar); 4.58 (s, 4H, -COCH₂O); 4.40-4.42 (t, 2H, -CH₂O); 4.16-4.29 (m, 4H, -CH₂O); 3.46-3.67(m, 95H, PEG chain,-CH and -SO₂Me); 3.00-3.36 (m, 8H, -CH₂); 1.37-1.39 (d, 3H, -CH₃).

¹³C-NMR (75 MHz, CD₂Cl₂, δ [ppm]) = 169.44; 160.04; 156.66; 149.37; 145.68; 129.10; 127.39; 127.17; 125.78; 125.47; 116.17; 115.54; 78.53; 70.80; 70.43; 70.13; 68.97; 68.20; 67.19; 45.52; 44.35; 41.47; 40.33; 39.44; 34.13; 30.25; 18.15.





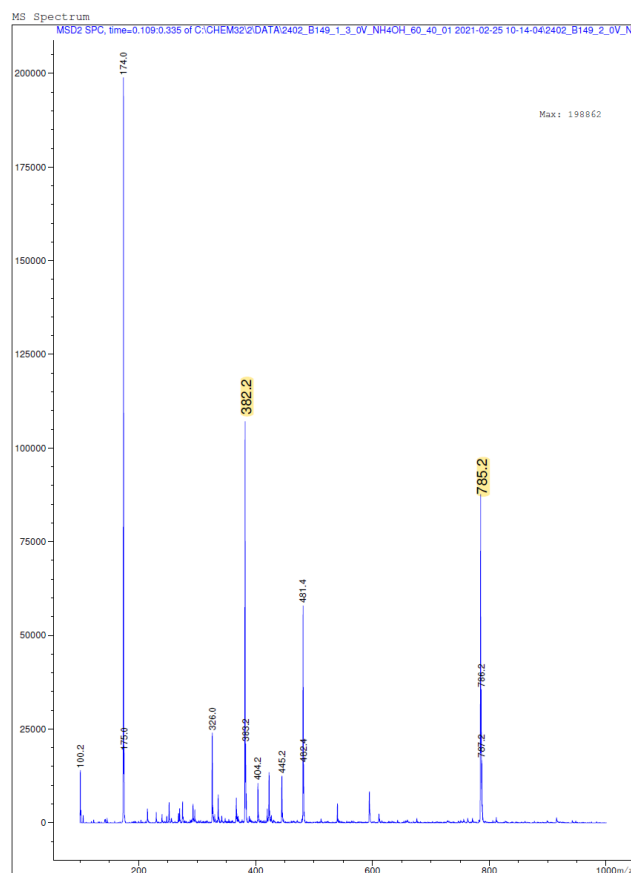
Appendix



(26) *Tert-butyl 3-((4-(5-(methylsulfonyl)-1,3,4-oxadiazol-2-yl)phenyl)amino)-3-oxopropanoate*

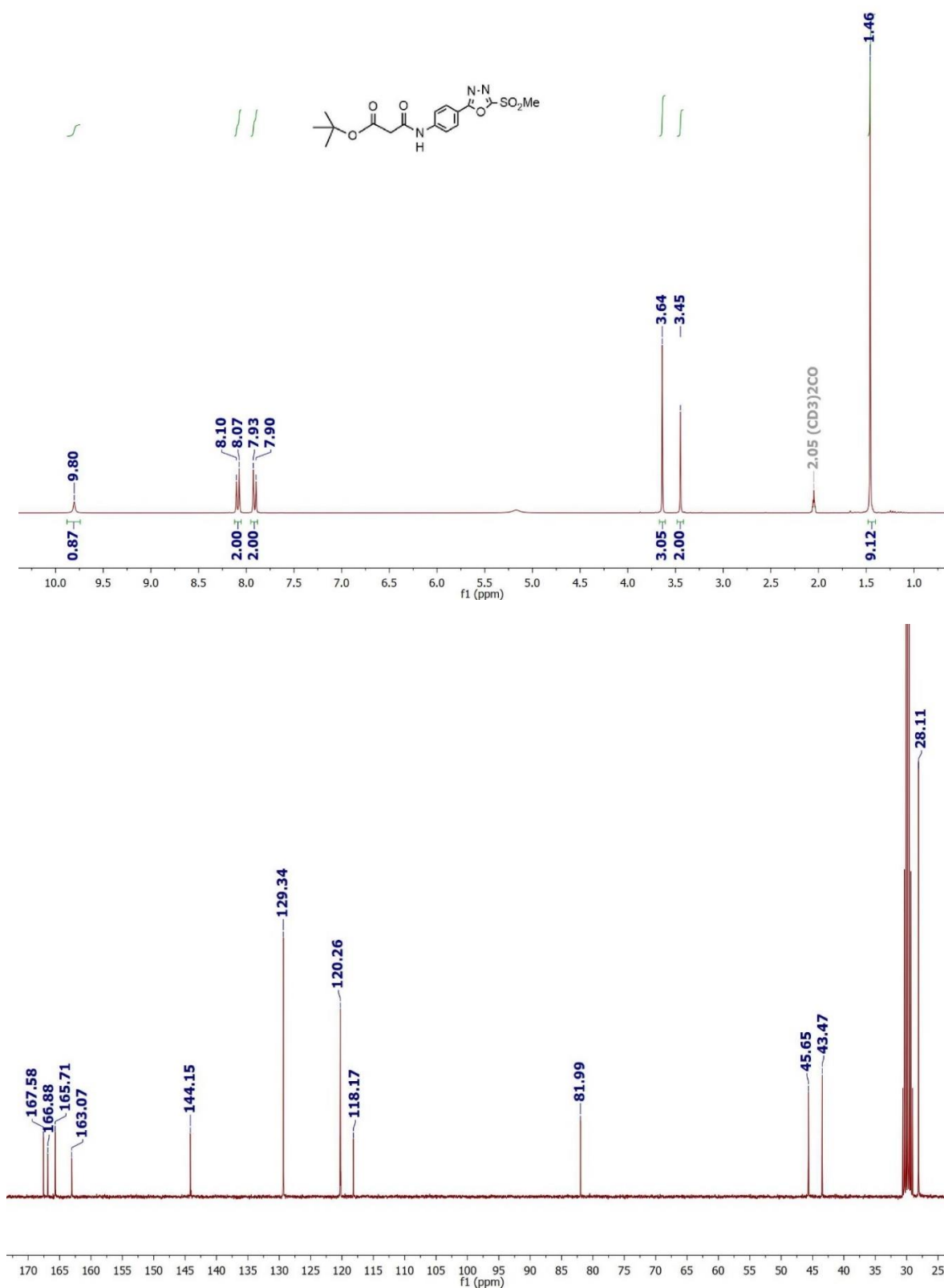
Tert-butyl malonate (2.5 eq., 0.52 mmol, 83.7 mg) was dissolved in 2 mL DMF at room temperature and purged with nitrogen, followed by addition of HOBT (2.5 eq., 0.52 mmol, 70.6 mg), HBTU (2.5 eq., 0.52 mmol, 198 mg) and DIPEA (3 eq., 0.63 mmol, 109 μ L). After 5 min of stirring, 4-(5-(methylsulfonyl)-1,3,4-oxadiazol-2-yl)aniline (1 eq., 0.21 mmol, 50 mg) was added. The reaction mixture was stirred for 2 h and DMF was removed by nitrogen flow. The crude was purified with preparative HPLC (20B to 95B, 280 nm, rt = 20 min) to obtain a pale yellow oil (23.9 mg, 30% yield).

ESI-MS⁺: 382.2 (M+H); 785.2 (2M+Na).



$^1\text{H-NMR}$ (300 MHz, acetone- d_6 , δ [ppm]): 9.8 (s, 1H, -NH); 8.07-8.10 (d, 2H, -CH Ar); 7.90-7.93 (d, 2H, -CH Ar); 3.64 (s, 3H, -SO₂Me); 3.45 (s, 2H, -CH₂); 1.46 (s, 9H, -C(CH₃)₃).

$^{13}\text{C-NMR}$ (75 MHz, acetone- d_6 , δ [ppm]) = 167.58; 166.88; 165.71; 163.07; 144.15; 129.34; 120.26; 118.17; 81.99; 45.64; 43.47; 28.11.



Appendix

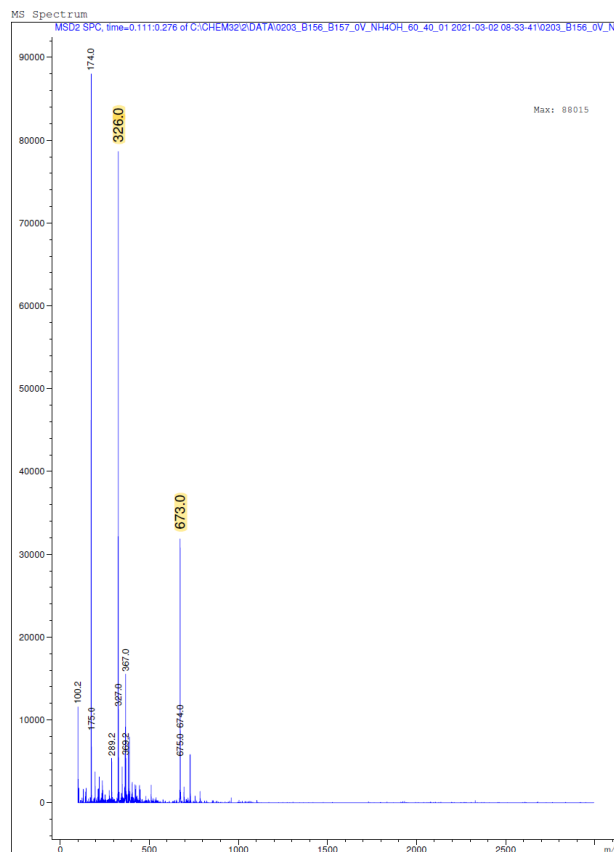
(27) 3-((4-(5-(methylsulfonyl)-1,3,4-oxadiazol-2-yl)phenyl)amino)-3-oxopropanoic acid

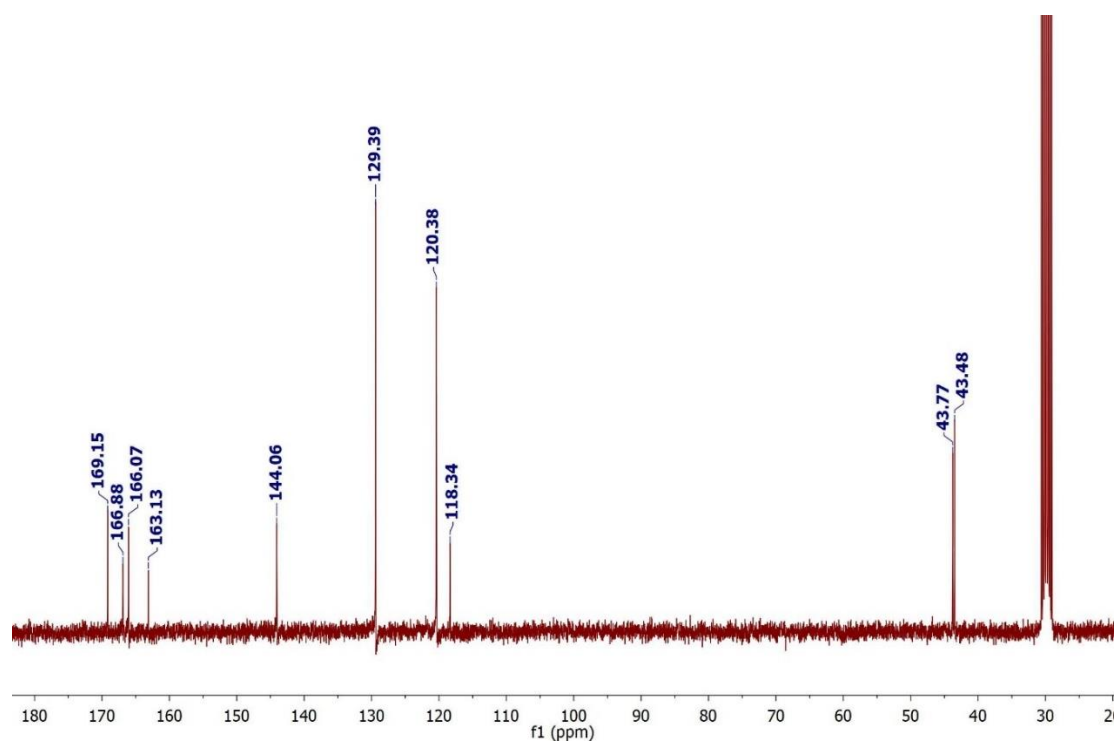
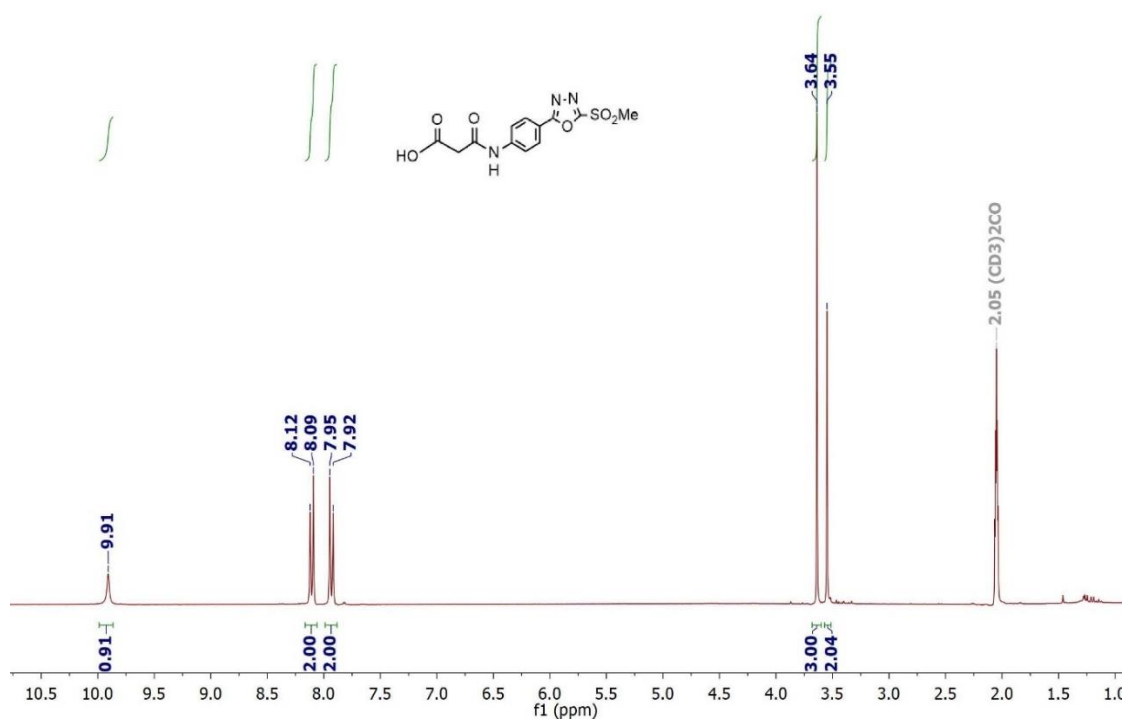
Tert-butyl 3-((4-(5-(methylsulfonyl)-1,3,4-oxadiazol-2-yl)phenyl)amino)-3-oxopropanoate (**26**) (95 mg) was dissolved in 2.5 mL TFA/dry DCM (1:1) at room temperature under nitrogen atmosphere, then stirred at room temperature for 1.5 h. Reaction completion was confirmed by TLC. TFA and DCM were removed by nitrogen flow. The crude was purified with preparative HPLC (5B to 95B, 280 nm, rt = 16 min) to obtain a pale yellow oil (55 mg, 68% yield).

ESI-MS⁺: 326.0 (M+H); 673.0 (2M+Na).

¹H-NMR (300 MHz, acetone-d₆, δ [ppm]): 9.91 (s, 1H, -NH); 8.09-8.12 (d, 2H, -CH Ar); 7.92-7.95 (d, 2H, -CH Ar); 3.64 (s, 3H, -SO₂Me); 3.55 (s, 2H, -CH₂).

¹³C-NMR (75 MHz, acetone-d₆, δ [ppm]) = 169.15; 166.88; 166.07; 163.13; 144.06; 129.39; 120.38; 118.34; 43.77; 43.48.





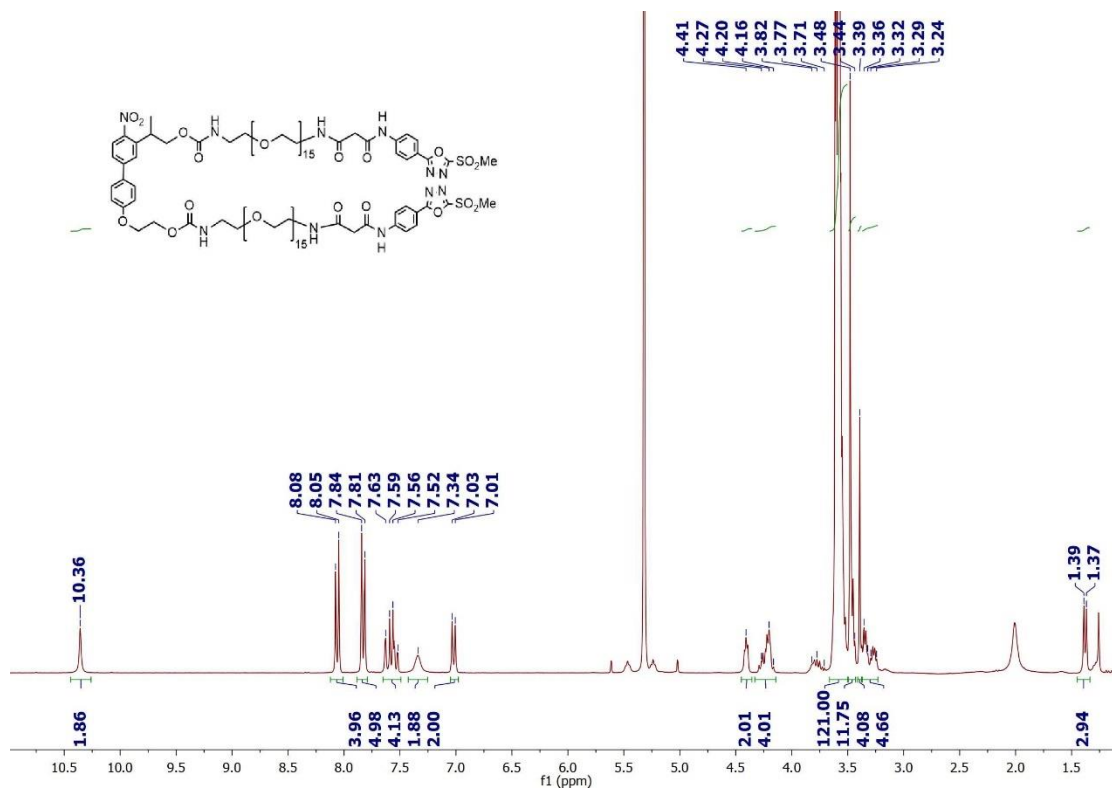
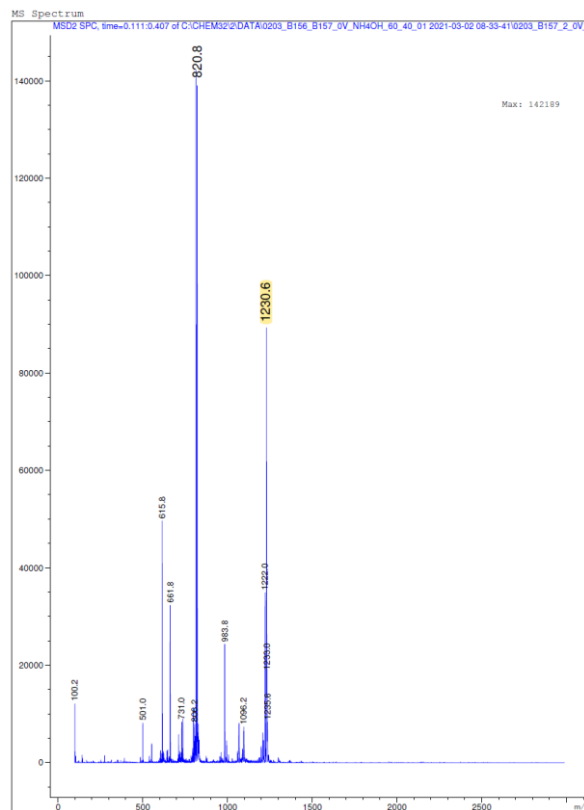
(28) PMNB(C-EG_n-Ox-MS)₂

3-((4-(5-(methylsulfonyl)-1,3,4-oxadiazol-2-yl)phenyl)amino)-3-oxopropanoic acid (27) (2.5 eq., 0.032 mmol, 10.3 mg) was dissolved in 0.8 mL DMF at room temperature and purged with nitrogen, followed by addition of HOBt (2.5 eq., 0.032 mmol, 4.3 mg), HBTU (2.5 eq., 0.032 mmol, 12.1 mg) and DIPEA (3 eq., 0.038 mmol, 6.8 μL). After 5 min of stirring, PMNB(C-EG₁₅-NH₂)₂ (**19**) (1 eq., 0.013 mmol, 20 mg) was added. The reaction mixture was stirred for 2 h and DMF was removed by nitrogen flow. The crude was purified with preparative HPLC (5B to 95B, 360 nm, rt = 30 min) to obtain a pale yellow oil (71% yield).

Appendix

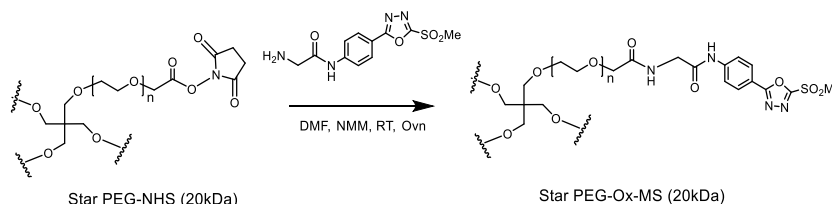
ESI-MS⁺: 1230 (M+2NH₄)².

¹H-NMR (300 MHz, CD₂Cl₂, δ [ppm]) = 10.36 (s, 2H, -NH); 8.05-8.08 (d, 4H, -CH Ar); 7.81-7.84 (d, 5H, -CH Ar); 7.52-7.63 (m, 4H, -CH Ar); 7.34 (s, 2H, -NH); 7.01-7.03 (d, 2H, -CH Ar); 4.40-4.42 (t, 2H, -CH₂O); 4.16-4.27 (m, 4H, -CH₂O); 3.52-3.65 (m, 121H, PEG chain and -CH); 3.48 (s, 10H, -SO₂Me and -CH₂); 3.24-3.44 (m, 8H, -CH₂); 1.37-1.39 (d, 3H, -CH₃).



5.2.4 Synthesis of star PEG-hydrogel precursors

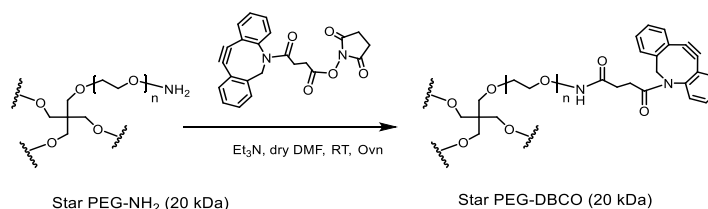
Star PEG-Ox-MS



2-amino-N-(4-(5-(methylsulfonyl)-1,3,4-oxadiazol-2-yl)phenyl)acetamide (10 eq., 100 μ mol, 30 mg) and NMM (15 eq., 150 μ mol, 40 μ L) were dissolved in 2 mL anhydrous DMF and purged with nitrogen for 15 min, and 20 kDa, star PEG-NHS (1 eq., 10 μ mol, 200 mg) in 1 mL anhydrous DMF was added to the solution with syringe under nitrogen atmosphere and the suspension was stirred overnight under room temperature. The crude was dialyzed against acetone and water (3x) to obtain a white polymer powder (188 mg, 94% yield) after freeze-drying. The substitution degree was calculated as 88% by $^1\text{H-NMR}$. The spectroscopic characterization data matched the values reported on the literature.

$^1\text{H-NMR}$ (300 MHz, CD_2Cl_2 , δ [ppm]) = 9.25 (s, 1H, -NH); 8.08 (d, 2H, -CH Ar); 8.04 (m, 1H, -NH); 7.86 (d, 2H, -CH Ar); 4.20 (d, 2H, - CH_2); 4.05 (s, 2H, - $\text{CH}_2\text{C}=\text{O}$ PEG); 3.50-3.68 (m, 440H, PEG chain); 3.48 (s, 3H, - SO_2Me).

Star PEG-DBCO



20 kDa, star PEG-NH₂ (1 eq., 5 μ mol, 100 mg), Et₃N (12 eq., 60 μ mol, 8.4 μ L) and DBCO-NHS (6 eq., 30 μ mol, 12 mg) were dissolved in 2 mL anhydrous DMF under nitrogen atmosphere and stirred overnight at room temperature. The crude was dialyzed against acetone and water (3x) to obtain a white polymer powder (95 mg, 95% yield) after freeze-drying. The substitution degree was calculated as 92% by $^1\text{H-NMR}$. The spectroscopic characterization data matched the values reported on the literature.

$^1\text{H-NMR}$ (300 MHz, CD_2Cl_2 , δ [ppm]) = 7.67 (d, H, -CH Ar); 7.51 (m, 1H, -CH Ar); 7.25-7.41 (m, 6H, -CH Ar); 6.10 (m, 1H, -NH); 5.14 (d, 1H, - CH_2NCO); 3.83 (m, 2H, - CH_2); 3.45-3.70 (m, 440H, PEG chain); 2.25-2.8 (m, 2H, - CH_2); 1.8-2.25 (m, 2H, - CH_2).

5.2.5 Photolysis studies of PMNB(E-PEG_n-SH)₂ and NB(E-EG_n-N₃)₂ in solution.

Solution of PMNB(E-PEG_n-SH)₂ and NB-E-(EG_n-N₃)₂ (0.1 μ M in ACN/H₂O (1:1)) were freshly prepared and introduced to a 400- μ L quartz cuvette (Hellma Analytics, Germany). The cuvette was placed in a

Appendix

with LUMOS 43 lamp source and light-exposed for increasing exposure times at $\lambda = 365$ nm ($I = 1.2$ J cm^{-2}) or $\lambda = 420$ nm ($I = 1.2$ J cm^{-2}). At selected exposure times, the UV/Vis spectrum of the solution was recorded. Additionally, one aliquot (15 μL) of the irradiated solution was taken, diluted to 100 μL with ACN/ H_2O (1:1), and 50 μL aliquot was analyzed by HPLC (method: 5B to 95B, 360 nm, 40 min). UV/Vis spectra and analytical chromatograms were plotted and analyzed with Origin 8.5. The conversion of the photolysis reaction was analyzed quantitatively by analytical HPLC by following the decay of the normalized value of the integral of the compound as a function of irradiation time.

5.3 Chapter 3

5.3.1 Hydrogels formation

Hydrogels were prepared by mixing solutions of star PEGs and crosslinkers in HEPES buffer (10-20 mM, pH 7.5-8) or PBS buffer (pH 7.4). The hydrogel precursors were separately dissolved in buffer. The solutions were combined at 1:1 molar ratio of functional groups and at equal volume. In a typical example, 2 mg of star PEG-Ox-MS and 0.52 mg of PMNB(E-PEG_n-SH)₂ were each dissolved in 20 μL HEPES (20 mM, pH 7.5), vortexed and centrifuged at 13,000 rpm to eliminate bubbles. 20 μL of star PEG-Ox-MS solution and 20 μL of PMNB(E-PEG_n-SH)₂ solution were combined at 25°C in an Eppendorf vial.

5.3.2 Blocking of unreacted -DBCO or -SH groups after hydrogel formation.

The precursors of PEG-T-E-PMNB or PEG-STz-C-PMNB hydrogels were freshly prepared in HEPES or PBS buffer, vortexed and centrifuged. Then the precursors are mixed in a PDMS mold (8 mm diameter), curing for 30-1h min and then incubated with O-(2-Azidoethyl)-O'-methyl-triethylene glycol (20 mM in Milli-Q water) or Mal-PEG-OMe (5kDa) (20 mM in PBS buffer) for 30 min at room temperature. Hydrogel was subsequently washed with Milli-Q water (3x) and started the photodegradation experiments immediately.

5.3.3 General procedure for gel preparation for LSM

Hydrogel were prepared in a μ -Dish with culture insert 4well (34 mm, Ibidi GmbH, Germany) in order to get a sharp edge for 2P degradation. In a representative example of sample preparation, 15 μL of star PEG-Ox-MS solution (fresh prepared) was drop casted onto a μ -Dish with culture insert 4well (34 mm, Ibidi GmbH, Germany), 15 μL of PMNB(E-PEG-SH)₂ solution (fresh prepared) was added at 25°C and the gelling mixture was let to cure for 1 h at 25°C in a humidified atmosphere. The obtained hydrogels were immersed in PBS buffer (pH 7.4) overnight at room temperature and then washed twice with PBS buffer. The culture insert 4-well was subsequently removed.

5.3.4 General procedure for gel preparation for NanoScribe

The experimental procedure is schematized in **Figure 5.1**. Glass slides ($\phi = 30$ mm, #1.5, Thermo scientific, Germany) were pre-functionalized as above with -SH groups or -N₃ groups for covalent fixation of the hydrogels and a PDMS mold ($\phi = 6$ mm) was placed on top. 15 μL of star PEG-Ox-MS

solution was drop casted on the glass slide inside the PDMS mold. 2.04 μL Alexa Fluor 555 (0.15 mM) or azide Fluor 545 (0.15 mM) was added and allowed to react for 3 min at 25°C. 5 μL of crosslinker solution was added at 25°C and let cure for 1 h in a closed chamber. After curing, the PDMS mold was removed and the hydrogels were immersed in PBS buffer (pH 7.4) overnight at room temperature.

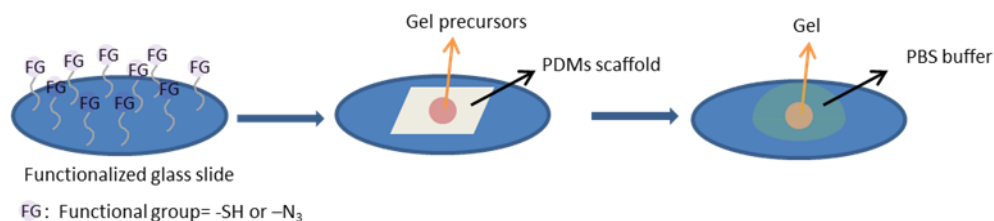


Figure 5.1 Hydrogel preparation procedure for NanoScribe

The hydrogel samples were mounted to a Nanoscribe GT photonic professional lithography system, equipped with a femtosecond laser (780 nm, up to 50 mW average power) and a 25x oil-immersion objective. The following exposure parameters were applied: speed= 5 mm s⁻¹ to 100 mm s⁻¹, and laser power= 5 mW to 25 mW. The patterns were written with computer aid design (CAD) model. After exposure at the Nanoscribe, the gels were imaged with Zeiss LSM 880. It should be noted that in order to avoid heating and dehydration, the hydrogels were immersed in PBS buffer to dissipate generated heat.

5.3.5 Spheroids preparation

100 μL from a suspension with a 5x10³ or 10x10³ cell mL⁻¹ were added in each well of 96 well, U-bottom, cell repellent plate (Greiner Bio-One, 650970). After cultured at 37°C under a humidified atmosphere containing 5 % CO₂ overnight, all spheroids were collected with a P1000 pipette with cut tip. Spheroid suspension was centrifuged 3 min at 200 rpm and the supernatant was removed.

5.3.6 3D encapsulation of spheroids in hydrogels

In a presentative experiment for PEG-SOx-C-PMNB with 5.25 wt% polymer concentration, star PEG-SH solution (8 wt%, 10 μL in sterile HEPES (20 mM, pH 7.5) with 0.9176% TCEP) and c[RGDfK(Mal)] (2 mM, 2.5 μL in sterile HEPES (20 mM, pH 7.5)) was prepared inside a sterile laminar flow and incubated for 5 min at room temperature in a Eppendorf vial. The spheroids prepared (6 μL) in the previous section was added and gently mixed. The above mixture (5.8 μL) was subsequently added into an ibidi® 15-well angiogenesis slide, followed by an addition of PMNB(C-EG₂₃-Ox-MS)₂ (4.2 μL), carefully mixed with pipette tip and let it cure for 30 min at 37 °C under a humidified atmosphere containing 5% CO₂. After gelation, medium (45 μL) was added to each well and substituted by fresh medium every 24 h during cell culture. The hydrogels were kept in HUVEC medium at 37 °C under a humidified atmosphere containing 5% CO₂.

5.3.7 Live/dead assay

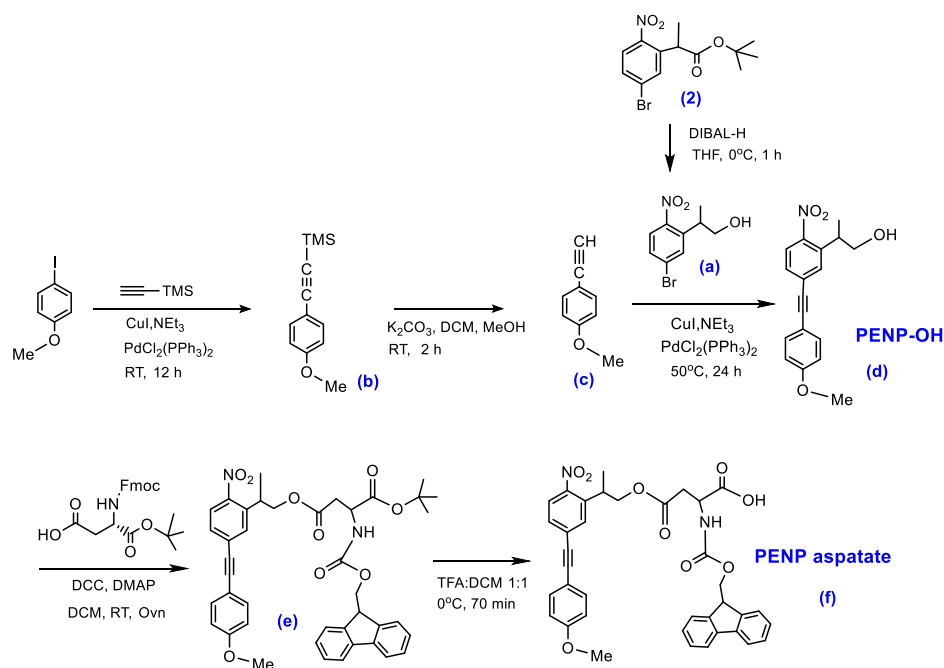
HUVEC spheroids were encapsulated in PEG-gels for 3 days. Cell culture medium was removed and a mixture of Fluorescein diacetate (FDA, 40 $\mu\text{g mL}^{-1}$) (Sigma, F7378) and Propidium iodide (PI, 30 $\mu\text{g mL}^{-1}$)

Appendix

¹) (Sigma, P4170) in PBS was added and incubated for 5 min at room temperature in dark. Then hydrogels were washed twice with PBS and imaged with Zeiss Cell Observer epifluorescence microscope and Zeiss LSM 880 confocal microscope with a 10x air objective.

5.4 Chapter 4

5.4.1 Synthesis PNEP-Asp



(a) 2-(5-bromo-2-nitrophenyl)propan-1-ol

Tert-butyl-2-(5-bromo-2-nitrophenyl)propanoate (**2**) (1 eq., 2.59 mmol, 0.854 g) was dissolved in 32 mL dry THF. DIBAL-H (3 eq., 7.76 mmol, 7.76 mL) (1M in THF) was subsequently added at 0°C. The reaction mixture was stirred for 3h at room temperature. 65 mL HCl solution (5 N) was added at 0°C and the reaction mixture was extracted with ethyl acetate. The combined organic phase was washed with brine; dried over Mg₂SO₄; evaporated and the crude product was purified by silica gel column chromatography (20% ethyl acetate/n-hexane) to obtain the title compound (0.357 g, 53% yield). The spectroscopic characterization data matched the values reported on the literature.

¹H-NMR (300 MHz, CDCl₃, δ [ppm]) = 7.64-7.67 (d, 1H, -CH Ar); 7.50 (d, 1H, -CH Ar); 7.48 (d, 1H, -CH Ar); 3.71-3.86 (m, 2H, -CH₂); 3.50-3.62 (m, 1H, -CH); 1.32-1.34 (d, 3H, -CH₃).

¹³C-NMR (75 MHz, CDCl₃, δ [ppm]) = 149.4; 140.5; 131.6; 130.4; 127.5; 67.6; 36.4; 17.4.

(c) 4-ethynylanisole ⁴

4-Iodoanisole (1 eq., 0.85 mmol, 200 mg) was dissolved in dry 0.8 mL Et₃N. Trimethylsilyl-acetylene (1.42 eq., 1.22 mmol, 0.18 mL) and Copper (I) iodide (0.05 eq., 0.042 mmol, 8 mg) were added to above solution and the mixture was maintained stirred under argon for 5 min.

Bis(triphenylphosphine)palladium(II) dichloride (0.05 eq., 0.042 mmol, 30 mg) was added. The reaction mixture was then stirred under argon at room temperature for 12 hours and reaction completion was confirmed by TLC. Ethyl acetate was added to dilute the mixture and filtered through a pad of celite. The mixture then extracted with ethyl acetate and the combined organic phase was washed with brine; dried over Mg_2SO_4 and evaporated. The crude product was then used without further purification and dissolved in a mixture of DCM (0.8 mL) and methanol (0.8 mL) under argon. Potassium carbonate (2 eq., 1.7 mmol, 235 mg) was added in one portion followed by KF on alumina (40 wt%, 94 mg). The mixture was stirred at room temperature for 2 hours, followed by extraction with DCM. The organic layer was washed with water and dried over Na_2SO_4 , evaporated and the crude product was subjected to silica gel column chromatography (5% ethyl acetate/n-hexane) to obtain a brown oil (100.5 mg, 89% yield). The spectroscopic characterization data matched the values reported on the literature.

$^1\text{H-NMR}$ (300 MHz, CDCl_3). δ = 7.42-7.44 (d, 2 H, -CH Ar); 6.83-6.85 (d, 2H, -CH Ar); 3.81 (s, 3 H, $-\text{OCH}_3$); 2.99 (s, H, -CH).

$^{13}\text{C-NMR}$ (75 MHz, CDCl_3 , δ [ppm]) = 160.07; 133.73; 114.30; 114.07; 83.80; 75.91; 55.43.

(d) 2-(5-((4-methoxyphenyl)ethynyl)-2-nitrophenyl)propan-1-ol

2-(5-bromo-2-nitrophenyl) propan-1-ol (**2**) (1 eq., 0.58 mmol, 151.4 mg) and 4-ethynylanisole (**c**) (1.3 eq., 0.76 mmol, 100 mg) were dissolved in 2 mL Et_3N . Copper(I) iodide (0.1 eq., 0.058 mmol, 11.1 mg) was subsequently added and the mixture was purged with argon for 5 min, followed by addition of bis(triphenylphosphine) palladium (II) dichloride (0.1 eq., 0.058 mmol, 40.9 mg). The reaction mixture was stirred under argon at 50°C for 24 hours, followed by dilution with ethyl acetate and filtration through a pad of celite. The mixture then extracted with ethyl acetate and the combined organic phase was washed with brine; dried over Na_2SO_4 ; evaporated and the crude product was purified by silica gel column chromatography (20% ethyl acetate/n-hexane) to obtain the pale yellow powder (121 mg, 67% yield).

ESI-MS⁺: 312.2 (M+H); 329.2 (M+NH₄).

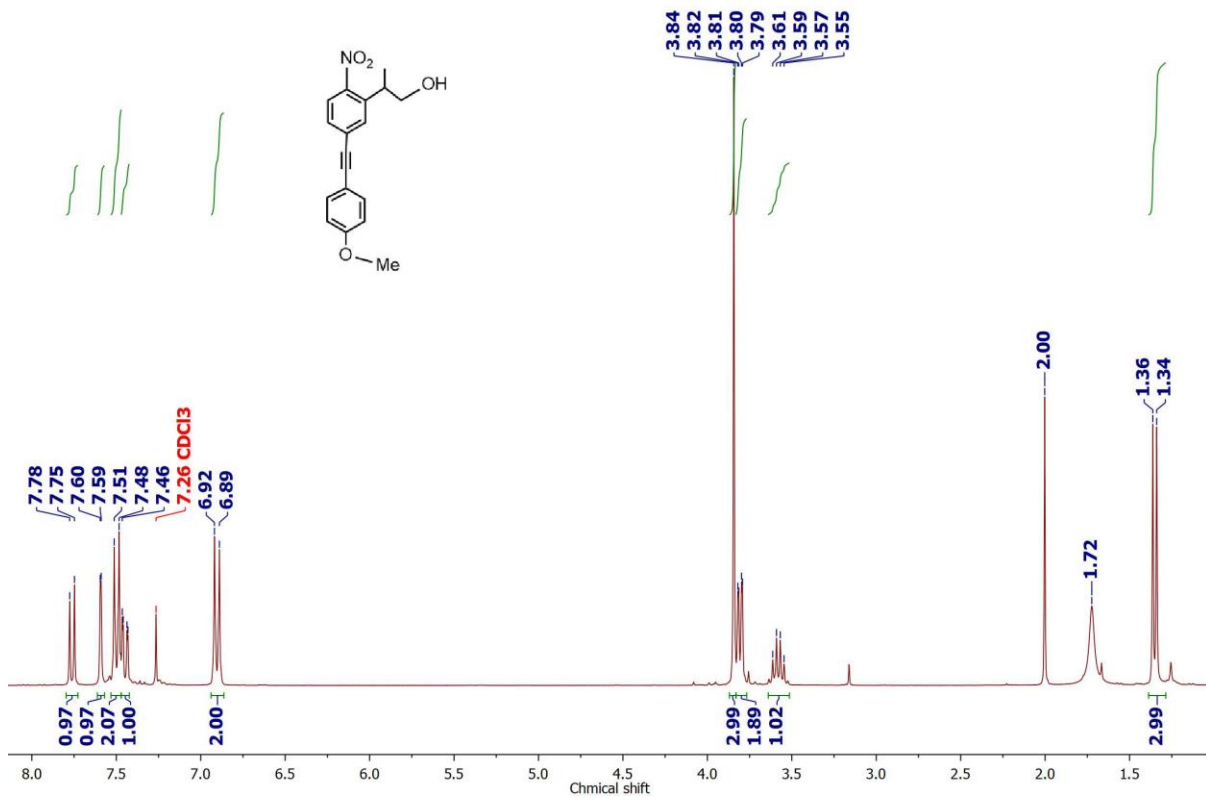
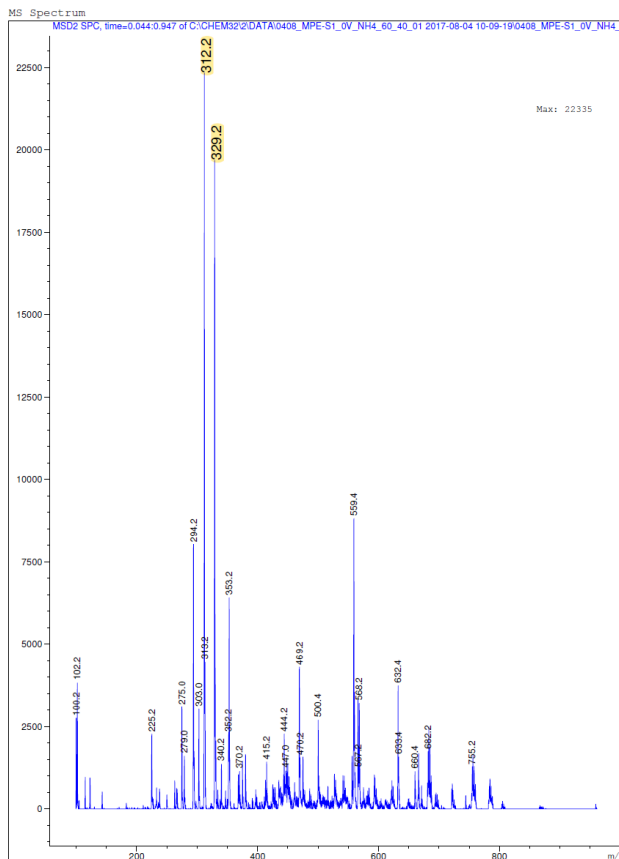
$^1\text{H-NMR}$ (300 MHz, CD_2Cl_2 , δ [ppm]) = 7.75-7.78 (d, 1H, -CH Ar); 7.60 (s, 1H, -CH Ar); 7.48-7.51 (d, 2H, -CH Ar); 7.43-7.46 (dd, 1H, -CH Ar); 6.89-6.92 (d, 2H, -CH Ar); 3.84 (s, 3H, $-\text{OCH}_3$); 3.79-3.82 (m, 2H, $-\text{CH}_2$); 3.55-3.61 (m, 1H, -CH); 1.34-1.36 (d, 2H, $-\text{CH}_3$).

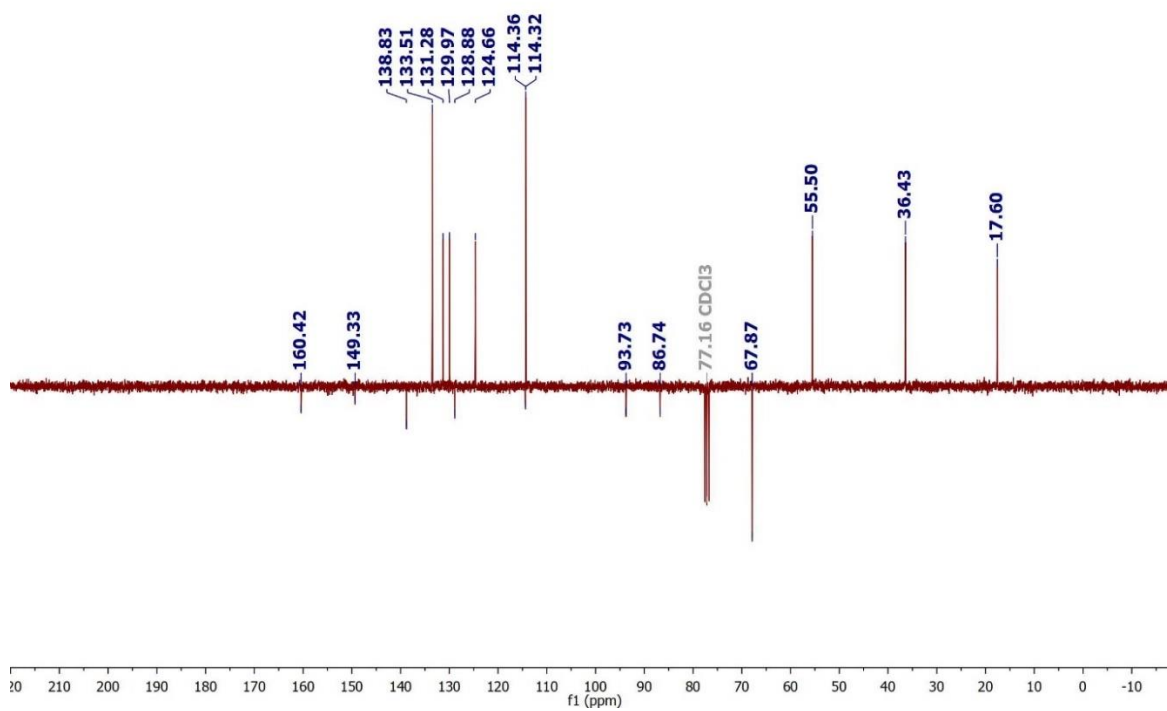
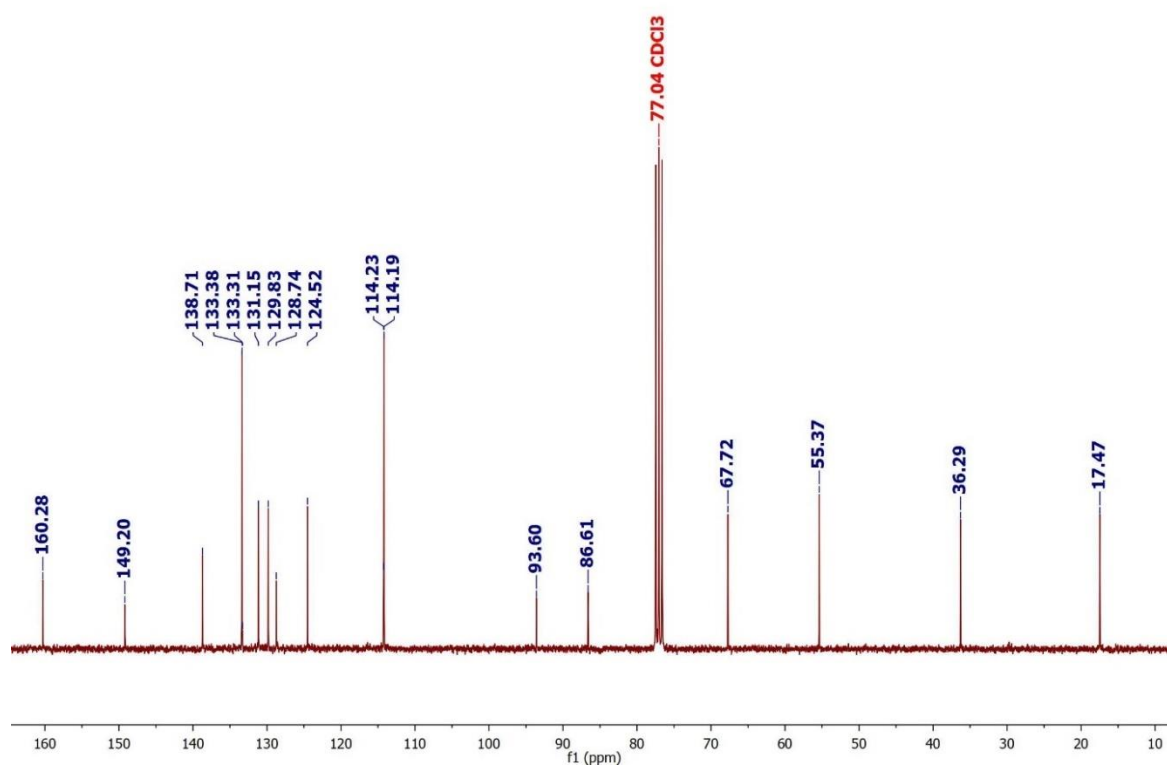
$^{13}\text{C-NMR}$ (75 MHz, CDCl_3 , δ): 160.28; 149.20; 138.71; 133.38; 131.15; 129.83; 128.74; 124.52; 114.23; 114.19; 93.60; 86.61; 67.72; 55.37; 36.29; 17.47.

Attached proton test (APT): -CH and $-\text{CH}_3$ signals positive and -C and $-\text{CH}_2$ signals negative.

$^{13}\text{C-NMR}$ (APT) (75 MHz, CDCl_3 , δ , APT): -C 160.42; 149.33; 138.83; 128.88; 114.36; 93.73; 86.74. -CH 133.51; 131.28; 129.97; 124.66; 114.32; 36.43. $-\text{CH}_2$ 67.87. $-\text{CH}_3$ 55.50; 17.60.

Appendix





Appendix

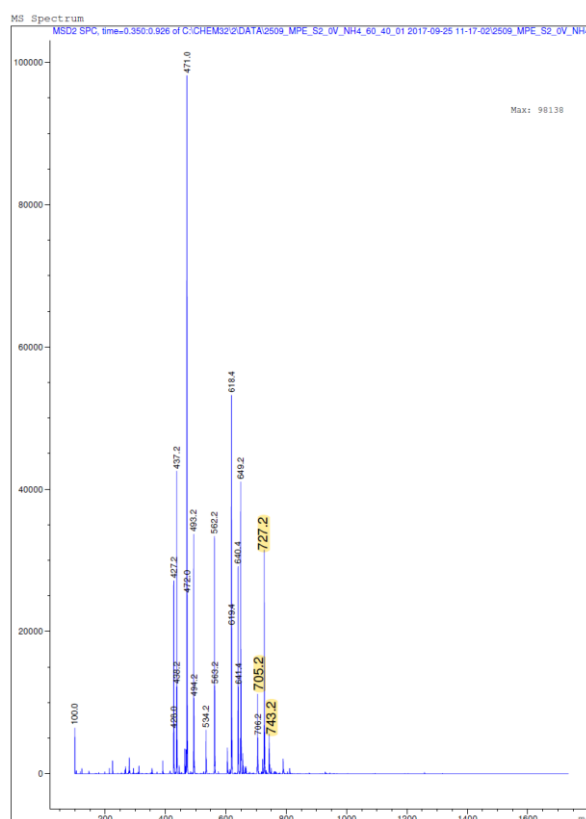
(e) α -tert-butyl δ -(2-(5-((4-methoxyphenyl)ethynyl)-2-nitrophenyl)propyl)-N-Fmoc-L-aspartate

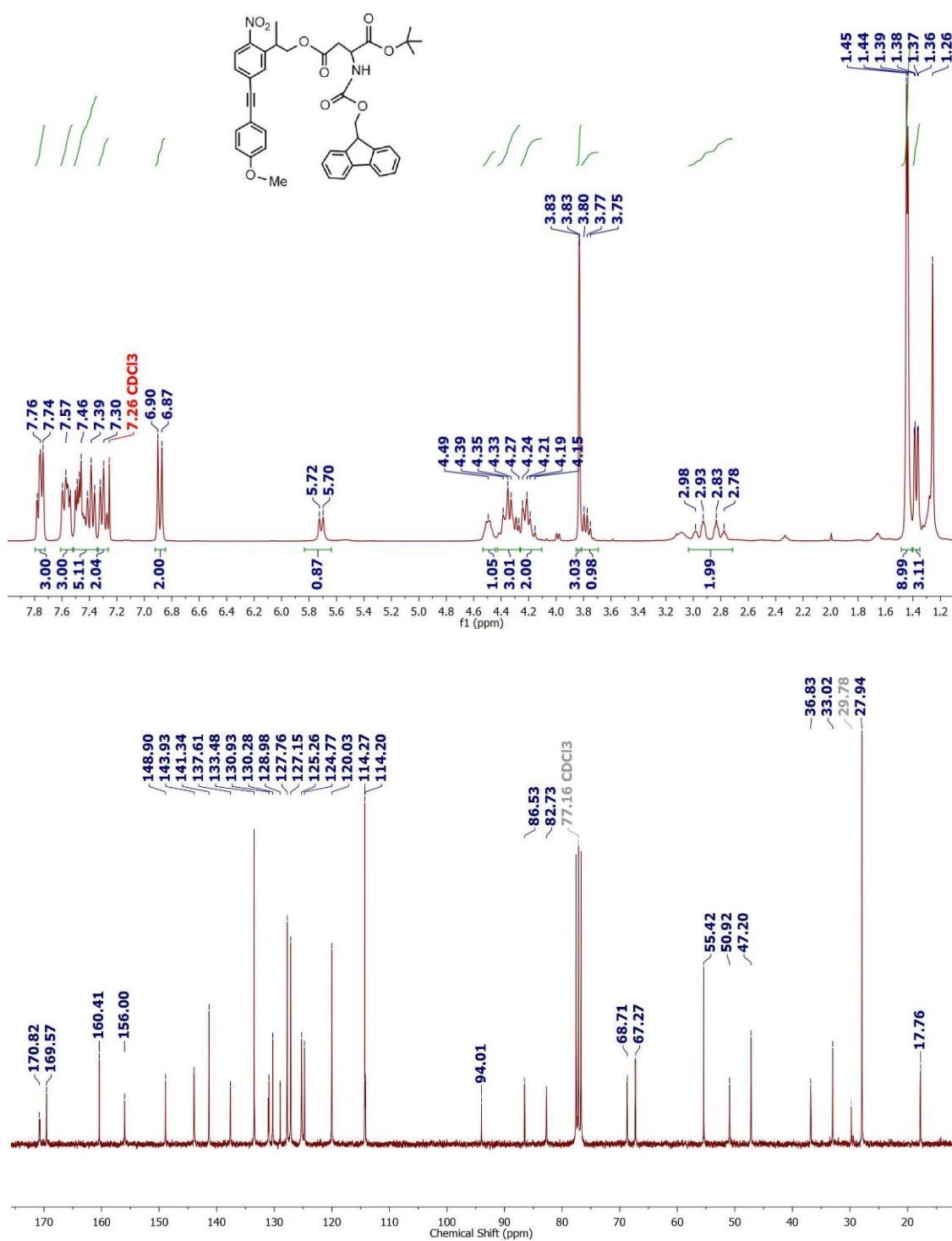
2-(5-((4-methoxyphenyl)ethynyl)-2-nitrophenyl)propan-1-ol (**d**) (1 eq., 0.32 mmol, 100 mg) was dissolved in 4 mL dry DCM under nitrogen atmosphere, and the following reagents were added in the specific order: α -tert-butyl N-Fmoc-L-aspartate (1 eq., 0.32 mmol, 132 mg), DCC (1 eq., 0.32 mmol, 66 mg) and DMAP (0.08 eq., 26 μ mol, 3.2 mg). The mixture was stirred overnight under nitrogen atmosphere at room temperature and subsequently saturated sodium bicarbonate solution was added (32 mL) followed by extraction with diethyl ether. The combined organic layer was washed with brine, dried over MgSO_4 and evaporated. The crude product was purified by prep HPLC (50 B to 95 B, 360 nm, 45 min, rt = 39 min) to obtain a yellow oil (129 mg, 57% yield) after freeze-drying.

ESI-MS⁺: 705.2 (M+H); 727.2 (M+Na); 743.2 (M+K).

¹H-NMR (300 MHz, CD_2Cl_2 , δ [ppm]) = 7.74-7.78 (m, 3H, -CH Ar); 7.54-7.60 (m, 3H, -CH Ar); 7.36-7.49 (m, 5H, -CH Ar); 6.87-6.90 (d, 2H, -CH Ar); 5.7-5.72 (d, 1H, -NH); 4.47-4.52 (m, 1H, -CH); 4.27-4.39 (m, 3H, -CH and -CH₂); 4.15-4.24 (m, 2H, -CH₂); 3.83 (s, 3H, -OCH₃); 3.75-3.80 (m, 1H, -CH); 2.78-2.98 (m, 2H, -CH₂); 1.44-1.45 (d, 9H, -C(CH₃)₃); 1.36-1.39 (dd, 3H, -CH₃).

¹³C-NMR (75 MHz, CDCl_3 , δ): 170.82; 169.57; 160.41; 156.00; 148.90; 143.93; 141.34; 137.61; 133.48; 130.93; 130.28; 128.98; 127.76; 127.15; 125.26; 124.77; 120.03; 114.27; 114.20; 94.01; 86.53; 82.73; 68.71; 67.27; 55.42; 50.92; 47.20; 36.83; 33.02; 27.94; 17.76.





(f) α -tert-butyl δ -(2-(5-((4-methoxyphenyl)ethynyl)-2-nitrophenyl)propyl)-L-aspartate

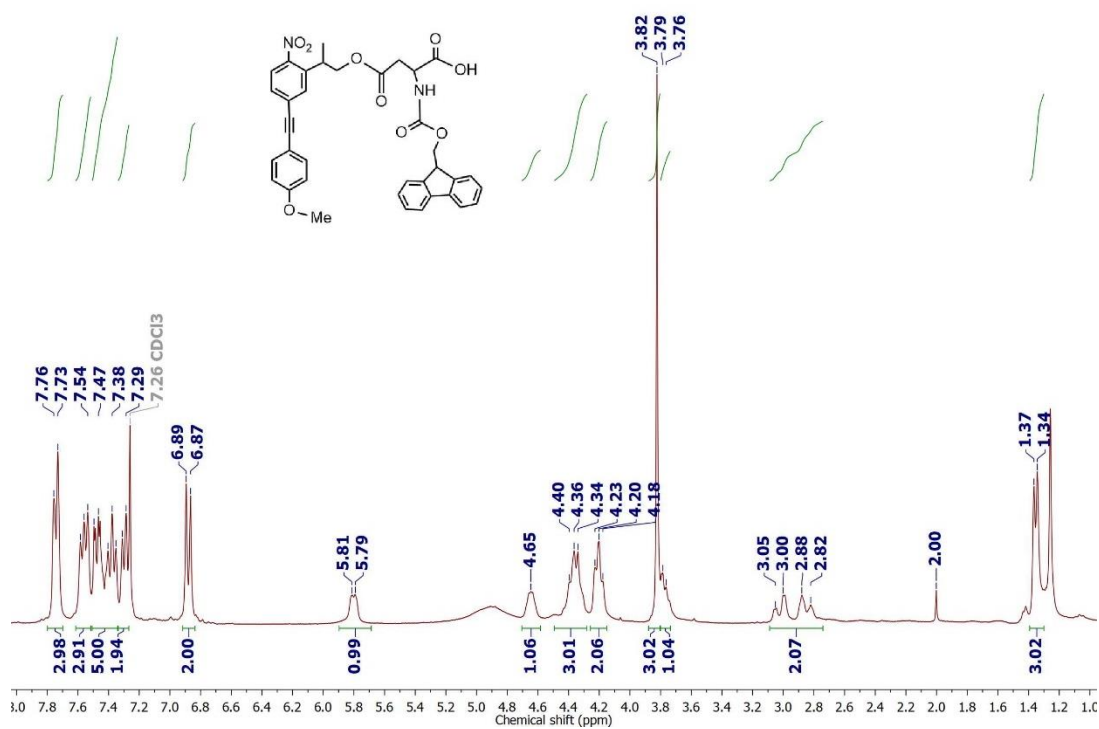
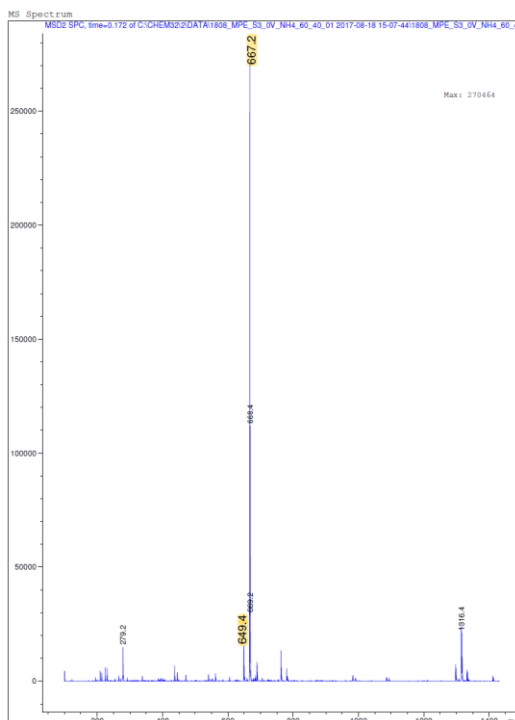
α -tert-butyl δ -(2-(5-((4-methoxyphenyl)ethynyl)-2-nitrophenyl)propyl)-N-Fmoc-L-aspartate (**e**) (1 eq., 0.082 mmol, 60 mg) was dissolved in 0.6 mL TFA:DCM (1:1) under argon atmosphere at 0°C for 70 min. The reaction mixture was stirred for 2 h and DMF was removed by nitrogen flow. The crude was purified with preparative HPLC (50B to 95B, 360 nm, rt = 33 min) to obtain a yellow oil (20 mg, 36% yield).

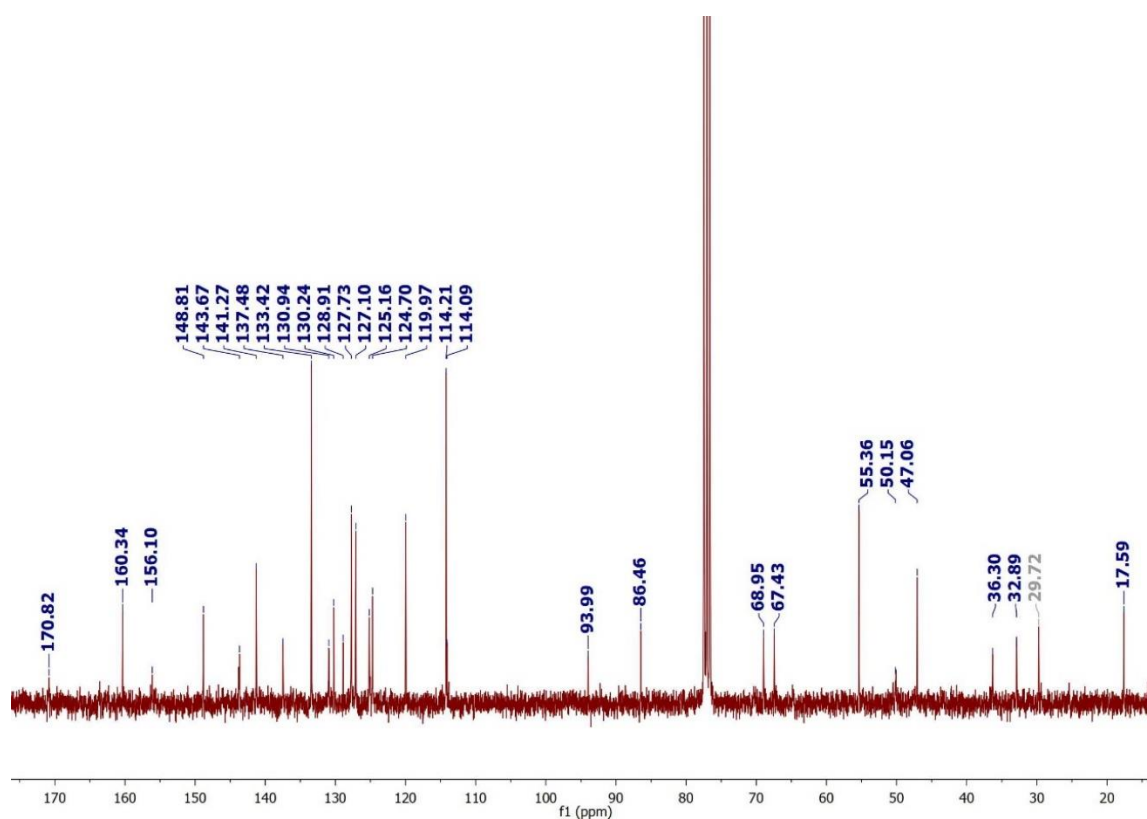
Appendix

ESI-MS⁺: 649.4 (M+H); 667.2 (M+NH₄).

¹H-NMR (300 MHz, CD₂Cl₂, δ [ppm]) = 7.73-7.76 (m, 3H, -CH Ar); 7.54-7.58 (m, 3H, -CH Ar); 7.35-7.49 (m, 5H, -CH Ar); 6.87-6.90 (d, 2H, -CH Ar); 5.79-5.81 (d, 1H, -NH); 4.65 (m, 1H, -CH); 4.34-4.40 (m, 3H, -CH and -CH₂); 4.18-4.23 (m, 2H, -CH₂); 3.82 (s, 3H, -OCH₃); 3.76-3.79 (m, 1H, -CH); 2.82-3.05 (m, 2H, -CH₂); 1.34-1.37 (d, 3H, -CH₃).

¹³C-NMR (75 MHz, CDCl₃, δ): 170.82; 160.34; 156.10; 148.81; 143.67; 141.47; 137.48; 133.42; 130.94; 130.24; 128.91; 127.73; 127.10; 125.16; 124.70; 119.97; 114.21; 114.09; 93.99; 86.46; 68.95; 67.43; 55.36; 50.15; 47.06; 36.30; 32.89; 17.59.





5.4.2 Stability study of Fmoc-Asp(PENP)-OH

Fmoc-Asp(PENP)-OH was freshly prepared in different mixtures (TFE/AcOH/ DCM 1:3:6, TFA/DCM/TIS 4:1:20 and PBS buffer) at room temperature and placed in a amber vial and maintained in the dark. At selected exposure times, one aliquot (50 μL) of the solution was taken and analyzed by HPLC (method: 20B to 95B, 360 nm, 40 min). The conversion of Fmoc-Asp(PENP)-OH was analyzed quantitatively by analytical HPLC by following the decay of the normalized value of the integral of the compound as a function of incubation time.

5.4.3 Synthesis of c[RGD(PENP)fc] by SPPS

Coupling of amino acids

Peptides were synthesized manually by SPPS from pre-loaded H-Gly-2-Cl-Trt resin (loading: 0.54 mmol g^{-1} , 0.054 mmol, 100 mg) and the next amino acids were coupled sequentially by adding the mixture solution of Fmoc-protected amino acids (2 eq., 0.108 mmol), HOBT (2 eq., 0.108 mmol, 14.6 mg), HBTU (2 eq., 0.108 mmol, 41 mg) and DIPEA (5.6 eq., 0.314 mmol, 54.6 μL) in 2 mL dry DMF with vigorous shaking for 2 h. The coupling solution was then filtered off and the resin was washed with DMF (5 x 2 mL). Fmoc protecting group was cleaved by 20% piperidine in DMF (1 mL, 2x10 min). The coupling procedure was summarised in **Table 5.1**.

Appendix

Table 5.1 Procedure for amino acid coupling

Steps	Reagent	Time	Amount
Coupling	Coupling mixture in DMF	2 h	-
Wash	DMF	5x1 min	2 mL/100 mg resin
Fmoc-cleavage	20% piperidine in DMF	2x10 min	1 mL/100 mg resin
Wash	DMF	5x1 min	2 mL/100 mg resin

Cleavage of peptide from resin

The linear peptide sequence was washed with DCM for 3 times and cleaved from resin by using TFE/AcOH/DCM (1:3:6) (3x30 min) with 10 mL solution of each. The solvents was then evaporated to obtain the crude linear peptide.

Cyclization

The crude linear peptide was dissolved in high dilution in dry DMF (30 mg/20 mL DMF), followed by addition of DPPA (3 eq.) and NaHCO₃ (5 eq.). The mixture was stirred for 48 h at room temperature. The solution was then filtered to remove the solid NaHCO₃ and evaporated. The obtained compound was then dissolved in acetone and precipitated in H₂O to obtain the cyclic peptide.

Cleavage of protecting groups

The protected cyclic peptide was dissolved in TFA/DCM/TIS (4:20:1) (20 mg in 1 mL) and stirred for 3.5-5 h at 0°C. Solution was removed by nitrogen flow. The obtained peptide was then dissolved in AcOH and precipitated in diethyl ether at 0°C. The crude purified with preparative HPLC (30B to 95B, 360 nm, rt = 25 min) to obtain a pale yellow powder (1.3 mg, 10% yield).

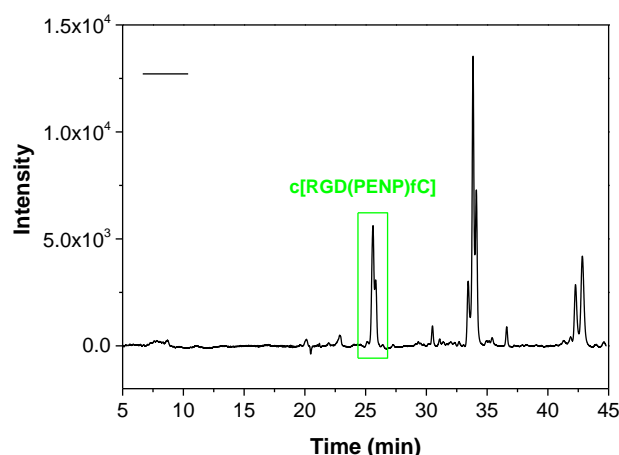


Figure 5.2 Preparative HPLC profile of c[RGD(PENP)fc]. $\lambda_{\text{detection}} = 360 \text{ nm}$.

Synthesis of c[RGD(PENP)fk-N₃]

c[RGDfk-N₃] (1 eq., 3.18 μmol , 2 mg) was dissolved in 0.1 mL dry DCM under nitrogen atmosphere, and the following reagents were added in the specific order: 2-(5-((4-methoxyphenyl)ethynyl)-2-nitrophenyl)propan-1-ol (**d**) (1 eq., 3.18 μmol , 1.0 mg), DCC (2 eq., 6.36 μmol , 1.33 mg) and DMAP

(0.16 eq., 0.51 μmol , 0.04 mg). The mixture was stirred overnight under nitrogen atmosphere at room temperature and the solvent was removed by nitrogen steam. The crude product was purified by prep HPLC (20 B to 95 B, 360 nm, 45 min, $t_r = 39$ min) to obtain a yellow oil (0.88 mg, 30% yield) after freeze-drying.

ESI-MS⁺: 923.2 (M+H).

5.4.4 Photolysis studies of Fmoc-Asp(PENP)-OH and c[RGD(PENP)fK-N₃] in solution.

Solution of Fmoc-Asp(PENP)-OH and c[RGD(PENP)fK-N₃] (0.2 mM in ACN/H₂O (1:1)) were freshly prepared and introduced to a 400- μL quartz cuvette (Hellma Analytics, Germany). The cuvette was placed in a with LUMOS 43 lamp source and light-exposed for increasing exposure times at $\lambda = 420$ nm ($I = 1.2$ J cm⁻²). At selected exposure times, the UV/Vis spectrum of the solution was recorded. Additionally, one aliquot (15 μL) of the irradiated solution was taken, diluted to 100 μL with ACN/H₂O (1:1), and 50 μL aliquot was analyzed by HPLC. UV/Vis spectra and analytical chromatograms were plotted and analyzed with Origin 8.5. The conversion of the photolysis reaction was analyzed quantitatively by analytical HPLC by following the decay of the normalized value of the integral of the compound as a function of irradiation time.

5.5 Reference

1. Schelkle, K. M.; Griesbaum, T.; Ollech, D.; Becht, S.; Buckup, T.; Hamburger, M.; Wombacher, R., Light-induced protein dimerization by one- and two-photon activation of gibberellic acid derivatives in living cells. *Angewandte Chemie (International ed. in English)* **2015**, *54* (9), 2825-9.
2. Paez, J. I.; Farrukh, A.; Valbuena-Mendoza, R.; Włodarczyk-Biegun, M. K.; del Campo, A., Thiol-Methylsulfone-Based Hydrogels for 3D Cell Encapsulation. *ACS Applied Materials & Interfaces* **2020**, *12* (7), 8062-8072.
3. Paez, J. I.; de Miguel-Jiménez, A.; Valbuena-Mendoza, R.; Rathore, A.; Jin, M.; Gläser, A.; Pearson, S.; del Campo, A., Thiol-Methylsulfone-Based Hydrogels for Cell Encapsulation: Reactivity Optimization of Aryl-Methylsulfone Substrate for Fine-Tunable Gelation Rate and Improved Stability. *Biomacromolecules* **2021**, *22* (7), 2874-2886.
4. Maity, A.; Sarkar, A.; Sil, A.; B. N, S. B.; Patra, S. K., Synthesis, photophysical and concentration-dependent tunable lasing behavior of 2,6-diacetylenyl-functionalized BODIPY dyes. *New Journal of Chemistry* **2017**, *41* (6), 2296-2308.

List of Scientific Contributions

Articles

1. Feng, J.; **Jiang, Q.**; Rogin, P.; W. de Oliveira, P.; Del Campo, A. Printed Soft Optical Waveguides of PLA Copolymers for Guiding Light into Tissue. *ACS Applied Materials & Interfaces*, 2020, 12 (18), 20287-20294.
2. Zheng, Y.; Liang, H.; Mitchell, Kim.; **Jiang, Q.**; Li, Bin.; Feng, Jun.; Del Campo, A. 4D hydrogel for dynamic cell culture with orthogonal, wavelength-dependent mechanical and biochemical cues. *Materials Horizons*, 2020, 7 111-120.
3. Zheng, Y.; Chen, Z.; **Jiang, Q.**; Feng, Jun.; Wu, Si.; Del Campo, A. Near-infrared-light regulated angiogenesis in a 4D hydrogel. *Nanoscale*, 2020, 12 (25), 13654-13661.
4. **Jiang, Q.**; Paez, J.I.; Valbuena-Mendoza, R.; De Miguel-Jiménez, A.; Del Campo, A. Two-photon photodegradable PEG-hydrogels for dynamic 3D cell culture. *2022 Manuscript in preparation*.

Talks

1. **Jiang, Q.**; Paez, J.I.; Del Campo, A. Two-Photon activatable chromophores for optoregulation of 3D cellular microenvironments. Doctoral Colloquia, May 2018, INM-Leibniz Institute for New Materials, Saarbrücken, Germany.
2. **Jiang, Q.**; Paez, J.I.; Del Campo, A. Two-photon degradable hydrogels for dynamic control of cellular microenvironments. Doctoral Colloquia, April 2019, INM-Leibniz Institute for New Materials, Saarbrücken, Germany.

Poster Presentations

1. **Jiang, Q.**; Paez, J.I.; Del Campo, A. Two-photon degradable hydrogels for dynamic control of cellular microenvironments. International Conference on Living Materials, February 2020, Universität des Saarlandes, Saarbrücken, Germany.
2. **Jiang, Q.**; Paez, J.I.; Zheng Y.; Del Campo, Two-photon degradable hydrogels for dynamic control of cellular microenvironments. 30th Conference of the European Society for Biomaterials (ESB), September 2019, Dresden, Germany.
3. **Jiang, Q.**; Paez, J.I.; Del Campo, A. Photodegradable Biomedical Adhesives for 3D Cell Encapsulation. Doctoral Day "Doctoral students from the Faculty of Natural Sciences and Technology present their doctoral topics, date November 2018, University of Saarland, Saarbrücken, Germany.
4. **Jiang, Q.**; Farrukh A.; Paez, J.I.; Del Campo, Optoregulation of 3D cellular microenvironments with NIR light; Cell Physics Conference, 11-13 October 2017, University of Saarland, Saarbrücken.
5. **Jiang, Q.**; Farrukh A.; Paez, J.I.; Del Campo, A. Two-Photon activatable chromophores for optoregulation of 3D cellular microenvironments. WE-Heraeus-Seminar on "Bio-inspired,

Nano- and Microstructured Surfaces: New Functionality by Material and Structure", May 2017, Bad Honnef, Germany.

Participation in Seminars

1. Carbohydrate chemistry; University of Saarland and HIPS, Summer 2017; Lecturer: Dr. Alexander Titz.
2. Cell culture basic course, Promo-cell academy, 30 July – 02 August 2019, Heidelberg, Germany.
3. European Summer School: Soft Matter and Smart Materials, University of Strasbourg, 01-05 May, Strasbourg, France.
4. Weekly INM scientific seminars (Colloquia), 2016 - 2019, INM-Leibniz Institute for new Materials, Saarbrücken, Germany.
5. Monthly Biointerface lectures, 2016 - 2019, INM-Leibniz Institute for new Materials, Saarbrücken, Germany.

Participation in soft skills seminars

1. Writing, Presenting, Networking – Tools for a Scientific Career, Symposium for Female Scientists, October 2019, INM-Leibniz Institute for new Materials, Saarbrücken, Germany.
2. Academic English, Doctoral Training Program of Saarland University (GradUS global), winter semester 2017 – 2018, University of Saarland, Saarbrücken, Germany.